TECHNISCHE
UNIVERSITÄT
WIEN
Vienna University of Technology

Institut für Verfahrenstechnik,
Umwelttechnik und
Technische Biowissenschaften

Masterthesis

Development of a Slug Analysis Tool for Slugging in Gas-Oil-Water Multiphase Pipelines and Comparison with Aspen Hysys

ausgeführt zum Zwecke der Erlangung des akademischen Grades eines Diplom-Ingenieurs
unter der Leitung von

Univ.Prof. Dipl.-Ing. Dr.techn. Herman Hofbauer
Inst. f. Verfahrenstechnik, Umwelttechnik und Techn. Biowissenschaften
E166

eingereicht an der Technischen Universität Wien

Fakultät für Maschinenwesen und Betriebswissenschaften

von

Mittlböck Sebastian
Matr.Nr.: 0825994
Pokornygasse 1a/6
1190 Wien

Wien, am 1. September 2014   Mittlböck Sebastian

Eidesstattliche Erklärung

Ich erkläre eidesstattlich, dass ich die Arbeit selbständig angefertigt, keine anderen als die angegebenen Hilfsmittel benutzt und alle aus ungedruckten Quellen, gedruckter Literatur oder aus dem Internet im Wortlaut oder im wesentlichen Inhalt übernommenen Formulierungen und Konzepte gemäß den Richtlinien wissenschaftlicher Arbeiten zitiert, durch Fußnoten gekennzeichnet bzw. mit genauer Quellenangabe kenntlich gemacht habe.

Wien, am 1. September 2014

Mittlböck Sebastian

Acknowledgment

Kurzfassung

Bei der Öl- und Gasförderung ist es eine der wichtigsten Aufgaben, den konstanten Transport der Mehrphasenströmung durch die Pipeline von der Produktionsbohrung zu den nachfolgenden Prozessen zu sichern. Die unterschiedlichen Anordnungen der Grenzflächen zwischen flüssiger und gasförmiger Phase machen es für einen Ingenieur zu einer schwierigen Aufgabe die Durchflusscharakteristika vorherzusagen.

Es wäre wünschenswert ein einfaches Werkzeug am Beginn eines Projektes zur Verfügung zu haben, mit dem es möglich ist das Mehrphasenverhlaten in Pipelines mit nur wenigen Eingabeparametern abzuschätzen. Um Wissen im Bereich der Mehrphasenströmung aufzubauen, wurde eine gründliche Literaturrecherche durchgeführt, auf deren Basis das Petals und Aziz Modell ausgewählt wurde. Darauf aufbauend wurde SEM-Flow, ein Programm zur Vorhersage von Mehrphasenströmung entwickelt. Um die Unabhängigkeit von anderen Programmen zu ermöglichen, wurde ein Modul zur Abschätzung der Eigenschaften von Flüssig- und Gasphase inkludiert und es ist darüber hinaus möglich, den Wärmeverlust über die Pipeline vorherzuberechnen. Für die Berechnung der Fluideigenschaften wird ein "black oil model" verwendet, wodurch es möglich ist, die Anzahl der Eingabeparameter gering zu halten.

Auf Grund des häufigen Auftretens der Pfropfenströmung wird spezielles Augenmerk auf diesen Bereich gelegt, wobei verschiedene Modelle zur Berechnung des Druckverlustes, des Flüssigkeitsinhaltes und der translatorischen Geschwindigkeit miteinander verglichen werden. Im Verlauf des Berechnungsprozesses ist es mehrmals nötig, die Nullstellen verschiedener Funktionen zu bestimmen. Damit die Berechnungszeit möglichst gering gehalten werden kann, wird das Pegasusverfahren als iterative Methode zur Nullstellenbestimmung vewendet. Um die Anwendbarkeit von SEM-Flow zu überprüfen, werden Ergebnisse wie Fluideigenschaften, Druckverlust und Parameter der Mehrphasenströmung mit dem kommerziellen Simulationsprogramm Aspen Hysys verglichen.

Abstract

During the oil and gas production process it is a crucial goal to ensure the constant transport of the multiphase flow in the pipeline from the producing wells to the downstream facilities. The multiple distributions of the interface between the liquid and gas phase make it difficult for engineers to predict the flow characteristics.

A simple tool, which estimates the multiphase flow behavior in pipelines with just a few input parameters is desirable, especially at the early stages of a project in order to estimate the order of magnitude. Based on a thorough literature review, which enables one to gain knowledge in the field of multiphase flow, the Petalas and Aziz model is selected. On this basis the multiphase flow prediction tool SEM-Flow is developed from scratch. To create a stand alone tool, SEM-Flow is capable of estimating the fluid properties of the gas and liquid phase, as well as the heat loss over the pipeline. A black oil model, which enables one to keep the number of required input parameters low is used.

Special emphasis is put on the slug flow region due to its frequent occurrence and several models to calculate the pressure drop, liquid hold up and translational velocity are compared. During the calculation process it is necessary to obtain several roots of functions. Therefore the Pegasus algorithm is used as iterative method to keep the computing time low.

To verify the applicability of SEM-Flow, the results like fluid properties, pressure drop and multiphase flow variables are compared to the commercial simulation software Aspen Hysys.

Contents

Chapter 1

Nomenclature

Latin letters	Description	Unit[1]
A	Pipe cross section area	$[m^2]$
$\tilde{A}$	Dimensionless pipe cross section area	$[-]$
A_c	Gas core area	$[m^2]$
$\tilde{A}_c$	Dimensionless gas core area	$[-]$
A_f	Liquid film area	$[m^2]$
$\tilde{A}_f$	Dimensionless liquid film area	$[-]$
A_G	Gas flow area	$[m^2]$
$\tilde{A}_G$	Dimensionless gas flow area	$[-]$
A_L	Liquid flow area	$[m^2]$
$\tilde{A}_L$	Dimensionless liquid flow area	$[-]$
A_T	Dimensionless parameter after [1]	$[-]$
B_G	Gas formation volume factor	$([ft^3/scf])$
B_o	Bond number	$[-]$
B_O	Oil formation volume factor	$([res^2\ bbl/STBO])$
B_{Ob}	Oil formation volume factor at p_b	$([res\ bbl/STBO])$
B_T	Dimensionless parameter after [1]	$[-]$
B_W	Water formation volume factor	$([res\ bbl/STBO])$
C_G	Gas input volume fraction	$[-]$
C_l	Lift coefficient	$[-]$
C_0	Distribution coefficient	$[-]$
c_O	Isothermal oil compressibility	$([1/psia])$
cp_G	Gas specific heat capacity	$[J/kg\ K]$
cp_L	Liquid specific heat capacity	$[J/kg\ K]$

---

[1]The units in round brackets are the English units. These units will be used in Sec. 6.3 due to the fact that no conversion of the empirical correlations to SI units is available. For more information see Sec. 6.3 .

[2]res = reservoir

Latin letters	Description	Unit
cp_O	Oil specific heat capacity	$[J/kg\ K]$
cp_W	Water specific heat capacity	$[J/kg\ K]$
C_T	Dimensionless parameter after [1]	$[-]$
D	Inner pipe diameter	$[m]$
D^*	Critical inner pipe diameter	$[m]$
D_b	Bubble diameter	$[m]$
D_c	Gas core diameter	$[m]$
Dev	Deviation SEM-Flow / Hysys	$[\%]$
$\overline{Dev}$	Average deviation SEM-Flow / Hysys	$[\%]$
D_f	Liquid film diameter	$[m]$
D_G	Gas hydraulic diameter	$[m]$
D_L	Liquid hydraulic diameter	$[m]$
D_o	Outer pipe diameter	$[m]$
D_T	Dimensionless parameter after [1]	$[-]$
$\frac{dp}{dL}$	Pressure gradient	$[Pa/m]$
E_c	Liquid hold up in the gas core	$[-]$
E_f	Liquid holdup in the film	$[-]$
E_G	Gas void fraction	$[-]$
E_L	Liquid hold up	$[-]$
E_{LS}	Slug liquid hold up	$[-]$
Eo	Eötvös number	$[-]$
f	Friction factor	$[-]$
f_c	Core friction factor	$[-]$
FE	Liquid fraction entrained	$[-]$
f_f	Friction factor film/pipe wall	$[-]$
f_G	Friction factor gas/pipe wall	$[-]$
f_i	Friction factor liquid/gas	$[-]$
f_L	Friction factor liquid/pipe wall	$[-]$
F_P	Flow pattern factor	$[-]$
Fr	Froude number	$[-]$
F_s	Slug frequency	$[1/s]$
f_s	Friction factor in the slug body	$[-]$
F_S	Shape factor	$[-]$
f_{SL}	Friction factor based on v_{SL}	$[-]$
F_T	Dimensionless parameter after [1]	$[-]$

Latin letters	Description	Unit
f_w	Water cut	$[-]$
g	Gravity	$[m/s^2]$
H_G	Gas specific enthalpy	$[J/kg]$
h_L	Liquid height	$[m]$
$\tilde{h}_L$	Dimensionless liquid height	$[-]$
H_O	Oil specific enthalpy	$[J/kg]$
$\dot{H}$	Enthalpy flow	$[W]$
H_W	Water specific enthalpy	$[J/kg]$
I^*	Modified inclination factor	$[-]$
k_G	Gas thermal conductivity	$[W/m\ K]$
k_L	Liquid thermal conductivity	$[W/m\ K]$
k_o	Air thermal conductivity	$[W/m\ K]$
k_O	Oil thermal conductivity	$[W/m\ K]$
k_{pipe}	Wall thermal conductivity	$[W/m\ K]$
K_T	Dimensionless parameter after [1]	$[-]$
k_W	Water thermal conductivity	$[W/m\ K]$
L	Pipe length	$[m]$
L_f	Slug film length	$[m]$
L_m	Mixing zone length	$[m]$
L_s	Liquid slug body length	$[m]$
$L_{segment_H}$	Equivalent horizontal pipe length	$[m]$
$L_{segment_V}$	Equivalent vertical pipe length	$[m]$
L_u	Slug unit length	$[m]$
$\dot{m}_G$	Gas mass flow rate	$[kg/s]$
$\dot{m}_L$	Liquid mass flow rate	$[kg/s]$
n	Number of data points	$[-]$
NB	Dimensionless number	$[-]$
$n_{Segment}$	Total number of segments	$[-]$
Nu	Nusselt number	$[-]$
N_x	Correction factor after [2]	$[m/s]$
N_y	Correction factor after [2]	$[m/s]$
p	Pressure	$[bara]\ ([psia])$
p_b	Bubble point pressure	$([psia])$
p_{pc}	Pseudo critical pressure	$([psia])$
p_{pr}	Reduced pressure	$([psia])$

Latin letters	Description	Unit
Pr	Prandtl number	$[-]$
p_{sep}	Actual separator pressure	$[bara]$ $([psia])$
q_G	Actual volumetric gas flow rate	$[m^3/s]$ $([ft^3/s])$
q_{Gsc}	Volumetric gas flow rate at standard conditions	$([ft^3/s])$
q_L	Actual volumetric liquid flow rate	$[m^3/s]$ $([ft^3/s])$
q_O	Actual volumetric oil flow rate	$[m^3/s]$ $([ft^3/s])$
q_{Osc}	Oil volumetric flow rate at standard conditions	$([ft^3/s])$
$\dot{Q}$	Heat flow	$[W]$
q_W	Actual volumetric water flow rate	$[m^3/s]$ $([ft^3/s])$
q_{Wsc}	Volumetric water flow rate at standard conditions	$([ft^3/s])$
R	Inner pipe radius	$[m]$
R_o	Outer pipe radius	$[m]$
Re	Reynolds number	$[-]$
R_p	Producing gas/oil ratio	$[Sm^3/m^3]$ $([scf/STB])$
R_s	Solution gas/oil ratio	$([scf/STB])$
R_{sW}	Solution gas/water ratio	$([scf/STB])$
R_{sW_b}	Corrected solution gas/water ratio	$([scf/STB])$
S	Salinity	$[\%]$
$\tilde{S}_f$	Dimensionless length film/pipe wall	$[-]$
S_G	Length gas/pipe wall	$[m]$
$\tilde{S}_G$	Dimensionless length gas/pipe wall	$[-]$
S_i	Length gas/liquid	$[m]$
$\tilde{S}_i$	Dimensionless length gas/liquid	$[-]$
S_L	Length liquid/pipe wall	$[m]$
$\tilde{S}_L$	Dimensionless length liquid/pipe wall	$[-]$
T	Average fluid temperature	$[^\circ C]$ $([^\circ F])$
T_o	Ambient fluid temperature	$[^\circ C]$
T_{pc}	Pseudo critical temperature	$([^\circ F])$
T_{pr}	Reduced temperature	$([^\circ F])$
T_{sep}	Actual separator temperature	$[^\circ C]$ $([^\circ F])$
T_T	Dimensionless parameter after [1]	$[-]$
U_i	Heat transfer coefficient fluid/pipe wall	$[W/m^2\ K]$
U_L	Single phase heat transfer coefficient	$[W/m^2\ K]$
U_o	Heat transfer coefficient air	$[W/m^2\ K]$
v_b	Bubble swarm rise velocity	$[m/s]$

Latin letters	Description	Unit
v_c	Gas core velocity	$[m/s]$
v_d	Elongated bubble drift velocity	$[m/s]$
$v_{dh\infty}$	v_d at high Re (horizontal)	$[m/s]$
$v_{dv\infty}$	v_d at high Re (vertical)	$[m/s]$
$v_{d\infty}$	v_d at high Re	$[m/s]$
v_f	Film velocity	$[m/s]$
v_G	Actual gas velocity	$[m/s]$
v_G^*	Critical gas velocity	$[m/s]$
v_{Gdb}	Velocity of dispersed bubbles in liquid slug	$[m/s]$
v_{Gs}	Velocity of the gas pocket in the slug	$[m/s]$
$\tilde{v}_G$	Dimensionless gas velocity	$[-]$
v_i	Slip velocity	$[m/s]$
v_L	Actual liquid velocity	$[m/s]$
v_L^*	Critical liquid velocity	$[m/s]$
v_{Ls}	Slug average liquid velocity	$[m/s]$
$\tilde{v}_L$	Dimensionless liquid velocity	$[-]$
v_M	Mixture velocity	$[m/s]$
v_o	Air velocity	$[m/s]$
v_{SG}	Superficial gas velocity	$[m/s]$
v_{SL}	Superficial liquid velocity	$[m/s]$
v_T	Translational velocity	$[m/s]$
W	Mass flow rate	$[kg/s]$
W_G	Gas mass flow rate	$[kg/s]$
W_L	Liquid mass flow rate	$[kg/s]$
x	Quality factor	$[-]$
X	Critical value for inclination angle	$[-]$
X_T	Dimensionless parameter after [1]	$[-]$
Z	Real gas deviation factor	$[-]$

Greek letters	Description	Unit
α	Pipe inclination angle	$[grad]$
α_{tot}	Total heat transfer coefficient	$[W/m^2\ K]$
β	Dimensionless coefficient	$[-]$
ΔV_{Wp}	Volume change due to pressure reduction	$[-]$

Greek letters	Description	Unit
ΔV_{WT}	Volume change due to temperature reduction	$[-]$
ΔH_{vap}	Latent heat of vaporization	$[J/kg]$
$\tilde{\delta}_L$	Dimensionless liquid film thickness	$[-]$
δ_L	Liquid film thickness	$[m]$
$\tilde{\delta}_{L_{min}}$	Minimum dimensionless liquid film thickness	$[-]$
ϵ	Pipe roughness	$[m]$
η	Slug length weighting factor	$[-]$
η_G	Gas Joule Thomson coefficient	$[K\ m^3/J]$
η_O	Oil Joule Thomson coefficient	$[K\ m^3/J]$
η_W	Water Joule Thomson coefficient	$[K\ m^3/J]$
γ	Bubble distortion coefficient	$[-]$
γ_{API}	API gravity	$[°API]$
γ_G	Specific gas gravity	$[-]$
γ_{G100}	Specific gas gravity at 100 psia p_{sep}	$[-]$
γ_{Gd}	Dissolved specific gas gravity	$[-]$
γ_{Gf}	Specific free gas gravity	$[-]$
γ_O	Specific gravity of stock tank oil	$[-]$
γ_{Wsc}	Specific water gravity at standard conditions	$[-]$
μ_c	Core dynamic viscosity	$[kg/m\ s]$
μ_G	Gas dynamic viscosity	$[kg/m\ s]$
μ_L	Liquid dynamic viscosity	$[kg/m\ s]$
μ_{LW}	Liquid dynamic viscosity at the pipe wall	$[kg/m\ s]$
μ_M	Mixture dynamic viscosity	$[kg/m\ s]$
μ_O	Oil dynamic viscosity	$[kg/m\ s]$
μ_{Od}	Dead oil viscosity	$[kg/m\ s]$
μ_s	Slug dynamic viscosity	$[kg/m\ s]$
μ_W	Water dynamic viscosity	$[kg/m\ s]$
ν_o	Air kinematic viscosity	$[m^2/s]$
ρ_c	Core density	$[kg/m^3]$
ρ_G	Gas density	$[kg/m^3]\ ([lbm/ft^3])$
ρ_L	Liquid density	$[kg/m^3]\ ([lbm/ft^3])$
ρ_M	Mixture density	$[kg/m^3]$
ρ_O	Oil density	$([lbm/ft^3])$
ρ_{Ob}	Oil density at p_b	$([lbm/ft^3])$
ρ_r	Reduced gas density	$([lbm/ft^3])$

Greek letters	Description	Unit
ρ_S	Slug density	$[kg/m^3]$
ρ_W	Water density	$([lbm/ft^3])$
σ_O	Gas/oil surface tension	$([dyne/cm])$
σ_W	Gas/water surface tension	$([dyne/cm])$
σ_L	Liquid surface tension	$[N/m]$ $([dyne/cm])$
σ_{Od}	Dead gas/oil surface tension	$([dyne/cm])$
σ_{Od100}	Dead gas/oil surface tension at $100°F$	$([dyne/cm])$
σ_{Od68}	Dead gas/oil surface tension at $68°F$	$([dyne/cm])$
σ_{W280}	Gas/water surface tension at $280°F$	$([dyne/cm])$
σ_{W74}	Gas/water surface tension at $74°F$	$([dyne/cm])$
τ_S	Shear stress in the slug body	$[Pa]$
τ_{Wf}	Shear stress film/pipe wall	$[Pa]$
τ_{WG}	Shear stress gas/pipe wall	$[Pa]$
τ_{Wi}	Shear stress gas/liquid	$[Pa]$
τ_{WL}	Shear stress liquid/pipe wall	$[Pa]$

Chapter 2

Introduction

2.1 Motivation

As the accessibility of oil and gas fields has decreased in the last few decades enhanced oil recovery measures are becoming more and more important. The rapidly increasing oil price has motivated the development of new secondary and tertiary oil recovery procedures and has made them economically viable for the oil and gas industry. For companies to continue oil and gas production profitably, the reliability and stability of the oil production and transportation must be ensured by all means. "One of the most pronounced challenges in meeting this goal is managing the complex hydraulics of pipelines used in gathering systems and to transport the oil and gas from wells to processing facilities."[3] Therefore it is important to predict multiphase flow behavior as accurately as possible, so that the multiphase flow mixture is constantly flowing and downstream equipment can be designed to meet the predicted requirements and to maintain uninterrupted service.

Usually part of this overall flow assurance[1] is a slug analysis. Slug flow is a common occurring flow phenomenon in pipelines and, at the same time, the most crucial one for downstream equipment such as separators. This slug analysis can be carried out with several sophisticated and costly software packages. The user must be a highly trained and experienced engineer. The duration of each simulation ranges from a couple of days to a week. The programs offer compositional fluid property models, which require a detailed characterization of the crude oil. A sophisticated heat transfer model is included in these software and they use robust and fast convergence methods. Moreover some of these simulation software have the advantage to perform detailed analysis of the system for complex operation methods (start up, shut downs).

In the conceptual phase however, a simplified tool is desirable, which allows experienced engineers to make an initial estimate of the multiphase flow behavior, on the basis of a small number of input data in order to be able to assess if further analysis is required.

---

[1]The term flow assurance refers to the ensuring of a constantly flowing hydrocarbon mixture in the pipeline. This involves, beside network modeling and transient multiphase simulation, a slug analysis and the prediction if hydrates, waxes or asphaltens deposit.

2.2 Statement of the problem

Of this thesis is the core objective the development of a simplified analysis tool in Microsoft Excel/VBA[2] to predict the multiphase flow behavior in a pipeline. This tool will be used primarily in the conceptual phase during the early stage of a project and should be able to predict the multiphase flow variables with as few input parameters as possible and the calculation process for the whole pipeline should be completed within a few minutes. By satisfying these requirements a lower accuracy is accepted, which is sufficient during the conceptual project phase.

Due to the fact, that the predominant flow pattern in pipelines is the slug flow pattern and this flow pattern is crucial for downstream equipment, special attention shall be paid to predicting the pressure drop, liquid hold up, slug length and slug velocity in this pattern. Therefore a comparison of different models to predict these properties shall be conducted. Nevertheless the tool must be capable of predicting the flow behavior and pressure drop over the whole pipeline.

In contrast to other highly sophisticated software that is available, this simplified tool will be only applicable to operational conditions in steady state. Thus start up and shut down processes cannot be predicted with this tool. Furthermore the inclination angle of the pipeline, which is calculated by the analysis tool, shall be limited to only small deviations from the horizontal angle. Although it is known, that in practice several slug flow mechanisms, such as hydrodynamic slugging or severe slugging cause slug flow in pipelines, the analysis tool is limited to hydrodynamic slugging only.

To assign priorities to the requirements on the analysis tool, the following list can be compiled, whereby the first point is the most important one. With this list the tool evaluation shall be made later on as well.

1. The analysis tool must be capable of predicting the pressured drop over the whole pipeline.

2. Identification of the flow patterns in the whole pipeline.

3. The slug properties, slug length and slug velocity must be calculated when the slug flow pattern occurs.

4. The liquid hold up and temperature loss must be predicted over the pipeline.

To predict the multiphase flow behavior, the analysis tool must be capable of calculating the temperature profile over the whole pipeline as well as to predict the fluid properties at the actual pressure and temperature in the pipeline.

---

[2]For more information concerning VBA see Sec. 7.1 .

2.3   Scope of the thesis

Following a brief summary of each chapter can be found:

Multiphase flow overview   A bridge from single phase flow, which is common knowledge, to multiphase flow is built. In multiphase flow it cannot be assumed for instance, that the pressure loss, due to a positive elevation change, is recovered in the downward section again. Due to the fact that depending on the author the symbols and the nomenclature can change in the field of multiphase flow, these variables must be defined.
The geometrical classification of the two phases in the pipe are called flow patterns or flow regimes. The determination of the flow pattern is crucial to apply the adequate calculation method for values like the pressure drop. In the last part of the chapter the different flow patterns in horizontal and vertical flow are defined and their development is described.

Multiphase flow prediction   A literature review was conducted to gain knowledge about different types of multiphase flow models. A summary of this literature review is presented highlighting the most important models. With this knowledge a mechanistically based model, the Petalas and Aziz model, is selected. This model can be divided in two sections: the determination of the flow pattern and the calculation of the pressure drop and liquid hold up. Different models are compared to calculate the properties in the slug flow region such as pressure drop, liquid hold up, slug length and slug velocity. These models as well as the main model by Petalas and Aziz are presented in detail.

Multiphase flow heat exchange   During the transportation of the multiphase flow mixture from the production well to the downstream equipment, the temperature of the fluids in the pipeline changes depending on the surrounding. The heat transfer between the fluids and the pipe surrounding, followed by a temperature change of the fluids in the pipeline, is an important matter with regard to the determination of the fluid properties. The overall heat balance as well as the determination of the heat transfer coefficients is presented in this chapter.

Fluid property correlation   The accurate prediction of the fluid properties is a prerequisite to successful pipeline design. To simulate the fluid properties two different approaches can be used: the black oil model and the compositional model. Although the accuracy of the data received from the compositional model would be higher, the black oil model is used in the analysis tool. The reason is that the black oil model only requires a few input data in contrast to the compositional model which is the requirement on the analysis tool. The black oil model equations are presented which are included in the analysis tool. For the latent heat of vaporization no correlation could be found in the literature which is why equations were derived by polynomial regression analysis of data calculated with Aspen Hysys.[3]

Multiphase flow simulation tool - SEM - Flow   The multiphase flow simulation tool SEM-Flow is programmed in visual basic and a modular approach is chosen as the program structure. The calculation was first evaluated with Mathcad to check for possible mistakes occurring in the code.

---

[3]For more information concerning Aspen Hysys see Sec. 8.2 .

The Frame-Module, which is the main module of the program, is the interface between the submodules. The submodules are called and parameters are passed there as well. Several equations, presented by Petalas and Aziz have to be solved with an iterative procedure. Thus numerical methods are identified to obtain the roots of these functions.

SEM-Flow simulation results   The validation of SEM-Flow is done by comparing the results to the results from a commercial simulation software, Aspen Hysys. At first the fluid properties and afterwords the results from the multiphase flow calculation are reviewed. The results and their interpretation are presented in this chapter.

Chapter 3

Multiphase flow overview

In the following chapter a bridge from single phase flow, which is common knowledge, to multiphase flow is built. In multiphase flow it cannot be assumed for instance, that the pressure loss, due to a positive elevation change, is recovered in the downward section again. Due to the fact, that depending on the author the symbols and the nomenclature can change in the field of multiphase flow, these variables must be defined.

The geometrical classification of the two phases in the pipe are called flow patterns or flow regimes. The determination of the flow pattern is crucial to apply the adequate calculation method for values like the pressure drop. In the last part of the chapter the different flow patterns in horizontal and vertical flow are defined and their development is described.

3.1   From single to multiphase flow

Nowadays the flow behavior of single phase flow is a well understood engineering topic and the methods for predicting the pressure drop or temperature profile over the whole pipeline are quite mature.[4] The pressure drop mainly depends on the Reynolds number, which is a function of fluid viscosity, fluid density, fluid velocity and pipeline diameter.[5] In single phase flow it is possible to calculate the actual velocity at every section from the continuity equation and also the pressure drop over the whole pipeline in a straightforward manner. A schematic image of a single phase flow pipeline is represented in Fig. 3.1 , where W is the mass flow rate and v is the actual velocity in the pipeline.
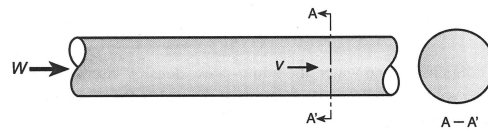
Figure 3.1: A single phase flow pipeline.[6]

Multiphase flow, as shown in Fig. 3.2 , can be characterized by simultaneously occurring gas and liquid phases. The phases in a multiphase flow pipeline can be distribute in many different geometrical configurations, which are called flow patterns or flow regimes. The calculation procedure of the pressure drop is different for every flow pattern and depends on a larger number of parameters than in single phase flow. Therefrom it can be seen, that it is crucial to determine the actual prevailing flow pattern to calculate the pressure drop or heat loss over the pipeline.[6]
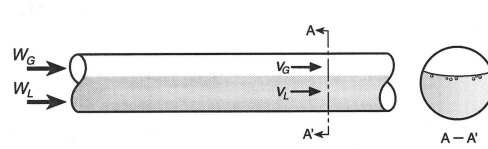
Figure 3.2: A multiphase flow pipeline.[6]

Another difference between single phase flow and multiphase flow, that should always be kept in mind, is that the pressure behavior in upward and downward inclined pipeline sections is different. In single phase flow the pressure loss, due to a positive elevation change, is recovered in the downward section again. In Fig. 3.3 (a) the pressure at position A is higher than at position B and the pressures at point A and C are the same. This effect cannot always be determined in multiphase flow pipelines due to the possibility of different flow patterns in the upward and downward sections of the pipeline, which is followed by a different pressure drop. So the pressure at point A and C will not be the same in the multiphase flow pipeline in Fig. 3.3 (b).[5]
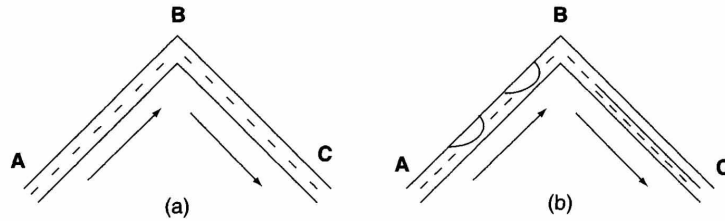
Figure 3.3: Single phase and multiphase flow through upward and downward inclined pipe sections.[5]

3.2   Multiphase flow variables

Unfortunately in the field of multiphase flow no general nomenclature or even a description of the core parameters exists, so that sometimes it can be difficult to compare different literature sources. Therefore these parameters will be defined and briefly explained in the following section.

3.2.1   Water cut

The water cut f_w is defined by the water volumetric flow divided by the total liquid volumetric flow. In Eq. 3.1 q_w is the water volumetric flow rate at standard conditions and q_o is the oil volumetric flow rate at standard conditions. It must be noted, that the water cut does not take into account, that the two liquid phases, water and oil, might flow at different velocities.[4]

$$f_w = \frac{q_w}{q_w + q_o} \tag{3.1}$$

3.2.2 Liquid hold up

The liquid hold up E_L is defined as the ratio of the volume of a pipe segment, which is occupied by liquid to the total volume of the pipe segment. In multiphase flow the liquid hold up can take values between 0 and 1, whereas in single phase flow it can only take the value 0 or 1.[7]

$$E_L = \frac{liquid\ volume\ in\ pipe\ segment}{total\ volume\ of\ pipe\ segment} \tag{3.2}$$

3.2.3 Gas void fraction

The remainder of the pipe segment, which is occupied by gas, is called gas void fraction. The gas void fraction E_G is thus defined as the ratio of the volume of a pipe segment, which is occupied by gas to the total volume of the pipe segment. In multiphase flow the gas void fraction can take values between 0 and 1, whereas in single phase flow it can only take the value 0 or 1.[7] The connection between the gas void fraction and the liquid hold up is presented by Eq. 3.4 .

$$E_G = \frac{gas\ volume\ in\ pipe\ segment}{total\ volume\ of\ pipe\ segment} \tag{3.3}$$

$$E_G = 1 - E_L \tag{3.4}$$

3.2.4 Superficial velocity

The superficial velocity of the gas (v_{SG}) or liquid phase (v_{SL}) is defined as the velocity, which the phase would have, if it would flow alone in the pipe. The superficial velocity is received by dividing the actual volumetric flow rate through the total pipe cross section area. It must be noted, that the superficial velocity is not the actual velocity of the respective phase but a theoretical parameter.[6]

$$v_{SL} = \frac{q_L}{A} \tag{3.5}$$

$$v_{SG} = \frac{q_G}{A} \tag{3.6}$$

3.2.5 Mixture velocity

The mixture velocity v_M is the the total volumetric flow rate of both phases divided by the total pipe section area. It is calculated from Eq. 3.7 .[6]

$$v_M = \frac{q_G + q_L}{A} \tag{3.7}$$

3.2.6 Actual velocity

As mentioned above, the superficial velocity is not the actual velocity of the phases in the pipe. The reason is that in reality, the phases are not occupying the whole pipe cross section area but only a fraction of it. Therefore the actual velocity is higher than the superficial velocity. The actual velocity of the liquid (v_L) and gas phase (v_G) is calculated from Eq. 3.8

and Eq. 3.9 by dividing the actual volumetric flow through the cross section area, occupied by the respective phase.[6]

$$v_L = \frac{q_L}{A_L} = \frac{q_L}{E_L A} \tag{3.8}$$

$$v_G = \frac{q_G}{A_G} = \frac{q_G}{E_G A} = \frac{q_G}{(1 - E_L)A} \tag{3.9}$$

3.3 Flow pattern in horizontal and vertical pipelines

The phase distribution in two phase flow can have many different geometrical configurations. These configurations are called flow patterns or flow regimes. The flow regimes differ from each other in the different interactions of the two phases, the results of which are different flow characteristics. The existence of the the different flow patterns is dependent on the following variables:

- The gas and liquid flow rate.

- The pipe diameter and the inclination angle of the pipe.

- The fluid properties of the two phases.

As one may expect, it is extremely important to determine the actual flow pattern for calculating the flow behavior in the pipe. Parameters, such as the pressure drop or the liquid hold up, are strongly dependent on the phase distribution and can vary over a wide range. Unfortunately two phase flow investigators did not agree on the definition and classification of the individual flow patterns. Their definition is arbitrary and based on observations in test pipelines in the laboratory. Therefore there is no objective approach and each author defines the transition from one pattern to another one differently. This is the reason why nowadays a lot of different flow patterns exist in the literature, which sometimes just have a different nomenclature. Different models for calculating multiphase flow behavior assume the existence of different flow patterns, which is why they sometimes cannot be compared to each other. Generally one can distinguish between flow patterns occurring in horizontal or vertical pipelines. A widely accepted flow pattern classification was made by Shoham.[8] Fig. 3.4 and Fig. 3.5 show the flow pattern existing in horizontal and vertical pipelines, which will be described next.

3.4 Horizontal flow patterns

In Fig. 3.4 one can see a possible classification of the existing flow patterns in horizontal flow, which are: dispersed bubble flow, annular flow, stratified flow, elongated bubble flow and slug flow.

3.4.1 Dispersed bubble flow

In this flow pattern the liquid phase is the continuous phase, in which the gas phase is dispersed as bubbles. The gas bubbles can either be located at the upper pipe wall or distributed over the whole cross sectional area. The liquid and gas phase move at the same velocity due to the high liquid flow rates. The dispersed bubble flow pattern arises either,
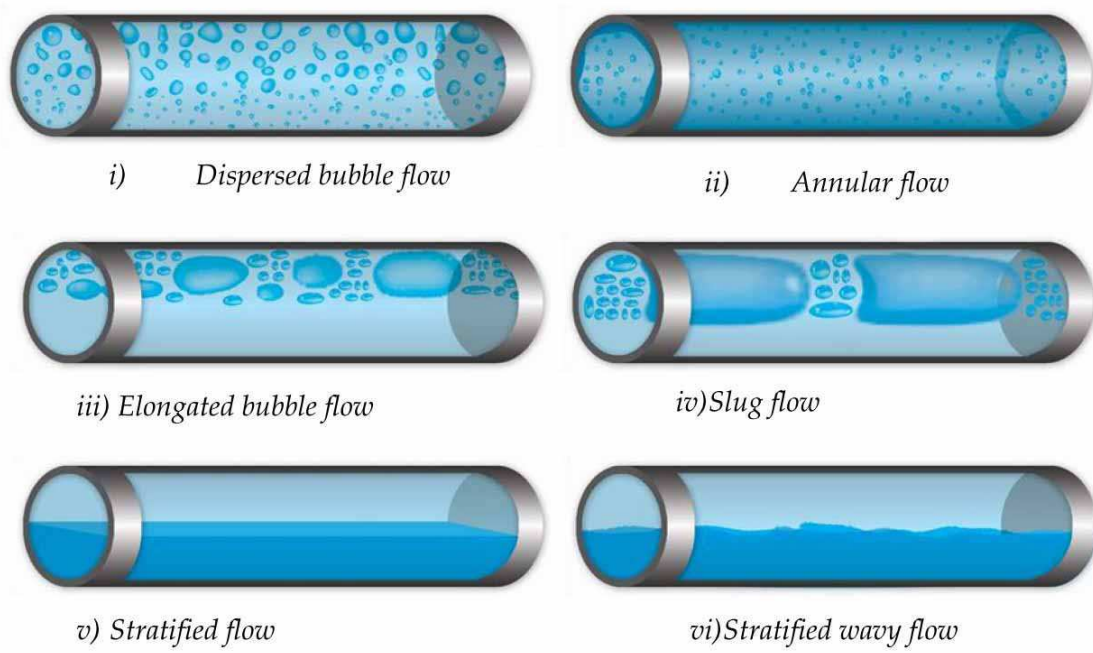
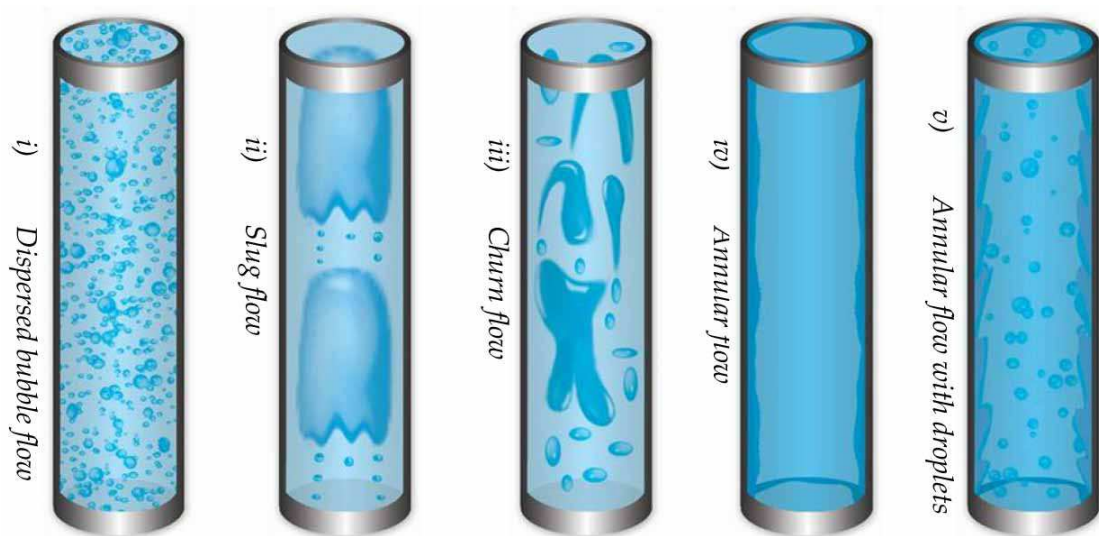Figure 3.4: Gas-liquid flow regimes in horizontal pipes.[4]

Figure 3.5: Gas-liquid flow regimes in vertical pipes.[4]

when bubbles are first suspended in the liquid, or, when gas pockets touching the pipe on the top collapse.[6]

3.4.2 Annular flow

In the annular flow pattern the gas phase flows at a very high velocity in the core of the pipe. In the gas phase liquid droplets may be dispersed as well. The liquid phase is flowing as a thin layer around the pipe wall and is surrounding the gas phase. The liquid film at the bottom is usually thicker than at the top of the pipe due to gravity. At high gas flow rates a larger amount of liquid will be dispersed in the gas phase, whereby a thin liquid layer remains at the pipe wall.[6]

3.4.3 Stratified flow

The gas and liquid phase are separated from each other in the stratified flow regime, where the liquid phase is, due to gravity reasons, flowing on the bottom of the pipe and the gas phase is flowing above the liquid layer. This flow pattern occurs at low gas and liquid flow rates. Stratified flow can be further divided in stratified smooth and, at higher gas flow rates, in stratified wavy flow.[6]

3.4.4 Intermittent flow

Elongated bubble flow and slug flow are usually summarized as intermittent flow. In intermittent flow gas and liquid are flowing alternately in the pipe. On the bottom of the pipe a liquid layer is flowing, which is overrun by the liquid slugs or plugs. The slugs are separated from each other by gas pockets. The flow behavior of slug flow and bubble flow is almost the same. The difference between these two flow patterns is, that the slug body in elongated bubble flow is considered to be free of entrained gas bubbles. In contrast to the elongated bubble flow, there are gas bubbles entrained in the liquid slug body, which are concentrated at the front end of the slug. Elongated bubble flow occurs at lower gas rates, whereby slug flow occurs at higher gas rates, when the slug front is in the form of an eddy. A detailed representation of a so called slug unit can be found in Fig. 3.7 , which will be explained in detail later on.[6]

3.4.5 Slug formation mechanisms

Slug flow can be induced by several different mechanisms. The derived slug forms are hydrodynamic slugging, terrain induced slugging, operationally induced slugging and severe slugging. Although it is the purpose of this thesis to take into account hydrodynamic slug flow only, the other forms of slug flow will be described briefly as well.

3.4.5.1 Hydrodynamic slugging

With an increase in gas velocity the surface between the gas and liquid phase becomes more and more wavy and the waves start to grow until they bridge the entire cross section area of the pipe. Therefrom the above described alternating gas and liquid units emerge. The larger the pipe, the longer these hydrodynamic slugs tend to be.[9]

3.4.5.2 Terrain induced slugging

Slug flow, caused by significant elevation change of the pipeline, is called terrain induced slugging. In hilly terrain the liquid tends to accumulate at the lowest points of the pipeline. If the pressure behind this liquid plug is large enough, the liquid is forced onward through the pipe forming the so called terrain induced slugs. This form of slug is most likely at low flow rates and low pressure.[9]

3.4.5.3 Severe slugging

If there is a riser in the pipeline or a steep upward inclined pipe segment, the terrain induced slugging is called severe slugging. As it was the case in terrain induced slugging, the liquid will accumulate at the bottom of the riser and is blocking the pipe and the passage for the gas flow. The gas pressure is building up until it is high enough to push the head of liquid up the riser and through the rest of the pipe. Fig. 3.6 shows the formation mechanism of severe slugs.[9]

Gas pressure similar at both sides of liquid.

Gas pressure builds up at upstream side.

Gas reaches lowest point and blows out the liquid.

Much of the liquid and gas has escaped. The flow is reduced and some liquid falls back.
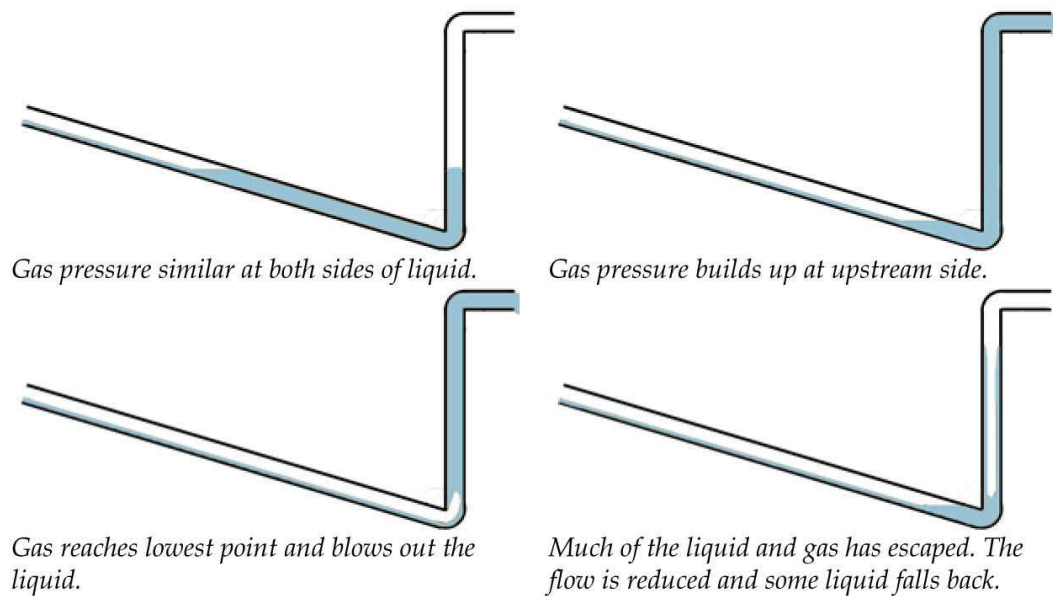
Figure 3.6: Severe slug formation.[4]

3.4.5.4 Operationally induced slugging

Several pipeline operations can initiate the formation of slugs. One possible pipeline operation is pigging. The pig, which moves through the pipe, pushes most of the liquid as a slug ahead of it. During the shut down process of a pipeline network, the liquid will accumulate at the lowest points of the pipeline. When the pipeline is restarted again, this accumulated liquid can form slugs as well. During depressurization or flow rate change the formation of slugs is possible as well.[9]

3.4.6 The unity cell concept

To get a better understanding of the slug flow pattern, it is practicable to simplify the flow by considering a single slug unit. This method of idealizing the slug flow is called the unity cell concept. This concept considers the slug flow to be a steady state phenomenon with constant average mass flow rates and stable slug length.

As is seen from Fig. 3.7 the slug unit has a total length of L_u. The unit consists of two main zones, the liquid slug body with length L_s and the stratified flow region with length L_f. When talking about the slug length it is referred to the total length of the slug L_u. The stratified or film region consists of a liquid film flowing on the bottom of the pipe and the gas pocket above it. Gas from the film region is entrained at the front end of the slug body forming the mixing zone (L_m).
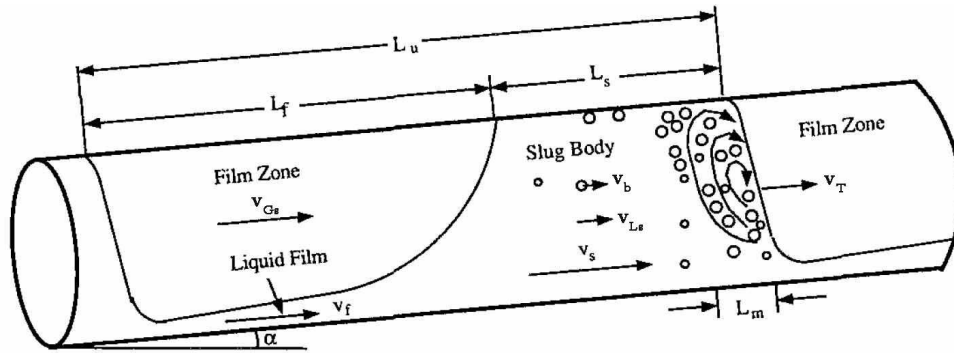
Figure 3.7: Physical model of a slug unit.[10]

As was previously described in Sec. 3.2.2 , the liquid hold up can be defined in the slug flow pattern as well. In contrast to the other flow patterns, in slug flow two liquid hold up values can be defined. First there is the overall liquid hold up of the slug unit E_L and secondly there is the slug liquid hold E_{LS}. This is the liquid hold up in the liquid slug body.

The velocity at the front of the slug v_T is called translational velocity and the velocity of the gas pocket is designated as v_{Gs}. The liquid in the film flowing below the gas pocket has the velocity v_f and the average liquid velocity is termed v_{Ls}.[11] When talking about the slug velocity it is always referred to the translational velocity. With the slug length and the slug velocity it is now possible to define the slug frequency as represented in Eq. 3.10 .

$$F_s = \frac{v_T}{L_u} \tag{3.10}$$

3.5 Vertical flow patterns

In Fig. 3.5 the flow patterns in vertical flows are presented. These patterns are designated as dispersed bubble flow, annular flow, churn flow and slug flow. As already stated, the analysis tool developed in this thesis is limited to only small deviations in the horizontal direction. However, a brief overview of flow patterns in vertical flow is necessary as well, and is provided here.

3.5.1   Dispersed bubble flow

The dispersed bubble flow pattern in vertical pipelines is similar to that in horizontal pipelines. The liquid phase is the continuous phase, in which the gas phase is dispersed as bubbles. Again the liquid and gas phase move at the same velocity, due to the high liquid flow rates.
The bubble flow pattern, which is not presented in Fig. 3.5 , looks the same as the dispersed bubble flow pattern. The only difference is, that the gas bubbles are larger than in dispersed bubble flow and that bubble flow occurs at lower flow rates. Due to the low flow rates and the sharp inclination in this flow regime, the two phases are not moving at the same velocity any more.[6]

3.5.2   Annular flow

Similar to the horizontal case the gas phase flows at a very high velocity in the core of the pipe and liquid droplets may be dispersed in this phase as well. The liquid phase is flowing as a thin layer around the pipe wall and is surrounding the gas phase. In contrast to the horizontal case the thickness of the liquid film is uniform around the pipe.[6]

3.5.3   Churn flow

The churn flow pattern is similar to the slug flow pattern. The difference is that no clear boundaries exist between the gas and the liquid phase. The churn flow pattern occurs at higher gas flow rates than the slug flow pattern, where the high gas flow rates cause the slugs to be blown through. The shape of the Taylor bubble is distorted and the so called churning occurs.[6]

3.5.4   Slug flow

In contrast to the horizontal slug flow pattern, where the gas bubble or pocket is situated on the top of the pipe, in the vertical case the bubble is almost symmetric around the pipe axis in the center of the pipe. The bubbles have almost the same size as the pipe itself and are surrounded by a thin liquid layer, which has the same thickness around the pipe. As it is the case in horizontal slug flow the gas pockets are separated from each other by the liquid slugs, whereby the thin liquid layer, surrounding the gas bubbles, is flowing downward.[6]
The above described unity cell concept is only applicable to horizontal and inclined pipelines. It cannot be used for vertical pipelines due to the different configuration of the phases.

Chapter 4

Multiphase flow prediction

A literature review is conducted to gain knowledge about different types of multiphase flow models. A summary of this literature review is presented, highlighting the most important models. With this knowledge a mechanistically based model, the Petalas and Aziz model, is selected. This model can be divided in two sections, the determination of the flow pattern and the calculation of the pressure drop and liquid hold up. Different models are compared to calculate the properties in the slug flow region such as pressure drop, liquid hold up, slug length and slug velocity. These models as well as the main model by Petalas and Aziz are presented in detail.

4.1 Flow pattern maps

Industries other than oil and gas have dealt with the simulation of flow behavior for more than a century now. During this time, a huge number of so called multiphase flow models have been developed, which are based on many different assumptions. The meaning of the term multiphase flow model depends on the degree of evolution of the model, but can generally be referred to as a composition of predicting the prevailing flow pattern and/or calculating variables like liquid hold up and pressure drop. A summary and classification of these multiphase flow models was presented by Brill and Arirachakaran [12] and further developed by Shippen and Bailey[13]. In Fig. 4.1 the models are classified on the level of physics involved in the calculation, which is presented on the vertical axis. On the horizontal axis three distinction criteria are plotted: first the year, the model was developed in and second the flow equation formulations, which are three general evolution stages of multiphase flow. Third the engineering application, which lists technical advancements in the multiphase flow models.[13]

4.1.1 Empirically based flow pattern maps

When looking on the vertical axis in Fig. 4.1 four categories are presented, starting from the single phase homogeneous category and ending at the sophisticated mechanistic models. The first multiphase flow models were considering the multiple phases as one pseudo single phase with an average velocity and average fluid properties. Further development led to empirically based models, which either considered slip between the phases and the existence of different flow patterns or not. The determination of the flow patterns was mainly practiced by visual observation. The received data were mapped on a two dimensional plot with lines representing the boundaries between the flow patterns, the so called flow pattern maps.
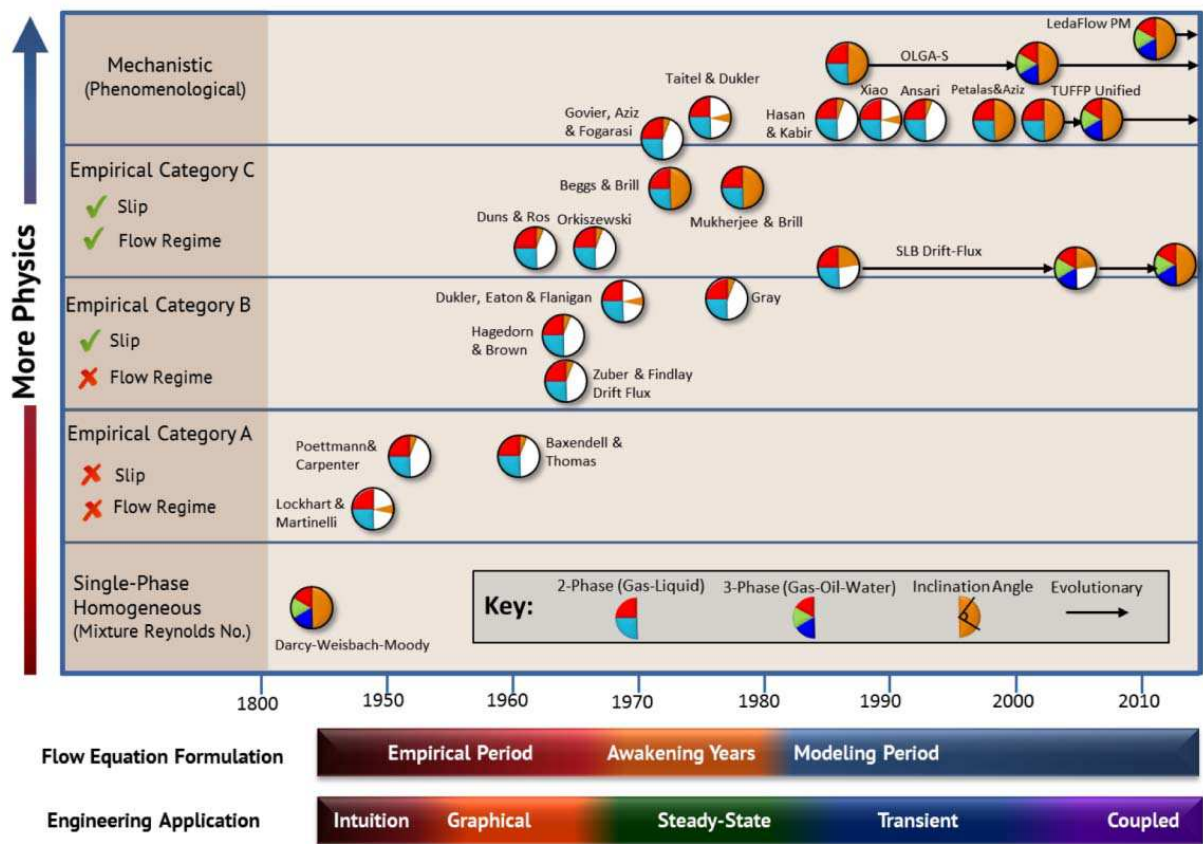
Figure 4.1: Evolution of multiphase flow models.[13]

4.1.1.1   The first models

The models by Poettman and Carpenter [14] and Baxendell and Thomas [15] were two of
the first methods for predicting the pressure drop in pipelines. These methods differ from
each other only in the correlation of friction factor, which is based on field data in both
methods. Fig. 4.2 shows the friction factor correlation developed for these methods. The
methods do not consider slip between phases or the occurrence of different flow regimes and
therefore should not be used any more.[16]
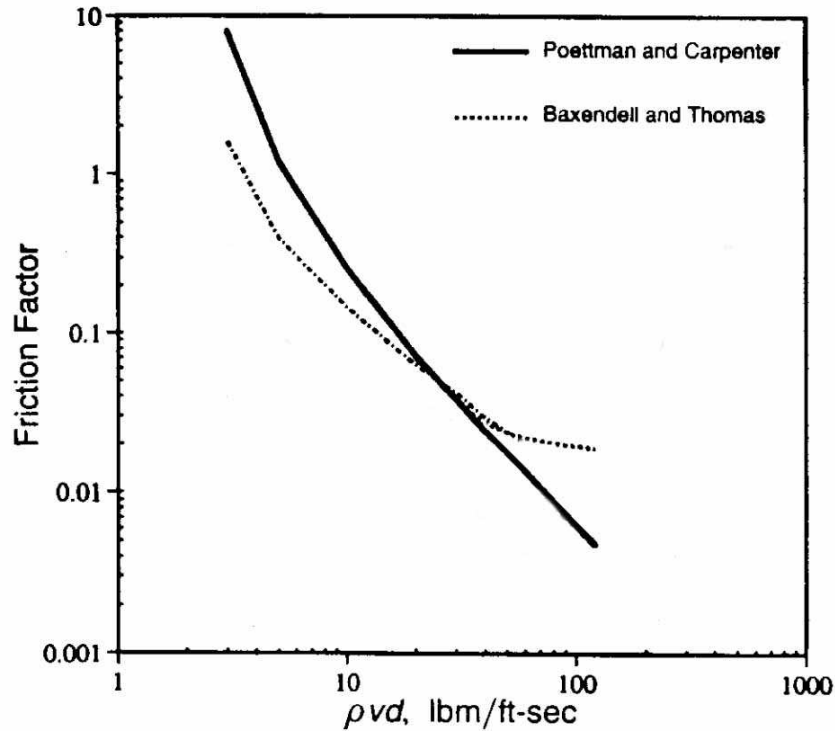
Figure 4.2: Friction factor correlations for the Poettman and Carpenter and the Baxendell
and Thomas model.[16]

4.1.1.2   The Aziz et al. model

In the 70s three of the most sophisticated empirically based models were developed. The
first, including a flow pattern map and taking slippage into account, was the model by Aziz
et al. [2], developed for vertical pipelines only. The previous models were reliable on the
conditions, under which the underlying field data were acquired only. The Aziz et al. model
therefore uses two correction factors for fluid properties, N_X and N_Y, which represent a
correction of the superficial gas and liquid velocity to extend the applicability of the model.
Fig. 4.3 shows the flow pattern map proposed by Aziz et al. for vertical flow.[16]

4.1.1.3   The Beggs and Brill model

The first method to predict flow behavior in pipes at all inclinations was the model by Beggs
and Brill [17]. Their work is based on experiments, done with an air water mixture at
varying pipe inclinations and flow conditions to observe the effect on holdup and pressure
gradient. As can be seen in the flow pattern map in Fig. 4.4 Beggs and Brill considered three

Figure 4.3: Flow pattern map after Aziz et al. for vertical pipes.[16]

flow regimes: segregated flow, intermittent flow and distributed flow. They further modified their flow pattern map to include a transition zone between segregated and intermittent flow, which is represented by the dashed lines in Fig. 4.4 . To account for various inclination angles, at first the flow regime and the matching liquid hold up is calculated, as if the pipe would be horizontal. Next a correction factor is calculated to adapt the liquid hold up to the inclination angle of the pipe and to be able to calculate the pressure d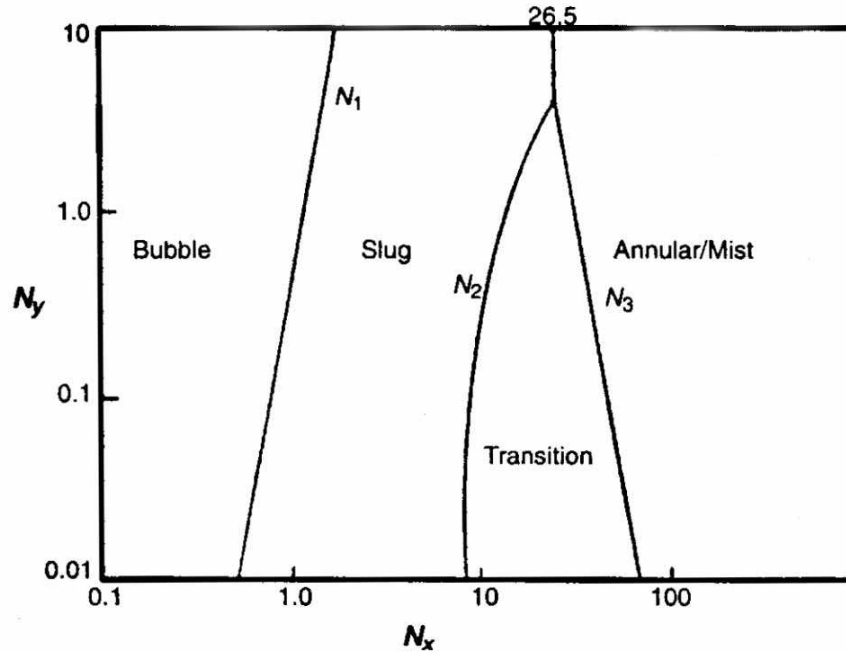rop. It has to be mentioned, that no change of the flow pattern due to the change of the inclination angle is accounted for in the Beggs and Brill model, which is why the designation of the flow patterns is only valid in horizontal pipelines.[16]

4.1.1.4 The Mandahane et al. model

An empirical model, which uses the superficial gas and liquid velocity as coordinate system is the model by Mandahane et al. [18]. Fig. 4.5 shows the flow pattern map, whereby Mandhane et al. are using a more detailed distinction between the several flow patterns. This model is based on a large database, but is only applicable to horizontal flow pipelines.[6]

4.1.2 Mechanistically based flow pattern maps

It is a disadvantage of empirically based models, that they are limited by the range of data on which they are based. Thus they cannot be used with confidence for different fluids and flow conditions, however they occur in the petroleum industry. In contrast mechanistic models are based on physical laws, which are less influenced by changing boundary conditions.[20]

4.1.2.1 The Taitel and Dukler model

Probably the first mechanistic flow model was developed by Taitel and Dukler [1]. Their model is applicable for steady state two phase flow in horizontal and slightly inclined ($\pm 10°$)
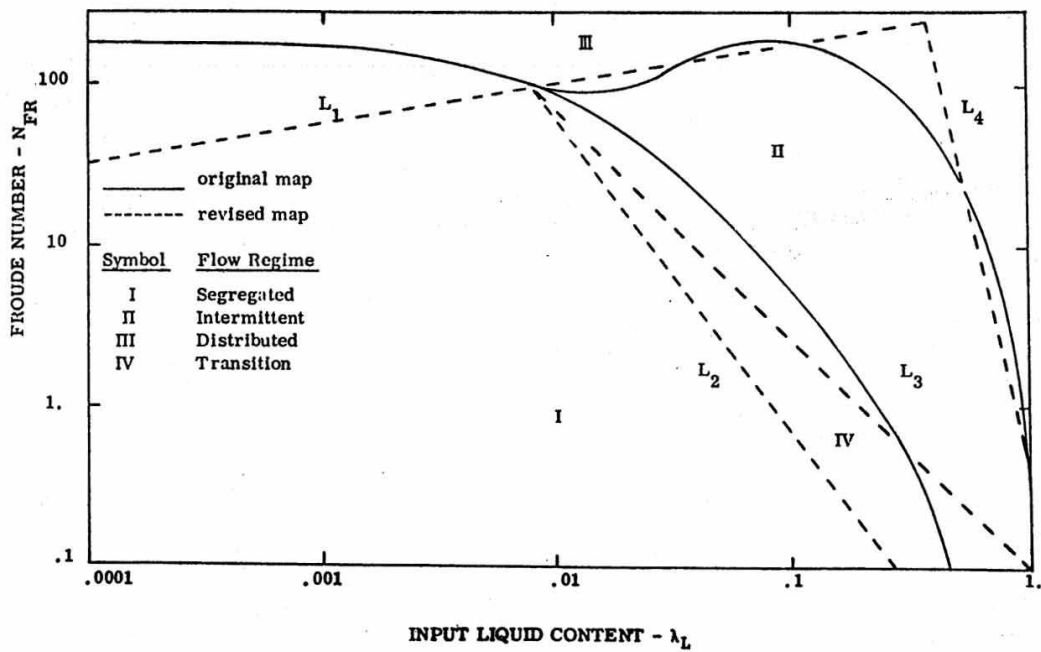
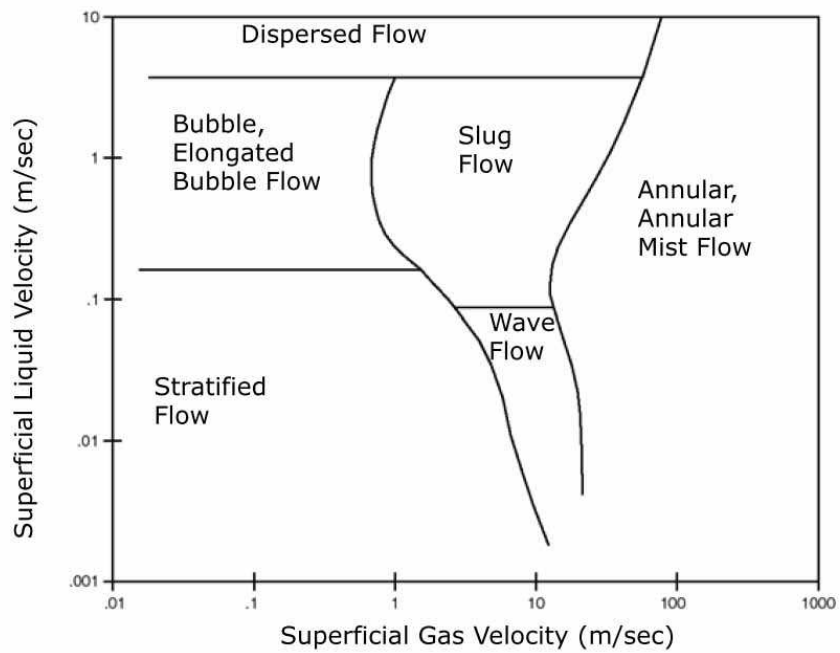Figure 4.4: Flow pattern map after Beggs and Brill for horizontal flow.[7]

Figure 4.5: Flow pattern map after Mandahane et al. for horizontal flow.[19]

pipelines. The transition criteria in the model by Taitel and Dukler are based on physical relationships rather than on pure empiricism.[4] The transition from one flow regime to the other is defined by different flow parameters in dimensionless form. As seen in Fig. 4.6 the several flow regimes are defined by transition curves. Curve A and B are defined by the coordinates F and X and curve C is defined by the coordinates K and X. Curve D is defined by the coordinates T and X.[5] For more details on the parameters and the model, please refer to the original paper by Taitel and Dukler[1].
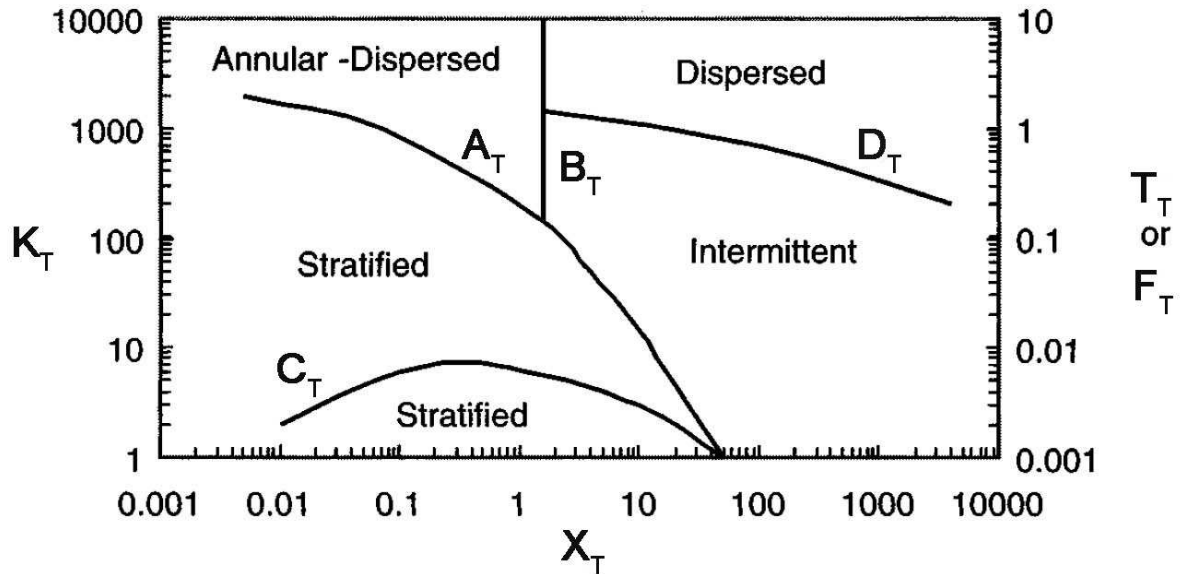
Figure 4.6: Flow pattern map after Taitel and Dukler.[1]

Taitel and Dukler were the first to develop a method for predicting the actual flow pattern, which was adopted by many authors after them. Therefore the Taitel and Dukler model can be denoted as the origin of the mechanistic models. The starting point of the flow pattern determination is the assumption that a dedicated flow pattern is stable. In the case of Taitel and Dukler they assume the stratified flow pattern to be stable. The flow variables, like the liquid level, are determined for the assumed flow pattern and a stability analysis is conducted. If the stratified flow pattern is found to be stable, this flow pattern occurs. Otherwise another flow pattern is assumed to be stable and the stability of this pattern is reviewed.[6]

4.1.2.2 The Xiao et al. model

Xiao et al. [10] developed a comprehensive mechanistic model for gas liquid two phase flow in horizontal and near horizontal pipelines. The mechanistic model first detects the prevailing flow pattern and then uses different correlations for each flow pattern to calculate liquid hold up and pressure drop in the pipeline. The flow pattern detection method is based on the model by Taitel and Dukler with some modifications. The Xiao et al. model considers four major flow pattern namely stratified flow, intermittent flow, annular flow and dispersed bubble flow.[10] Fig. 4.7 shows a typical flow pattern map by Xiao et al. for an air water pipeline. The flow regimes are separated from each other by the five lines representing the transition criteria. For a detailed description of the Xiao et al. model it is referred to the

original paper.[10] The calculation of the pressure drop and liquid hold in the slug flow pattern can be found as well in Sec. 4.4.1 .
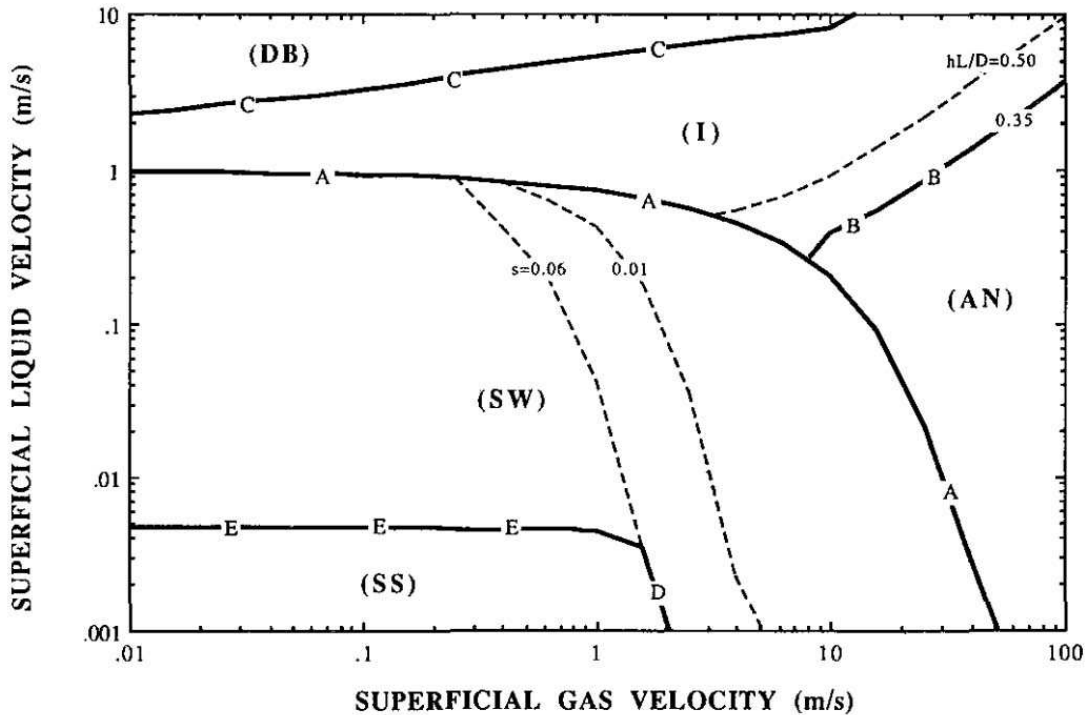
Figure 4.7: Flow pattern map after Xiao et al. ($-1°$ inclination).[10]

4.1.2.3   The Petalas and Aziz model

One of the most recent mechanistic models for multiphase flow in pipes is the model by Petalas and Aziz [20]. As the model by Xiao et al. this model is divided into a model for predicting the flow pattern and several methods for calculating the pressure drop and liquid hold up in the respective flow pattern. The big advantage of the model by Petalas and Aziz is its applicability to all pipe inclinations.[20] No further information on the model will be given here and the reader should reference Sec. 4.3 .

4.2   Model selection process

As it is the objective of the thesis to develop an analysis tool to predict the multiphase flow behavior in pipelines, a model must be selected which is capable of predicting the flow pattern and to calculate the core parameters as liquid hold up and pressure drop. At first a thorough literature review was conducted to gain knowledge about different types of multiphase flow models and to be able to compare different models among each other. In Sec. 4.1 a summary of this literature review is presented highlighting the most important models in each category.

At the beginning the usage of an easily programmable empirical model was taken into consideration. Most of these models do not consider many flow patterns and are using relatively simple calculation procedures, which could be easily programmed. As it was already mentioned, the empirically based multiphase flow models have several weaknesses. Empirical

models are developed from a limited data set, which makes them weak, if the boundary conditions differ from the original one. The first models treat the multiphase flow as a homogeneous mixture which leads to poor predictions of the flow behavior.[16] Even by further development, the empirically based models cannot overcome these weaknesses and were therefore not taken into consideration for the analysis tool any more. Thus it was decided to select a mechanistically based multiphase flow model.

Many mechanistic multiphase flow models nowadays have reached a high degree of complexity. Flow pattern determination has been investigated as well through linear stability theory in several models, which is mathematically complex and the solution process would require high computing power.[10] Due to the fact, that the analysis tool shall be coded in Excel/VBA, this computing power might not be available, which is why the balance between sufficient calculation accuracy and low calculation time must be kept in mind in the model selection process.

Finally the decision was made between two models, the Xiao et al. model [10] and the Petalas and Aziz model [20]. Both models are mainly based on the approaches made by Taitel and Dukler [1], whereas the Petalas and Aziz model is applicable to all pipeline inclinations. Although this is not required, it is seen as an advantage to the Xiao et al. model. Even if a mechanistic model is used, empiric so called closure relationships are required, for instance for friction factor correlations. Petals and Aziz have conducted numerous experiments to overcome known weaknesses of these closure relationships. They have included these results in their model and moreover have put special effort in predicting the pressure drop in the slug flow pattern.[20] For reasons mentioned above it was decided finally to choose the Petalas and Aziz model as the core model for the analysis tool.

4.3   The Petalas and Aziz model[1]

The Petalas and Aziz model [20] is one of the most recent mechanistic models for multiphase flow prediction in pipelines published in 1998. This model is based on fundamental physical laws and is applicable to all pipe inclinations. Like all mechanistic models the model after Petalas and Aziz requires several empirical closure relationships as well. In contrast to other models, Petalas and Aziz developed new closure relationships, if those available in the literature, were not satisfying. They developed new empirical correlations for the stratified, annular and intermittent flow regime. The Petalas and Aziz model is mainly based on the work by Taitel and Dukler [1] and Barnea [21]. Besides these models, parts were taken from Oliemans [22] and Taitel et al. [23] whereby this list is not intended to be exhaustive. The model can be divided in two sections: first the determination of the flow pattern and second the calculation of the pressure drop and the liquid hold up for the respective pattern.[20]

4.3.1   Flow pattern determination

When predicting the flow pattern, at first it is assumed, that a particular flow pattern is present in the pipe. Next the stability of this assumed flow pattern is reviewed by various criteria. Each criteria is formulated as an equation and can be plotted as well. Fig. 4.8 shows the flow pattern map by Petalas and Aziz where each criteria is represented by one transition line. The first flow regime, the stability of which is reviewed, is the dispersed

---

[1]The following section is based on the paper after Petals and Aziz [20]. In favor of a simple legibility a continuous citation is renounced for Sec. 4.3

bubble flow. If this regime is not stable, then the stability of the stratified flow pattern is evaluated. The total procedure for the flow pattern determination is illustrated in Fig. 4.9 .
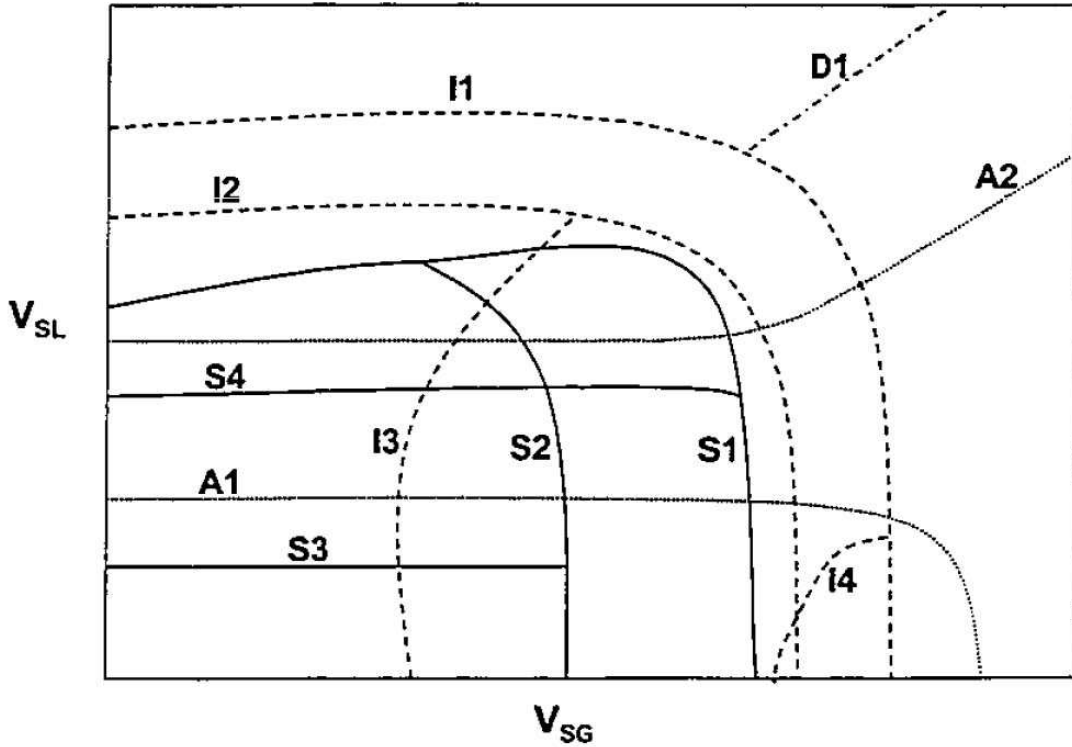
Figure 4.8: Flow pattern map after Petalas and Aziz.[20]

4.3.1.1   Dispersed bubble flow

The first boundary criterion that limits the dispersed bubble flow, is the transition between slug and dispersed bubble flow. A transition from intermittent flow to dispersed bubble flow occurs, when the slug liquid hold up E_{LS}, represented by Eq. 4.1 , is smaller than the value of the maximum volumetric packing density of the dispersed gas bubbles, which is associated with 0.52. This transition is represented by line I1 in Fig. 4.8 .

$$E_{LS} = \frac{1}{1 + \left(\frac{v_M}{8.66}\right)^{1.39}} \tag{4.1}$$

The second criterion determines the transition from dispersed bubble flow to froth flow. This transition occurs when the above mentioned packing density is exceeded (Eq. 4.2). This transition criterion is shown by line D1 in Fig. 4.8 .

$$C_G = \frac{v_{SG}}{v_M} \tag{4.2}$$

If $E_{LS} < 0.48$ and $C_G \leq 0.52$ the criteria is fulfilled and dispersed bubble flow is stable. Otherwise the stability of stratified flow is examined afterwards.
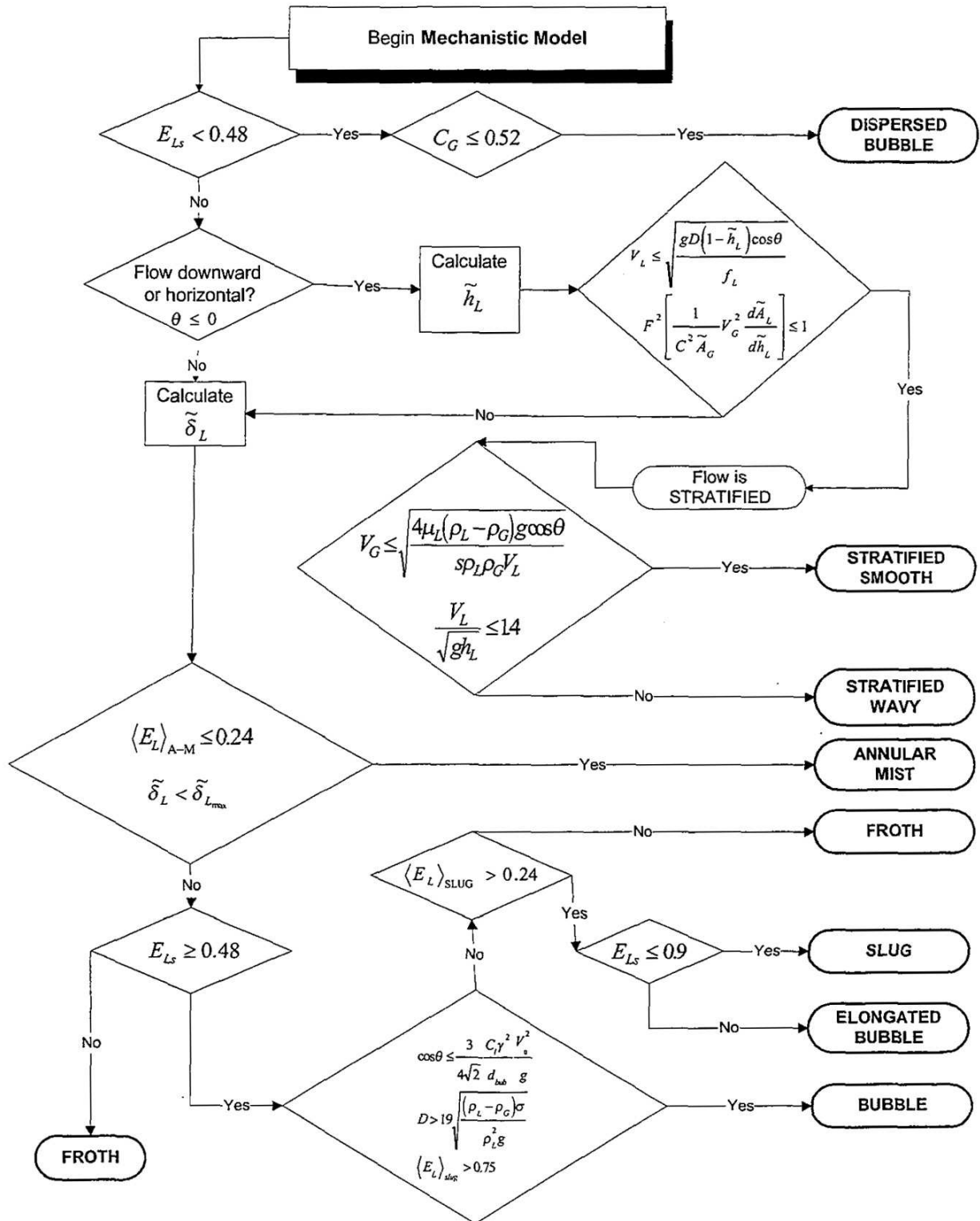
Figure 4.9: Overall flow chart for flow pattern determination.[20]

4.3.1.2   Stratified flow

In Fig. 4.10 a sketch of the stratified flow geometry can be seen, representing the core variables. A_G and A_L are the flow areas of the two phases and S_G, S_L and S_i representing the length between gas respectively liquid and the pipe wall and the length of the interface between gas and liquid. The Petalas and Aziz model limits stratified flow to horizontal and downward angles only. To check if stratified flow is stable, the liquid height h_L has to be determined which can be obtained by writing the momentum balance equations for the gas (Eq. 4.4) and the liquid (Eq. 4.3) phase.
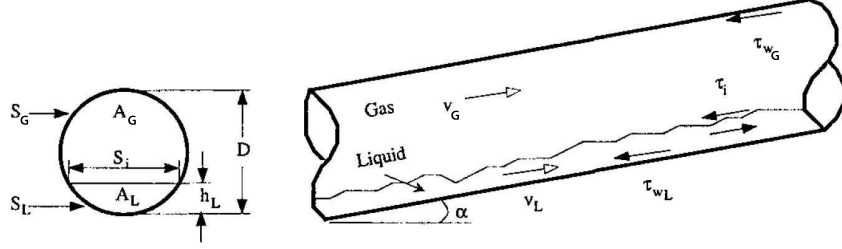
Figure 4.10: Physical model for stratified flow.[10]

$$- A_L \left(\frac{dp}{dL} \right) - \tau_{wL} S_L + \tau_i S_i - \rho_L A_L g \sin \alpha = 0 \tag{4.3}$$

$$- A_G \left(\frac{dp}{dL} \right) - \tau_{wG} S_G - \tau_i S_i - \rho_G A_G g \sin \alpha = 0 \tag{4.4}$$

By eliminating the pressure gradient the two equations can be combined and by using the geometric relationships from Eq. 4.6 to Eq. 4.12 expressed in terms of the dimensionless liquid height $\tilde{h}_L = \frac{h_L}{D}$. Eq. 4.5 represents the combined momentum balance equation before making it dimensionless.

$$\tau_{wG} \frac{S_G}{A_G} - \tau_{wL} \frac{S_L}{A_L} + \tau_i S_i \left(\frac{1}{A_L} + \frac{1}{A_G} \right) - (\rho_L - \rho_G) g \sin \alpha = 0 \tag{4.5}$$

$$\tilde{A}_L = 0,25 \left[\pi - \arccos(2\tilde{h}_L - 1) + \left(2\tilde{h}_L - 1 \right) \sqrt{1 - \left(2\tilde{h}_L - 1 \right)^2} \right] \tag{4.6}$$

$$\tilde{A}_G = 0,25 \left[\arccos(2\tilde{h}_L - 1) - \left(2\tilde{h}_L - 1 \right) \sqrt{1 - \left(2\tilde{h}_L - 1 \right)^2} \right] \tag{4.7}$$

$$\tilde{S}_L = \pi - \arccos(2\tilde{h}_L - 1) \tag{4.8}$$

$$\tilde{S}_G = \arccos(2\tilde{h}_L - 1) \tag{4.9}$$

$$\tilde{S}_i = \sqrt{1 - \left(2\tilde{h}_L - 1 \right)^2} \tag{4.10}$$

$$\tilde{v}_L = \frac{\pi}{4\tilde{A}_L} \tag{4.11}$$

$$\tilde{v}_G = \frac{\pi}{4\tilde{A}_G} \tag{4.12}$$

The shear stresses in Eq. 4.5 are given by Eq. 4.13 to Eq. 4.15 .

$$\tau_{wG} = \frac{f_G \rho_G v_G^2}{2} \tag{4.13}$$

$$\tau_{wL} = \frac{f_L \rho_L v_L^2}{2} \tag{4.14}$$

$$\tau_i = \frac{f_i \rho_G v_i |v_i|}{2} \tag{4.15}$$

The velocity in Eq. 4.15 is defined as $v_i = (v_G - v_L)$ and a new relationship for the inter facial friction factor is introduced by Petalas and Aziz (Eq. 4.16) using the Froude number represented by Eq. 4.17 .

$$f_i = \left(0.004 + 0.5 * 10^{-6} Re_{SL}\right) Fr_L^{1.335} \left(\frac{\rho_L D g}{\rho_G v_G^2}\right) \tag{4.16}$$

$$Fr_L = \frac{v_L}{\sqrt{g h_L}} \tag{4.17}$$

According to Petalas and Aziz the friction factor in Eq. 4.13 can be obtained from standard methods with the Reynolds number defined in Eq. 4.18 . The hydraulic diameter is $D_G = \frac{4A_G}{(S_G + S_i)}$.

$$Re_G = \frac{D_G \rho_G v_G}{\mu_G} \tag{4.18}$$

For laminar flow ($Re < 2000$) the Fanning friction factor equation (Eq. 4.19) is taken and for turbulent flow the Colebrook equation (Eq. 4.20) is selected.[24]

$$f = \frac{16}{Re} \tag{4.19}$$

$$\frac{1}{\sqrt{f}} = 3.48 - 4\log\left(\frac{2\epsilon}{D} + \frac{9.35}{Re\sqrt{f}}\right) \tag{4.20}$$

For the friction factor between the liquid phase and the wall (Eq. 4.14) Petalas and Aziz introduced a new empirical correlation presented in Eq. 4.21 where f_{SL} is obtained from standard methods with the Reynolds number shown in Eq. 4.22 .

$$f_L = 0.452 f_{SL}^{0.731} \tag{4.21}$$

$$Re_{SL} = \frac{D \rho_L v_{SL}}{\mu_L} \tag{4.22}$$

Now Eq. 4.5 can be solved for $\tilde{h}_L$ with an iterative procedure. The approach for this iterative solution process will be explained in Sec. 7.9 . Having determined the liquid height, the stability of the stratified flow pattern can be examined now by two criteria. At first the gas velocity v_G^*, that is sufficient causing large enough waves, that can bridge the pipe, is determined from Eq. 4.23 . In this equation if $\cos\alpha \leq 0.02$, $\cos\alpha = 0.02$ is substituted.

$$v_G^* = \left(1 - \frac{h_L}{D}\right)\sqrt{\frac{(\rho_L - \rho_G)gA_G\cos\alpha}{\rho_G\frac{dA_L}{dh_L}}} \qquad (4.23)$$

A transition from stratified flow to annular flow can occur when the liquid velocity v_L^* (Eq. 4.24) is high enough even at low gas velocities.

$$v_L^* = \sqrt{\frac{gD\left(1 - \tilde{h}_L\right)\cos\alpha}{f_L}} \qquad (4.24)$$

Stratified flow is stable if $\alpha \leq 0$, the gas velocity v_G is smaller than v_G^* and $v_L \leq v_L^*$. The transition criteria including the gas velocity is represented by transition line S1 and the one including the liquid velocity by S4 in Fig. 4.8 . Furthermore there could be made a distinction between stratified smooth and stratified wavy flow with the Petalas and Aziz model. Due to the fact, that no distinction is made in calculating the pressure drop and liquid hold up it is not included in the flow analysis tool and therefore not further explained here.

4.3.1.3   Annular flow

In Fig. 4.11 a schematic diagram of annular flow is given, where A_f and A_c are the area of flow of the liquid and the gas phase respectively. S_i is the length between liquid and gas and S_L is the length between liquid and the pipe wall. The treatment of the annular flow pattern is similar to stratified flow and starts with defining the momentum balance equations.
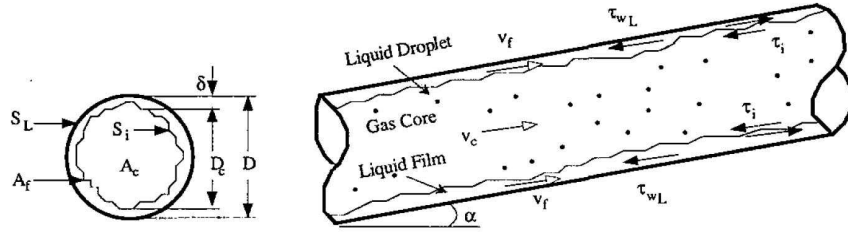
Figure 4.11: Physical model for annular flow.[10]

$$-A_f\left(\frac{dp}{dL}\right) - \tau_{wL}S_L + \tau_i S_i - \rho_L A_f g\sin\alpha = 0 \qquad (4.25)$$

$$-A_c\left(\frac{dp}{dL}\right) - \tau_i S_i - \rho_c A_c g\sin\alpha = 0 \qquad (4.26)$$

The pressure drop in Eq. 4.25 and Eq. 4.26 again can be eliminated (Eq. 4.27) and with the geometric relationships from Eq. 4.28 to Eq. 4.32 the combined momentum balance equation can be expressed as a function of the dimensionless liquid film thickness $\tilde{\delta}_L = \frac{\delta_L}{D}$ and the liquid fraction entrained FE.

$$-\tau_{wL}\frac{S_L}{A_f} + \tau_i S_i\left(\frac{1}{A_f} + \frac{1}{A_c}\right) - (\rho_L - \rho_c)g\sin\alpha = 0 \qquad (4.27)$$

$$\tilde{A}_f = \frac{\pi}{4} \left(1 - \left(1 - 2\tilde{\delta}_L \right)^2 \right) \tag{4.28}$$

$$\tilde{A}_c = \frac{\pi}{4} \left(1 - 2\tilde{\delta}_L \right)^2 \tag{4.29}$$

$$\tilde{A} = \frac{\pi}{4} \tag{4.30}$$

$$\tilde{S}_i = \pi \left(1 - 2\tilde{\delta}_L \right) \tag{4.31}$$

$$\tilde{S}_L = \pi \tag{4.32}$$

The shear stresses are given by Eq. 4.33 and Eq. 4.34 whereby the required velocities of the gas core v_c and the liquid film v_f are defined by Eq. 4.35 and Eq. 4.36 respectively.

$$\tau_{wL} = \frac{f_f \rho_L v_f^2}{2} \tag{4.33}$$

$$\tau_i = \frac{f_i \rho_c (v_c - v_f)|v_c - v_f|}{2} \tag{4.34}$$

$$v_c = \frac{v_{SG} + v_{SL}FE}{\left(1 - 2\tilde{\delta}_L \right)^2} \tag{4.35}$$

$$v_f = \frac{v_{SL}(1 - FE)}{4\tilde{\delta}_L \left(1 - \tilde{\delta}_L \right)} \tag{4.36}$$

The interfacial friction factor f_i is calculated from Eq. 4.37 . The core friction factor f_c as well as the friction factor for the liquid film f_f are calculated with Eq. 4.19 or Eq. 4.20 using the Reynolds number in the core (Eq. 4.38) and film Reynolds number (Eq. 4.39) respectively. The diameters D_c and D_f are defined as $D_c = D(1 - 2\tilde{\delta}_L)$ and $D_f = 4\tilde{\delta}_L(1 - \tilde{\delta}_L)D$.

$$\frac{f_i}{f_c} = 0.24 \left(\frac{\sigma_L}{\rho_c v_c^2 D_c} \right)^{0.085} Re_f^{0.305} \tag{4.37}$$

$$Re_c = \frac{\rho_c v_c D_c}{\mu_c} \tag{4.38}$$

$$Re_f = \frac{\rho_L v_f D_f}{\mu_L} \tag{4.39}$$

The values not defined so far, are the liquid fraction entrained FE and the values in the core with the subscripts c. With Eq. 4.40 the liquid fraction entrained is defined by Eq. 4.41 .

$$N_B = \frac{\rho_G v_{SG}^2 \mu_L^2}{\sigma_L^2 \rho_L} \tag{4.40}$$

$$\frac{FE}{1 - FE} = 0.735 N_B^{0.074} \left(\frac{v_{SG}}{v_{SL}} \right)^{0.2} \tag{4.41}$$

The liquid hold up in the gas core E_c which is related to the liquid fraction entrained can be calculated from Eq. 4.42 . The core density and the core viscosity respectively are defined by Eq. 4.43 and Eq. 4.44 .

$$E_c = \frac{v_{SL}FE}{v_{SG} + v_{SL}FE} \tag{4.42}$$

$$\rho_c = E_c\rho_L + (1 - E_c)\rho_G \tag{4.43}$$

$$\mu_c = E_c\mu_L + (1 - E_c)\mu_G \tag{4.44}$$

$\tilde{\delta}_L$ can be examined with an iterative procedure again. The transition from annular to intermittent flow is based on the observation, that the minimum interfacial shear stress causes a change in the velocity profile and an instability of the annular flow pattern. This minimum shear stress condition is obtained from Eq. 4.45 .

$$2f_f\frac{\rho_L}{\rho_L - \rho_c}\frac{v_{SL}^2(1 - FE)^2}{gD\sin\alpha} - \frac{E_f^3\left(1 - \frac{3}{2}E_f\right)}{2 - \frac{3}{2}E_f} = 0 \tag{4.45}$$

With Eq. 4.46 the minimum film height, at which the minimum shear stress occurs can be determined using an iterative procedure. The transition from annular to intermittent flow is shown by line A1 in Fig. 4.8 .

$$E_f = 4\tilde{\delta}_{L_{min}}(1 - \tilde{\delta}_{L_{min}}) \tag{4.46}$$

The second transition mechanism from annular flow occurs at high liquid flow rates, when the liquid film can become large enough to bridge the pipe. This is said to happen, when the liquid hold up E_L exceeds one half of the value of the volumetric packing density of a gas bubble, which is 0.52. Line A2 in Fig. 4.8 shows this criterion. The determination of the liquid hold up in the annular flow pattern is explained in Sec. 4.3.2.3 . If both criteria are fulfilled namely $\tilde{\delta}_L < \tilde{\delta}_{L_{min}}$ and $E_L \leq 0.24$ annular flow is stable. Otherwise bubble flow is examined next.

4.3.1.4   Bubble flow

Bubble flow can exist if the pipe diameter is large enough that the Taylor bubble velocity exceeds the bubble velocity. The critical pipe diameter is calculated from Eq. 4.47 .

$$D^* = 19\left(\frac{(\rho_L - \rho_G)\sigma_L}{\rho_L^2 g}\right)^{\frac{1}{2}} \tag{4.47}$$

The second limiting case for bubble flow is the angle of inclination. It must be large enough to prevent migration of bubbles to the top wall of the pipe. The critical value is determined from Eq. 4.48 .

$$X = \frac{3v_b^2}{4\sqrt{2}}\left(\frac{C_l\gamma^2}{gD_b}\right) \tag{4.48}$$

Several constants are defined by Petalas and Aziz namely the lift coefficient $C_l = 0.8$, the bubble distortion coefficient $\gamma = 1.3$ and the bubble diameter $D_b = 7$. The bubble swarm rise velocity can be determined from Eq. 4.49 .

$$v_b = 1.41 \left(\frac{g(\rho_L - \rho_G)\sigma_L}{\rho_L^2} \right)^{\frac{1}{4}} \sin \alpha \tag{4.49}$$

A transition from intermittent flow to bubble flow occurs, when the gas void fraction in slug flow drops below the critical value of 0.25, which is represented by line I3 in Fig. 4.8 . The determination of the liquid hold up in the slug flow regime can be found in Sec. 4.3.1.5 . If the pipe diameter D is greater than D^*, $\cos \alpha \le X$ and $E_L > 0.75$ bubble flow is stable. Otherwise intermittent flow is examined next.

4.3.1.5   Intermittent flow

Slug flow and elongated bubble flow are classified as intermittent flow patterns. In Fig. 3.7 the physical model of a slug unit is presented. A transition from slug flow occurs when there is not sufficient liquid for slug formation available. The liquid hold up needed to determine the stability of slug flow is calculated from Eq. 4.50 , which is derived from an overall mass balance over a slug-bubble unit.

$$E_L = \frac{E_{LS}v_T + v_{Gdb}(1 - E_{LS}) - v_{SG}}{v_T} \tag{4.50}$$

The liquid hold up in the slug body is calculated from Eq. 4.1 . The translational velocity of the elongated bubble v_T is calculated from Eq. 4.51 , where the distribution coefficient C_0 is taken from an empirical equation introduced by Petalas and Aziz (Eq. 4.52). The modified Reynolds number in Eq. 4.52 is defined by Eq. 4.53 .

$$v_T = C_0 v_M + v_d \tag{4.51}$$

$$C_0 = (1.64 + 0.12 \sin \alpha) Re_{ML}^{-0.031} \tag{4.52}$$

$$Re_{ML} = \frac{\rho_L v_M D}{\mu_L} \tag{4.53}$$

v_d is the elongated bubble drift velocity which is determined by Eq. 4.54 . In this equation the friction factor for $f_M < 1$ is $f_M = 0.316\sqrt{Re_\infty}$ and otherwise is set to 1. The Reynolds number is defined by Eq. 4.55 .

$$v_d = f_M v_{d\infty} \tag{4.54}$$

$$Re_\infty = \frac{\rho_L v_{d\infty} D}{2\mu_L} \tag{4.55}$$

The elongated bubble drift velocity at high Reynolds numbers $v_{d\infty}$, is given by Eq. 4.56 . The drift velocity of the bubbles in a horizontal system is given by Eq. 4.57 with the Bond number defined by Eq. 4.58 .

$$v_{d\infty} = v_{dh\infty} \cos \alpha + v_{dv\infty} \sin \alpha \tag{4.56}$$

$$v_{dh\infty} = \left(0.54 - \frac{1.76}{Bo^{0.56}} \right) \sqrt{\frac{gD(\rho_L - \rho_G)}{\rho_L}} \tag{4.57}$$

$$Bo = \frac{(\rho_L - \rho_G)}{\sigma_L} gD^2 \tag{4.58}$$

For a vertical system the elongated bubble drift velocity is given by Eq. 4.59 and the coefficient β can be calculated from Eq. 4.60 .

$$v_{dv\infty} = 0.345 \left(1 - e^{-\beta}\right) \sqrt{\frac{gD(\rho_L - \rho_G)}{\rho_L}} \tag{4.59}$$

$$\beta = Boe^{(3.278 - 1.424 \ln Bo)} \tag{4.60}$$

The last parameter, which has to be defined, is the velocity of the dispersed bubbles in the liquid slug v_{Gdb} (Eq. 4.61). C_0 again is calculated from Eq. 4.52 and the rise velocity of the dispersed bubbles is determined by Eq. 4.62 . In certain situations v_{Gdb} can become negative. In case of these situations v_{Gdb} is then set to 0. The liquid hold up can now be calculated from Eq. 4.50 . If E_L becomes greater than 1, it is set to C_L (Eq. 4.63).

$$v_{Gdb} = C_0 v_M + v_b \tag{4.61}$$

$$v_b = 1.53 \left(\frac{g(\rho_L - \rho_G)\sigma_L}{\rho_L^2}\right)^{\frac{1}{4}} \sin \alpha \tag{4.62}$$

$$C_L = \frac{v_{SL}}{v_M} \tag{4.63}$$

Intermittent flow is stable if $E_L > 0.24$. If the liquid hold up in the slug body E_{LS} is greater than 0.90, elongated bubble flow exists, otherwise the flow pattern is slug flow. If none of the flow pattern discussed so far is stable, the flow regime is designated froth flow, which is a transitional state between the other flow patterns.

4.3.2   Calculation of pressure drop and liquid hold up

After having determined the flow pattern the next step is to calculate the pressure drop and the liquid hold up, which are dependent on the present flow pattern.

4.3.2.1   Dispersed bubble flow

For dispersed bubble flow the liquid hold up is calculated from Eq. 4.64 , whereby v_{Gdb} is taken from Eq. 4.61 . The distribution coefficient C_0 and the rise velocity of the dispersed bubbles in the liquid slug v_b is determined as it was done in slug flow and can therefore be taken from Eq. 4.52 and Eq. 4.62 respectively. If $v_{Gdb} \leq 0$ the liquid hold up is obtained from Eq. 4.65 .

$$E_L = 1 - \frac{v_{SG}}{v_{Gdb}} \tag{4.64}$$

$$E_L = 1 - \frac{v_{SG}}{C_0 v_M} \tag{4.65}$$

If the value of E_L, calculated by one of the two equations, is greater than 1, E_L is set equal to C_L (Eq. 4.63).

The pressure gradient for dispersed bubble flow is calculated from Eq. 4.66 . The friction factor is determined again by standard methods with the Reynolds Number in Eq. 4.67 .

$$-\left(\frac{dp}{dL}\right) = \frac{2f_M v_M^2 \rho_M}{D} + \rho_M g \sin\alpha \tag{4.66}$$

$$Re_M = \frac{D\rho_M v_M}{\mu_M} \tag{4.67}$$

The mixture values, needed in Eq. 4.66 and Eq. 4.67 , can be determined with the liquid hold up from Eq. 4.68 and Eq. 4.69 respectively.

$$\rho_M = E_L \rho_L + (1 - E_L)\rho_G \tag{4.68}$$

$$\mu_M = E_L \mu_L + (1 - E_L)\mu_G \tag{4.69}$$

4.3.2.2   Stratified flow

The liquid hold up for stratified flow is derived from geometric considerations by Eq. 4.70 . The pressure drop can be calculated either from Eq. 4.3 or Eq. 4.4 .

$$E_L = \frac{A_L}{A} \tag{4.70}$$

4.3.2.3   Annular flow

The liquid hold up in annular flow is derived from geometric considerations as well. When the liquid film thickness is known the liquid hold up is calculated from Eq. 4.71 . The pressure drop is calculated from Eq. 4.25 or Eq. 4.26 .

$$E_L = 1 - \left(1 - 2\tilde{\delta}_L\right)^2 \frac{v_{SG}}{v_{SG} + FE v_{SL}} \tag{4.71}$$

4.3.2.4   Bubble flow

The gas void fraction is defined by Eq. 4.72 . The translational bubble velocity is calculated by Eq. 4.73 , whereby C_0 is set to 1.2 in this case. v_b is calculated from Eq. 4.62 and the gas void fraction is limited between $0 \leq E_G \leq C_G = \frac{v_{SG}}{v_M}$. The liquid hold up is calculated straight forward as $E_L = 1 - E_G$.

$$E_G = \frac{v_{SG}}{v_T} \tag{4.72}$$

$$v_T = C_0 v_M + v_b \tag{4.73}$$

The pressure gradient for bubble flow is given by Eq. 4.74 and the friction factor f_{ML} is obtained from standard methods with the Reynolds number $Re = \frac{D\rho_M v_M}{\mu_M}$.

$$-\left(\frac{dp}{dL}\right) = \frac{2f_{ML} v_M^2 \rho_M}{D} + \rho_M g \sin\alpha \tag{4.74}$$

4.3.2.5   Intermittent flow

There is not a distiction made between the intermittent flow regimes of slug flow and elongated bubble flow when calculating the pressure drop and the liquid hold up. The calculation process for the liquid hold up has already been outlined in Sec. 4.3.1.5 . The pressure drop in intermittent flow could be calculated by writing the momentum balance over a slug-bubble unit as it was done by many authors before Petalas and Aziz. Petalas and Aziz however stated, that there are no reliable methods for calculating the slug length L_s or the film length L_f. Thus they introduced the weighting factor η, which is related to $\frac{L_s}{L_u}$ and is calculated from Eq. 4.75 on the condition that $\eta \leq 1$.

$$\eta = C_L^{(0.75-E_L)} \tag{4.75}$$

The pressure drop defined by Petalas and Aziz is outlined by Eq. 4.76 . In this equation the frictional pressure gradient for the slug portion is obtained from Eq. 4.77 .

$$-\left(\frac{dp}{dL}\right) = \rho_M g \sin\alpha + \eta \left(\frac{dp}{dL}\right)_{fr_{SL}} + (1-\eta)\left(\frac{dp}{dL}\right)_{fr_{AM}} \tag{4.76}$$

$$\left(\frac{dp}{dL}\right)_{fr_{SL}} = \frac{2f_{ML}v_M^2\rho_M}{D} \tag{4.77}$$

The friction factor in Eq. 4.77 is calculated from either Eq. 4.19 or Eq. 4.20 with the Reynolds number used for bubble flow. To determine the frictional pressure gradient based on annular flow (Eq. 4.78) the shear stress is defined as it was done in the annular flow pattern (Eq. 4.79).

$$\left(\frac{dp}{dL}\right)_{fr_{AM}} = \frac{4\tau_{wL}}{D} \tag{4.78}$$

$$\tau_{wL} = \frac{f_f\rho_L v_f^2}{2} \tag{4.79}$$

The film velocity is calculated as in annular flow by Eq. 4.36 where the liquid film height is defined by Eq. 4.80 . The liquid fraction entrained FE is calculated from Eq. 4.41 with the dimensionless number NB defined by Eq. 4.40 .

$$\tilde{\delta}_L = \frac{1}{2}\left(1 - \sqrt{(1-E_L)\frac{FEv_{SL}+v_{SG}}{v_{SG}}}\right) \tag{4.80}$$

When the liquid film height is less than $1*10^{-4}$ the frictional pressure gradient based on annular flow is not calculated from Eq. 4.78 but from Eq. 4.81 . f_M is calculated from standard methods with the Reynolds number used in dispersed bubble flow.

$$\left(\frac{dp}{dL}\right)_{fr_{AM}} = \frac{2f_M v_M^2\rho_M}{D} \tag{4.81}$$

4.3.2.6   Froth flow

Petalas and Aziz assume that froth flow is a transition zone between dispersed bubble flow and annular flow and between slug flow and annular flow. To calculate values for the liquid hold up and the pressure drop it is thus proposed to interpolate between the appropriate

boundary regimes. This process would involve a number of iteration procedures and thereby increasing the computation time. Therefore it is not included in the analysis tool. If froth flow is the present flow pattern, the liquid hold up and the pressure drop are calculated as if intermittent flow would occur. This approach is supported by the fact, that other authors like Xiao et al. [10] do not include the froth flow pattern at all, but include this region in the intermittent flow regime as well.

4.4   Model comparison in the slug flow pattern

The most common flow pattern in multiphase flow pipelines and, at the same time, the one which can cause the most problems for downstream equipment, is the slug flow pattern. This is the reason, why it was one task to put special attention in predicting the pressure drop and liquid hold up in this flow pattern. Moreover, methods to calculate the slug length and the slug velocity should be compared.

In the following section the methods, which are selected for comparison are summarized. It should be stated here, that although different models might be used in the slug flow region, the basic model still is the model by Petalas and Aziz. The flow pattern determination for all flow regimes as well as the pressure drop and liquid hold up calculation procedures for the other flow patterns is not effected by the utilization of a different model in the slug flow pattern.

4.4.1   The Xiao et al. model

To calculate the pressure drop and the liquid hold up in slug flow, a second model is chosen, the model by Xiao et al. [10]. The core equation for calculating the liquid hold up is the same as used by Petalas and Aziz (Eq. 4.50), while slightly different methods are used to calculate the translational velocity (Eq. 4.82) and the velocity of the dispersed bubbles in the liquid slug (Eq. 4.83).

$$v_T = C_0 v_M + 0.35\sqrt{gD}\sin\alpha + 0.54\sqrt{gD}\cos\alpha \tag{4.82}$$

$$v_{Gdb} = 1.2 v_M + 1.53 \left(\frac{\sigma_L g(\rho_L - \rho_G)}{\rho_L^2}\right)^{\frac{1}{4}} E_{LS}^{0.1}\sin\alpha \tag{4.83}$$

The variable C_0 in Eq. 4.82 takes the value 1.2 for turbulent flow and 2 for laminar flow. E_{LS} is calculated by Eq. 4.1 . Contrary to Petals and Aziz, Xiao et al. are writing a force balance over a slug unit to calculate the pressure drop in the slug flow regime (Eq. 4.84).[10]

$$-\left(\frac{dp}{dL}\right) = \rho_M g\sin\alpha + \frac{1}{L_u}\left[\left(\frac{\tau_S\pi D L_s}{A}\right) + \left(\frac{(\tau_{wf}S_f + \tau_{wG}S_G)L_f}{A}\right)\right] \tag{4.84}$$

To determine the slug unit length (Eq. 4.85) the liquid hold up in the film region E_f has to be calculated from Eq. 4.86 using Eq. 4.87 .[10]

$$L_u = L_s\frac{v_{Ls}E_{LS} - v_f E_f}{v_{SL} - v_f E_f} \tag{4.85}$$

$$E_f = \frac{\theta - \sin\theta}{2\pi} \tag{4.86}$$

$$\theta = 2\arccos\left(1 - 2\tilde{h}_f\right) \tag{4.87}$$

As one can see in Eq. 4.87 the dimensionless liquid height has to be calculated as was done in stratified flow. Xiao et al. are therefore using a similar approach to Petalas and Aziz. At first the combined momentum balance equation for the film region is written (Eq. 4.88).[10]

$$\tau_{wG}\frac{S_G}{A_G} - \tau_{wf}\frac{S_f}{A_f} + \tau_i S_i\left(\frac{1}{A_f} + \frac{1}{A_G}\right) - (\rho_L - \rho_G)g\sin\alpha = 0 \tag{4.88}$$

The shear stresses can be calculated by Eq. 4.89 to Eq. 4.91 . The friction factor f_i takes a constant value $f_i = 0.0142$ and the values for f_f and f_G are calculated from Eq. 4.19 or Eq. 4.20 using the Reynolds number Eq. 4.92 and Eq. 4.93 respectively. The hydraulic diameters are $D_L = \frac{4A_L}{S_L}$ and $D_G = \frac{4A_G}{(S_G+S_i)}$.[10]

$$\tau_{wf} = \frac{f_f\rho_L|v_f|v_f}{2} \tag{4.89}$$

$$\tau_{wG} = \frac{f_G\rho_G|v_{Gs}|v_{Gs}}{2} \tag{4.90}$$

$$\tau_i = \frac{f_i\rho_G|v_{Gs} - v_f|(v_{Gs} - v_f)}{2} \tag{4.91}$$

$$Re_f = \frac{\rho_L v_f D_L}{\mu_L} \tag{4.92}$$

$$Re_G = \frac{\rho_G v_{Gs} D_G}{\mu_G} \tag{4.93}$$

The liquid velocity in the slug body v_{Ls}, the liquid velocity in the film region v_f and the gas velocity in the film region v_{Gs} are defined by Eq. 4.94 to Eq. 4.96 .[10]

$$v_{Ls} = \frac{v_M - v_{Gdb}(1 - E_{LS})}{E_{LS}} \tag{4.94}$$

$$v_f = v_T - \frac{(v_T - v_{Ls})E_{LS}}{E_f} \tag{4.95}$$

$$v_{Gs} = \frac{v_M - v_f E_f}{1 - E_f} \tag{4.96}$$

With the geometric relations in Eq. 4.97 to Eq. 4.101 the combined momentum balance equation can be solved for $\tilde{h}_f$ with an iterative procedure.[10]

$$\tilde{A}_f = 0.25\left[\pi - \arccos(2\tilde{h}_f - 1) + \left(2\tilde{h}_f - 1\right)\sqrt{1 - \left(2\tilde{h}_f - 1\right)^2}\right] \tag{4.97}$$

$$\tilde{A}_G = 0.25\left[\arccos(2\tilde{h}_f - 1) - \left(2\tilde{h}_f - 1\right)\sqrt{1 - \left(2\tilde{h}_f - 1\right)^2}\right] \tag{4.98}$$

$$\tilde{S}_f = \pi - \arccos(2\tilde{h}_f - 1) \tag{4.99}$$

$$\tilde{S}_G = \arccos(2\tilde{h}_f - 1) \tag{4.100}$$

$$\tilde{S}_i = \sqrt{1 - \left(2\tilde{h}_f - 1\right)^2} \tag{4.101}$$

Now the slug unit length can be determined from Eq. 4.85 by using the empirical correlation for the slug length presented in Eq. 4.102 when $D \geq 0.0381\,\mathrm{mm}$ or $L_s = 30D$ when $D < 0.0381\,\mathrm{mm}$.[10]

$$\ln L_s = -26.6 + 28.5(\ln D + 3.67)^{0.1} \tag{4.102}$$

The last term that has to be determined before the pressure drop can be calculated is the shear stress in the slug body τ_s (Eq. 4.103). The friction factor f_s is obtained from standard methods with $Re_s = \frac{\rho_s v_M D}{\mu_s}$ and the values with the subscript s are calculated from Eq. 4.104 and Eq. 4.105 .[10]

$$\tau_s = \frac{f_s \rho_s v_M^2}{2} \tag{4.103}$$

$$\rho_s = E_{LS}\rho_L + (1 - E_{LS})\rho_G \tag{4.104}$$

$$\mu_s = E_{LS}\mu_L + (1 - E_{LS})\mu_G \tag{4.105}$$

4.4.2   Slug translational velocity

The methods to calculate the translational slug velocity are similar in both models to Petalas and Aziz (Eq. 4.51) and Xiao et al.(Eq. 4.82). A third model to determine this velocity by Bendiksen [25] is compared with those, which were originally used in Petalas and Aziz and Xiao et al. . The translational velocity is calculated by Eq. 4.106 , where C_0 is determined by Eq. 4.107 and U_0 by Eq. 4.108 . Both are dependent on the Froude number $Fr_M = \frac{v_M}{\sqrt{gD}}$.

$$v_T = C_0 v_M + U_0 \tag{4.106}$$

$$C_0 = \begin{cases} 1.05 + 0.15\sin\alpha^2 & Fr_M \leq 3.5 \\ 1.2 & Fr_M > 3.5 \end{cases} \tag{4.107}$$

$$U_0 = \begin{cases} (0.35\sin\alpha + 0.54\cos\alpha)\sqrt{gD} & Fr_M \leq 3.5 \\ 0.35\sqrt{gD}\sin\alpha & Fr_M > 3.5 \end{cases} \tag{4.108}$$

4.4.3   Liquid hold up

The determination of the liquid hold up E_L in the slug flow pattern by Petalas and Aziz and Xiao et al. is derived from the same equation. A second method for calculating the liquid hold up is introduced by Cook and Behnia [26]. The velocities in Eq. 4.109 are already defined in the previous sections.

$$E_L = \frac{v_{SL} + E_{LS}v_T - E_{LS}v_M}{v_T} \tag{4.109}$$

4.4.4   Slug length

It is a difficult task to predict the average slug length in a pipeline and only empirical models exist. Different models can predict highly different values for the average slug length, which is why they in fact cannot be compared and careful usage of the received values is recommended. The three most used empirical correlations are presented. The first equation (Eq. 4.110) by Brill et al. [27] correlates the mean slug length to the pipe diameter and the mixture velocity. Eq. 4.111 is a modification of the correlation by Brill et al. made by Norris [28], which excludes the mixture velocity. The last correlation by Scott et al. [29] modifies the correlation by Norris. D is given in inch and L_s is given in feet in the following empirical equations.

$$\ln L_s = -2.663 + 5.441(\ln D)^{0.5} + 0.059(\ln v_M) \tag{4.110}$$

$$\ln L_s = -2.099 + 4.859(\ln D)^{0.5} \tag{4.111}$$

$$\ln L_s = -25.4144 + 28.4948(\ln D)^{0.1} \tag{4.112}$$

Chapter 5

Multiphase flow heat exchange

During the transportation of the multiphase flow mixture from the production well to the downstream equipment, the temperature of the fluids in the pipeline changes depending on the surrounding. The heat transfer between the fluids and the pipe surrounding, followed by a temperature change of the fluids in the pipeline, is an important matter with regard to the determination of the fluid properties. By changing temperatures the viscosity can alter and the density is affected significantly.[30]

Heat flow in single phase flow pipelines is well studied and many correlations are available to calculate the heat loss by determining the heat transfer coefficients for the fluid, the pipe wall and the surrounding. In a multiphase flow pipeline the correlations to estimate the heat transfer coefficients are not as straight forward as they have been in single phase flow and are also less reliable.[4]

5.1 Overall heat balance

To calculate the heat loss in a pipeline the total heat balance is applied. Fig. 5.1 is a schematic representation of an inclined pipeline with the temperature and enthalpy values at the entrance $(\dot{H}_i, T_i)$ and at the end of the pipeline $(\dot{H}_{i+1}, T_{i+1})$. $\dot{Q}$ is the heat flow between the multiphase fluid mixture and the surrounding. The overall heat balance can be written as shown in Eq. 5.1 .

$$\dot{H}_i + \dot{Q} = \dot{H}_{i+1} \tag{5.1}$$

The enthalpy flows in Eq. 5.1 can be calculated with the procedure shown in Sec. 6.3.21 . To determine the heat flow $\dot{Q}$ the total heat transfer coefficient α_{tot} must be calculated first. From Eq. 5.2 the heat flow can then be calculated with the ambient fluid temperature T_o and the average fluid temperature T.

$$\dot{Q} = \alpha_{tot}\pi(T - T_o)L \tag{5.2}$$

5.2 Heat transfer coefficients

The total heat transfer coefficient is a combination of the heat transfer coefficients of each layer. In case of an overground pipeline there are three layers with three heat transfer coefficients. One heat transfer coefficient between fluid and pipe wall (U_i), one for the pipe wall and one convective heat transfer coefficient (U_o) for the air surrounding the pipeline
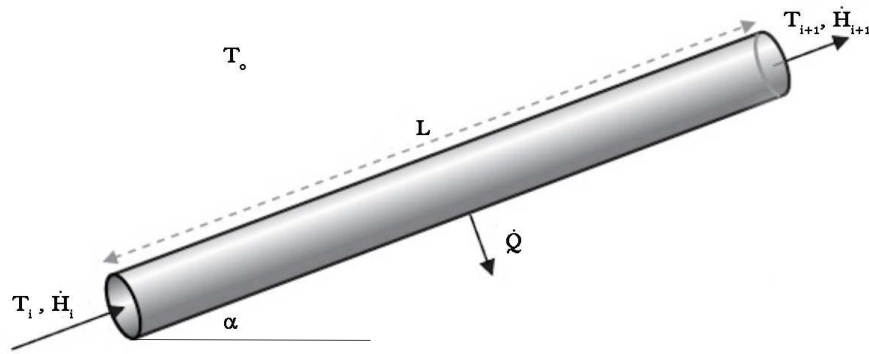
Figure 5.1: Heat balance over a pipeline segment.

have to be calculated. Fig. 5.2 shows a schematic of these layers.[30] The heat transfer coefficients for the pipe wall and for the surroundings can be calculated in a straight forward manner. Unfortunately the heat transfer coefficient for the multiphase mixture is influenced by numerous parameters such as the flow pattern, the liquid hold up and the inclination angle of the pipeline.

In the literature many correlations can be found in order to predict the heat transfer coefficient in multiphase flow pipelines at all inclinations and for all flow patterns. A comprehensive literature review was conducted by Kim et al. [31] identifying two phase flow heat transfer correlations available in the literature. A general two phase heat transfer correlation for all pipeline inclinations and flow patterns is presented by Ghajar and Kim [32] and Kim and Ghajar [33] and will be explained in Sec. 5.2.1 . The total heat transfer coefficient can then be calculated from Eq. 5.3 .[34]
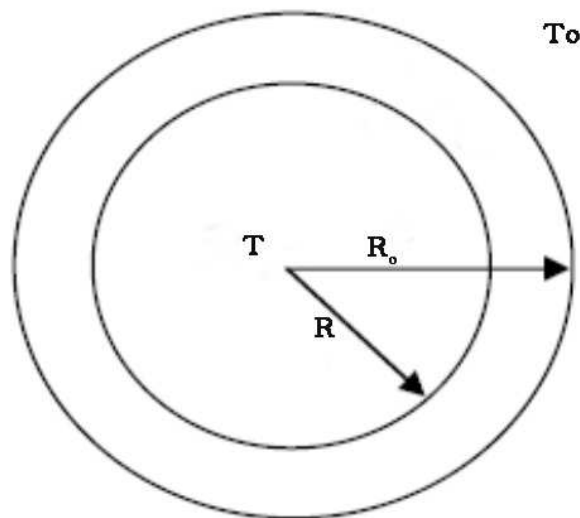

Figure 5.2: Schematic picture of the pipeline layers.

$$\alpha_{tot} = \frac{1}{\frac{1}{\frac{DU_i}{2}} + \frac{\ln\left(\frac{D_o}{D}\right)}{k_{pipe}} + \frac{1}{\frac{D_oU_o}{2}}} \tag{5.3}$$

5.2.1   Heat transfer coefficient between fluid and pipe wall

In Eq. 5.4 the heat transfer coefficient for two phase flow in pipelines is presented. U_L is representing the single phase heat transfer coefficient. Several correlations this coefficient could be calculated with are available in the literature, however the correlation after Sieder and Tate [35] is recommended.[34] The heat transfer coefficient by Sieder and Tate is given by Eq. 5.5 .

$$U_i = F_P U_L \left[1 + C \left(\frac{x}{1-x}\right)^m \left(\frac{1-F_P}{F_P}\right)^n \left(\frac{Pr_G}{Pr_L}\right)^p \left(\frac{\mu_L}{\mu_G}\right)^q (I^*)^r \right] \tag{5.4}$$

$$U_L = 0.027 Re_L^{\frac{4}{5}} Pr_L^{\frac{1}{3}} \left(\frac{k_L}{D}\right) \left(\frac{\mu_L}{\mu_{LW}}\right)^{0.14} \tag{5.5}$$

The insitu Reynolds number is calculated from Eq. 5.6 and the Prandtl number for the gas and the liquid phase can be calculated from Eq. 5.7 and Eq. 5.8 respectively.[34]

$$Re_L = \frac{4\dot{m}_L}{\pi \mu_L D \sqrt{E_L}} \tag{5.6}$$

$$Pr_L = \frac{cp_L \mu_L}{k_L} \tag{5.7}$$

$$Pr_G = \frac{cp_G \mu_G}{k_G} \tag{5.8}$$

The quality x in Eq. 5.4 is defined by Eq. 5.9 . To account for different flow patterns the flow pattern factor F_P (Eq. 5.10) is introduced, which tries to capture the realistic shape of the gas liquid interface. F_S in Eq. 5.10 represents the shape factor, which is a modification of the Froude number and defined by Eq. 5.11 .[34]

$$x = \frac{\dot{m}_G}{\dot{m}_G + \dot{m}_L} \tag{5.9}$$

$$F_P = E_L + (1 - E_L)F_S^2 \tag{5.10}$$

$$F_S = \frac{2}{\pi} \arctan\left(\sqrt{\frac{\rho_G(v_G - v_L)^2}{gD(\rho_L - \rho_G)}}\right) \tag{5.11}$$

To account for the effect of inclination an inclination factor is proposed, which includes the effect of the surface tension as well. This factor is defined by Eq. 5.12 whereby the Eötvös number is given by Eq. 5.13 .[34]

$$I^* = 1 + Eo|\sin\alpha| \tag{5.12}$$

$$Eo = \frac{(\rho_L - \rho_G)gD^2}{\sigma_L} \tag{5.13}$$

Finally in Tab. 5.1 the missing empirical values are listed, which are necessary to calculate heat transfer coefficient in Eq. 5.4 .[34]

Table 5.1: Empirical factors for Eq. 5.4

Variable	Value
C	0.55
m	0.1
n	0.4
p	0.25
q	0.25
r	0.25

5.2.2   Convective heat transfer coefficient

To calculate the convective heat transfer coefficient for the outermost layer, the Nusselt number hast to be determined at first (Eq. 5.14).[30]

$$Nu_o = 0.3 \frac{0.62 Re_o^{\frac{1}{2}} Pr_o^{\frac{1}{3}}}{\left[1 + \left(\frac{0.4}{Pr_o}\right)^{\frac{2}{3}}\right]^{\frac{1}{4}}} \left[1 + \left(\frac{Re_o}{282}\right)^{\frac{5}{8}}\right]^{\frac{4}{5}} \tag{5.14}$$

The thermal conductivity (Eq. 5.15), kinematic viscosity (Eq. 5.16) and Prandtl number (Eq. 5.17) for air can be derived from simple linear functions.[30]

$$k_o = 6.55 * 10^{-5} T_o + 0.00594 \tag{5.15}$$

$$\nu_o = 0.0818 * 10^{-6} T_o - 8.6471 * 10^{-6} \tag{5.16}$$

$$Pr_o = -1.587 * 10^{-4} T_o + 0.759 \tag{5.17}$$

With the Reynolds number (Eq. 5.18) including the air velocity v_o the convective heat transfer coefficient can be calculated with Eq. 5.19 .[30]

$$Re_o = \frac{v_o D_o}{\nu_o} \tag{5.18}$$

$$U_o = \frac{k_o Nu_o}{D_o} \tag{5.19}$$

Chapter 6

Fluid property correlations

The accurate prediction of the fluid properties is the prerequisite to successful pipeline design. To simulate the fluid properties two different approaches can be used, the black oil model and the compositional model. Although the accuracy of the data received from the compositional model would be higher the black oil model is used in the analysis tool. The reason therefore is that the black oil model only requires a few input data in contrast to the compositional model which is the requirement on the analysis tool. In the following section the black oil model equations are presented which are included in the analysis tool. For the latent heat of vaporization no correlation could be found in the literature which is why equations are derived by polynomial regression analysis of data calculated with Aspen Hysys.

6.1 Reuqired fluid properties

As we can see in Sec. 4 multiphase flow prediction models make use of various fluid properties. The accurate prediction of the physical properties is the prerequisite to successful pipeline design.[36] Fluids encountered in a multiphase flow stream are normally water and hydrocarbons in the liquid and gaseous phase. All the fluid properties depend in principle on the actual temperature, the pressure and the fluid composition.[7] In Tab. 6.1 the properties, required by the multiphase flow prediction models, are listed. The liquid properties refer to the liquid phase, which is a composition of oil and water. Thus the fluid properties of this phase are a mixture of oil and water properties.

6.2 Available calculation models

To simulate the fluid properties two different approaches can be used, the black oil model and the compositional model. In the black oil model, which is also called constant composition model, it is assumed that the chemical composition of oil and gas remains constant over time. It defines the oil as a liquid phase, containing gas, such as hydrocarbons produced from the oil reservoir. In this model a set of equations is used to calculate the core parameters, the fluid properties are calculated with. These crucial parameters are the solution gas/oil ratio R_s, the oil formation volume factor B_O, the solution gas/water ratio R_{sW}, the water formation volume factor B_W and the real gas deviation factor Z.[36]

The compositional model on the other hand, determines the amount of the feed that exists in the vapor and liquid phases and the composition of each phase, for a given composition of the fluid mixture. If the composition of each phase is known, it is further possible to calculate

Table 6.1: Required fluid properties.

Fluid property	Symbol
Liquid density	ρ_L
Gas density	ρ_G
Liquid dynamic viscosity	μ_L
Gas dynamic viscosity	μ_G
Liquid surface tension	σ_L
Liquid thermal conductivity	k_L
Gas thermal conductivity	k_G
Liquid specific heat capacity	cp_L
Gas specific heat capacity	cp_G
Enthalpy flow	$\dot{H}$
Latent heat of vaporization	ΔH_{vap}

the fluid properties such as density and viscosity. The accuracy of the data, received from the compositional model, is highly dependent on the accuracy of the compositional input data. In contrast to the black oil model the compositional model does not assume the composition of the oil and gas phase to be constant why complex phase effects such as retrograde condensation are considered as well.[36]

6.3   The black oil model

Comparing the black oil model and the compositional model it is obvious, that the compositional model has a higher accuracy in predicting the fluid properties of the hydrocarbon mixture. On the other hand the black oil model only requires a few input data in contrast to the compositional model, which requires the detailed composition of the mixture.
As it was the requirement on the analysis tool to perform the flow calculation with as few input parameters as possible, the black oil model was chosen despite it's lack of accuracy.
In the literature several black oil model equations are available. In the following section only those equations are presented, which are included in the analysis tool as well. It must be mentioned here, that the following empirical equations are given in English units. Due to the empirically derived coefficients in these equations, it is not possible to transform the equations itself to SI units but only the results. Therefore in the nomenclature (Chapter 1) the English units are given as well for the parameters used in the following section.

6.3.1   Input parameter

The main input parameters for the black oil model beside pressure and temperature are the API gravity γ_{API} and the specific gas gravity γ_G. The API gravity is a standard to measure the density of a petroleum oil using the specific oil gravity. Eq. 6.1 gives the API gravity, whereby γ_O is the specific gravity of stock tank oil at $60°F/60°F$. The specific oil gravity is the ratio of the oil density to the water density.[16]

$$\gamma_{API} = \frac{141.5}{\gamma_O} - 131.5 \tag{6.1}$$

The specific gas gravity is the ratio of the gas density to the density of air at the actual separator conditions p_{sep} and T_{sep} (normally standard conditions). To calculate the actual flows of gas and liquid, the black oil model requires the producing gas/oil ratio R_p as an input parameter. This is the ratio of gas to oil from a producing well. Finally the liquid flow rate q_L and the water cut f_W are needed so that the actual flow rates of the gas and liquid phase can be calculated.[16]

6.3.2 Solution gas oil ratio

The solution gas/oil ratio is defined as the volume of gas dissolved in one stock tank barrel of oil at the actual pressure and temperature.[16] With increasing pressure a crude oil will absorb gas into solution and with decreasing pressure, the gas will evolve from the oil.[7] Eq. 6.2 presents the solution gas oil ratio after Vazquez and Beggs [37], where the values of the coefficients are presented in Tab. 6.2 .[16]

$$R_s = C_1 \gamma_{G100} p^{C_2} \exp\left[C_3 \left(\frac{\gamma_{API}}{T + 460} \right) \right] \tag{6.2}$$

Table 6.2: Coefficients for Eq. 6.2 after Vazquez and Beggs.

Coefficient	$\gamma_{API} \leq 30$	$\gamma_{API} > 30$
C_1	0.0362	0.0178
C_2	1.0937	1.1870
C_3	25.7245	23.931

In Eq. 6.2 the specific gas gravity γ_{G100} refers to a separator pressure of 100 psig and is given by Eq. 6.3 .[16]

$$\gamma_{G100} = \gamma_G \left(1 + 5.912 * 10^{-5} \gamma_{API} T_{sep} \log \frac{p_{sep}}{114.7} \right) \tag{6.3}$$

6.3.3 Oil formation volume factor

The oil formation volume factor is used to predict the change in volume of the oil with changing pressure and temperature. The reason for the volume change is a combination of compressibility effects, thermal expansion and mass transfer.[7] With increasing pressure the oil formation volume factor B_O increases until the bubble point pressure p_b is reached. Above the bubble point pressure the oil formation volume factor decreases, because the oil stops dissolving more gas. Thus different equations are used to determine the oil formation volume factor above and below the bubble point pressure. After Vazequez and Beggs [37] the bubble point pressure is calculated from Eq. 6.4 with the constants in Tab. 6.3 .[16]

$$p_b = \left[\left(\frac{C_1 R_p}{\gamma_{G100}} \right) 10^{-C_3 \frac{\gamma_{API}}{T+460}} \right]^{C_2} \tag{6.4}$$

Table 6.3: Coefficients for Eq. 6.4 after Vazquez and Beggs.

Coefficient	$\gamma_{API} \leq 30$	$\gamma_{API} > 30$
C_1	27.62	56.18
C_2	0.914328	0.84246
C_3	11.172	10.393

For the oil formation volume factor below the bubble point pressure Vazquez and Beggs proposed Eq. 6.5 and above the bubble point pressure Eq. 6.6 .

$$B_O = 1 + C_1 R_s + (T - 60) \left(\frac{\gamma_{API}}{\gamma_{G100}} \right) (C_2 + C_3 R_s) \tag{6.5}$$

$$B_O = B_{Ob} \exp \left[-c_o (p - p_b) \right] \tag{6.6}$$

The coefficients for Eq. 6.5 can be found in Tab. 6.4 . To calculate the oil formation volume factor above the bubble point pressure, B_{Ob} is calculated from Eq. 6.5 by replacing R_s by R_p and the isothermal compressibility of oil c_O is calculated from Eq. 6.7 after Vazquez and Beggs.[16]

Table 6.4: Coefficients for Eq. 6.5 after Vazquez and Beggs.

Coefficient	$\gamma_{API} \leq 30$	$\gamma_{API} > 30$
C_1	$4.677 * 10^{-4}$	$4.670 * 10^{-4}$
C_2	$1.751 * 10^{-5}$	$1.1 * 10^{-5}$
C_3	$-1.811 * 10^{-8}$	$1.337 * 10^{-9}$

$$c_O = \frac{-1.433 + 5R_s + 17.2T - 1.18\gamma_{G100} + 12.61\gamma_{API}}{10^5 p} \tag{6.7}$$

6.3.4   Specific gravity of free and dissolved gas

When pressure declines, gas will evolve from the crude oil. First methane vaporizes followed by hydrocarbons with higher molecular weight. Thus the gravity of the free and dissolved gas changes due to the different boiling points of the hydrocarbons.[7] In the literature there are no equations available for calculating the dissolved gas gravity (γ_{Gd}), wherefore Fig. 6.1 after Katz et al. [38] is used to predict it.[16]
The specific gravity of free gas (γ_{Gf}) can be obtained from a material balance calculation (Eq. 6.8).[7]

$$\gamma_{Gf} = \frac{R_p \gamma_G - R_s \gamma_{Gd}}{R_p - R_s} \tag{6.8}$$

6.3.5   Oil density

The calculation method for the oil density above the bubble point pressure differs from the one below the bubble point pressure. The bubble point pressure is calculated from Eq. 6.4
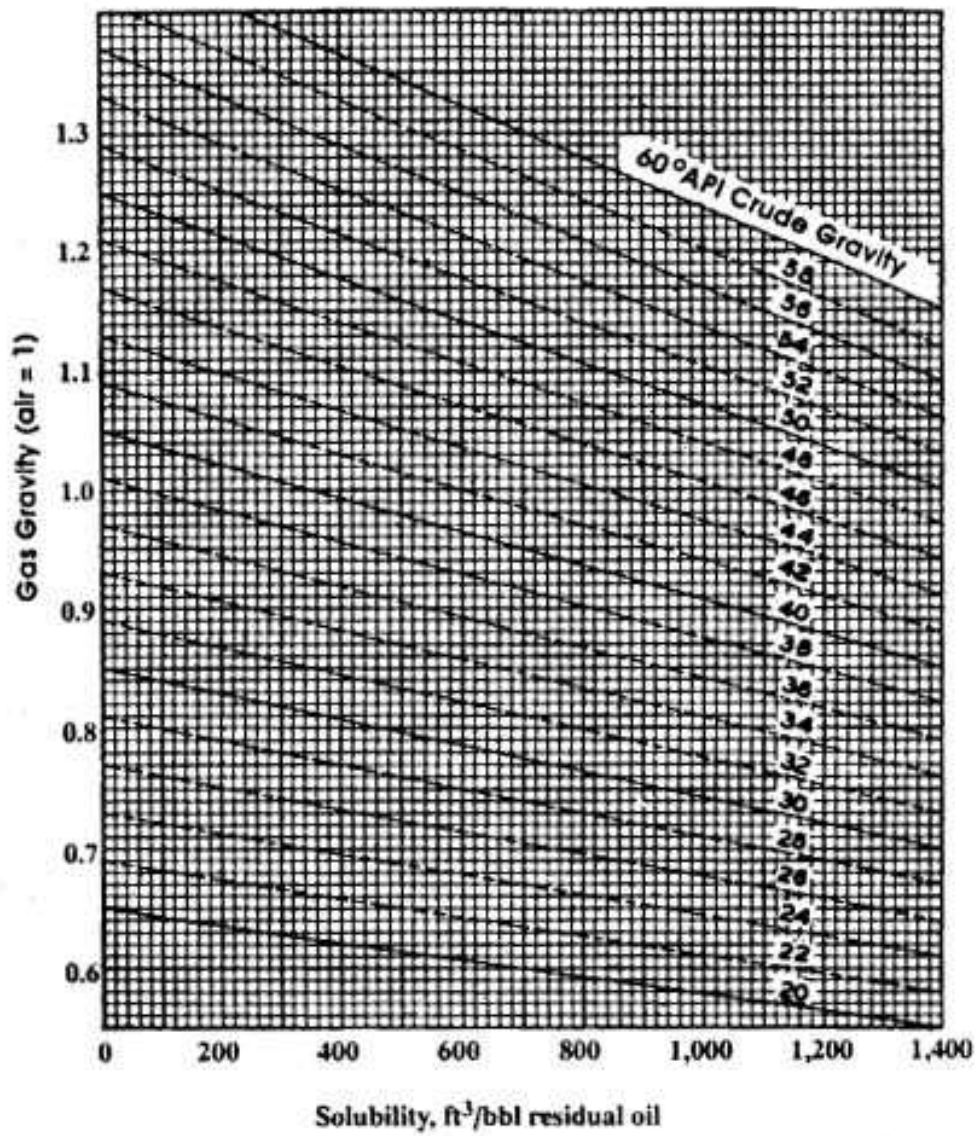
Figure 6.1: Representation of the Katz et al. dissolved gas gravity correlation.[16]

again. Below the bubble point pressure Eq. 6.9 is used. The density above the bubble point pressure is calculated by first determining the density at the bubble point pressure (Eq. 6.10) and then using Eq. 6.11 .[16]

$$\rho_O = \frac{62.4\gamma_O + 0.0136R_s\gamma_{Gd}}{B_O} \tag{6.9}$$

$$\rho_{Ob} = \frac{62.4\gamma_O + 0.0136R_p\gamma_G}{B_{Ob}} \tag{6.10}$$

$$\rho_O = \rho_{Ob} \exp\left[c_O(p - p_b)\right] \tag{6.11}$$

6.3.6   Oil viscosity

When determining the oil viscosity, at first the so called dead oil viscosity is calculated. This is the viscosity of the oil without dissolved gas at atmospheric pressure and at the actual temperature. The empirical correlation for the dead oil viscosity proposed by Kartoatmodjo and Schmidt [39] is given by Eq. 6.12 .[16]

$$\mu_{Od} = 16 * 10^8 T^{-2.8177} \log\left(\gamma_{API}\right)^{5.7526\log(T)-26.9718} \tag{6.12}$$

The oil viscosity decreases with increasing pressure up to the bubble point pressure. Above the bubble point pressure the viscosity is increasing with rising pressure. The bubble point pressure is again determined from Eq. 6.4 . Below the bubble point pressure Kartoatmodjo and Schmidt proposed Eq. 6.13 to calculate the oil viscosity, which is in fact a correction of the dead oil viscosity.[16]

$$\mu_O = -0.06821 + 0.9824f + 0.0004034f^2 \tag{6.13}$$

$$f = \left(0.2001 + 0.8428 * 10^{-0.000845R_s}\right)\mu_{Od}^{(0.43+0.5165y)}$$

$$y = 10^{-0.00081R_s}$$

Above the bubble point pressure the oil viscosity is determined from Eq. 6.14 after Kartoatmodjo and Schmidt . μ_{Ob} represents the saturated crude oil viscosity at bubble point pressure calculated from Eq. 6.13 .[16]

$$\mu_O = 1.0081\mu_{Ob} + 0.001127(p - p_b)\left(-0.006517\mu_{Ob}^{1.8148} + 0.038\mu_{Ob}^{1.590}\right) \tag{6.14}$$

6.3.7   Gas oil surface tension

Baker and Swerdloff [40] present empirical correlations in the form of graphs (Fig. 6.2), where the dead oil surface tension is correlated with temperature and API gravity. The equation for the dead oil surface tension at $68°F$ and $100°F$ is presented by Eq. 6.15 and Eq. 6.16 respectively.[16]

$$\sigma_{Od_{68}} = 39 - 0.2571\gamma_{API} \tag{6.15}$$
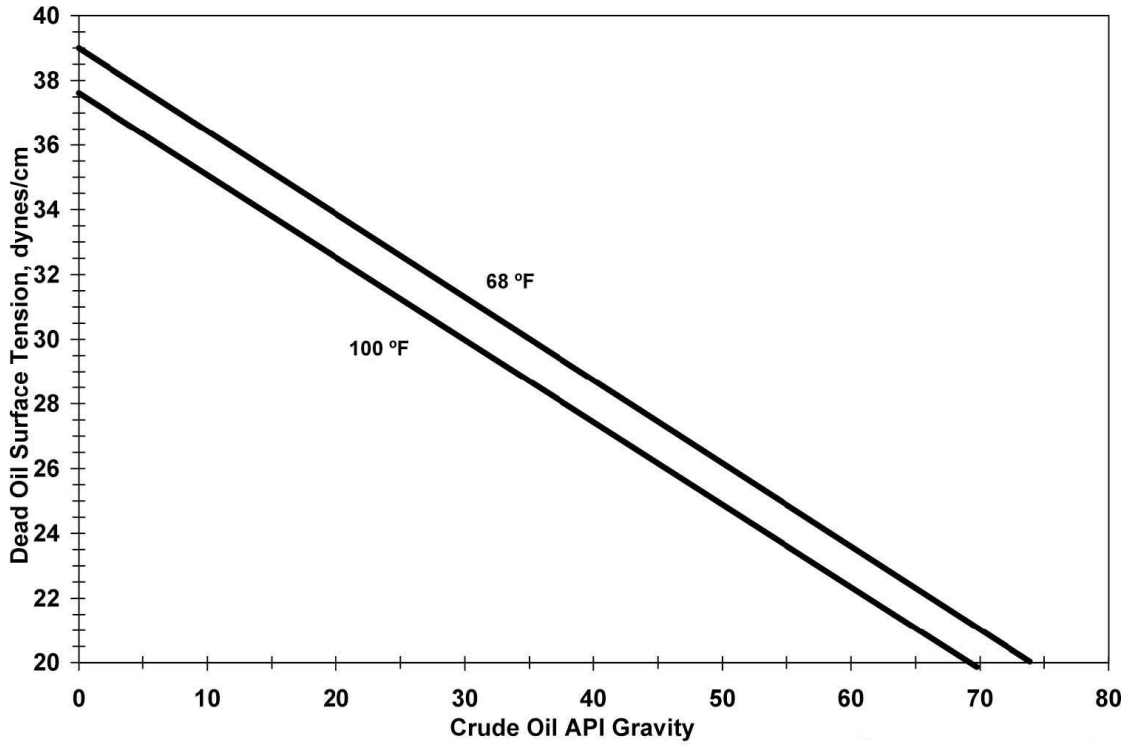
$$\sigma_{Od_{100}} = 37.5 - 0.2571\gamma_{API} \tag{6.16}$$

Figure 6.2: Surface tension of crude oils at atmospheric pressure.[16]

For temperatures, greater than $100°F$, $\sigma_{Od_{100}}$, and for temperatures smaller than $68°F$, $\sigma_{Od_{68}}$ is used. Between $100°F$ and $68°F$ the value is derived from linear interpolation.[41] Eq. 6.17 shows a summary of the calculation process for the gas oil surface tension.

$$\sigma_{Od} = \begin{cases} \sigma_{Od_{68}} & T \leq 68°F \\ \sigma_{Od_{68}} - \frac{(T-68)\left(\sigma_{Od_{68}} - \sigma_{Od_{100}}\right)}{32} & 68°F < T < 100°F \\ \sigma_{Od_{100}} & 100°F \leq T \end{cases} \qquad (6.17)$$

With increasing pressure gas is dissolved in the oil, which reduces the surface tension. Baker and Swerdloff therefore provided a correction factor (Eq. 6.18) to calculate the live oil surface tension (Eq. 6.19).[16]

$$\left(\frac{\sigma_O}{\sigma_{Od}}\right) = \exp\left(-8.6306 * 10^{-4}p\right) \qquad (6.18)$$

$$\sigma_O = \sigma_{Od}\left(\frac{\sigma_O}{\sigma_{Od}}\right) \qquad (6.19)$$

6.3.8   Solution gas water ratio

The solubility of the components of a hydrocarbon gas in water is inversely proportional to their molecular weight. Methane is the most soluble component in a hydrocarbon gas mixture. To calculate the solubility of gas in water, Ahmed [42] proposed Eq. 6.20 , which is corrected for the effect of water salinity by Eq. 6.21 .[16]

$$R_{sW} = A + Bp + Cp^2 \qquad (6.20)$$

$$A = 2.12 + 3.45 * 10^{-3}T - 3.59 * 10^{-5}T^2$$

$$B = 0.0107 - 5.26 * 10^{-5}T + 1.48 * 10^{-7}T^2$$

$$C = -8.75 * 10^{-7} + 3.9 * 10^{-9}T - 1.02 * 10^{-11}T^2$$

$$R_{sW_b} = R_{sW}C_s \tag{6.21}$$

$$C_s = 1 - (0.0753 - 0.000173T)S$$

6.3.9   Water formation volume factor

The water formation volume factor B_W decreases with decreasing pressure, no matter, if the pressure is above or below the bubble point pressure. According to McCain [43] the water formation volume factor B_W can be calculated from Eq. 6.22 .[43]

$$B_W = (1 - \Delta V_{WT})(1 + \Delta V_{Wp}) \tag{6.22}$$

$$\Delta V_{Tt} = -1.00010 * 10^{-2} + 1.33391 * 10^{-4}T + 5.50654 * 10^{-7}T^2$$

$$\Delta V_{Wp} = -1.95301 * 10^{-9}pT - 1.72834 * 10^{-13}p^2T - 3.58922 * 10^{-7}p - 2.25341 * 10^{-10}p^2$$

6.3.10   Water density

At standard conditions the density of pure water is $62.4 \quad lbm/ft^3$. By neglecting gas solubility in water the density of water can be calculated from Eq. 6.23 .[16]

$$\rho_W = \frac{62.4\gamma_{Wsc}}{B_W} \tag{6.23}$$

6.3.11   Water viscosity

Only few data are available on viscosity of oilfield water. Van Wingen [44] reported the effect of temperature on water viscosity which is presented in Eq. 6.24 .[7]

$$\mu_W = \exp\left(1.003 - 1.479 * 10^{-2}T + 1.982 * 10^{-5}T^2\right) \tag{6.24}$$

6.3.12   Gas water surface tension

The gas water surface tension can be computed from Eq. 6.25 and Eq. 6.26 which give values for the surface tension at $74°F$ and $280°F$ respectively. With linear interpolation values for the surface tension between these two temperatures can be derived (Eq. 6.27).[16]

$$\sigma_{W_{74}} = 75 - 1.108 p^{0.349} \tag{6.25}$$

$$\sigma_{W_{280}} = 53 - 0.1048 p^{0.637} \tag{6.26}$$

$$\sigma_G = \begin{cases} \sigma_{W_{74}} & T = 74°F \\ \sigma_{W_{74}} - \frac{(T-74)\left(\sigma_{W_{74}} - \sigma_{W_{280}}\right)}{206} & 74°F < T < 280°F \\ \sigma_{W_{280}} & T = 280°F \end{cases} \tag{6.27}$$

6.3.13   Liquid fluid properties

So far the determination of the oil and water fluid properties have been presented. By using a black oil model, the properties of oil and water are combined considering no slippage between the phases. The liquid density, viscosity and surface tension can thus be determined from Eq. 6.28 , Eq. 6.29 and Eq. 6.30 .[16]

$$\rho_L = \rho_W f_W + \rho_O (1 - f_W) \tag{6.28}$$

$$\mu_L = \mu_W f_W + \mu_O (1 - f_W) \tag{6.29}$$

$$\sigma_L = \sigma_W f_W + \sigma_O (1 - f_W) \tag{6.30}$$

6.3.14   Real gas deviation factor

The starting point in determining the gas fluid properties is to calculate the real gas deviation factor Z. This factor is used to define the deviation from the ideal gas behavior. Before the Z-factor can be determined, the pseudo critical as well as the reduced pressure and temperature must be determined. For the pseudo critical values Standing [45] developed two empirical equations, Eq. 6.31 and Eq. 6.32 .[16]

$$p_{pc} = 677 + 15\gamma_G - 37.5\gamma_G^2 \tag{6.31}$$

$$T_{pc} = 168 + 325\gamma_G - 12.5\gamma_G^2 \tag{6.32}$$

With the pseudo critical temperature and pressure the pseudo reduced pressure and temperature can be estimated next, which is given by Eq. 6.33 and Eq. 6.34 .[16]

$$p_{pr} = \frac{p}{p_{pc}} \tag{6.33}$$

$$T_{pr} = \frac{T + 460}{T_{pc}} \tag{6.34}$$

Dranchuk and Abou-Kassem [46] present an empirical equation to calculate the Z-factor.
Eq. 6.35 presents this correlation and the needed constants are presented in Tab. 6.5 . The
reduced gas density is defined as $\rho_r = \frac{0.27 p_{pr}}{Z T_{pr}}$. As one can see, Eq. 6.35 is an implicit equation
in Z which is why an iterative method must be used to solve the equation.[16]

$$
\begin{aligned}
Z =& \left(A_1 + \frac{A_2}{T_{pr}} + \frac{A_3}{T_{pr}^3} + \frac{A_4}{T_{pr}^4} + \frac{A_5}{T_{pr}^5} \right) \rho_r + \left(A_6 + \frac{A_7}{T_{pr}} + \frac{A_8}{T_{pr}^2} \right) \rho_r^2 \\
& - A_9 \left(\frac{A_7}{T_{pr}} + \frac{A_8}{T_{pr}^2} \right) \rho_r^5 + A_{10} \left(1 + A_{11}\rho_r^2 \right) \frac{\rho_r^2}{T_{pr}^3} \exp\left(-A_{11}\rho_r^2 \right) + 1
\end{aligned}
\tag{6.35}
$$

Table 6.5: Coefficients for Eq. 6.35 after Dranchuk and Abou-Kassem.

Coefficient	Value
A_1	0.3265
A_2	-1.07
A_3	-0.5339
A_4	0.01569
A_5	-0.05165
A_6	0.5475
A_7	-0.7361
A_8	0.1844
A_9	0.1056
A_{10}	0.6134
A_{11}	0.7210

6.3.15   Gas formation volume factor

From the real gas law, the gas formation volume factor can be calculated with Eq. 6.36 .[16]

$$
B_G = 0.0283 \frac{Z(T + 460)}{p}
\tag{6.36}
$$

6.3.16   Gas density

The gas density is derived from the real gas law as well (Eq. 6.37), whereby the specific
gravity of the free gas γ_{Gf} is used instead of the gas specific gravity γ_G.[16]

$$
\rho_G = \frac{2.7 \gamma_{Gf} p}{Z(T + 460)}
\tag{6.37}
$$

6.3.17   Gas viscosity

Lee et al. [47] present a set of empirical equations for calculating the gas viscosity. First the molecular weight is calculated from Eq. 6.38 and then the viscosity is derived from Eq. 6.39 .[16]

$$M_G = 28.97 * \gamma_G \tag{6.38}$$

$$\mu_G = 10^{-4} K \exp \left[X \left(\frac{\rho_G}{62.4} \right)^Y \right] \tag{6.39}$$

$$K = \frac{(9.4 + 0.02 M_G)(T + 460)^{1.5}}{209 + 19 M_G + (T + 460)}$$

$$X = 3.5 + \frac{986}{T + 460}$$

$$Y = 2.4 - 0.2X$$

6.3.18   Actual volumetric flow rate

Although the actual flow rates are no fluid properties, their determination is included in this chapter. At first the volumetric flow rates at standard conditions are determined with Eq. 6.40 to Eq. 6.42 .

$$q_{Wsc} = q_L f_W \tag{6.40}$$

$$q_{Osc} = q_L - q_{Wsc} \tag{6.41}$$

$$q_{Gsc} = q_{Osc} R_p \tag{6.42}$$

Afterwards the actual flow rates are calculated, using the formation volume factors and the gas solubilities, Eq. 6.43 to Eq. 6.45 .

$$q_W = \frac{q_{Wsc} B_W 5.614}{86400} \tag{6.43}$$

$$q_O = \frac{q_{Osc} B_O 5.614}{86400} \tag{6.44}$$

$$q_G = \frac{(q_{Gsc} - q_{Osc} R_s - q_{Wsc} R_{sW_b}) B_G}{86400} \tag{6.45}$$

6.3.19   Thermal conductivity

The ability of a material to conduct energy is called thermal conductivity. A material with a high thermal conductivity can transfer heat at a higher rate than one with a low thermal conductivity.[48] In contrast to the previous sections the equations are given in SI units again from now on.

6.3.19.1   Water thermal conductivity

The thermal conductivity of water can be estimated with Eq. 6.46   after Deming and Chapman.[49]

$$k_W = \begin{cases} 0.5648 + 1.878 * 10^{-3}T - 7.231 * 10^{-6}T^2 & 0°C \le T \le 137°C \\ 0.6020 + 1.309 * 10^{-3}T - 5.140 * 10^{-6}T^2 & 137°C \le T \le 300°C \end{cases} \tag{6.46}$$

6.3.19.2   Oil thermal conductivity

The oil thermal conductivity can be derived from Eq. 6.47 .[48]

$$k_O = \begin{cases} 0.2389 - 4.593 * 10^{-4}(T + 273.15) + 2.676 * 10^{-7}(T + 273.15)^2 & 0°C \le T < 240°C \\ 0.075 & T \ge 240°C \end{cases}$$
$$\tag{6.47}$$

6.3.19.3   Liquid thermal conductivity

The liquid thermal conductivity is a composition of the oil thermal conductivity and the water thermal conductivity and can be calculated with Eq. 6.48 .

$$k_L = k_W f_W + k_O(1 - f_W) \tag{6.48}$$

6.3.19.4   Gas thermal conductivity

The gas thermal conductivity can be derived from Eq. 6.49 .[48]

$$k_G = \begin{cases} -0.0969 + 4.37 * 10^{-4}(T + 273.15) & 0°C \le T < 120°C \\ 0.075 & T \ge 120°C \end{cases} \tag{6.49}$$

6.3.20   Specific heat capacity

The heat capacity is defined as the amount of heat, which is required to raise the temperature of that substance by one degree. The specific heat capacity is the heat capacity per unit mass of the substance.[50]

6.3.20.1   Water specific heat capacity

Empirical equations for the specific heat capacity of pure water, as a function of temperature, are proposed by Somerton [51]. Eq. 6.50 shows these correlations, whereby it is proposed by Waples and Waples [50], that the correlation between 20 °C and 290 °C can be extrapolated down to 0 °C.[50]

$$cp_W = \begin{cases} \frac{4245 - 1.841T}{\rho_W} & 20°C \le T \le 290°C \\ \frac{3703}{\rho_W} \exp\left[-0.00481(T - 290) - 0.000234(T - 290)^2\right] & 290°C < T \le 370°C \end{cases} \tag{6.50}$$

6.3.20.2   Oil specific heat capacity

Gambill [52] proposed Eq. 6.51 to predict the specific heat capacity of oils as a function of temperature and specific oil gravity.

$$cp_O = \frac{1684 + 3.389T}{\sqrt{\gamma_O}} \tag{6.51}$$

6.3.20.3   Liquid specific heat capacity

The liquid specific heat capacity is a composition of the oil specific heat capacity and the water specific heat capacity and can be calculated with Eq. 6.52 .

$$cp_L = cp_W f_W + cp_O(1 - f_W) \tag{6.52}$$

6.3.20.4   Gas specific heat capacity

To calculate the gas specific heat capacity, Waples and Waples [50] proposed a fourth order polynomial (Eq. 6.53). The coefficients in Eq. 6.53 have the form of Eq. 6.54 and the values are given in Tab. 6.6 , whereby the pressure is given MPa.

$$cp_G = AT^4 + BT^3 + CT^2 + DT + E \tag{6.53}$$

$$Coefficient = C_1 P^4 + C_2 P^3 + C_3 P^2 + C_4 P + C_5 \tag{6.54}$$

Table 6.6: Values for Eq. 6.54 after Waples and Waples.

Coefficient	C_1	C_2	C_3	C_4	C_5
A	$-2.03 * 10^{-7}$	$5.7 * 10^{-5}$	-0.00518	0.132	-0.181
B	$2.84 * 10^{-7}$	$-7.88 * 10^{-5}$	0.00714	-0.188	0.207
C	$-1.42 * 10^{-6}$	$3.88 * 10^{-4}$	-0.03513	0.980	-0.872
D	$2.95 * 10^{-7}$	$-7.97 * 10^{-5}$	0.00725	-0.222	0.533
E	$-2 * 10^{-7}$	$5.46 * 10^{-5}$	-0.00519	0.193	1.928

6.3.21   Black oil enthalpy

For calculating the heat loss over the pipeline, the enthalpy of the multiphase mixture has to be calculated at a dedicated pressure and temperature. The black oil fluid enthalpy model (2009 Method), presented in the Pipesim user guide [53], is chosen to calculate the enthalpy. At first the enthalpies of the water phase, oil phase and gas phase are determined from Eq. 6.55 to Eq. 6.57 .

$$H_W = cp_W T - \eta_W cp_W p \tag{6.55}$$

$$H_O = cp_O T - \eta_O cp_O p \tag{6.56}$$

$$H_G = cp_G T - \eta_G cp_G p + \Delta H_{vap} \tag{6.57}$$

The Joule Thomson coefficients are determined from Eq. 6.58 to Eq. 6.60 and the total enthalpy flow of the fluid is given by Eq. 6.61 .

$$\eta_G = \frac{1}{\rho_G cp_G} \left(\frac{T}{Z} \frac{\partial Z}{\partial T} \right) \tag{6.58}$$

$$\eta_O = -\frac{1}{\rho_O cp_O} \tag{6.59}$$

$$\eta_W = -\frac{1}{\rho_W cp_W} \tag{6.60}$$

$$\dot{H} = H_G \dot{m}_G + H_W \dot{m}_W + H_O \dot{m}_O \tag{6.61}$$

6.3.22   Latent heat of vaporization

To calculate the fluid enthalpy in Sec. 6.3.21 , the latent heat of vaporization is needed. Unfortunately no equations for calculating the latent heat of vaporization for a hydrocarbon mixture could be found in the literature. Therefore equations were derived by polynomial regression analysis of data calculated with Aspen Hysys[1].

The latent heat of vaporization is plotted against the pressure whereby the pressure is varied between 1 and 40 bara. This procedure is performed for six different specific gas gravities, which is presented in Fig. 6.3 . In Tab. 6.7 the polynomial equations for each specific gas gravity are listed. Values for the latent heat of vaporization for gas gravities between the listed values can be calculated by linear interpolation.

Table 6.7: Polynomial equations for the latent heat of vaporization.

γ_G	Polynomial equation
0.553	$\Delta H_{vap} = -0.004p^3 + 0.2379p^2 - 12.009p + 518.08$
0.593	$\Delta H_{vap} = -0.0025p^3 + 0.1839p^2 - 10.925p + 656.49$
0.653	$\Delta H_{vap} = -0.0018p^3 + 0.1402p^2 - 9.0574p + 664.4$
0.673	$\Delta H_{vap} = -0.0015p^3 + 0.1117p^2 - 7.8026p + 666.41$
0.713	$\Delta H_{vap} = -0.0012p^3 + 0.0895p^2 - 6.8576p + 666.15$
0.753	$\Delta H_{vap} = -0.001p^3 + 0.0719p^2 - 6.1286p + 664.84$

---

[1]For more information concerning Hysys see Sec. 8.2 .
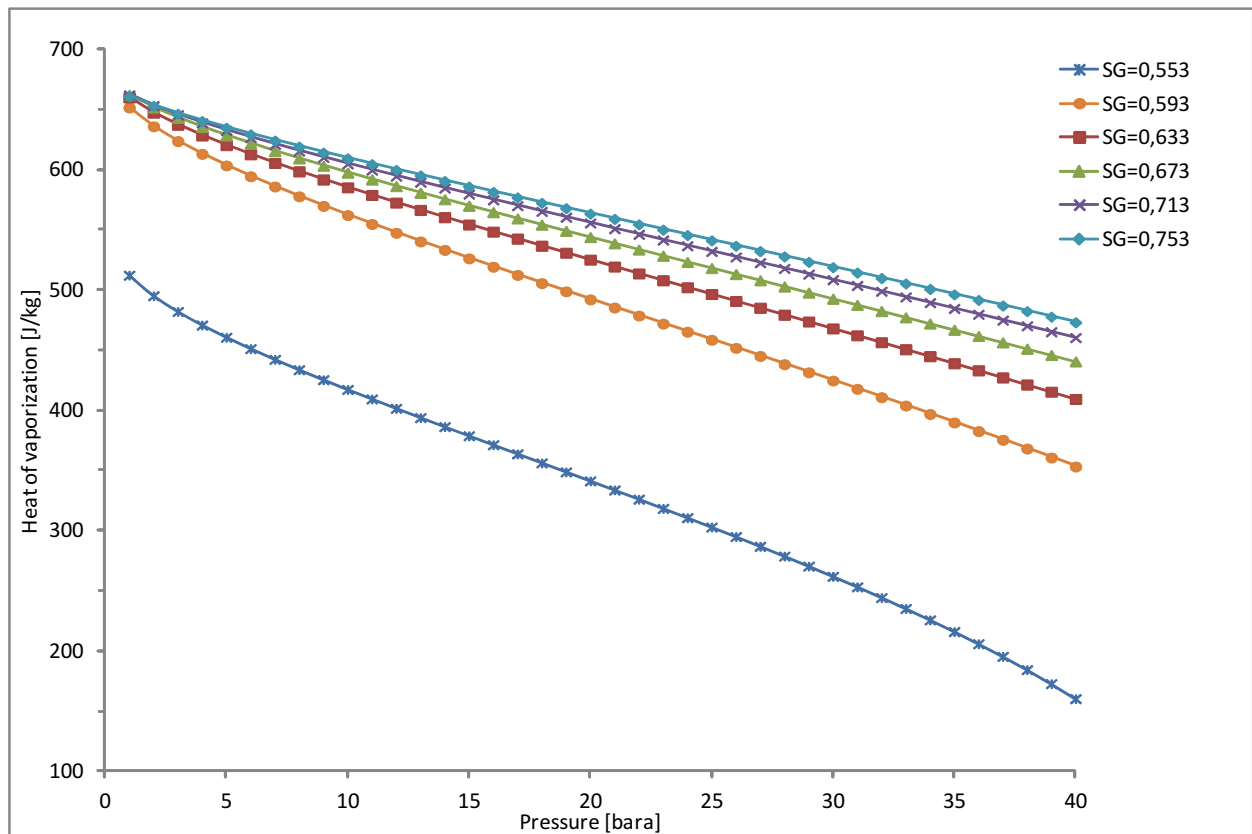
Figure 6.3: Latent heat of vaporization as a function of pressure for six specific gas gravities (SG).

Chapter 7

Multiphase flow simulation tool - SEM-Flow

The multiphase flow simulation tool SEM-Flow is programmed in visual basic and a modular approach is chosen for the program structure. The calculation was first evaluated with Mathcad to check for possible mistakes occurring in the code.

The Frame-Module, which is the mainmodule of the program, is the interface between the submodules. The submodules are called and parameters are passed there as well. Several equations, presented by Petalas and Aziz, have to be solved with an iterative procedure. Thus numerical methods are identified to obtain the roots of these functions.

7.1 Visual basic for applications

Visual basic for applications (VBA) is a programming environment, that is included in Microsoft Excel. VBA is a complete programming language, which can be used only with Microsoft Office applications such as Excel. Components like worksheets, that are known from the Microsoft Excel environment, can be used and manipulated by the programmer. To create visual basic code it is necessary to use the visual basic editor, which can be accessed from the Microsoft Excel window. Visual basic for applications can be seen as a dialect of the Microsoft visual basic programming language and thus is a complete programming language.[54]

7.2 The modular structure

Considering the previous sections a large number of calculations have to be performed to predict the flow behavior in a pipeline. In order to structure the program and to simplify the understanding, a modular approach is chosen for the program structure. Furthermore this modular programming approach enables the modification of parts of the program without influencing the whole program. Besides this, the possibility to evaluate the reduced parts of the program instead of the whole program at once, is another advantage, which makes a modular architecture desirable. Thus the program is split up in the smallest parts which are possible.

The smallest independent modules in VBA are called functions, which are analogous to the ones built-in in Excel. In Excel, these built-in functions (for example the *SUM()* function), can be used in spreadsheet formulas. A function is passed one or more values and it always

returns at least one value. It is possible to create your own function in VBA, which can be used then the same way as the built-in functions. The multiphase flow simulation tool is structured in independent modules, that can be called by other modules and variables are passed between each of these modules.

A crucial task during programming is the verification of the code in order to avoid mistakes, especially in the complex equations. Therefore the calculation after Petalas and Aziz was first calculated with Mathcad[1]. The big advantage of this program is the clear presentation of the equations and the automatically computing of engineering units. Thus it was possible to validate the results of the VBA functions based on the Mathcad results.

7.3   Architecture of the algorithm

The mainmodule of the multiphase flow simulation tool (SEM-Flow) is designated as Frame-Module and can be seen as the skeleton of the program, where all strings run together. The mainmodules with a short description are listed below:

Frame Skeleton of the algorithm where the other modules are called.

FluidProperty Return fluid property values and call submodules (Tab. 7.1).

MultiphaseFlow Examine stability of flow pattern and calculate pressure drop and liquid hold up. The function of the submodules are explained in Sec. 7.7 .

The calculation of the pressure drop and heat loss over the pipeline requires an iterative procedure in principle. The starting point for the calculation could be the inlet (oil well) or the outlet of the pipeline (before facility inlet). In SEM-Flow the pressure drop and heat loss calculation are performed from the outlet to the inlet of the pipeline. The reason therefore is, that this is the commonly needed direction in practice because the pressure at the outlet is fixed due to the fact that the downstream facilities operate at a fixed pressure.

At first the data from the Input-Interface (Sec. 7.4) are read, which are then passed to the other modules. Then the pipeline is divided into increments (Increment-Module) and the calculation procedure is repeated for each increment.[2]

7.3.1   First concept of the algorithm

By developing the overall coupling algorithm for SEM-Flow, an approach was considered first, which uses a double iteration procedure. In Fig. 7.1 the flow chart of the algorithm is presented. The pressure and temperature at the increment outlet (p_{Outlet}, T_{Outlet}) of the first increment are known. The pressure and temperature at the inlet of the increment ($p_{Assumed}, T_{Assumed}$) are assumed and the average pressure and temperature in the increment can be calculated. Now the fluid properties are calculated at the average temperature and pressure. In the Multiphase-Flow-Module the flow pattern is determined first, and the pressure at the increment inlet is calculated. $p_{Assumed}$ is compared with p_{Inlet} and if the difference between the two values does not exceed the convergence criterion, the Heat-Loss-Module is called next. Otherwise the first iteration loop is entered by setting the pressure

---

[1]Mathcad is a computer algebra software primarily intended for the verification, validation and documentation of engineering calculations.

[2]A pipeline consists of several segments which are defined as a connected part of the pipeline with the same inclination. Each segment is further divided in slices with a dedicated length designated as increments.

at the inlet of the first increment, to the pressure, just calculated. The procedure described so far is then repeated with the new average pressure until the calculated values of p_{Inlet} are sufficiently close to each other.
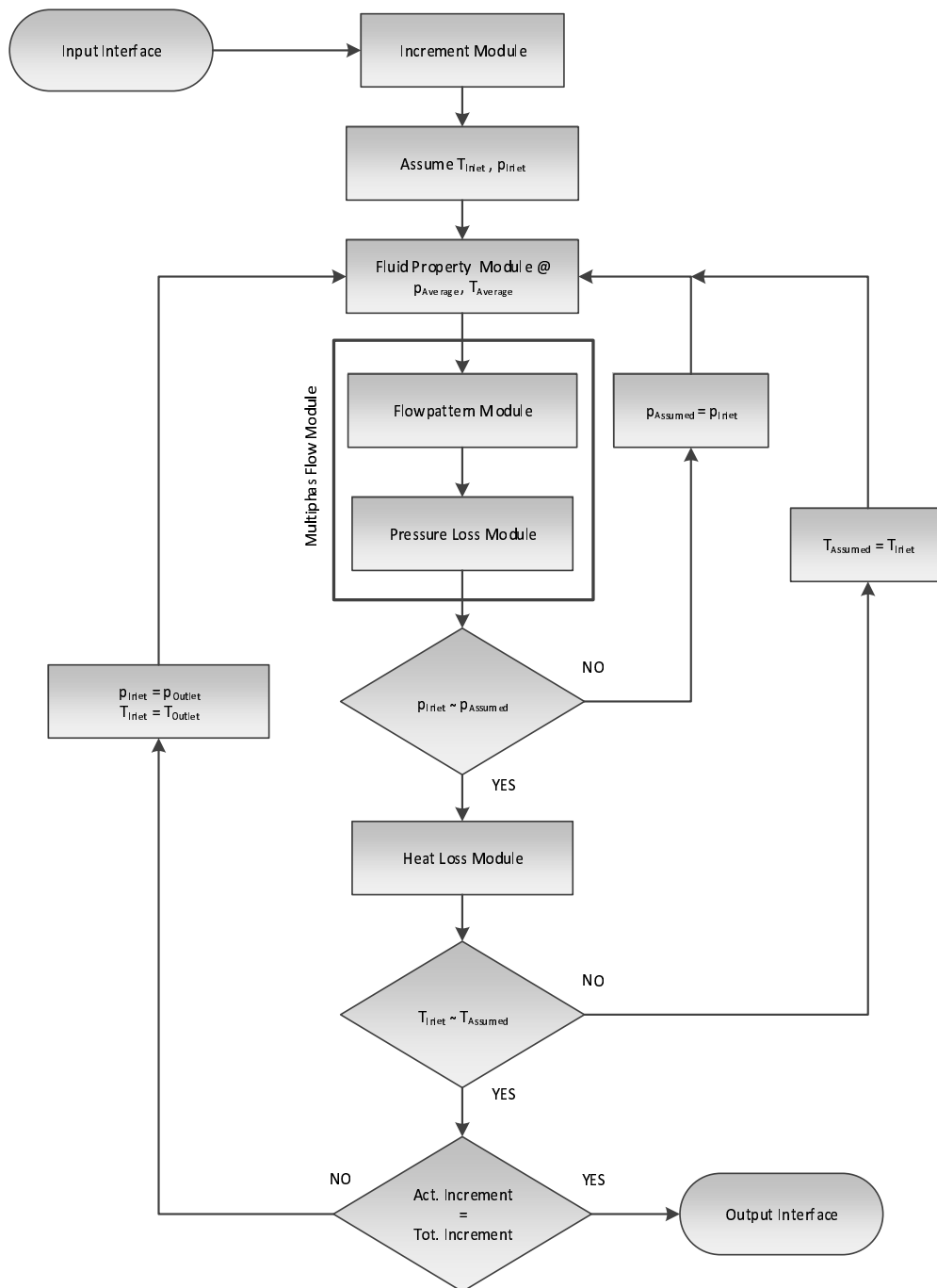

Figure 7.1: Flow chart of the coupling algorithm (first approach).

T_{Inlet} is calculated in the Heat-Loss-Module, with the temperature at the outlet of the increment. As it was done afterwards the Multiphase-Flow-Module $T_{Assumed}$ is compared with T_{Inlet}. If the difference exceeds the convergence criterion, the second iteration loop is entered by setting the assumed value of the temperature at the inlet to the just calculated value. Otherwise the temperature and the pressure at the inlet of the first increment have been determined and those values are taken as the outlet values for the next increment. The

procedure is repeated till the last increment is reached and the pressure drop and temperature loss over the whole pipeline is known.

By further evaluation of this first approach, there were concerns, that problems with the convergence of this procedure could occur. If, for example, the difference between the assumed and the calculated pressure is large, it is possible, that a different flow pattern is determined in the second iteration loop. The pressure drop can be highly different in different flow patterns however, which can lead to large steps between the several iteration loops. Thus convergence cannot be ensured.

7.3.2   The implemented algorithm

To overcome the convergence problem, the original algorithm was further developed. The new coupling algorithm is presented in Fig. 7.2 . In this approach no pressure and temperature at the inlet of the increment are assumed. The pressure and temperature at the increment outlet are used to calculate the fluid properties however. This assumption is based on the fact that the length of one increment is chosen sufficiently small, so that the pressure and temperature change is within the limit. The flow pattern and the pressure drop are calculated in the Multiphase-Flow-Module again. To check, if the assumed increment length is sufficiently short, a pressure drop of 5% based on the outlet pressure is set as the maximum allowed pressure drop in one increment. If this limit is exceeded, the number of increments is increased, decreasing the increment length.

The temperature loss over the increment is calculated in the Heat-Loss-Module next. The limit for the temperature loss is set to 5% again, based on the temperature at the outlet of the increment. If the limit is exceeded, the number of increments is increased again. A third criteria is included in the algorithm by checking, if the fluid properties at the increment outlet and inlet do not differ from each other more than $\pm 5\%$. The procedure is repeated till the last increment is reached and the pressure drop and temperature loss over the whole pipeline are known.

It is assumed, that the new algorithm overcomes the convergence problem and the calculation time is decreased as well by choosing a good value of the initial increment number. A code fragment of the Frame-Module is presented in Appendix A (Sec. A.1).

7.4   Input/Output-Interface

The input and output pages are the interface between the user and SEM-Flow. The interfaces are set up in a way that one can immediately print a report including the input data and the results. An example of these interfaces is presented in Appendix B. On the first sheet (Input Data) the user has to specify all relevant data for the multiphase flow calculation. Most data do not need any additional explanation. The only thing that should be mentioned is the definition of the initial pressure and temperature. It was mentioned earlier that the calculation in SEM-Flow starts at the outlet of the pipeline. Thus the temperature and pressure at the outlet of the pipeline have to be defined which is described as initial pressure and temperature (p_{Outlet}, T_{Outlet}).

On the second page (Elevation profile) the user has to define the pipeline profile. At first the total number of segments has to be defined and then the horizontal length and vertical height have to be defined for each segment. The length and height of each segment are defined in Fig. 7.3 . It must be mentioned that both, the length and height are defined as
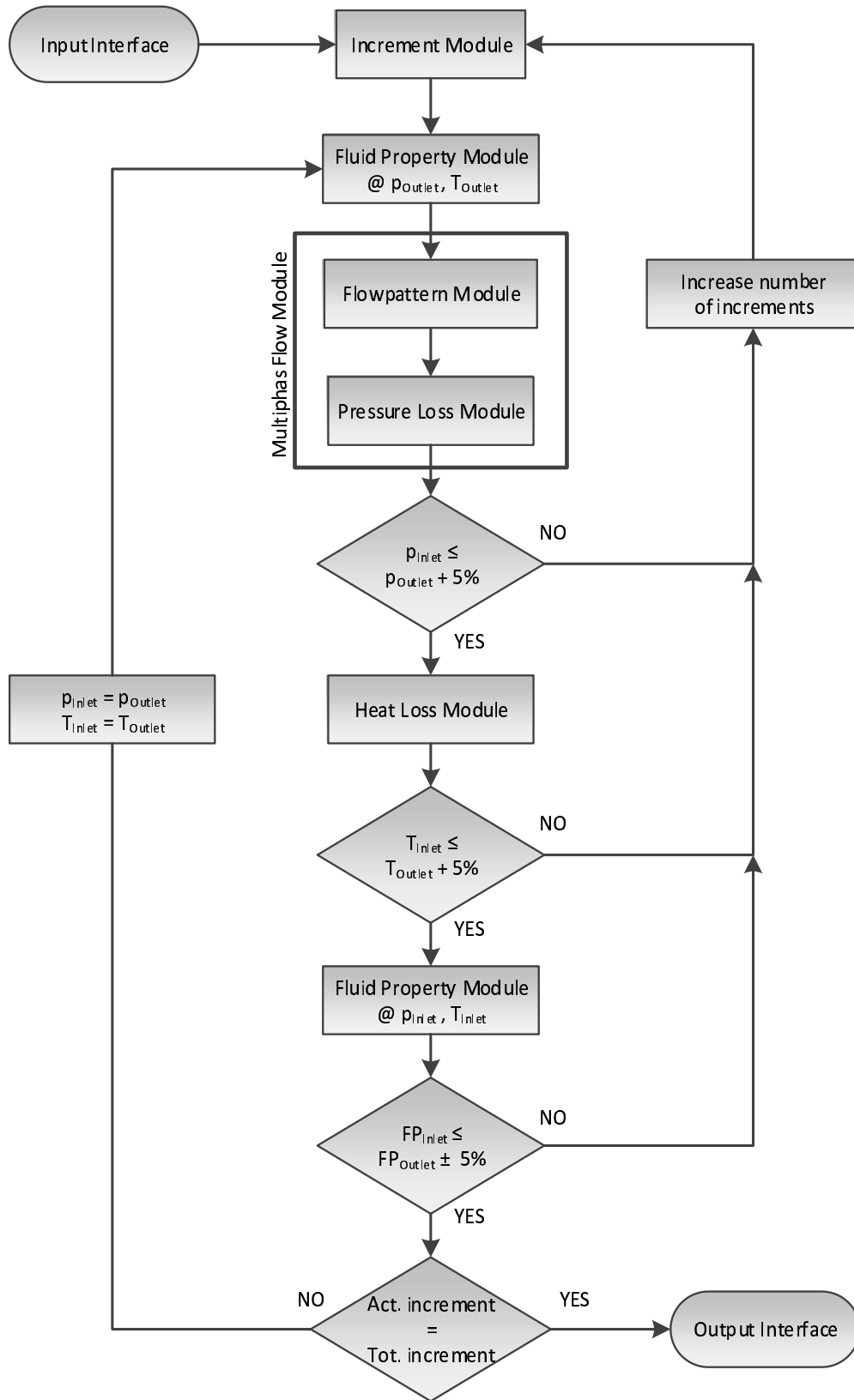
Figure 7.2: Flow chart of the coupling algorithm (final approach).

relative values for each segment. Thus the length and the height for each single segment are entered instead of the sum of the previous segments. The calculation process in SEM-Flow is started by pressing the "Start calculation"button.

The Output-Interface is divided in four pages. First there is a summary of the output data. The pressure loss, temperature loss as well as the flow pattern at the pipeline outlet are presented. If slug flow is the prevailing flow pattern at the outlet the translational velocity and the slug length at the outlet are presented as well. Additionally three detailed output pages are available. One is showing the fluid properties for each increment. One is showing the multiphase flow properties such as liquid hold up and flow pattern for each increment and one is presenting the slug properties for those increments where slug flow occurs.

7.5   Increment-Module

It was mentioned in Sec. 7.3 , that the pressure drop and heat loss calculations are performed for one pipeline increment after the other. It was not defined however what the term "increment" refers to.

The elevation profile of the pipeline is defined by the user and entered in the Input-Interface. For this purpose the whole pipeline is divided into segments, whereby a segment is defined as a connected part of the pipeline with the same inclination. The total number of segments $n_{segment}$, the equivalent horizontal pipe length $L_{segment_H}$ and the equivalent vertical pipe length $L_{segment_V}$ are read from the Input-Interface. Now it is possible to calculate the pipe length L and the inclination angle α for each segment.

Next every segment is divided into increments, wherefore the pressure drop and heat loss calculations are performed. Fig. 7.3 shows an example of one segment divided into n increments. The first approach to define the number of increments was to divide the segment length by the pipeline diameter. It was assumed, that the distance of one pipe diameter would be sufficient to satisfy the requirements of small temperature and pressure changes over the increment. It was found out later by testing the program, that the increment number became very high in case of a long pipeline with a small diameter. Due to the high number of increments the computing time increased dramatically. Furthermore it was found out, that the pressure drop and heat loss was constantly smaller than the defined 5%, which indicates that the increment length is assumed too short.

Thus the initial number of increments was set to five for each segment. If the pressure drop or temperature loss exceed the 5%, the number of increments is then increased by 25%. By this process the number of increments is just increased as high as necessary and the computing time is improved.

7.6   Fluid-Property-Module

The purpose of the Fluid-Property-Module is to return the values listed in Tab. 6.1 at a dedicated temperature and pressure. Thus, when the Fluid-Property-Module is called, the variable input parameters are pressure and temperature beside the fixed parameters, such as API gravity or specific gas gravity.

In the mainmodule of the Fluid-Property-Module the submodules are called and the parameters are passed. In Tab. 7.1 the submodules and the respective return parameters are listed. In Sec. 6.3 it is mentioned, that the empirical equations for the fluid property calculation are given in English units. Therefore the transmission parameters pressure, temperature,
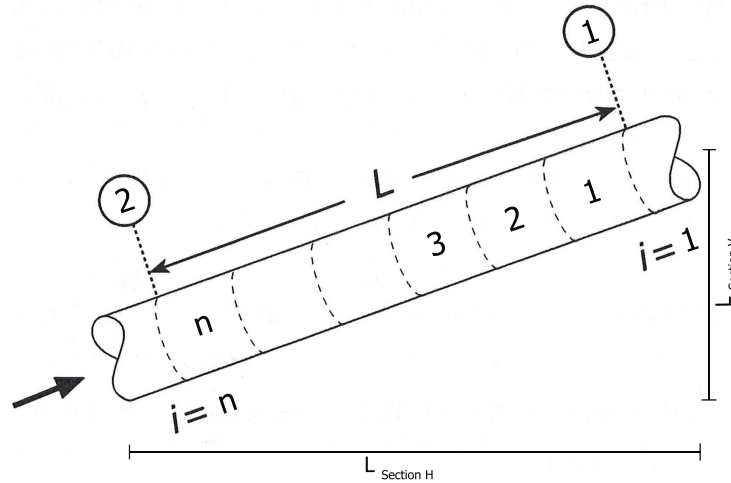
Figure 7.3: Segment divided into increments.

liquid flow rate and producing gas oil ratio are first converted from SI units to English units. The Fluid-Property-Module then works with the English units before converting the return values to SI units again.

Table 7.1: Fluid property submodules.

Module	Return parameters
OilFormationVolumeFactor	$\gamma_{G100}, R_s, p_b, B_O, C_0, B_{Ob}$
SpecificGasGravity	γ_{Gd}, γ_{Gf}
OilDensity	ρ_O
OilViscosity	μ_O
OilSurfaceTension	σ_O
WaterFormationVolumeFactor	B_W
WaterProperties	$\rho_W, \mu_W, \sigma_W, R_{sW_b}$
GasDeviationFactor	Z
GasProperties	ρ_G, μ_G, B_G
ThermalConductivity	k_W, k_O, k_G, k_L
SpecificHeatCapacity	cp_W, cp_O, cp_G, cp_L
HeatofVap	ΔH_{vap}

7.7   Multiphase-Flow-Module

The mainmodule in the Multiphase-Flow-Module can be seen as an umbrella, spanning over the several submodules. As it is given by the Petals and Aziz model, at first the stability of the flow pattern is examined before the pressure drop and liquid hold up are calculated, depending on the prevailing flow pattern. Therefore the submodules in the Multiphase-Flow-Module can be organized in two module categories, the Flow-Pattern-Modules and the

Pressure-Loss-Modules. For each flow pattern, defined by Petalas and Aziz, there are at least two modules, one calculating the parameters to check the stability of the flow pattern and one to calculate the pressure drop and liquid hold up.

In the mainmodule the submodules are called and the stability criteria as stated by Petalas and Aziz are checked with the returned values from the respective Flow-Pattern-Module. If the criteria are fulfilled the Pressure-Loss-Module of the flow pattern is called, otherwise the next criteria is reviewed. The output values of the Multiphase-Flow-Module to the Frame-Module are the flow pattern, the pressure drop $\frac{dp}{dL}$ and the liquid hold up E_L of the increment. In Fig. 7.4 the flow chart of the Multiphase-Flow-Module is presented. The modules with a short description and notes are presented next:

DispersedBubbleFlow To check the stability of the dispersed bubble flow pattern the liquid volume fraction in the slug E_{LS} and C_G are calculated and returned.

PHDispersedBubbleFlow If the dispersed bubble flow pattern is found to be stable, this module calculates the pressure drop and the liquid hold up for dispersed bubble flow. In this module the function to calculate the Colebrook friction factor is defined. The function uses fixed point iteration to solve the equation. In Appendix A (Sec. A.2) the code of the function is presented.

StratifiedFlow To determine the liquid height, the combined momentum balance equation has to be solved with an iterative procedure. At first the functions for the necessary variables, like the geometric relations are programmed. Afterwards all the functions are included in one function, which takes the liquid height as an input parameter besides others and the output parameter is the value, calculated with the combined momentum balance equation. The iterative procedure is explained in Sec. 7.9 . With the liquid height v_G^* and v_L^* are determined and returned to the Multiphase-Flow-Module. Moreover the determined liquid height is returned as well, because it will be needed to calculate the pressure drop.

PHStratifiedFlow As it is mentioned in Sec. 4.3.2.2 , the pressure drop could be calculated either from Eq. 4.3 or Eq. 4.4 . The iterative determination of the liquid height is not an exact procedure. This means, that the value, returned by the function defined in the previous section, will never become 0. Thus the pressure drops, calculated from the equations, cannot have exactly the same value. To overcome this inaccuracy the arithmetic mean is chosen as output pressure drop.

AnnularFlow The calculation procedure for the liquid film thickness is the same as for the liquid height in stratified flow. To check the stability of annular flow the minimum film height has to be determined next. Therefore an additional module designated as AnnularFlowStability, is programmed, which calculates the minimum liquid film thickness iteratively as well.

PHAnnularFlow The liquid hold up is calculated with the determined liquid film thickness. Two equations can be used to calculate the pressure drop, which is why the arithmetic mean of those values is selected again.
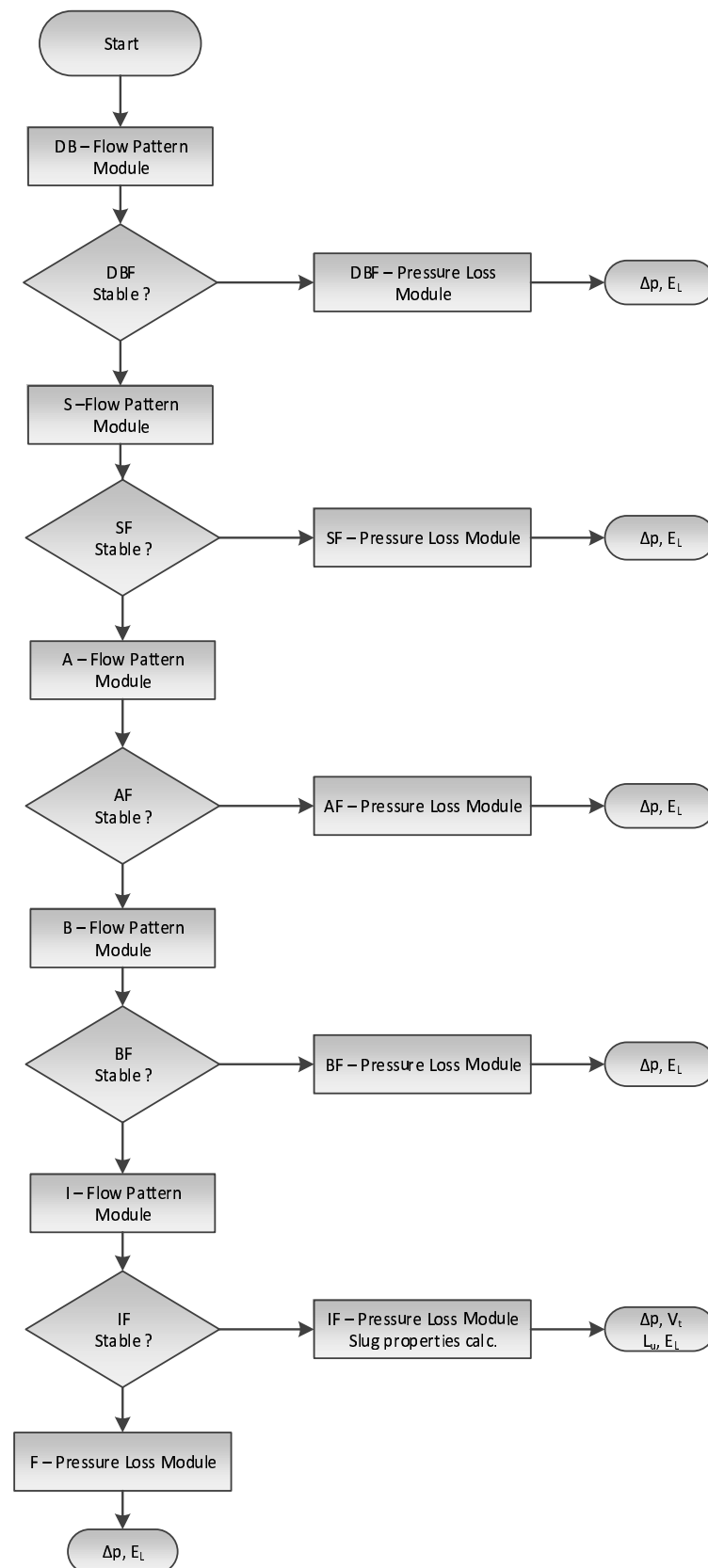
Figure 7.4: Flow chart of the Multiphase-Flow-Module.

BubbleFlow For checking the stability of the bubble flow pattern, the critical angle, critical diameter and the liquid hold up in the slug flow regime are determined in this module. The functions, needed for determining the liquid hold up in the slug flow regime, are programmed in the module IntermittentFlow and just called here.

PHBubbleFlow If the bubble flow pattern is found to be stable, this module calculates the pressure drop and the liquid hold up in a straight forward manner.

IntermittentFlow To determine the stability of intermittent flow, the liquid hold up is calculated first. The slug liquid hold up is calculated next to distinguish between slug flow and elongated bubble flow.

PHIntermittentFlow The liquid hold up is already calculated in the module IntermittentFlow. The pressure gradient is calculated here and returned to the Multiphase Flow Module. If intermittent flow is found to be stable the slug properties are returned to the Output-Interface.

7.8 Heat-Loss-Module

The Heat-Loss-Module is used to determine the temperature at the inlet of the increment. Fig. 7.5 shows the flow chart of the Heat Loss Module. At first the Fluid-Property-Module is called to determine the fluid properties at T_{Outlet} and p_{Outlet}. With these values first each heat transfer coefficient is calculated and then combined to the total heat transfer coefficient. In Eq. 5.5 , one can see that the dynamic viscosity at the pipe wall is needed. To calculate this value, the fluid temperature at the inner pipe wall would be required. An additional iterative procedure with a high risk not to converge would be needed. Thus the temperature at the inner pipe wall is set equal to the temperature at the outer pipe wall. Of course it is known, that these temperatures are not the same. On the one hand it is assumed, that the difference between these two temperatures is small, thus not effecting the calculation of the dynamic viscosity too much and on the other hand another time consuming iterative procedure shall be avoided. Therefore this inaccuracy is accepted. With the total heat transfer coefficient the heat flow between the fluid and the surrounding is calculated now.
The next step is to calculate the enthalpy at the inlet and at the outlet of the increment. The temperature T_{Outlet} and the pressure p_{Outlet} are already known. To calculate the fluid properties and in the sequel the enthalpy value at the increment inlet, the temperature T_{Inlet} must be assumed first. As a first guess the temperature at the inlet is set to T_{Outlet}. Now the overall heat balance is solved. If the correct temperature is assumed, the heat balance is fulfilled.
The above described procedure is put in one function again, which has the temperature T_{Inlet} as the variable input parameter and returns the value from the heat balance. The temperature at the end of the increment is determined with an iterative procedure.

7.9 Numerical methods

In the previous sections it was mentioned several times, that an iterative procedure must be used to find the root of a function. In Fig. 7.6 the combined momentum balance equation
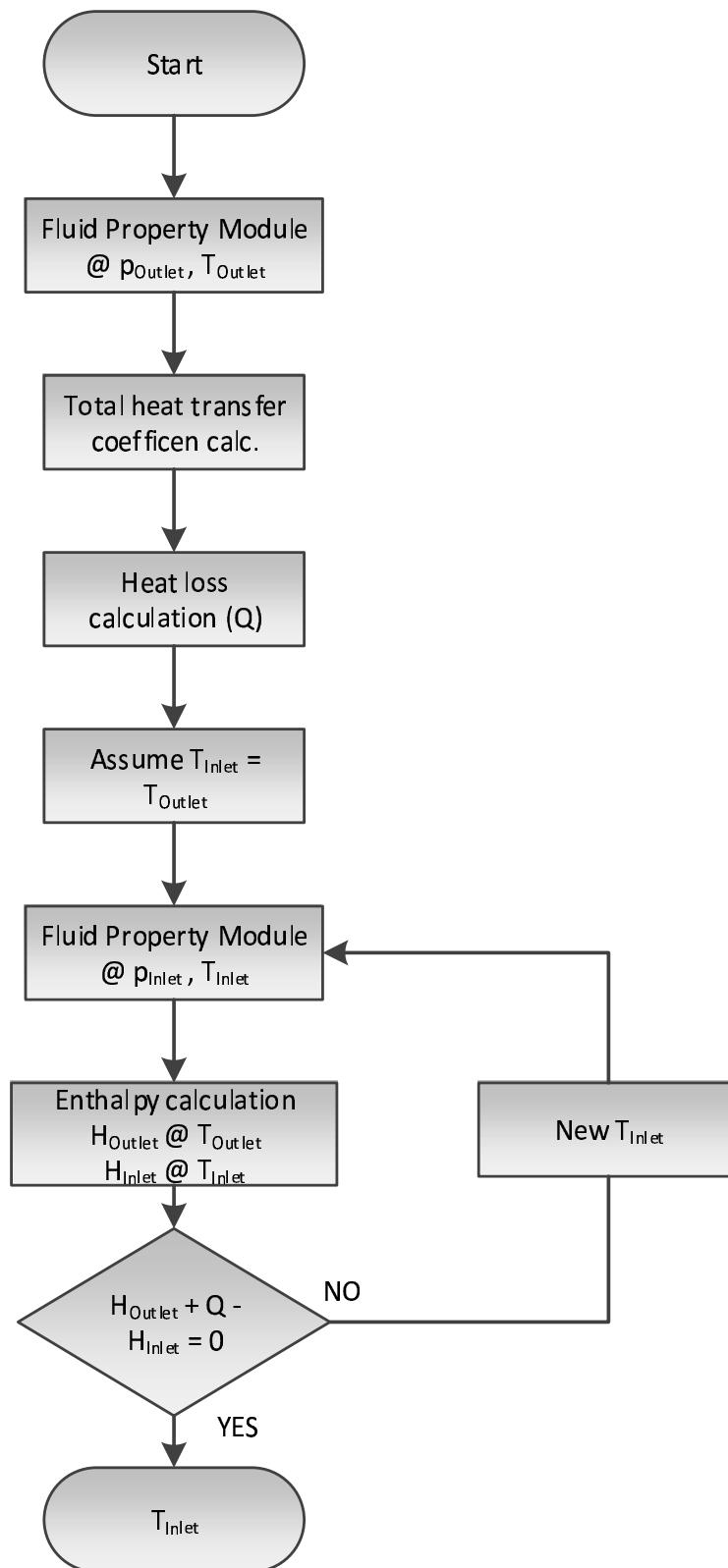
Figure 7.5: Flow chart of Heat Loss Module.

for stratified flow as a function of the dimensionless liquid height is presented as an example. The root must be obtained by successive approximations beginning with an initial estimate. In the literature a large number of methods are presented to obtain the roots of a function.[55]
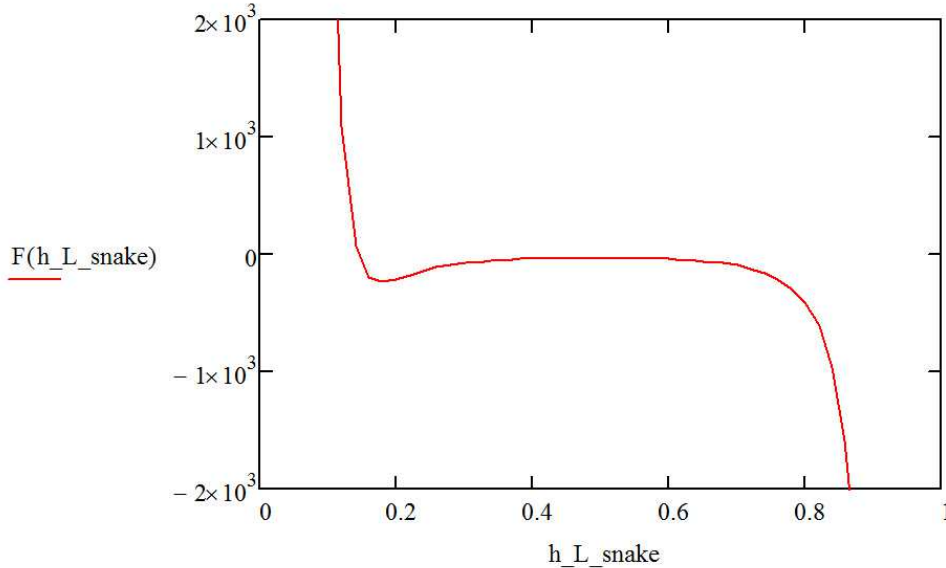

Figure 7.6: Plot of the combined momentum balance equation for stratified flow as a function of the dimensionless liquid height.

The first iteration method, that was taken into account, was the regula falsi, which is a combination of the bisection method and the secant method. In Fig. 7.7 the graphical procedure of this method is presented. At first one has to find two values x_0 and x_1 so that $f(x_0)$ and $f(x_1)$ are of opposite sign. Thus it is ensured, that at least one root is between these values. Now the interval, which contains the root is shrunk by determining a new value for x_1. This is done by drawing the secant through $(x_0, f(x_0))$ and $(x_1, f(x_1))$. The intersection with the x-axis is the new value x_2. The equation for the intersection is presented by Eq. 7.1 .[55]

$$x_2 = x_1 - f(x_1)\frac{x_0 - x_1}{f(x_0) - f(x_1)} \tag{7.1}$$

Now the value of $f(x_2)$ is determined. If the value is positive, x_2 and x_1 are used to repeat the process. Otherwise x_2 and x_0 are used. The process is repeated till the intersection is sufficiently close to the root.[55]

In Fig. 7.7 , it can be seen that for the presented function only one boundary $(x_1, x_2, ...)$ is changing, why it might take a long time to approach the root. Thus the regula falsi is improved leading to the Pegasus algorithm. Fig. 7.8 shows the graphical procedure of this method. The difference is, that a factor γ_i (Eq. 7.2) is defined, $f(x_{i-1})$ is multiplied with. Thereby it is ensured that both boundaries are moving closer to the root. The equation for the intersection is now modiefed to Eq. 7.3 .[55]

$$\gamma_i = \frac{f(x_i)}{f(x_i) + f(x_{i+1})} \tag{7.2}$$

$$x_2 = x_1 - f(x_1)\frac{x_0 - x_1}{\gamma_i f(x_0) - f(x_1)} \tag{7.3}$$
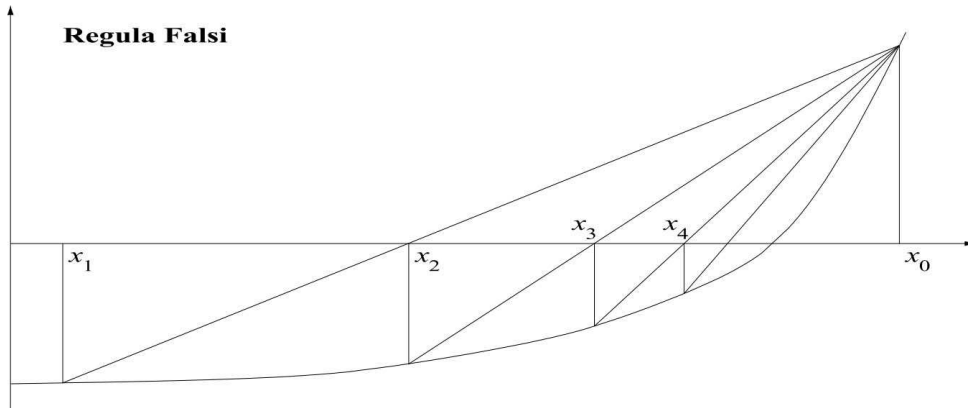
Figure 7.7: Graphical procedure of the regula falsi.
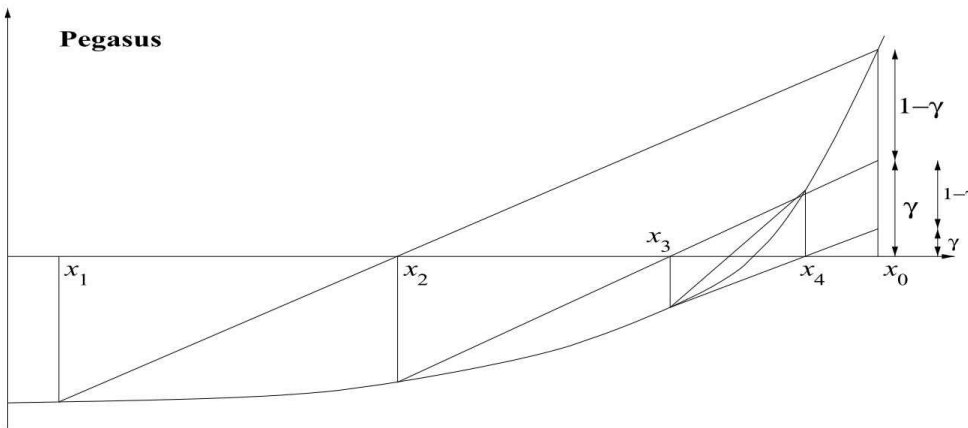
Figure 7.8: Graphical procedure of the Pegasus algorithm.

In SEM-Flow the Pegasus algorithm is used to obtain the roots of several functions. The code for determining the liquid height in stratified flow is presented in Appendix A (Sec. A.3).

At first the starting values x_0 and x_1 have to be determined. It is known, that $\tilde{h}_L$ can only take values between 0 and 1. Thus the lower boundary is set to 0.000001 and the upper boundary is increased by 0.01 till $f(x_0)f(x_1) < 0$ (line 15 to 45). If the starting values are too far apart from each other, problems with the Pegasus algorithm can occur and the time to obtain the root is increased dramatically. Thus the value of the lower boundary is increased by 0.001 as long as $f(x_0)f(x_1) < 0$ (line 49-63).

Having determined the starting values, the Pegasus algorithm can be applied now (line 77 to 120). With the values $f(x_0)$ and $f(x_1)$ the interception is calculated and the boundary values for the next iteration loop are defined. The loop is repeated till the exit condition (line 120) is fulfilled. Two possible exit conditions are defined. The first one is $f(x_n) < 0.0001$. This means, that the value, calculated by the combined momentum balance equation, is almost 0. Sometimes it can happen, that x_n is not changing its value any more and no better approximation of the liquid height can be obtained. Therefore a second exit condition is implemented. The last ten values of x_n are saved to the array $x()$ (line 107). If the sum of the deviations is smaller than 10^{-10} the second exit condition is fulfilled.

Chapter 8

SEM-Flow simulation results validation

The validation of SEM-Flow is done by comparing the results to the results from a commercial simulation software, Aspen Hysys. At first the fluid properties and afterwards the results from the multiphase flow calculation are reviewed. The results and their interpretation are presented in the present chapter.

8.1 The validation approach

To validate the results from SEM-Flow the simulation software Aspen Hysys is used. It must be stated here that, although it is a recognized and widely used engineering simulation tool, it is as well just a model to describe real processes. For a rigorous verification of the developed program, SEM-Flow, field tests and laboratory experiments would have to be conducted, which is however beyond the scope of this thesis. Thus, the results presented in this section are the deviations between two models, but should not be misunderstood as an error between SEM-Flow and the reality. Nevertheless the validation can show, whether the SEM-Flow simulation results have a reasonable deviation and show a similar tendency.

The validation of SEM-Flow is divided into two parts. At first the Fluid-Property-Module is checked, comparing values, such as oil density at different fluid compositions and in dedicated pressure and temperature ranges between SEM-Flow and Aspen Hysys. Afterwards the functionality of the entire program is evaluated by comparing the pressure drop, the temperature loss and the multiphase flow parameters over the whole pipeline.

8.2 Aspen Hysys

Aspen Hysys is a powerful engineering simulation software, that enables the user to model and optimize several process plants. Hysys uses thermodynamic models to predict the properties of fluid mixtures ranging from well defined light hydrocarbon systems to complex oil mixtures. The so called Pipe Segment Operation enables the user to simulate a wide variety of piping situations such as single or multiphase flow. It offers a heat transfer estimation and several pressure drop correlations. In Tab. 8.1 the correlation models, available in Aspen Hysys are listed. Additionally the model applicability to horizontal and vertical flow is presented. It is possible to select different calculation models for horizontal, vertical and inclined pipe flow.[19]

Table 8.1: Available pressure drop calculation models in Aspen Hysys.[19]

Model	Horizontal Flow	Vertical Flow
Aziz, Govier and Fogarasi	NO	YES
Baxendell and Thomas	Use with care	YES
Beggs and Brill (1973)	YES	YES
Beggs and Brill (1979)	YES	YES
Duns and Ros	NO	YES
Gregory, Aziz, Mandhane	YES	NO
Hagedorn and Brown	NO	YES
HTFS Homogeneous	YES	YES
HTFS Liquid Slip	YES	YES
Olgas2000	YES	YES
Orkisewski	NO	YES
Poettman and Carpenter	NO	YES
Tulsa 99	NO	YES
Tulsa unified model (2-Phase)	YES	YES
Tulsa unified model (3-Phase)	YES	YES

8.3   Fluid property validation

To evaluate the accuracy of the fluid property prediction by SEM-Flow it was the aim to cover a broad range of temperature, pressure and fluid composition combinations. This approach makes it possible to determine the acceptable working area of the Fluid-Property-Module. According to its API gravity, crude oil can be classified as light oil, medium oil and heavy oil. The same classification can be applied to gases according to the specific gas gravity. For the first three fluid combinations a heavy, medium and light oil is combined with a medium gas. The second three combinations combine a medium oil with a heavy, medium and light gas. In Tab. 8.2 and Tab. 8.3 the six fluid combinations are summarized. These six cases are set up in Aspen Hysys by combining a gas stream, an oil stream and a water stream with a Mixer Operation, thereby producing a single outlet stream. An example of this setup is presented in Fig. 8.1 . The Peng-Robinson equation of state is used as the thermodynamic model in Hysys.

The pressure is varied from 10 to 40 bara using a step of 10 bar and for each pressure the temperature is varied from 10 to 80 °C using a step of 10 °C. Thereby for each fluid property 192 cases are set up, resulting in 192 data points, that are used for the evaluation.

8.3.1   Results

The deviation between SEM-Flow and Hysys is calculated in percent first. Eq. 8.1 shows this calculation at the example of the oil density. Afterwards the absolute maximum, the absolute minimum and the average deviation are determined for each fluid property. The average deviation is calculated after Eq. 8.2 . Additionally the number of values which
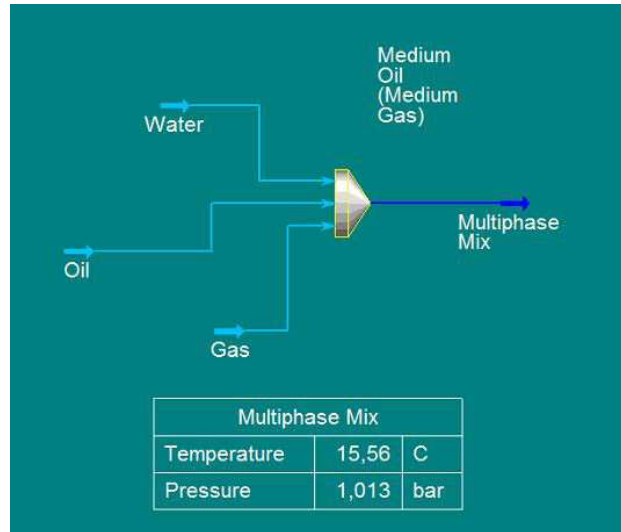
Figure 8.1: Mixer Operation in Aspen Hysys.

Table 8.2: Fluid combinations with varying API gravities. (LO=light oil, MO=medium oil, HO=heavy oil, MG=medium gas)

Combination	LO - MG	MO - MG	HO - MG	Unit
γ_{API}	48.63	35.15	21.02	$[°API]$
γ_G	0.60	0.60	0.58	$[-]$
T_{sep}	15.56	15.56	15.56	$[°C]$
p_{sep}	1.01	1.01	1.01	$[bara]$
R_p	1112.60	716.13	342.91	$[Sm^3/m^3]$
f_W	0.89	0.84	0.72	$[-]$
q_L	6788.86	7196.1	8432.23	$[Sm^3/d]$
S	0.00	0.00	0.00	$[\%]$

Table 8.3: Fluid combinations with varying specific gas gravities. (LG=light gas, MG=medium gas, HG=heavy gas, MO=medium oil)

Combination	LG - MO	MG - MO	HG - MO	Unit
γ_{API}	34.79	36.73	36.11	$[°API]$
γ_G	0.58	0.65	0.75	$[-]$
T_{sep}	15.56	15.56	15.56	$[°C]$
p_{sep}	1.01	1.01	1.01	$[bara]$
R_p	724.36	716.12	694.76	$[Sm^3/m^3]$
f_W	0.84	0.84	0.83	$[-]$
q_L	7185.47	7196.1	7222.19	$[Sm^3/d]$
S	0.00	0.00	0.00	$[\%]$

are underestimated is calculated in percent. Therefrom one can see, if a fluid property is
constantly under- or overestimated.

$$Dev_{\rho_O} = \frac{\rho_{O_{SEM}} - \rho_{O_{Hysys}}}{\rho_{O_{Hysys}}} * 100 \tag{8.1}$$

$$\overline{Dev}_{\rho_O} = \frac{1}{n} \sum_{i=1}^{n} |Dev_{\rho_O,i}| \tag{8.2}$$

In Tab. 8.4 a summery of the deviations for each fluid property is presented. To get a better
overview where deviations reach critical values, the maximum deviations are presented in
Fig. 8.2 . There it shows, that the deviation for most values is within a range of 20%, which
presents an acceptable value. Fluid properties with a higher deviation are the oil viscosity,
the gas/oil surface tension and the gas and water thermal conductivity. To make a qualified
statement, it is however not enough to take the maximum deviation values into account
only. It could happen, in case of the oil viscosity for example, that just a few data points
have a large deviation. In this case it would be a misinterpretation to assume that this
value is predicted with that large deviation over the whole pressure and temperature range.
Thus the average deviation has to be reviewed as well. From Fig. 8.3 it can be seen, that
the average deviation for the before mentioned properties, is constantly smaller than the
maximum deviation. In case of the oil viscosity, the average deviation (31%) is relatively
small compared to the maximum deviation (123%). Therefore it is assumed, that only a few
data points have that big deviation, which would make it possible to define a working area,
in which the deviation is within an acceptable range. Thus further evaluation of the fluid
properties with large deviations is conducted in the present section.

8.3.1.1   Oil density

To evaluate, what the deviations of the properties depend on mostly, the deviation is plotted
over temperature for the several pressures and fluid compositions. To have the opportunity
to compare a property with a marginal deviation and those with higher deviations, the oil
density is reviewed first which has a maximum deviation of 4%.
In Fig. 8.4 the deviation is plotted over temperature for a constant gas and varying oil
compositions. For the same API gravity the deviation is in the same range for all pressures,
whereby the fluid combination with the medium API gravity has the lowest deviation over
the whole pressure and temperature range. The temperature has the largest influence on the
deviation of the results for all fluid compositions. The presentation of the other properties
with low deviations can be found in Appendix C.
When keeping the oil composition constant with a varying gas composition (Fig. 8.5), a
similar behavior can be observed. For the same specific gas gravity the deviation is in the
same range and temperature has a greater influence again. The smallest average deviation
is found for the gas with the lowest specific gas gravity.

8.3.1.2   Oil viscosity

The oil viscosity has a maximum deviation of 123%, occuring with a medium API gravity
and high specific gas gravity at $10°C$. Fig. 8.6 shows that the deviation is hardly influenced
by the gas composition at high temperatures. At low temperatures however, the deviation
increases as specific gas gravity increases. The smallest deviation for the whole temperature

Table 8.4: Summary of deviations for each fluid property.

Fluid property	Maximum deviation [%]	Minimum deviation [%]	Average deviation [%]	Underst. [%]
Gas density	17.75	-0.016	3.72	11.98
Oil density	4.28	0.012	1.32	51.56
Water denstiy	-1.74	-0.018	0.73	75.00
Gas viscosity	-6.76	0.0049	1.95	67.93
Oil viscosity	123.07	0.058	31.83	75.00
Water viscosity	11.38	5.23	8.89	0.00
Actual vol. gas flow rate	7.21	0.027	2.43	13.021
Actual vol. oil flow rate	-15.44	0.019	4.39	69.27
Actual vol. water flow rate	-1.985	0.031	1.02	87.50
Gas/oil surface tension	-53.85	0.77	26.30	99.48
Gas/water surface tension	-10.503	-4.24	7.86	100.00
Gas spez. heat capacity	6.66	0.0011	2.09	79.69
Oil spez. heat capacity	-5.22	-1.33	3.53	100.00
Water spez. heat capacity	-3.18	-0.002	1.23	68.23
Gas thermal conductivity	87.95	5.012	41.29	0.00
Oil thermal conductivity	20.048	0.018	6.17	28.65
Water thermal conductivity	-45.013	-7.085	26.58	100.00
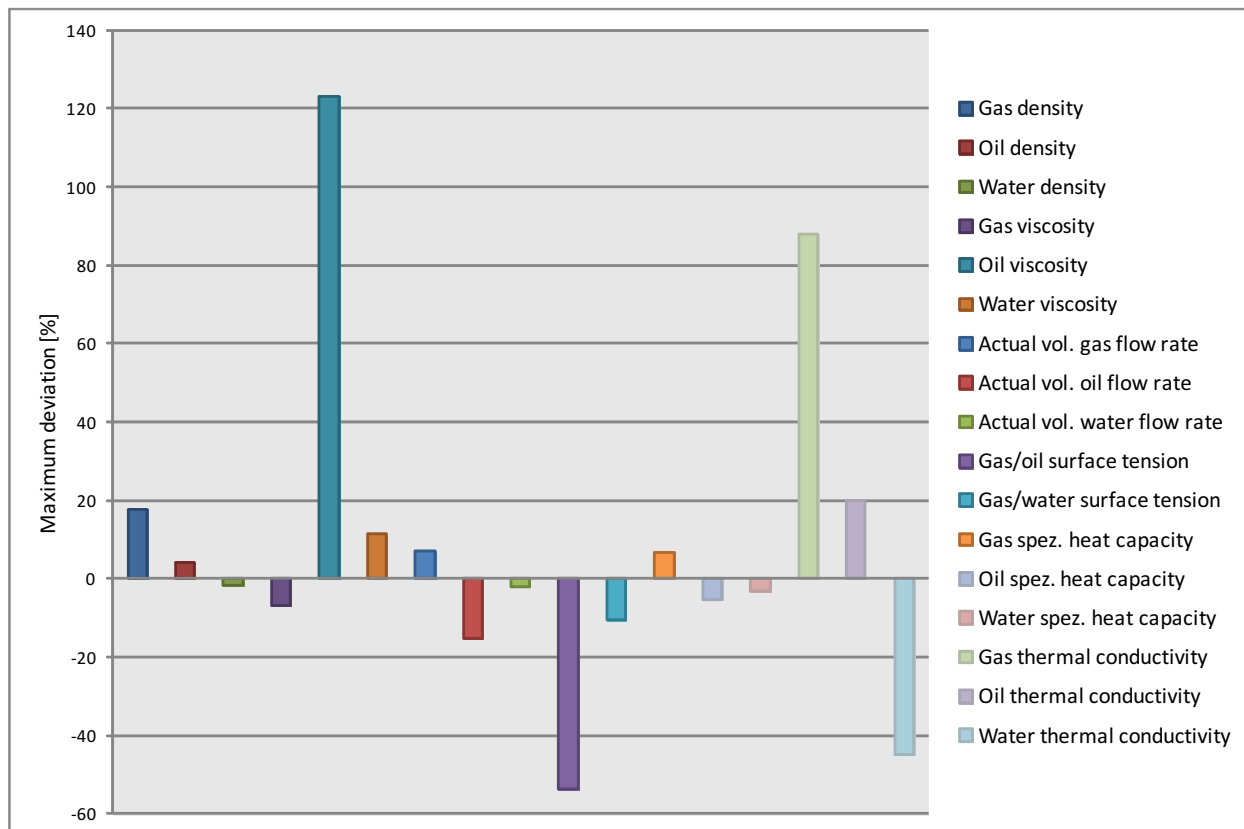
Figure 8.2: Maximum deviations of the fluid properties.
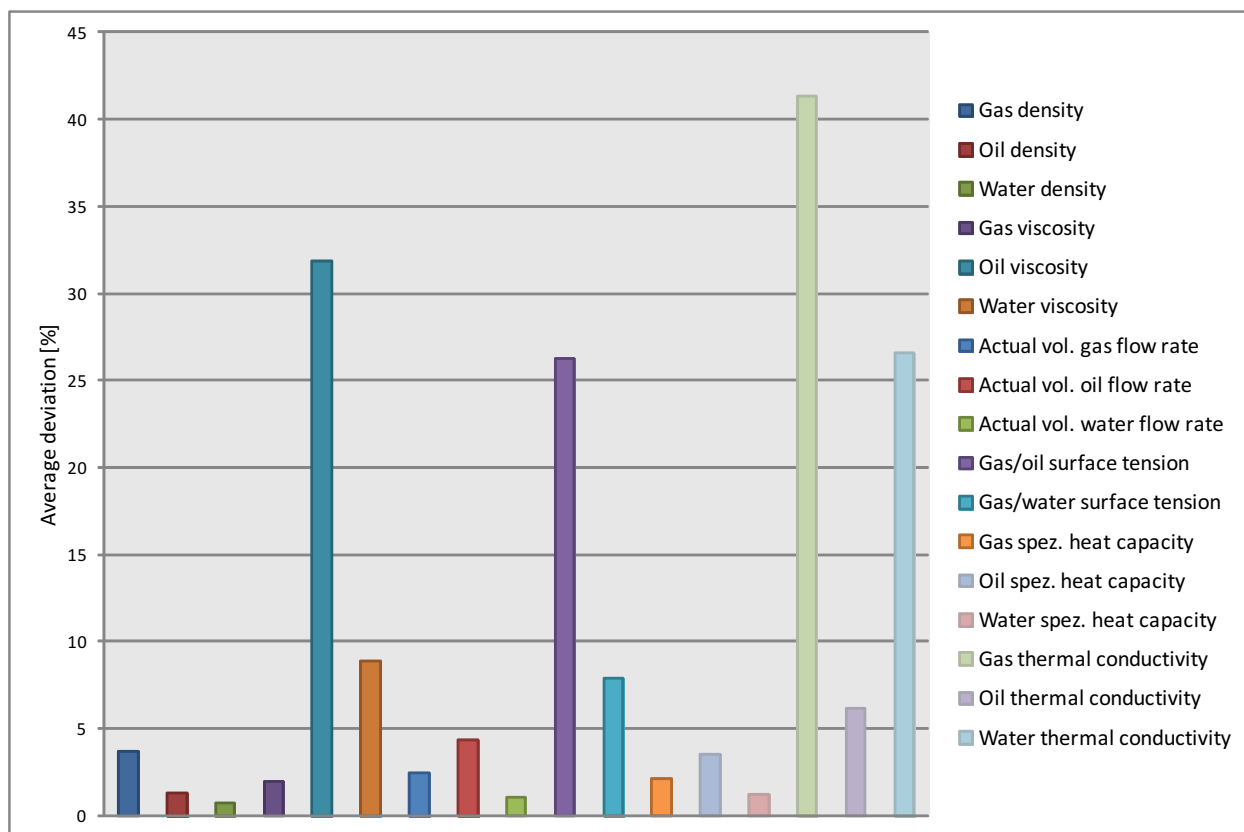
Figure 8.3: Average deviations of the fluid properties.
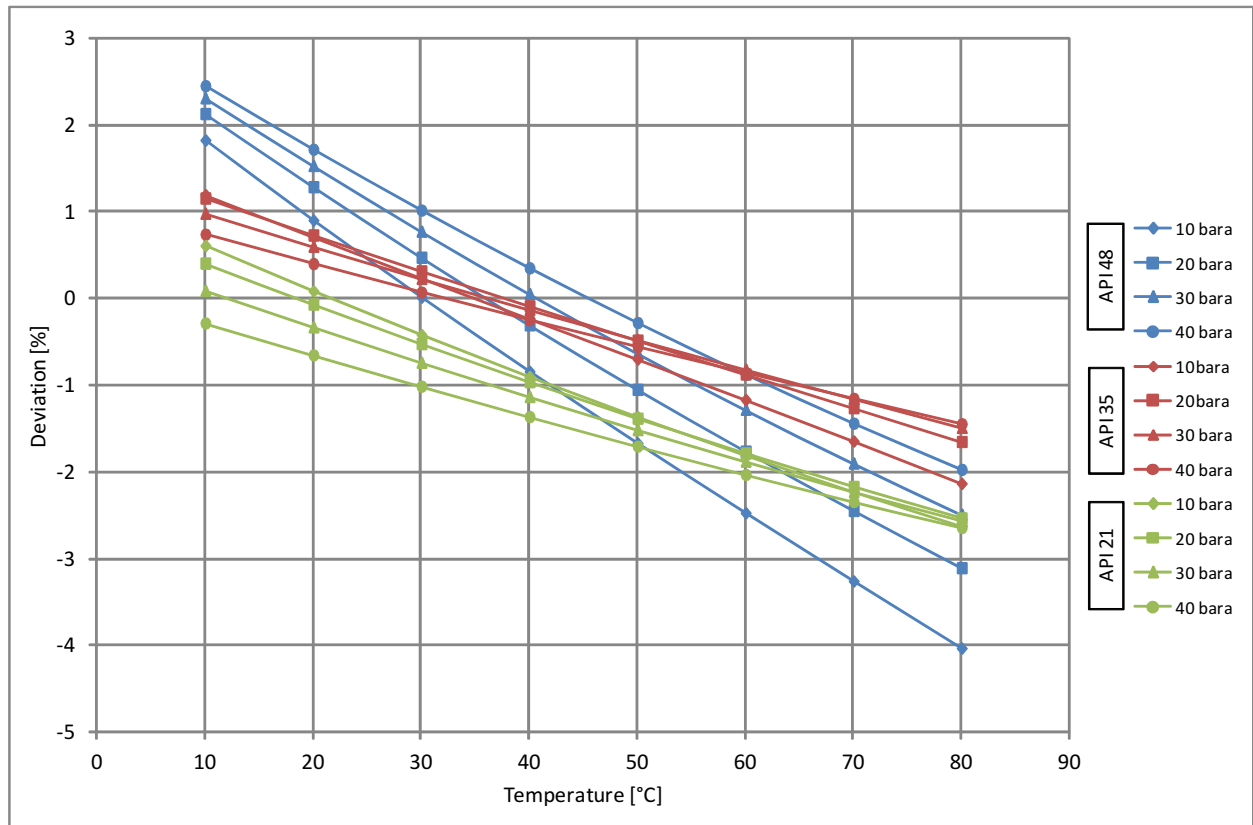
Figure 8.4: Deviation of the oil density for varying API gravities.
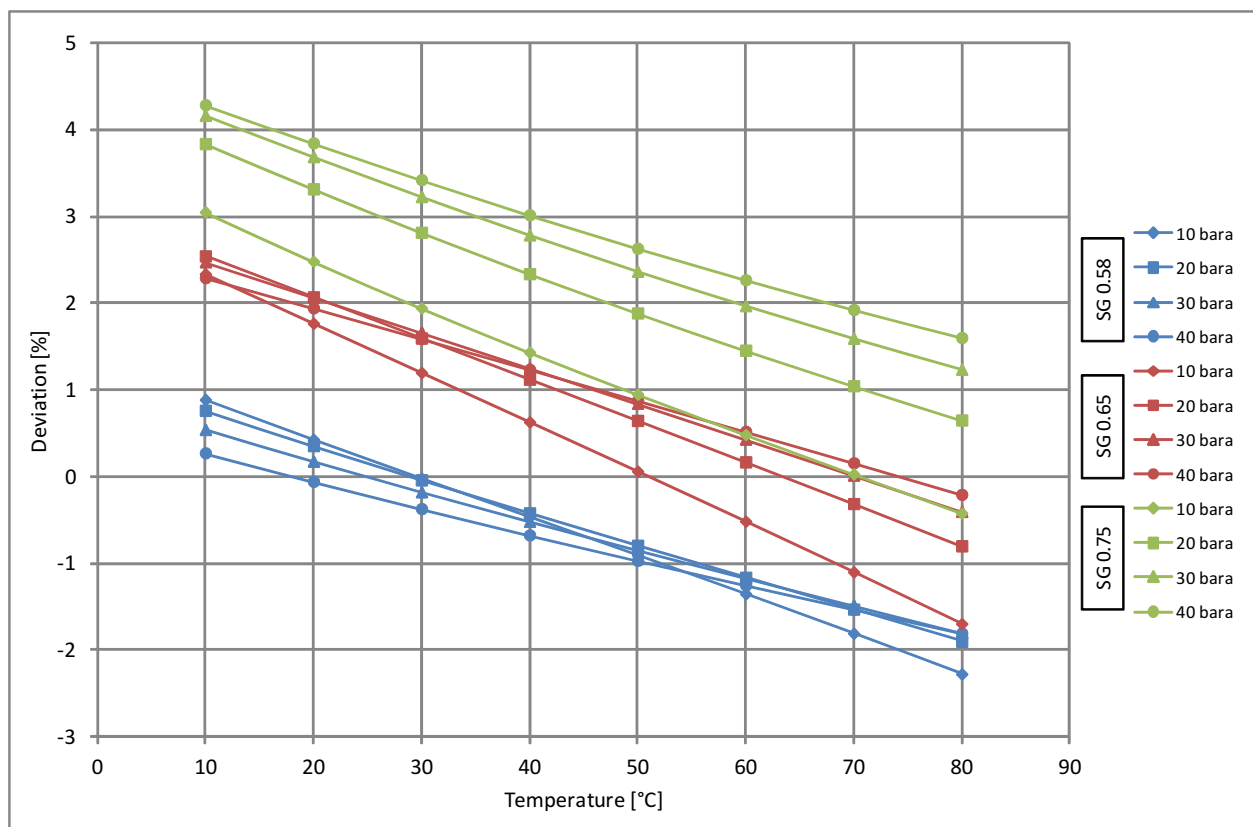
Figure 8.5: Deviation of the oil density for varying specific gas gravities.

and pressure range occurs in case of the medium specific gas gravity. For all gas compositions the smallest deviation is found between 30 and 60 °C.
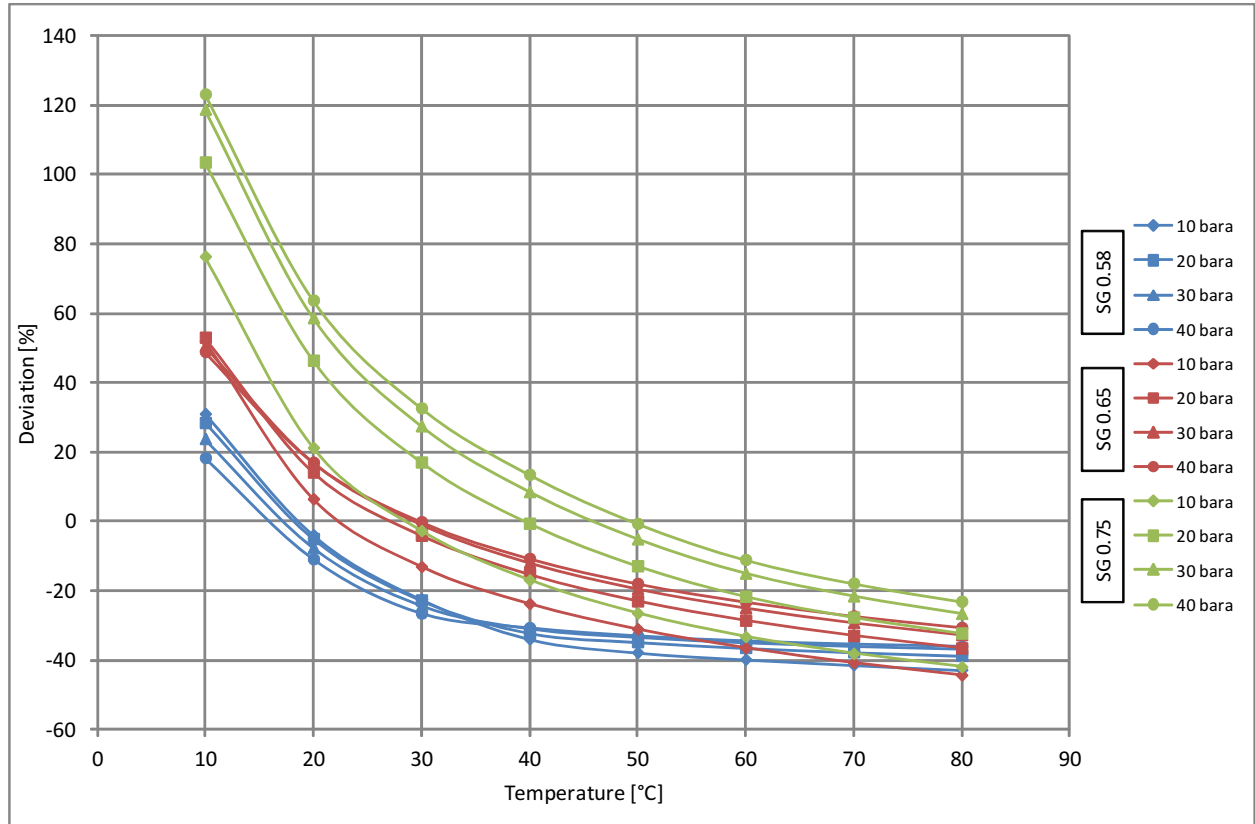
Figure 8.6: Deviation of the oil viscosity for varying specific gas gravities.

In Fig. 8.7 the deviation of the oil viscosity is plotted for variable API gravities. The influence of the pressure on the deviation is negligible, whereas the temperature has a great influence. The smallest average deviation over the whole range of pressure and temperature occurs for oils with a medium and heavy API gravity. The highest deviation occurs at low temperatures again.

8.3.1.3   Oil surface tension

The oil surface tension is underestimated by SEM-Flow compared to Hysys for all ranges of fluid composition, temperature and pressure. In case of a variable API (Fig. 8.8) or specific gas gravity (Fig. 8.9), the shape of the deviation curves is approximately parallel within the same fluid composition group. In case of increasing temperature the deviation decreases. The pressure has a large influence on the deviation, whereby the deviation increases with increasing pressure. The lower the API gravity of the oils and the specific gas gravity of the gases are, the higher the deviation becomes.

8.3.1.4   Water thermal conductivity

Due to the fact, that the water phase is not influenced by the oil and gas composition, the deviation of the water thermal conductivity is independent of API and specific gas gravity (Fig. 8.10 , Fig. 8.10) . The pressure has no influence on the deviation as well. Thus the
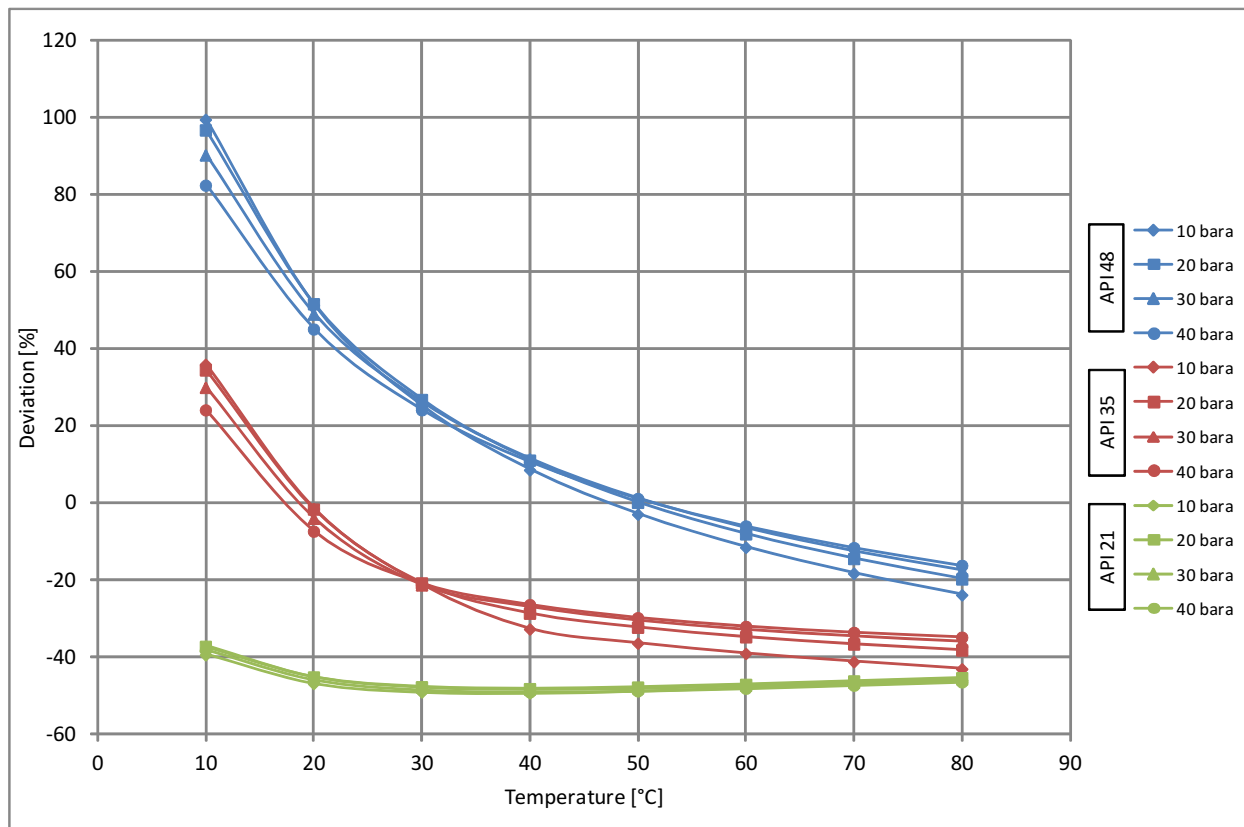
Figure 8.7: Deviation of the oil viscosity for varying API gravities.
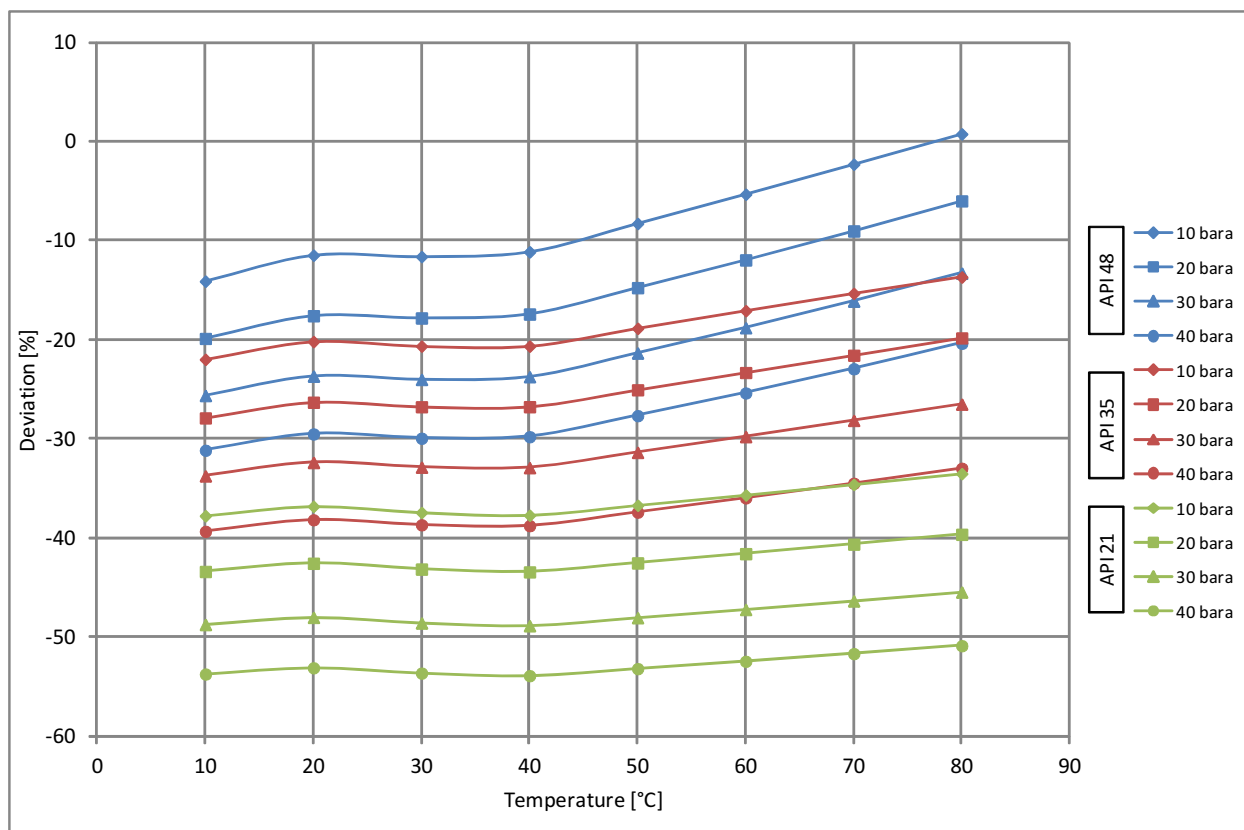
Figure 8.8: Deviation of the oil surface tension for varying API gravities.
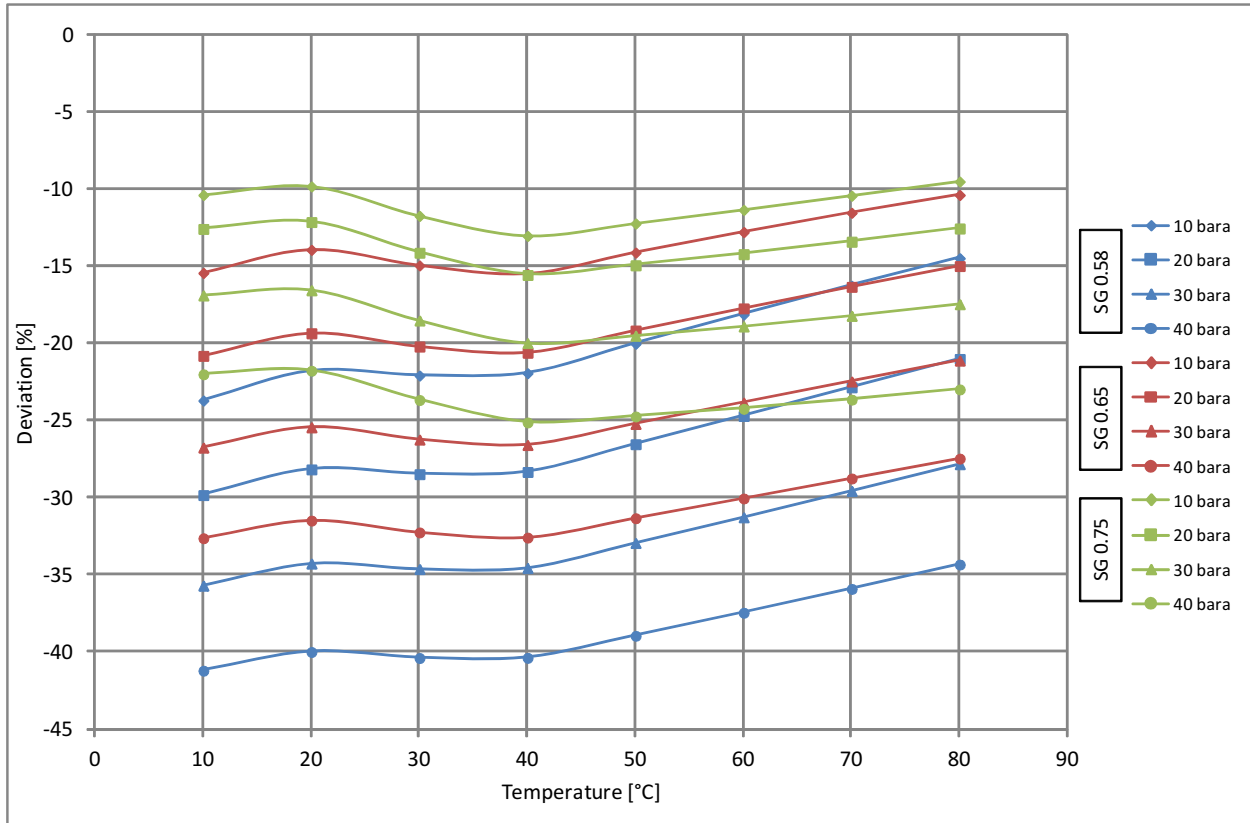
Figure 8.9: Deviation of the oil surface tension for varying specific gas gravities.

deviation is influenced by the temperature only and at low temperatures the best results are achieved.

8.3.1.5   Gas thermal conductivity

Changing the oil composition has a negligible influence on the gas composition. Thus the deviation of the gas thermal conductivity in Fig. 8.12 is almost independent of the API gravity. The temperature has the highest influence and the pressure has a minor influence on the deviation of the gas thermal conductivity. Variable gas compositions of course have an influence on the deviation (Fig. 8.13). With increasing specific gas gravity the deviation of the gas thermal conductivity increases as well.

8.3.2   Conclusion of the fluid property validation

The results of the fluid property prediction are very good for most fluid properties and only a few present larger deviations. By comparing the deviations of the fluid properties in Sec. 8.3 , no general connection between fluid composition and deviation can be found applicable to all properties in the same way. The equations used for the water thermal conductivity in Hysys and SEM-Flow both seem to be independent of pressure and fluid composition. In SEM-Flow the influence of temperature is higher than in Hysys. The water thermal conductivity is included in the liquid thermal conductivity. Thus its influence on the overall simulation results is strongly dependent on the water cut. It is constantly underestimated, which leads to a decrease of the heat transfer coefficient. A small heat transfer coefficient will lower the heat loss over the pipeline.
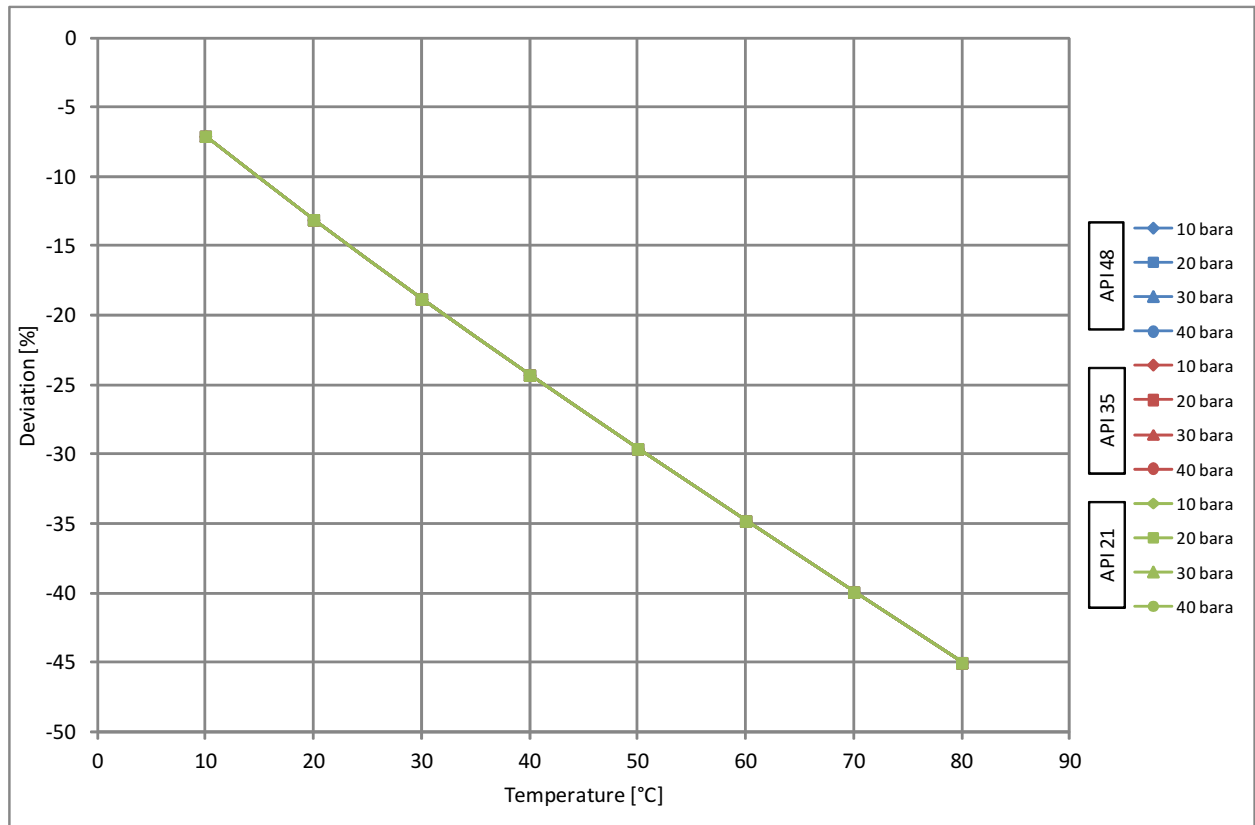
Figure 8.10: Deviation of the water thermal conductivity for varying API gravities.
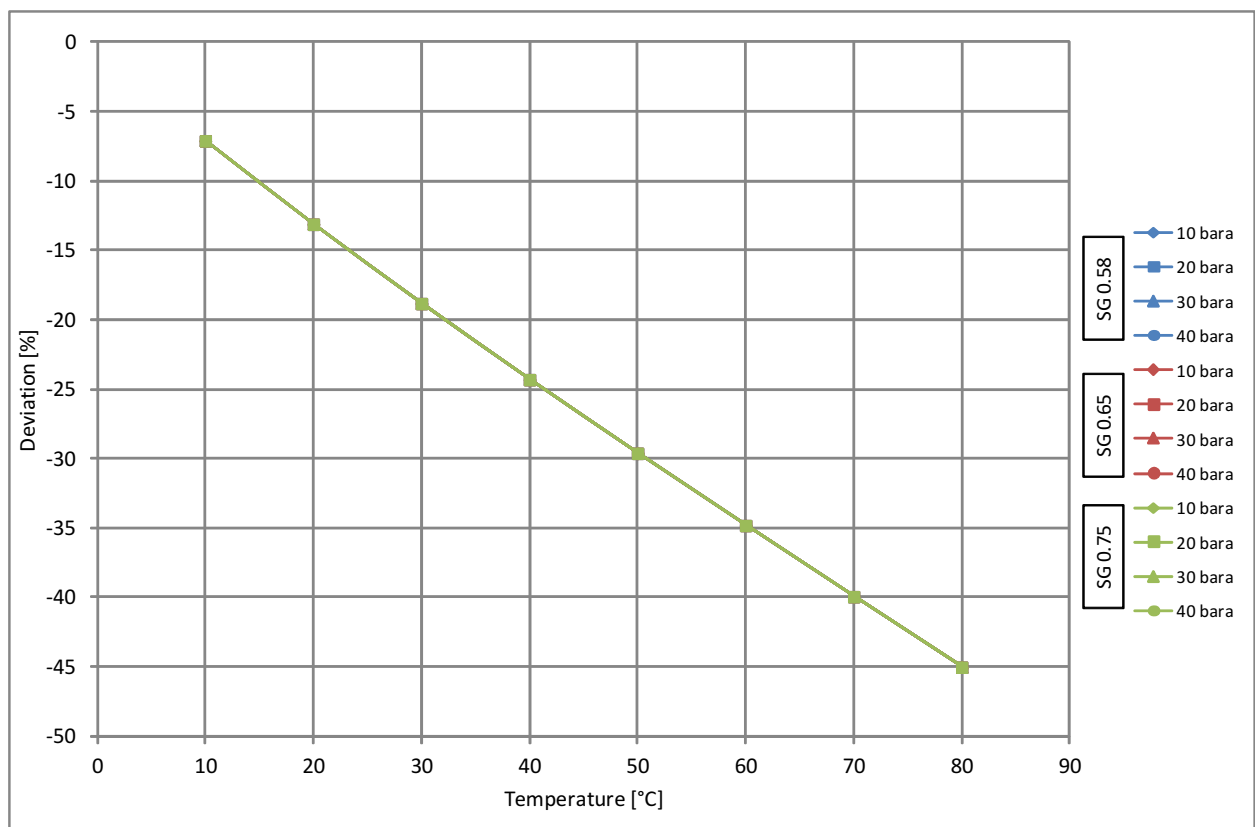
Figure 8.11: Deviation of the water thermal conductivity for varying specific gas gravities.
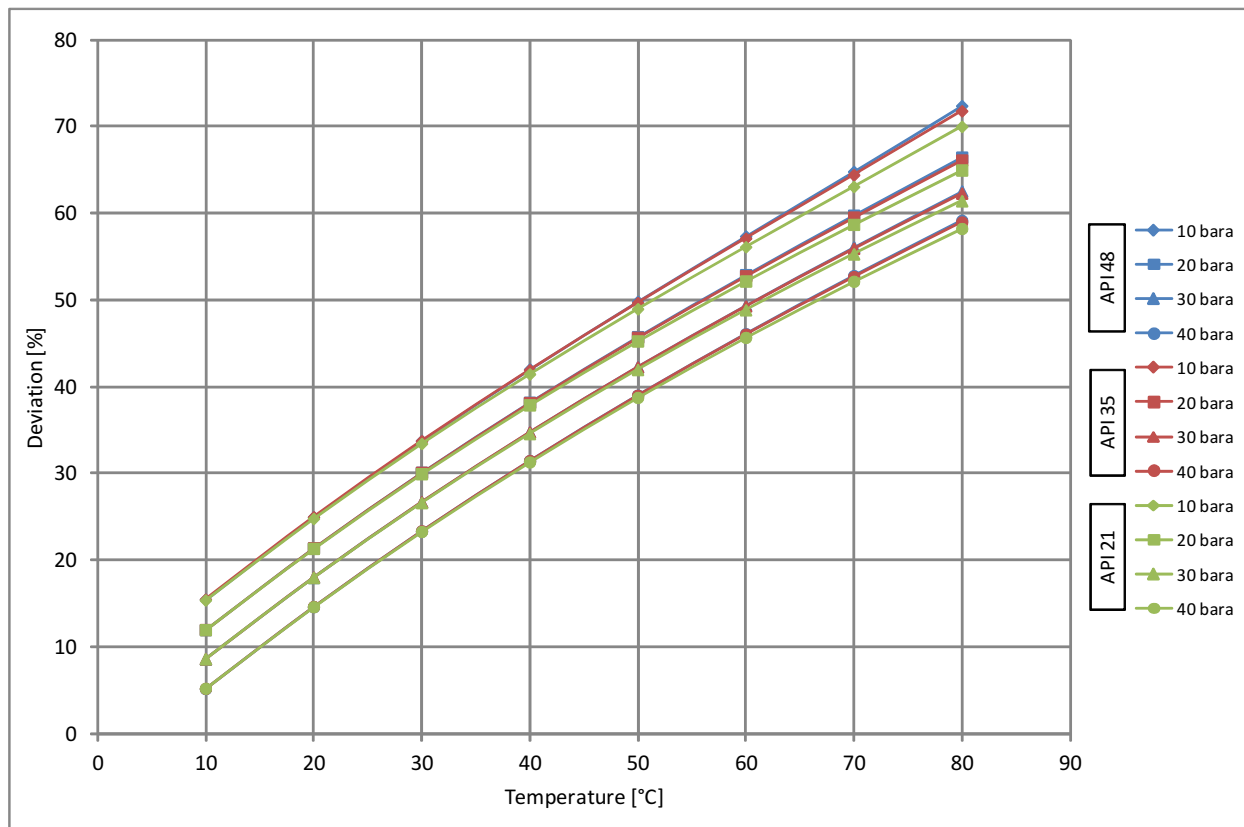
Figure 8.12: Deviation of the gas thermal conductivity for varying API gravities.
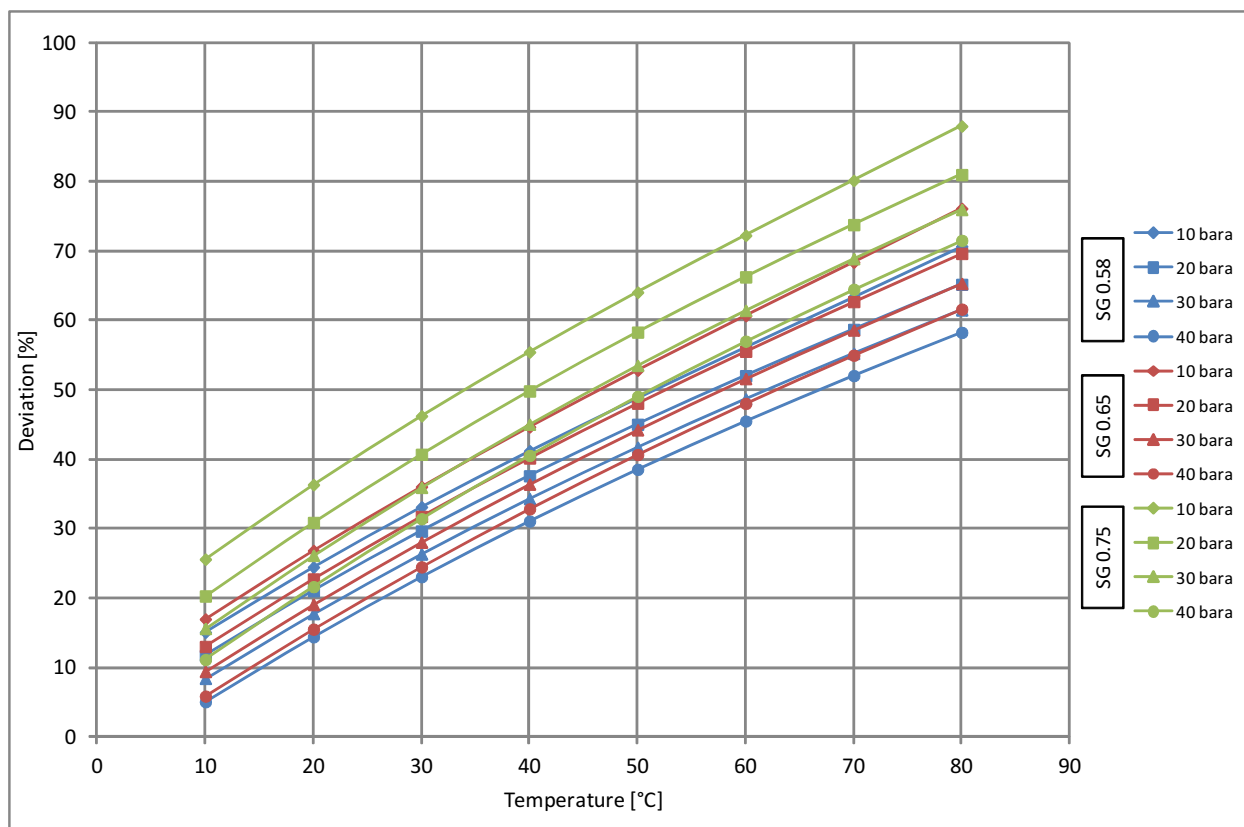
Figure 8.13: Deviation of the gas thermal conductivity for varying specific gas gravities.

The equation, which is used to calculate the gas thermal conductivity (Eq. 6.49) in SEM-Flow, is independent of the gas composition. As seen from Fig. 8.13 this assumption is not permitted due to the fact, that the deviation increases with increasing specific gas gravity. Again the influence of the temperature is weighted in a higher way in SEM-Flow than in Hysys. The gas thermal conductivity influences the heat transfer coefficient between fluid and pipe wall over the Prandl number. It is constantly overestimated by SEM-Flow, which might lead to a lower heat loss over the pipeline again.

It is stated, that the equation used to calculate the oil surface tension can primarily be used between 20 and 38 °C. From Fig. 8.8 and Fig. 8.9 it occurs, that even in this range large deviations occur. It seems as if the deviation decreases for temperatures, higher than 40 °C but increases for temperatures, smaller than 20 °C. The oil surface tension is needed to calculate the liquid surface tension. The influence of the liquid surface tension on the pressure drop or heat loss cannot be derived easily. It is known however, that the surface tension mostly influences the stability of the flow patterns and thus influences the pressure drop as well.

The oil viscosity is influenced by the temperature over the dead oil viscosity. This equation does not seem to be applicable to low temperatures. At 10 °C the deviation is around 100%, whereas for temperatures greater than 30 °C, it decreases to less than 40%. The oil viscosity is used to calculate the liquid viscosity which mainly influences the Reynolds number. The oil viscosity is underestimated at 70%, which increases the Reynolds number. With an increasing Reynolds number the friction factor decreases thereby lowering the pressure drop. With the previous observations it is tried to define a working area by setting a maximum allowable percentage of deviation. For getting a useful working area the maximum deviation is set to 50%. Due to the fact, that the influence of the thermal conductivities is assumed to be small, on the overall simulation result the working area is defined without taking them into consideration. In Tab. 8.5 the temperature and pressure ranges, in which the deviation does not exceed 50%, is presented for each fluid combination. The results, when taking the thermal conductivities into consideration as well, are presented in Tab. 8.6 .

Table 8.5: Working area, in which the deviation is smaller than 50% (excluding the thermal conductivities). (LO=light oil, MO=medium oil, HO=heavy oil, LG=light gas, MG=medium gas, HG=heavy gas)

Combination	p_{min} [bara]	p_{max} [bara]	T_{min} [°C]	T_{max} [°C]
LO - MG	10	40	30	80
MO - MG	10	40	10	80
HO - MG	10	30	10	80
LG - MO	10	40	10	80
MG - MO	10	40	20	80
HG - MO	10	40	30	80

Table 8.6: Working area, in which the deviation is smaller than 50% (including the thermal conductivities). (LO=light oil, MO=medium oil, HO=heavy oil, LG=light gas, MG=medium gas, HG=heavy gas)

Combination	p_{min} [bara]	p_{max} [bara]	T_{min} [°C]	T_{max} [°C]
LO - MG	10	40	30	50
MO - MG	10	40	10	50
HO - MG	10	30	10	50
LG - MO	10	40	10	50
MG - MO	10	40	20	50
HG - MO	10	40	30	50

8.4   Multiphase flow validation

To check the requirements on SEM-Flow, presented in Sec. 2.2 a so called Pipe Segment Operation is used. As can be seen in Fig. 8.14 , the Pipe Segment Operation requires an inlet, an outlet, as well as an energy stream, whereby temperature, pressure and volumetric flow rate must be defined for one stream. The pipe segment, presented on the flow sheet is only a symbol, which can represent a whole pipeline or a single segment. For each segment in the Pipe Segment Operation the diameter, the equivalent length and the elevation change must be entered. Furthermore the pipe flow correlations for horizontal, vertical and inclined pipe segments must be selected.
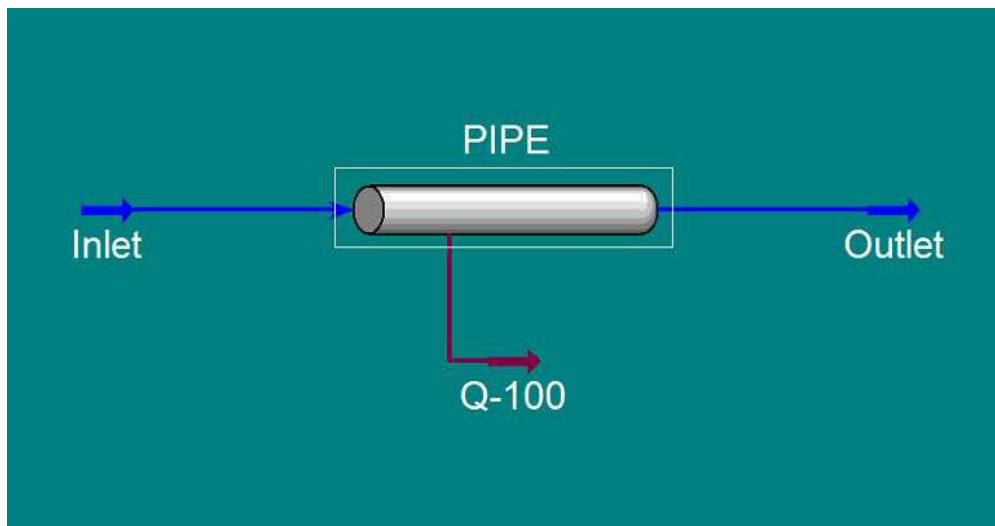
Figure 8.14: Pipe Segment Operation with inlet and outlet stream.

The multiphase flow validation is divided into two parts. First, individual pipe segments and then, a multisegment pipeline are used. In both cases the fluid composition is kept constant. In case of the individual segments, a pipeline with a length of 500 m and a constant diameter is used and the inclination angle is varied between 0 and ± 90 °. The setup is presented in Tab. 8.7 . Furthermore three different flow conditions are set up in the horizontal segment by varying the volumetric gas and liquid flow rates. The input parameters for those three

Table 8.7: Setup for individual pipe segments.

Inclination angle [$grad$]	0	30	60	90	-30	-60	-90
Pipe length [m]	500	500	500	500	500	500	500
p_{Outlet} [$bara$]	20	20	20	20	20	20	20
T_{Outlet} [$°C$]	40	40	40	40	40	40	40
Pipe inner diameter [m]	0.152	0.152	0.152	0.152	0.152	0.152	0.152
Wall thickness [m]	0.01	0.01	0.01	0.01	0.01	0.01	0.01
Pipe roughness [m]	0.0015	0.0015	0.0015	0.0015	0.0015	0.0015	0.0015
Wall thermal cond. [W/mK]	50	50	50	50	50	50	50
Ambient temperature [$°C$]	20	20	20	20	20	20	20
Air velocity [m/s]	1	1	1	1	1	1	1

Table 8.8: Initial flow conditions for individual pipeline profile. (SF=Stratified flow; AF=Annular flow; IF=Intermittent flow

Flow condition	SF	AF	IF	Unit
γ_{API}	35.71	35.45	36.08	[$°API$]
γ_G	0.61	0.59	0.63	[$-$]
T_{sep}	15.56	15.56	15.56	[$°C$]
p_{sep}	1.01	1.01	1.01	[$bara$]
R_p	219.38	1827.52	57.15	[Sm^3/m^3]
f_W	0.025	0.03	0.021	[$-$]
q_L	148.45	1234.61	3180.51	[Sm^3/d]
S	0.00	0.00	0.00	[$\%$]

conditions are presented in Tab. 8.8 .

As it was mentioned earlier, several correlation methods are compared to calculate the properties in the slug flow region. Four different correlation combinations are defined therefore and are presented in Tab. 8.9 .

Table 8.9: Correlation combinations for the slug flow region. (P&A=Petalas and Aziz, P&A comp.=Petalas and Aziz comparison, Xiao=Xiao et al., Xiao comp.=Xiao et al. comparison)

Correlation combination	Pressure drop calculation	Translational velocity	Liquid hold up	Slug length
P&A	After Sec. 4.3.2.5	After Eq. 4.51	After Eq. 4.50 with Eq. 4.51	After Eq. 4.110 to Eq. 4.112
P&A comp.	After Sec. 4.3.2.5	After Eq. 4.106	After Eq. 4.109 with Eq. 4.106	After Eq. 4.110 to Eq. 4.112
Xiao	After Sec. 4.4.1	After Eq. 4.82	After Eq. 4.50 with Eq. 4.82	After Eq. 4.110 Eq. 4.112
Xiao comp.	After Sec. 4.4.1	After Eq. 4.106	After Eq. 4.109 with Eq. 4.106	After Eq. 4.110 to Eq. 4.112

In the second part an elevation profile consisting of eleven connected segments is defined. To push SEM-Flow to its limits an extreme profile is chosen, which contains several steep up- and downward inclined and even a vertical segment. The profile is presented in Fig. 8.15 . It should be mentioned that such a profile is very unlikely to occur in a real case, but it can show the deviations between the models more obviously however. In Tab. 8.10 the setup is presented. A different pipeline inner diameter is chosen to enlarge the reviewed range.

Table 8.10: Setup for multisegment pipeline profile.

Description	Value	Unit	Description	Value	Unit
p_{Outlet}	20	$[bara]$	γ_{API}	35.90	$[°API]$
T_{Outlet}	40	$[°C]$	γ_G	0.61	$[-]$
Pipe inner diameter	0.3084	$[m]$	T_{sep}	15.56	$[°C]$
Wall thickness	0.01	$[m]$	p_{sep}	1.01	$[bara]$
Pipe roughness	0.0015	$[m]$	R_p	125.22	$[Sm^3/m^3]$
Wall thermal cond.	50	$[W/mK]$	f_W	0.03	$[-]$
Ambient temperature	20	$[°C]$	q_L	5811.1	$[Sm^3/d]$
Air velocity	1	$[m/s]$	S	0	$[\%]$

By setting up the Pipe Segment Operation, a pipe flow correlation must be chosen. The available correlations have already been presented in Tab. 8.1 . At first, three correlations are chosen and the pressure drop, calculated with each of them is compared. The deviation between the largest and the smallest pressure drop is 155% as can be seen from Fig. 8.16 . The reason for this deviation is, on the one hand, that different assumptions are made within the different models but, on the other hand, that an extreme pipeline profile and starting pressure are chosen which maximices the differences between the models. To evaluate the
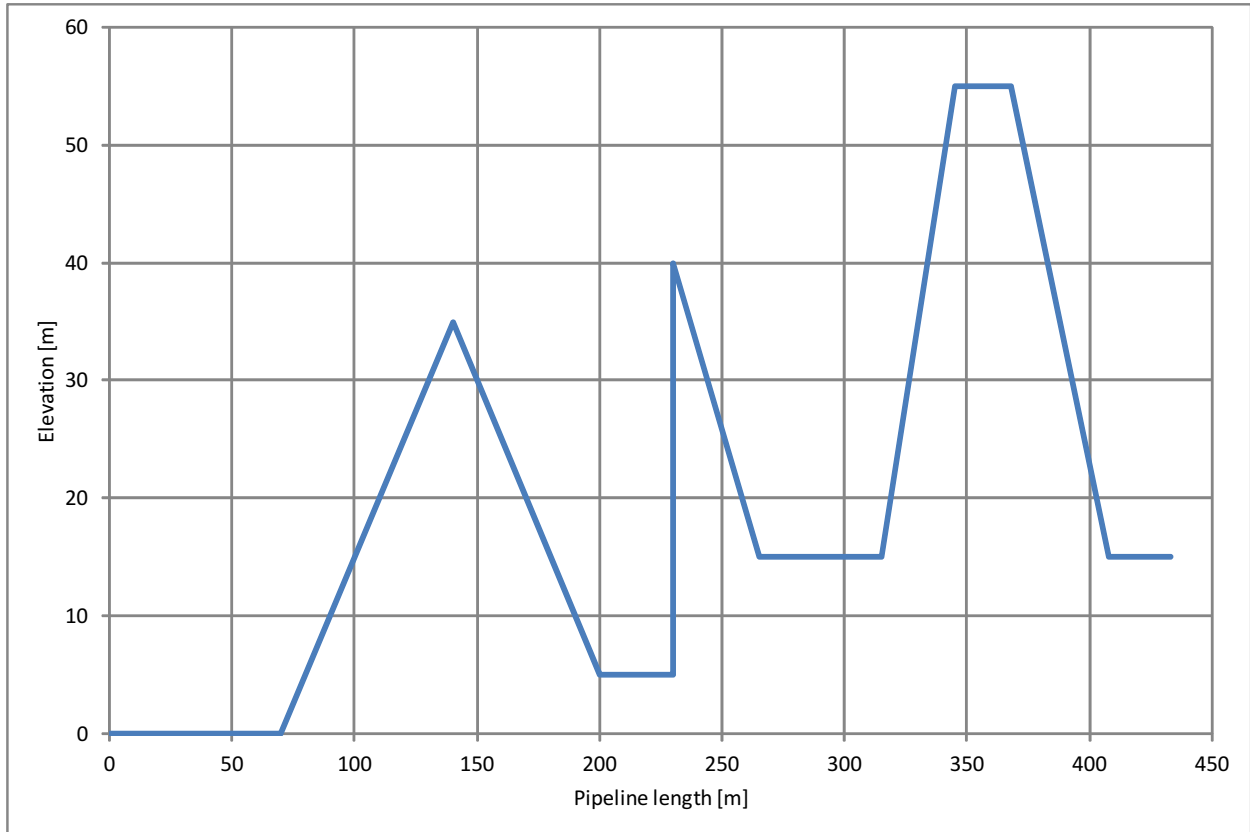
Figure 8.15: Pipeline elevation profile.

influence of pressure and pipeline inclination on the deviation between the models, the input pressure is reduced to 5 bara first. From Fig. 8.17 it can be seen, that the deviation reduces to 77%. Next a more moderate pipeline profile is defined (Fig. 8.18). From Fig. 8.19 it can be seen, that the influence of the pipeline profile on the deviation is small. The deviation only reduces to 146%. In Fig. 8.20 the results for the lower pressure and the moderate pipeline profile are presented.

For further comparison the Tulsa pipe flow correlation is chosen. On the one hand this correlation can be seen as a lower limit of the pressure drop. It constantly predicts the lowest pressure drop. Therefrom a statement can be derived, whether SEM-Flow is more or less conservative. On the other hand, Tulsa is the only pipe flow correlation, which has the same classification of flow patterns as defined by Petalas and Aziz.

8.4.1   Results individual segments

On the basis of the priority list in Sec. 2.2 the evaluation is conducted. Each value, calculated with SEM-Flow is compared to the results from the Tulsa method and the deviation is calculated. Eq. 8.3 gives an example of the deviation calculation. Concerning to pressure and temperature the deviations are calculated between the pressure and temperature loss over the whole pipeline. For the liquid hold up, the slug length and the translational velocity, the deviation is calculated for each increment and then the absolute average deviation is determined. Whenever slug flow occurs, the several methods to calculate the pressure drop, the liquid hold up, the translational velocity and the slug length are compared.
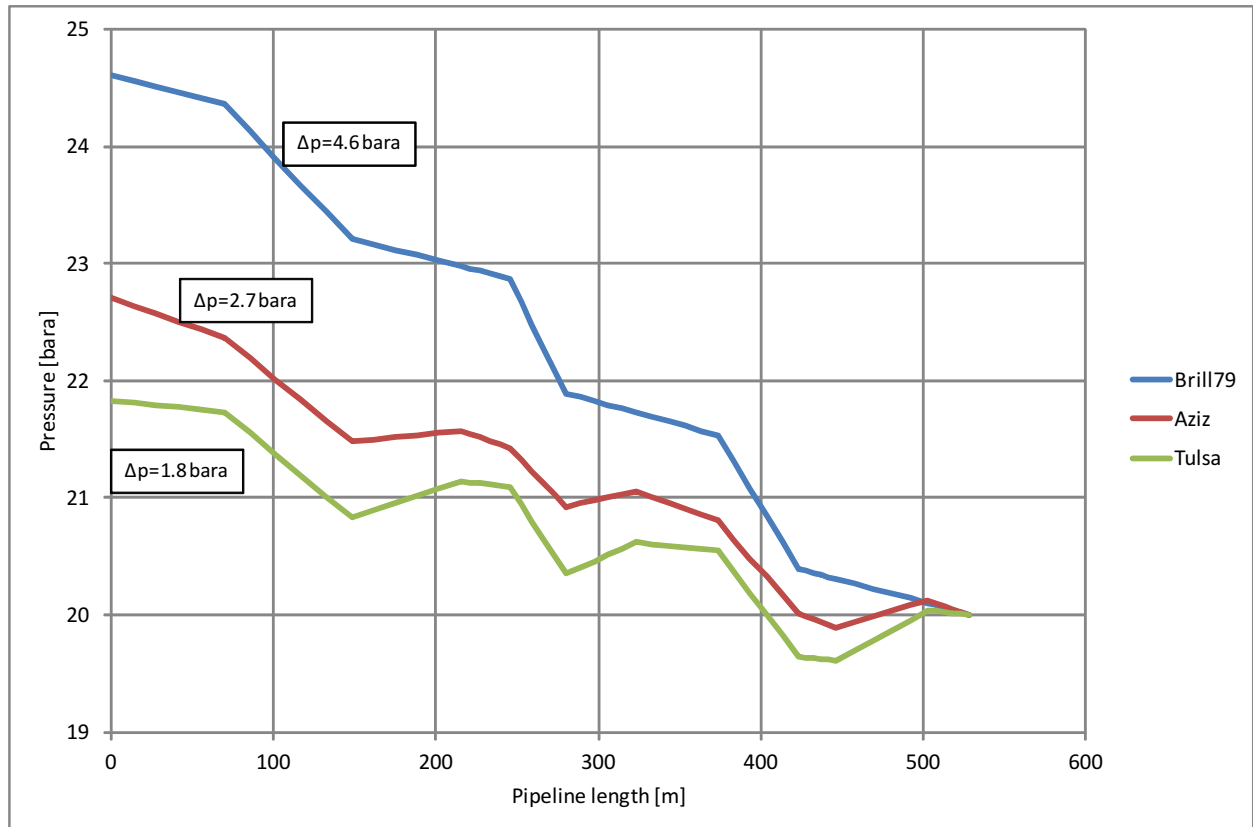
Figure 8.16: Pipe flow correlation comparison. (20 bara, steep profile)
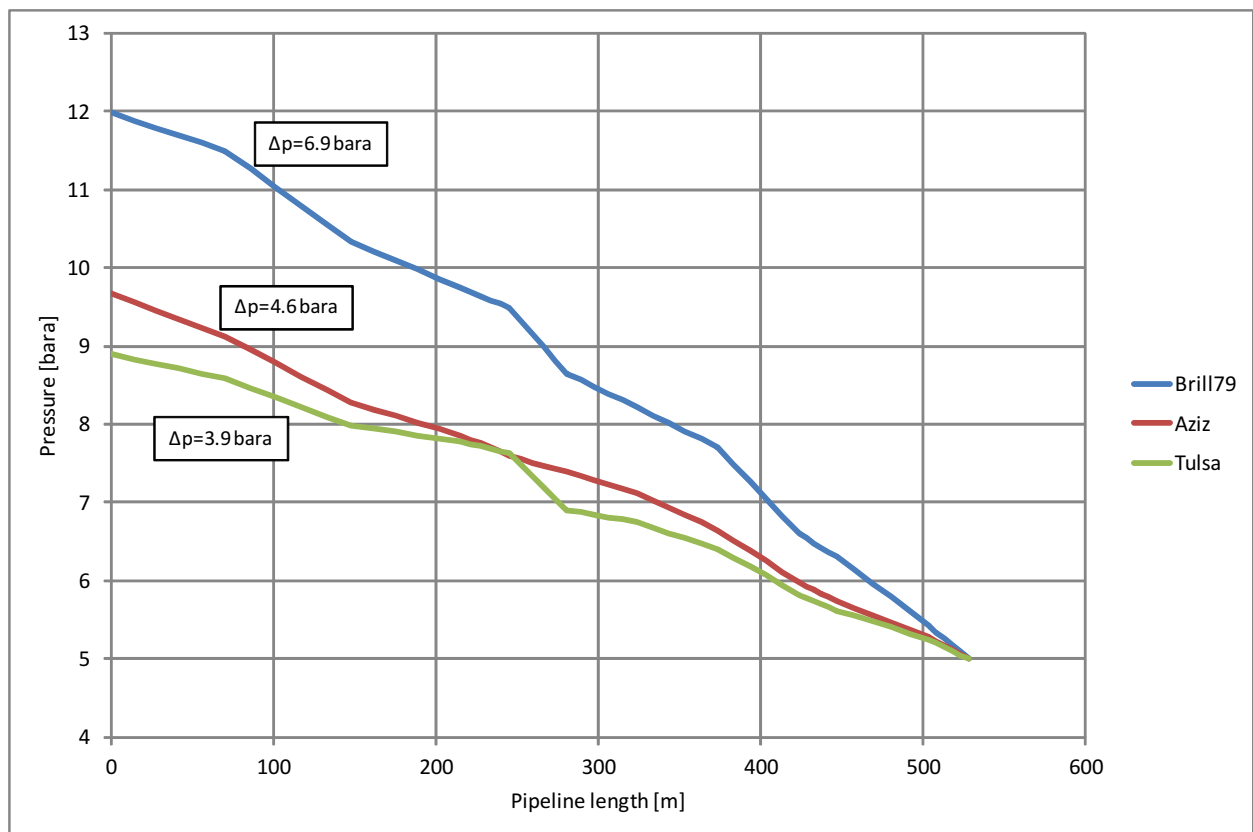
Figure 8.17: Pipe flow correlation comparison. (5 bara, steep profile)
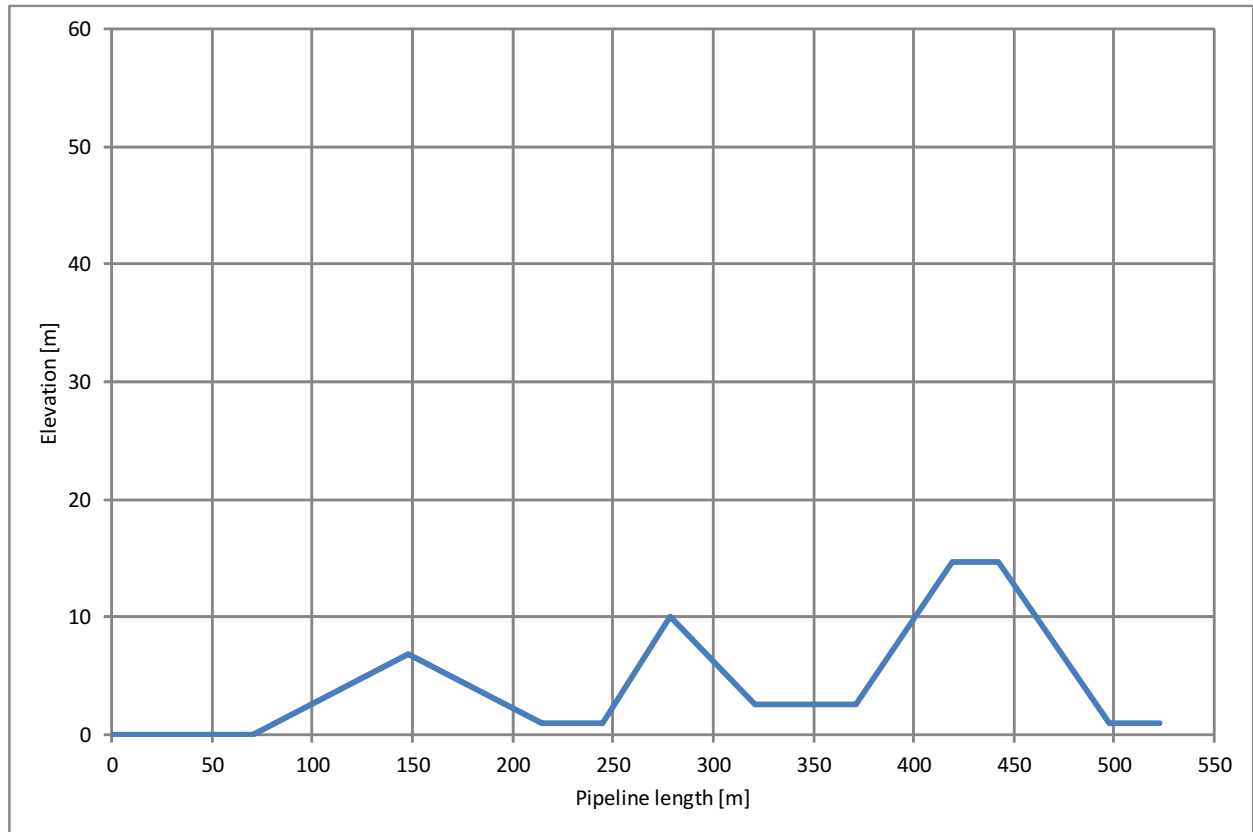
Figure 8.18: Pipeline elevation profile. (moderate)
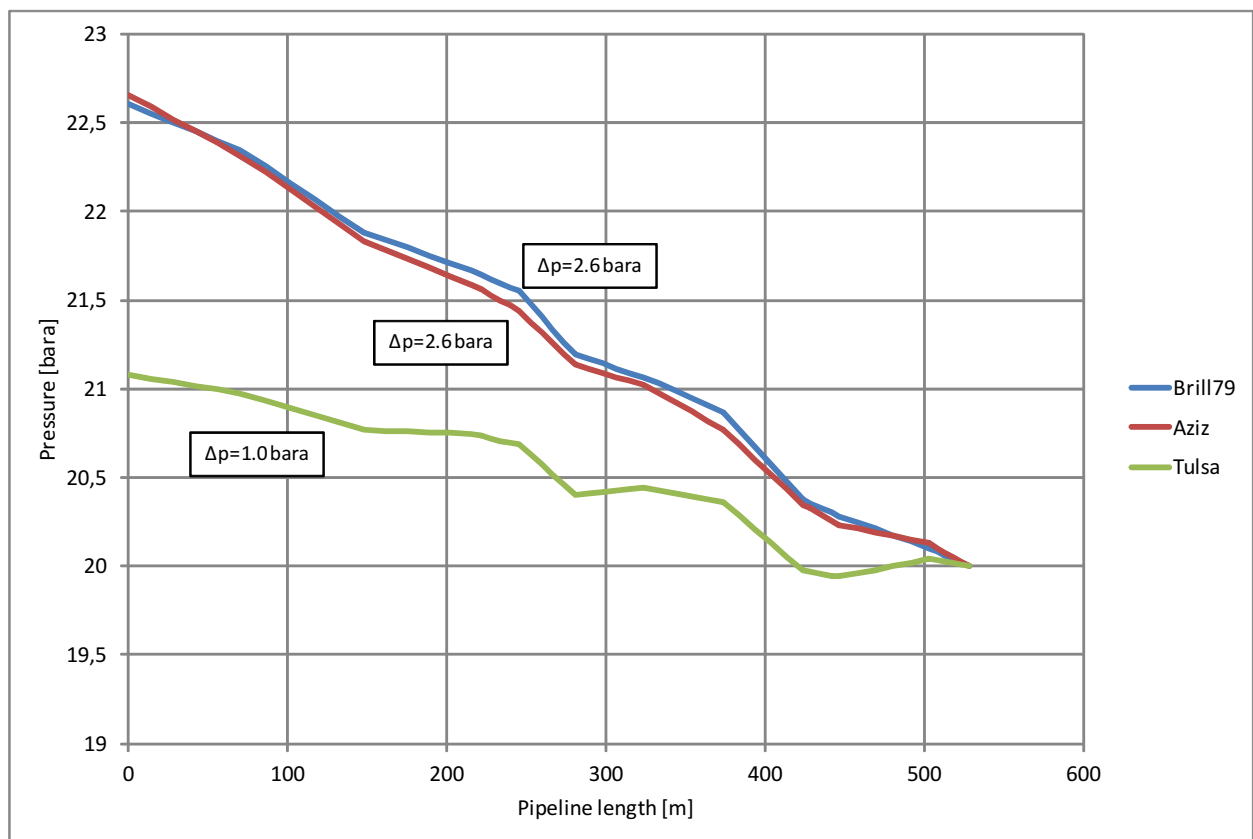
Figure 8.19: Pipe flow correlation comparison. (20 bara, moderate profile)
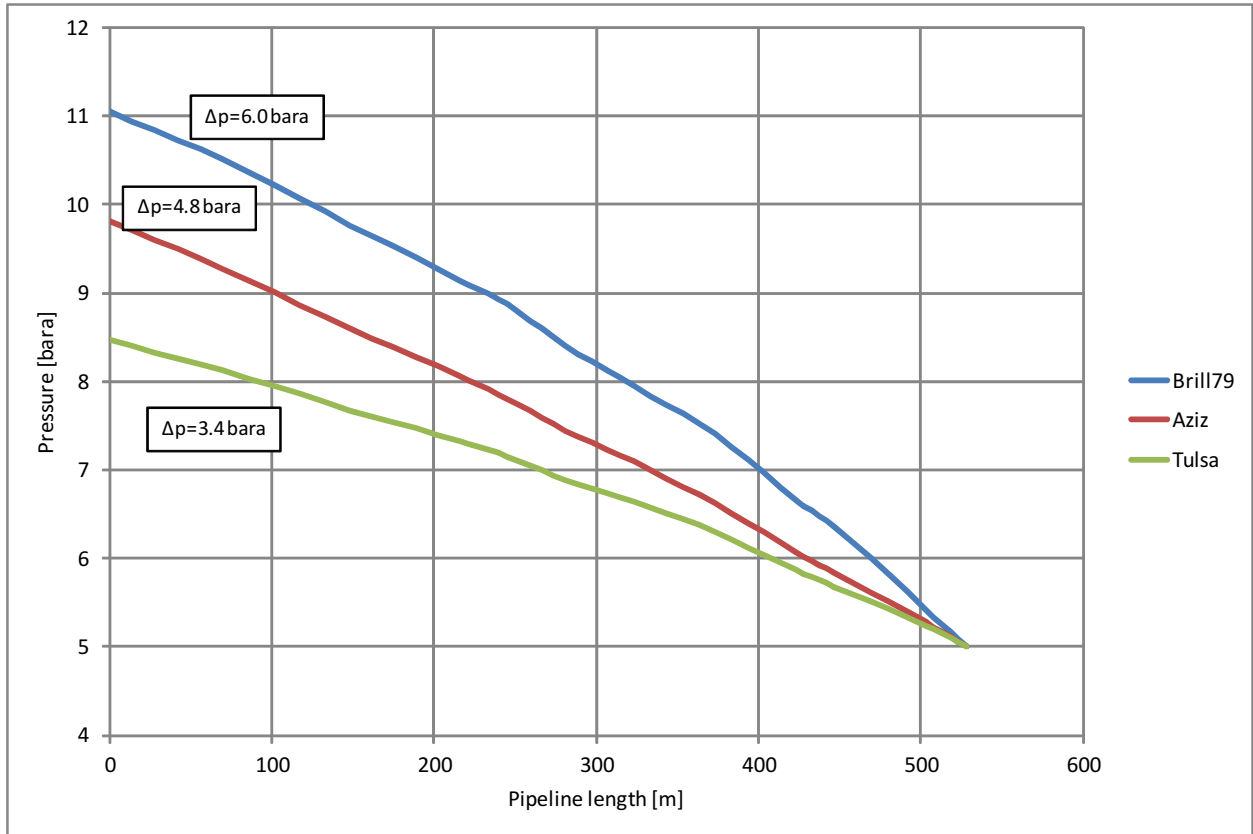
Figure 8.20: Pipe flow correlation comparison. (5 bara, moderate profile)

$$Dev_{\Delta p} = \frac{\Delta p_{SEM} - \Delta p_{Hysys}}{\Delta p_{Hysys}} * 100 \tag{8.3}$$

8.4.1.1   Pressure drop

At first the pressure drop of each segment, calculated with the model after Petalas and Aziz is reviewed. In Fig. 8.21 to Fig. 8.23 the deviation is plotted for each inclination angle for the three different initial flow conditions. It must be noted here that, although stratified flow is set in the horizontal pipeline segment for example, the flow pattern might change with changing pipeline inclination and flow conditions.

In case of the SF-condition (Fig. 8.21) the pressure drop is underestimated except for an angle of -60°. One can see, that the deviation is increasing with increasing inclination. For the AF-case it does not seem that the inclination angle has an influence on the deviation. The biggest deviation occurs at 90° upward inclination. The reason therefore might be different assumptions of the distribution of the liquid and gas phase although both models predict annular flow. In the IF-case, the pressure drop predicted by Petalas and Aziz is higher than the one by the Tulsa model. For -60° and -90° extreme deviations occur, compared to the other inclination angles. The reason therefore could be the fact that different flow patterns are predicted for this angles by Petalas and Aziz and Tulsa, as will be reviewed later on. The detailed evaluation can be found in Appendix C (Sec. C.2).

In Fig. 8.24 and Fig. 8.25 the pressure drop deviations for slug flow are presented. As one can see, the flow pattern changes to slug flow in the SF-case (Fig. 8.24), when the pipeline has an upward inclination. For the other inclination angles slug flow does not occur
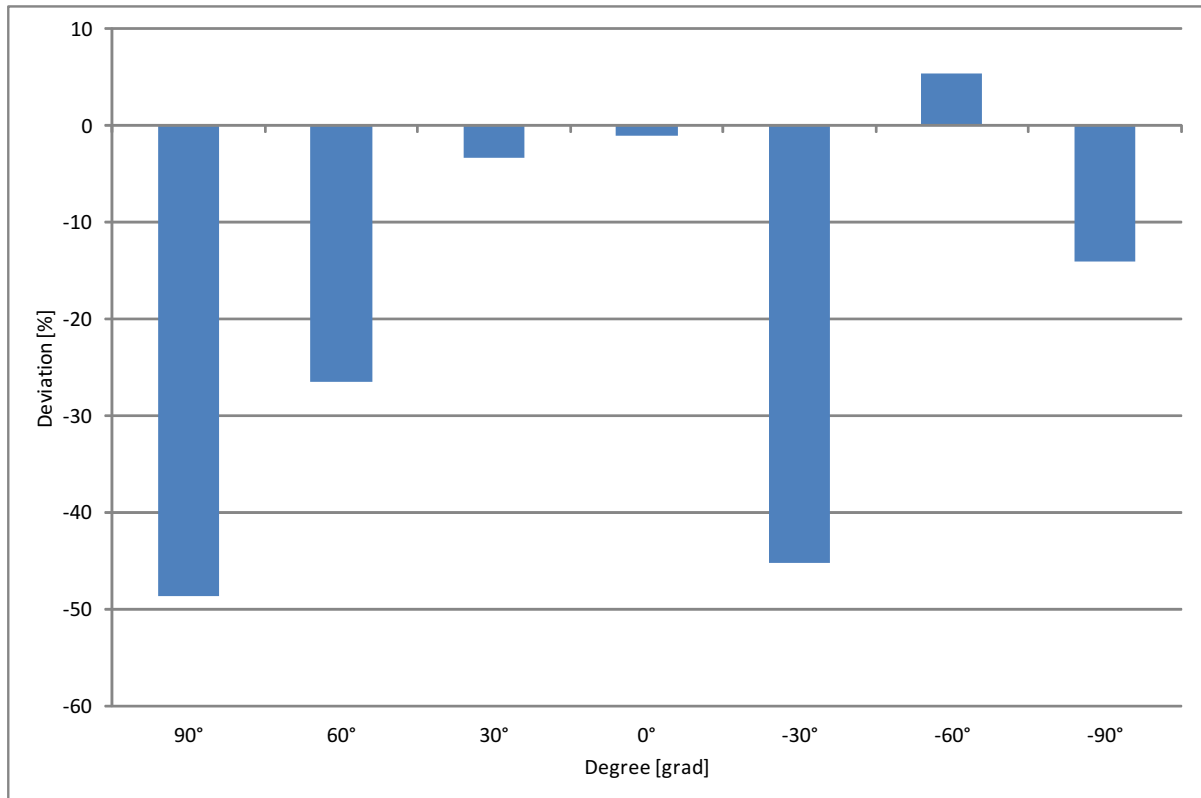
Figure 8.21: Deviation of pressure drop between Petalas and Aziz and Tulsa over the pipeline inclination. (initial flow condition = SF)
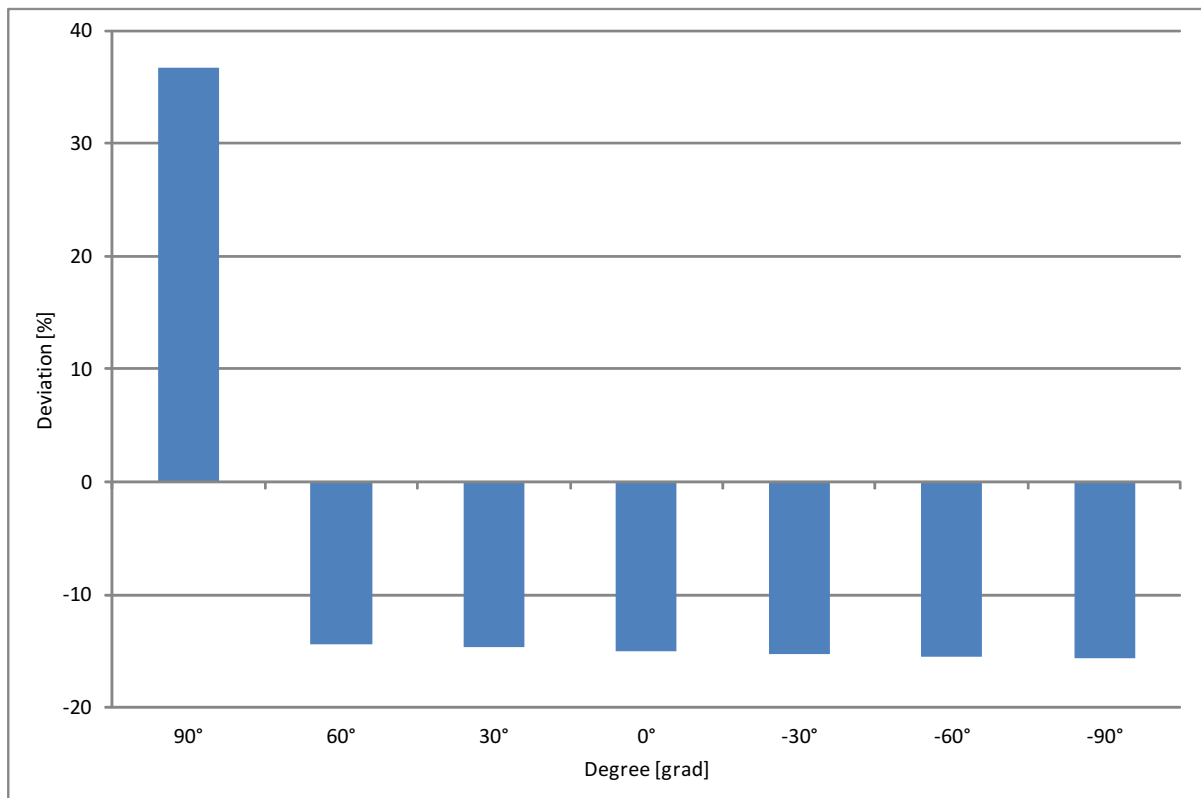
Figure 8.22: Deviation of pressure drop between Petalas and Aziz and Tulsa over the pipeline inclination. (initial flow condition = AF)
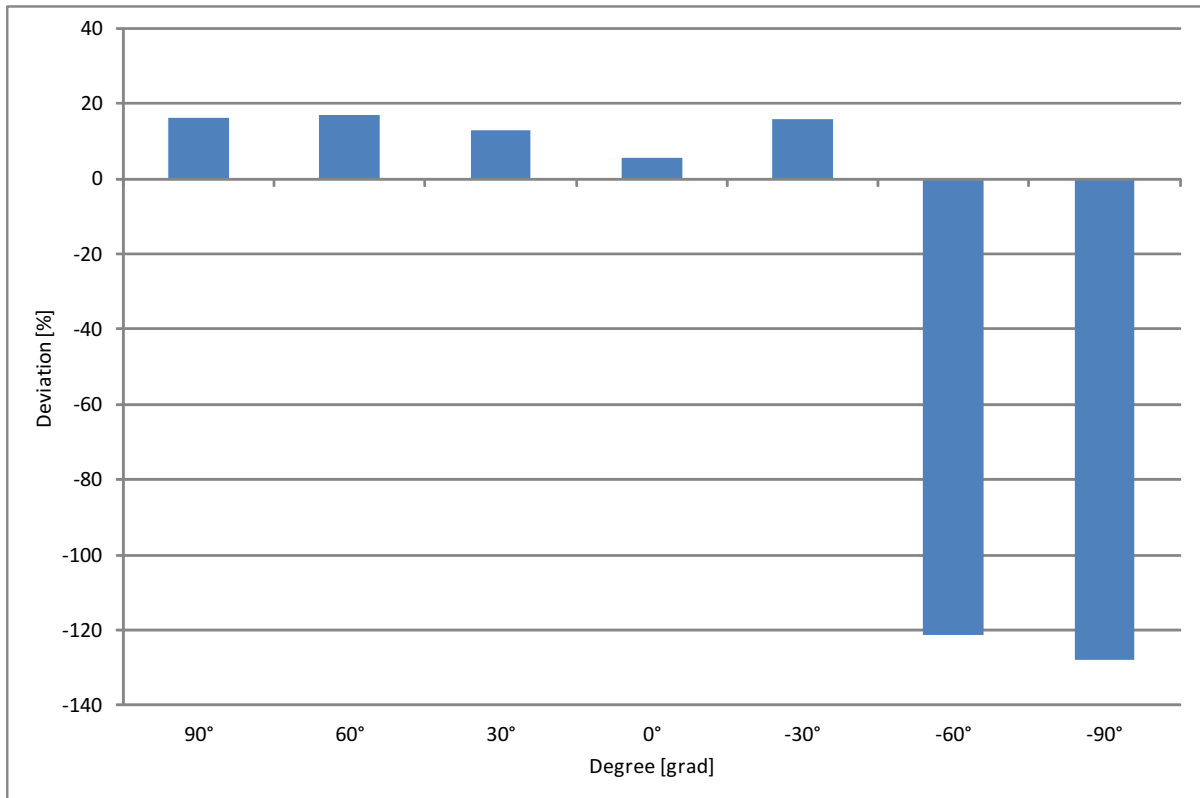
Figure 8.23: Deviation of pressure drop between Petalas and Aziz and Tulsa over the pipeline inclination. (initial flow condition = IF)

why no comparison can be conducted. The smallest deviation constantly appears for the "Xiao comp." model. This observation can be made as well for the IF-case (Fig. 8.25). Unfortunately, an error occurred for negative inclinations within the "Xiao model", why no comparison can be made in this cases. The high deviations for the three negative inclinations can be explained by the differently predicted flow patterns again. No plot is available for the AF-case because slug flow does not occur under this flow conditions.

8.4.1.2   Flow pattern

In Tab. 8.11 the flow patterns, which are predicted by Hysys and SEM-Flow are listed. The flow pattern does not change within one segment. A change just occurs for varying flow conditions and inclination angles. For 80% of the cases the flow patterns match. Differences occur for downward inclined pipelines, where different assumptions are made between the models obviously. Twice intermittent flow is predicted by Hysys, but no slug properties are calculated. Thus, it is assumed that elongated bubble flow, which is an intermittent flow pattern as well, occurs for example. This could be the reason, why no slug flow properties are predicted by the software.

8.4.1.3   Slug flow properties

The slug flow properties can be reviewed only if slug flow occurs and both models predict slug flow. As it was mentioned earlier, the predicted flow patterns are different in Hysys and SEM-Flow for negative inclinations and the IF-case. For the AF-case slug flow does not occur at all.
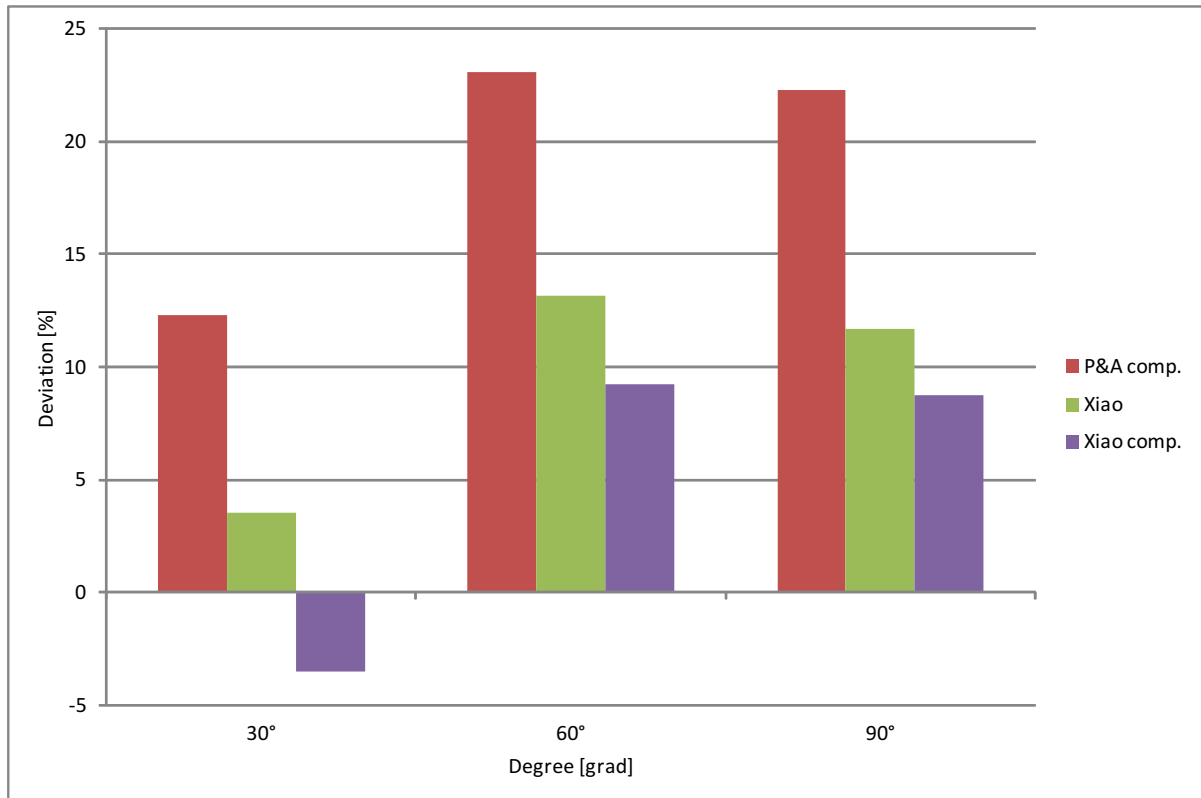
Figure 8.24: Deviation of pressure drop in the slug flow pattern over the pipeline inclination. (initial flow condition = SF)
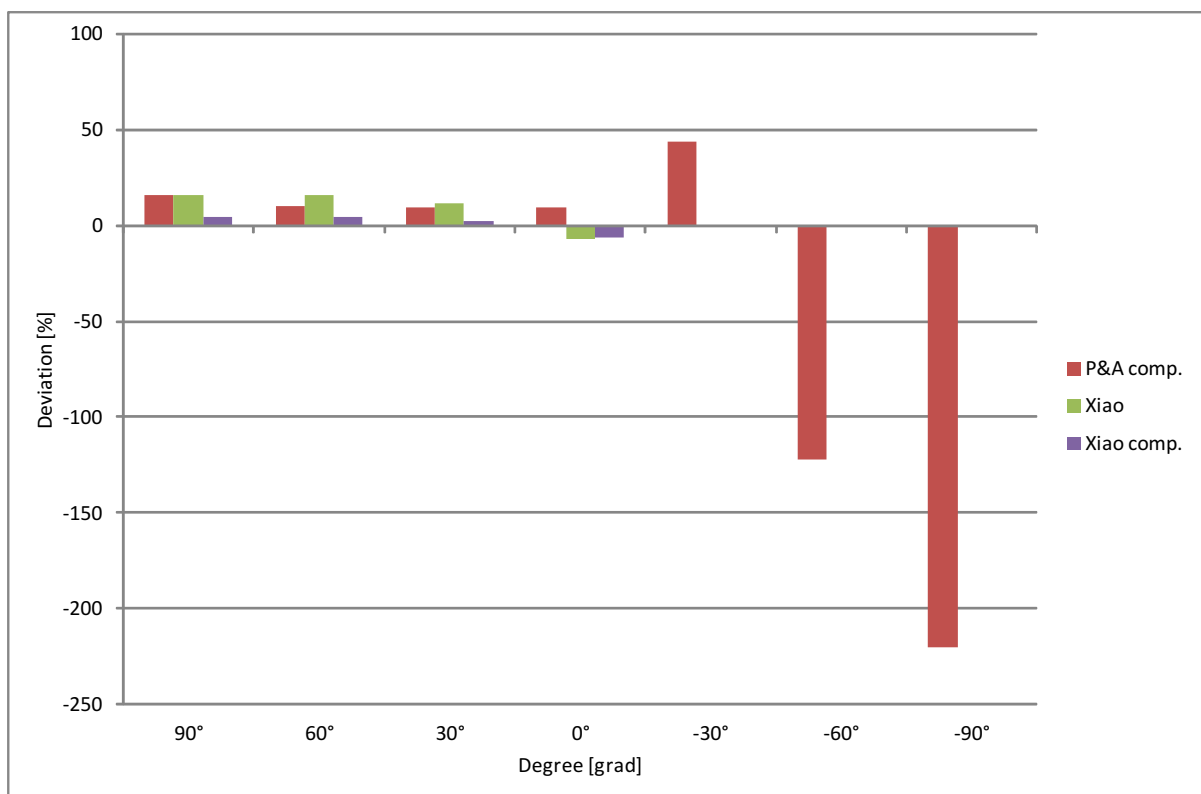
Figure 8.25: Deviation of pressure drop in the slug flow pattern over the pipeline inclination. (initial flow condition = IF)

Table 8.11: Comparison of the flow pattern prediction.

Initial flow condition	Angle	Hysys	SEM-Flow
SF	0°	Stratified flow	Stratified flow
SF	30°	Slug flow	Slug flow
SF	60°	Slug flow	Slug flow
SF	90°	Slug flow	Froth flow
SF	−30°	Stratified flow	Stratified flow
SF	−60°	Stratified flow	Stratified flow
SF	−90°	Annular flow	Annular flow
AF	0°	Annular flow	Annular flow
AF	30°	Annular flow	Annular flow
AF	60°	Annular flow	Annular flow
AF	90°	Annular flow	Annular flow
AF	−30°	Annular flow	Annular flow
AF	−60°	Annular flow	Annular flow
AF	−90°	Annular flow	Annular flow
IF	0°	Slug flow	Slug flow
IF	30°	Slug flow	Slug flow
IF	60°	Slug flow	Slug flow
IF	90°	Slug flow	Slug flow
IF	−30°	Intermittent flow	Slug flow
IF	−60°	Stratified flow	Slug flow
IF	−90°	Intermittent flow	Slug flow

The four correlation combinations are compared to predict the slug translational velocity. In Fig. 8.26 the average deviation of the translational velocity is plotted for those angles, where slug flow occurs. The deviation of "Xiao comp." is the smallest, independent of inclination angle and flow condition (Fig. 8.27).
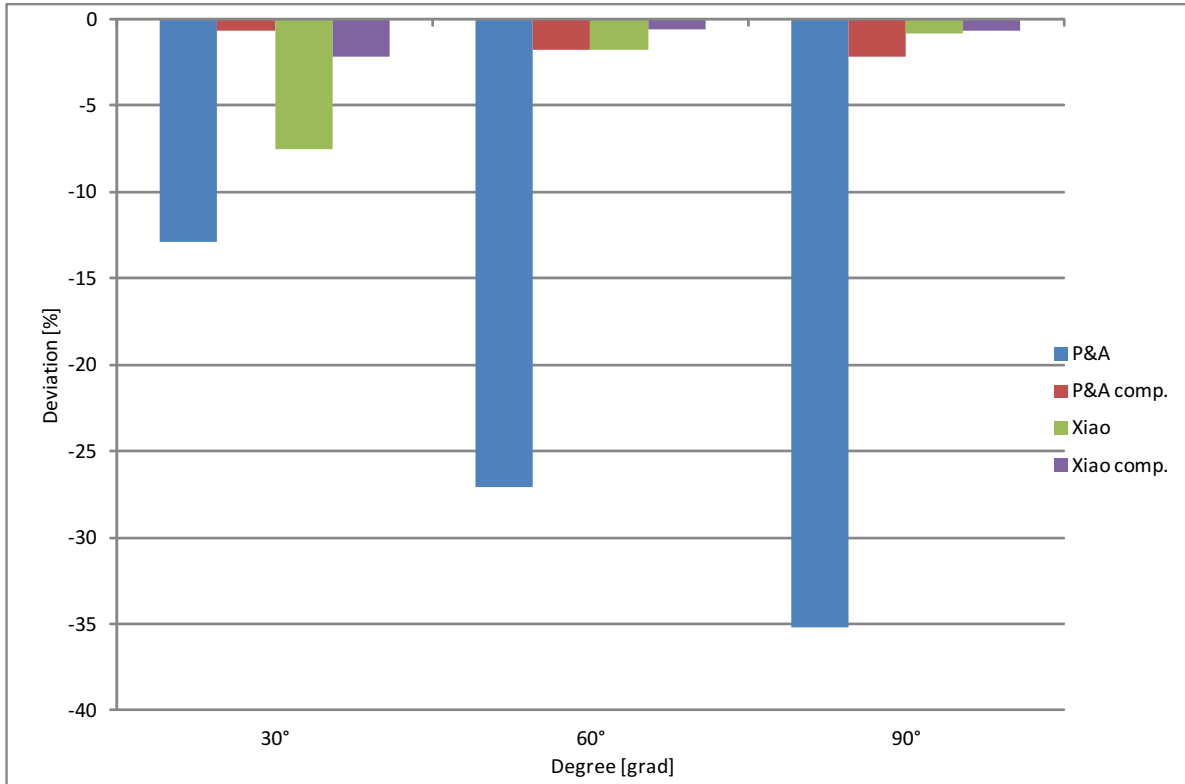
Figure 8.26: Avergae deviation of the slug translational velocity. (initial flow condition = SF)

As it was already mentioned in Sec. 4.4.4 , the prediction of the slug length is based on pure empiricism. That is the reason why highly different values are calculated with the different equations. As can be seen from Tab. 8.12 , the best accordance between Hysys and SEM-Flow is found for the Norris correlation.

8.4.1.4   Liquid hold up

By reviewing the liquid hold up, no clear connection between the inclination angle and the deviation can be found. The deviation is dependent on the prevailing flow condition however. From Fig. 8.28 to Fig. 8.30 it can be seen, that the highest deviations occur for stratified flow and the lowest deviations occur for slug flow.
The several models to calculate the liquid hold up in the slug flow pattern are compared again (Fig. 8.31 , Fig. 8.32). The dependence of the deviation on the prevailing flow pattern can be observed as well. The lowest average deviation occurs between Xiao comp. and Tulsa.

8.4.1.5   Temperature

The temperature deviation is as well dependent on the flow pattern instead of the inclination angle (Fig. 8.33 , Fig. 8.34). The highest deviations occur for intermittent flow (Fig. 8.35), if the flow pattern is predicted differently in SEM-Flow and Hysys. This is an indicator for the fact, that the influence of the flow pattern on the temperature loss calculation is weighted
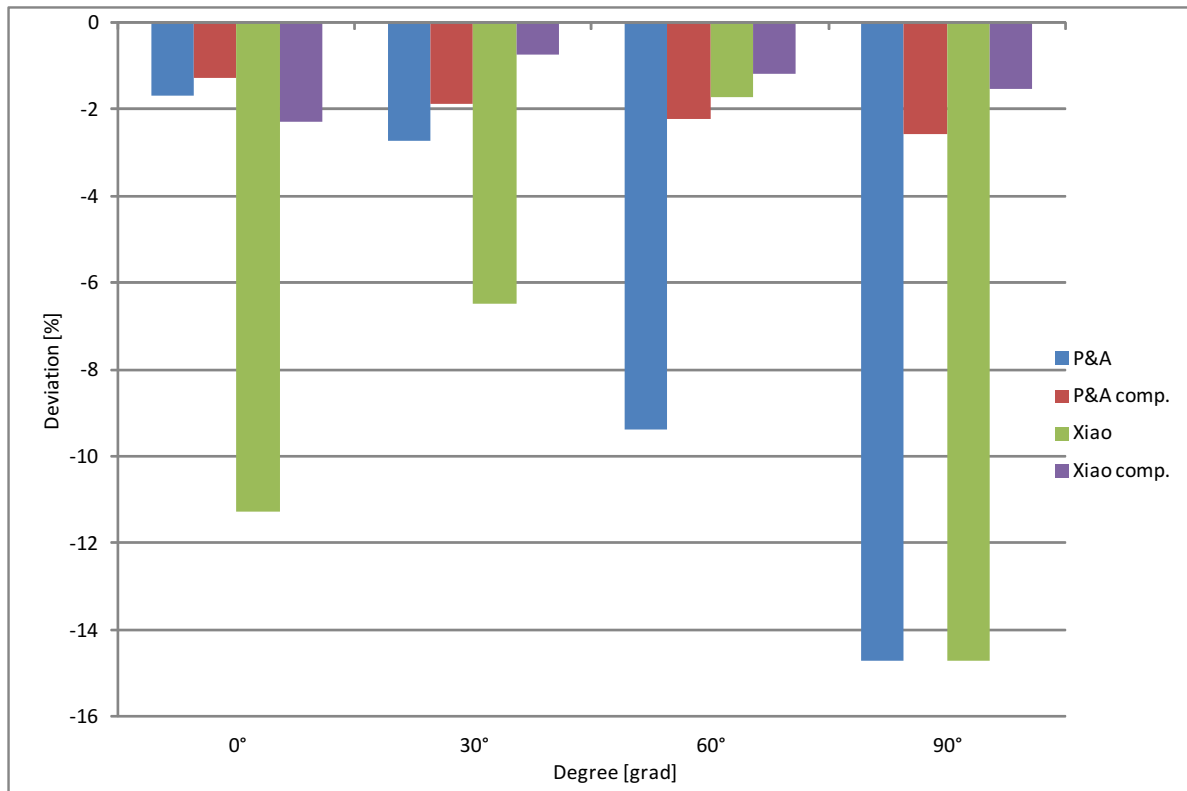
Figure 8.27: Avergae deviation of the slug translational velocity. (initial flow condition = IF)
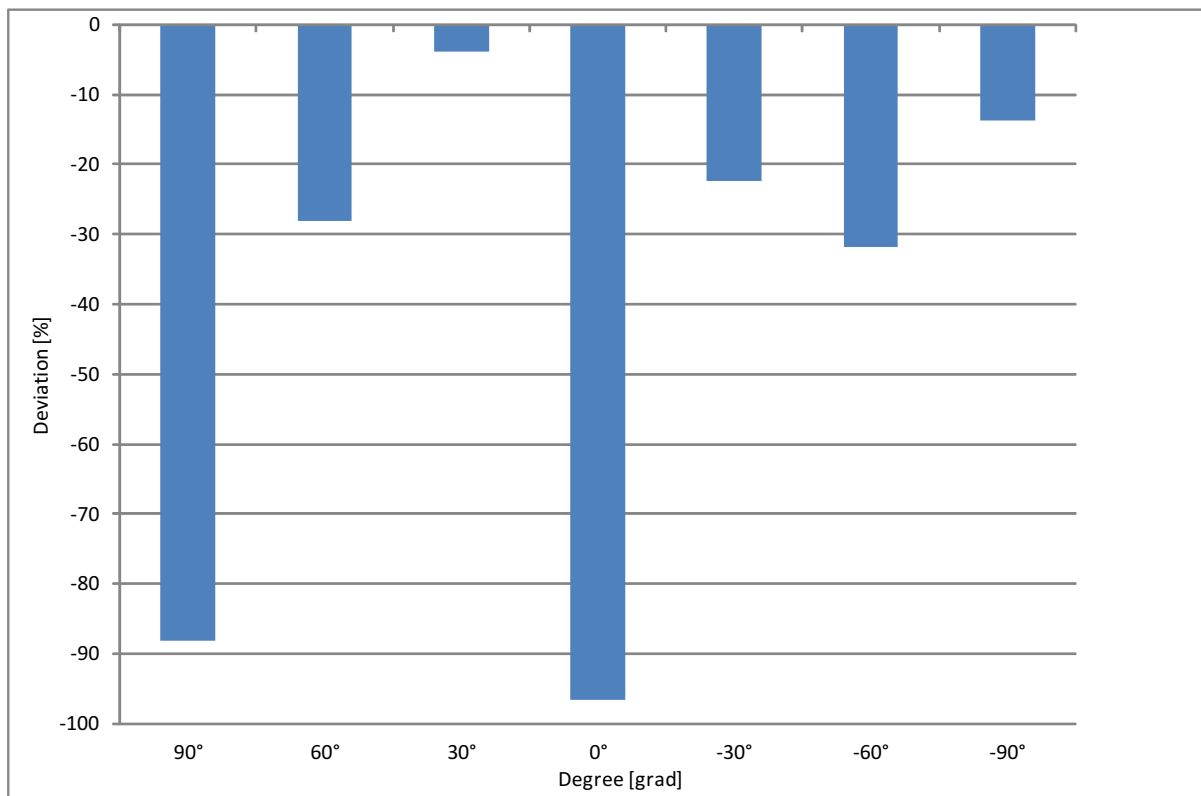
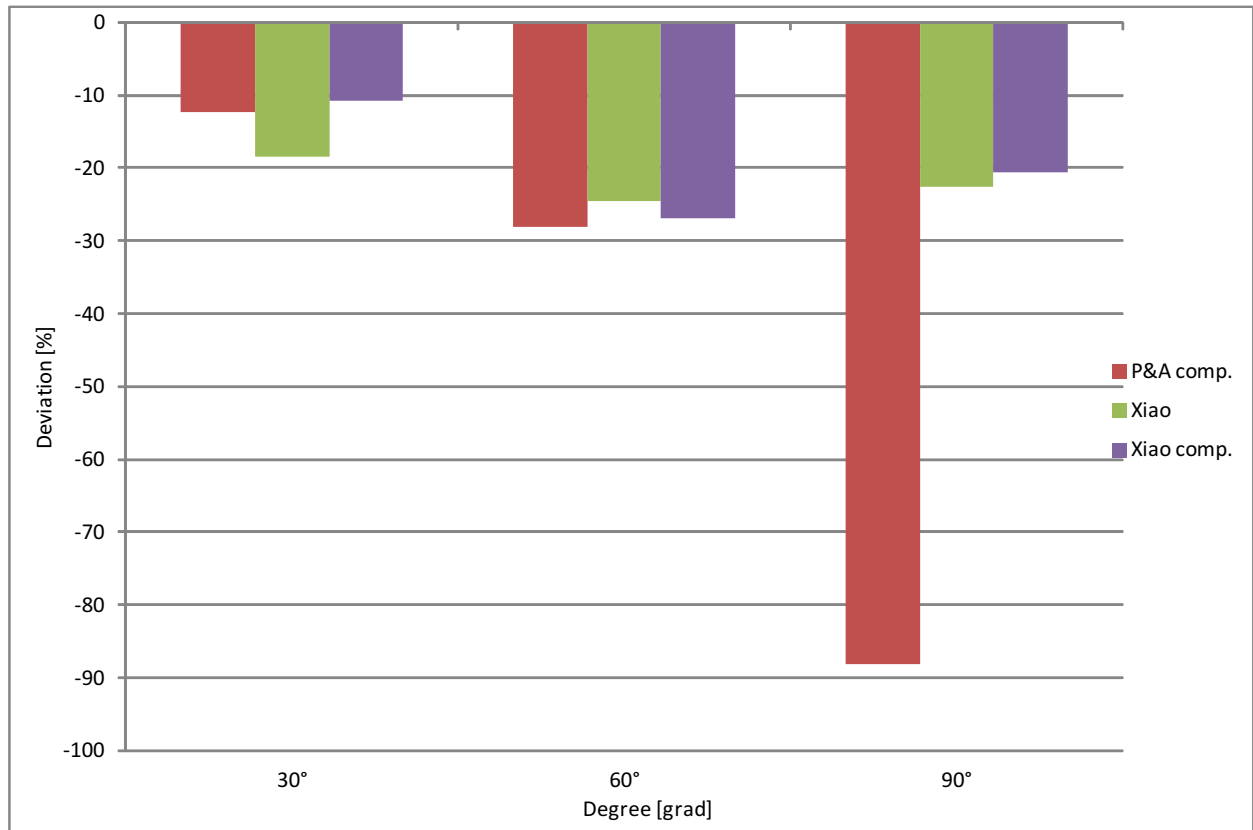Figure 8.28: Average deviation of liquid hold up between Petalas and Aziz and Tulsa. (initial flow condition = SF)

Table 8.12: Average deviation of the slug length. (NS=no slug flow in the pipeline, OF=different flow pattern in Hysys and SEM-Flow)

Initial flow condition	Angle	Brill [m]	Norris [m]	Scott [m]
SF	0°	NS	NS	NS
SF	30°	-154.10	-91.30	-9908.19
SF	60°	-265.97	-175.75	-14326.20
SF	90°	-731.30	-527.82	-32745.56
SF	−30°	NS	NS	NS
SF	−60°	NS	NS	NS
SF	−90°	NS	NS	NS
AF	0°	NS	NS	NS
AF	30°	NS	NS	NS
AF	60°	NS	NS	NS
AF	90°	NS	NS	NS
AF	−30°	NS	NS	NS
AF	−60°	NS	NS	NS
AF	−90°	NS	NS	NS
IF	0°	-5.50	-29.10	-3609.06
IF	30°	-208.79	-109.93	-10882.96
IF	60°	-262.30	-147.47	-12846.56
IF	90°	-277.58	-158.30	-13413.19
IF	−30°	OF	OF	OF
IF	−60°	OF	OF	OF
IF	−90°	OF	OF	OF
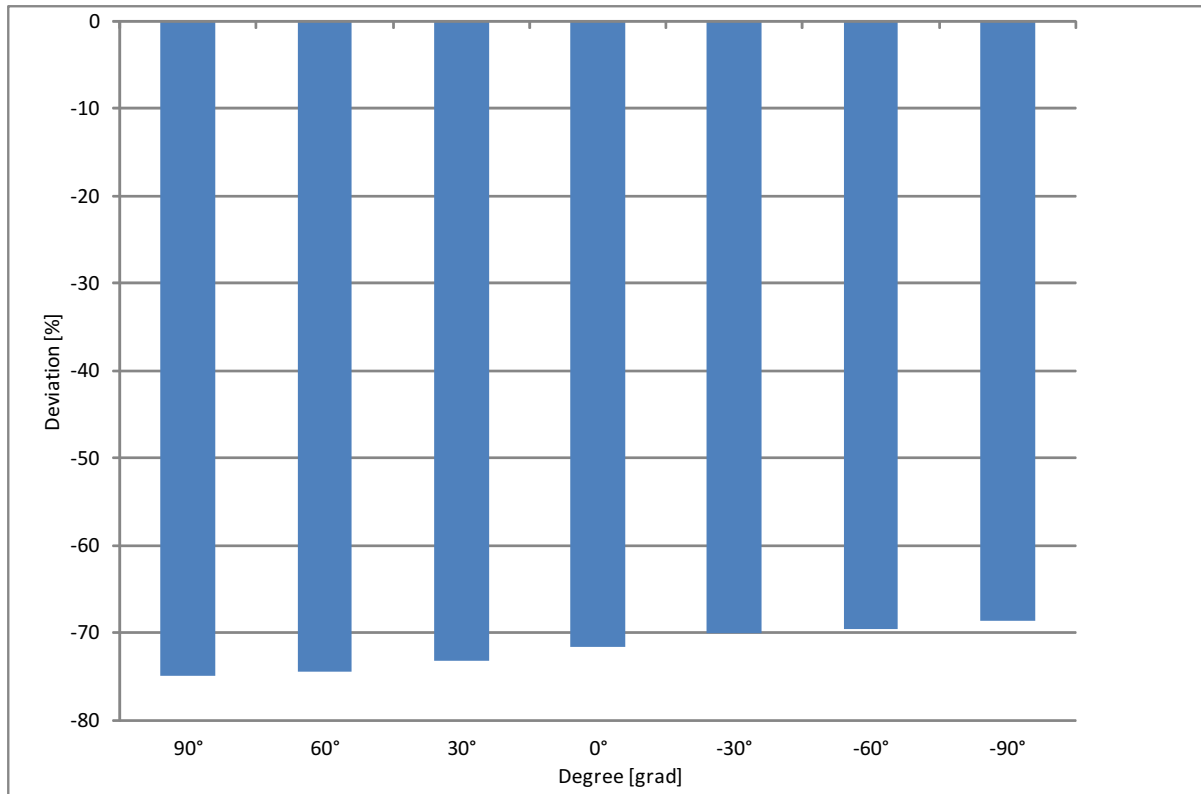
Figure 8.29: Average deviation of liquid hold up between Petalas and Aziz and Tulsa. (initial flow condition = AF)
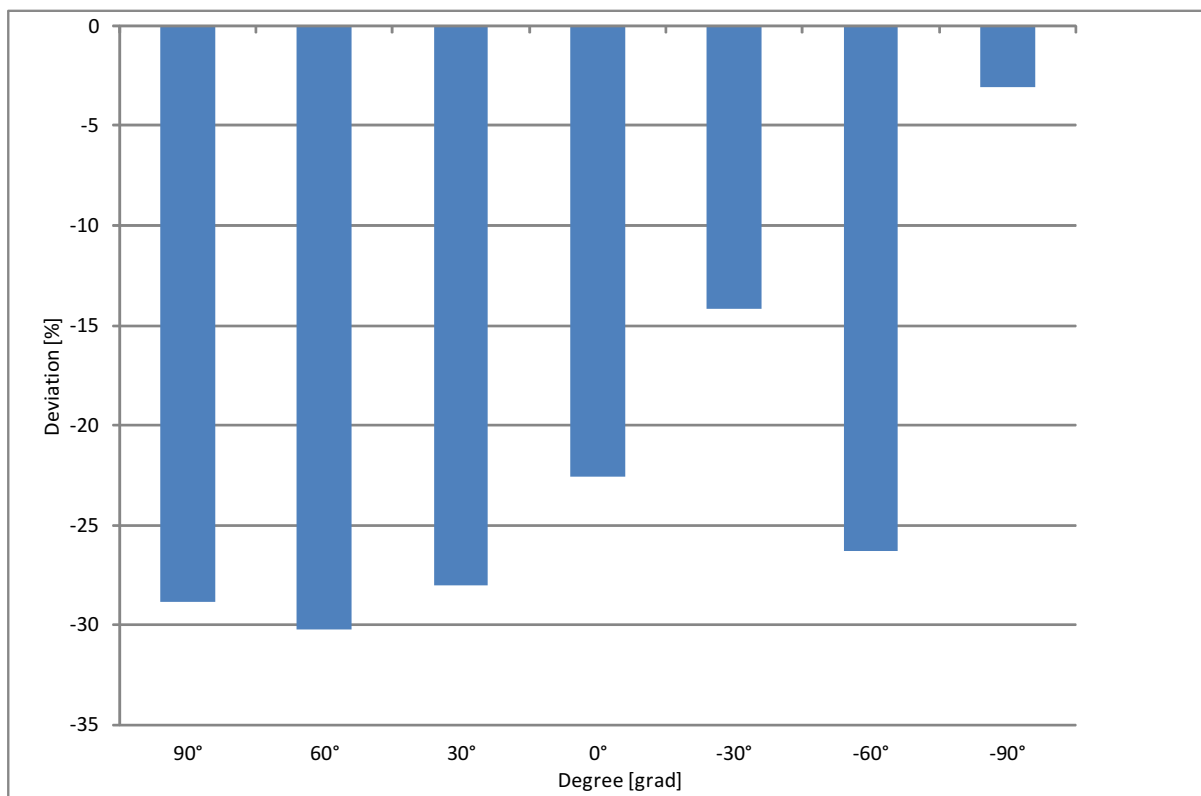
Figure 8.30: Average deviation of liquid hold up between Petalas and Aziz and Tulsa. (initial flow condition = IF)

Figure 8.31: Average deviation of liquid hold up. (initial flow condition = SF)
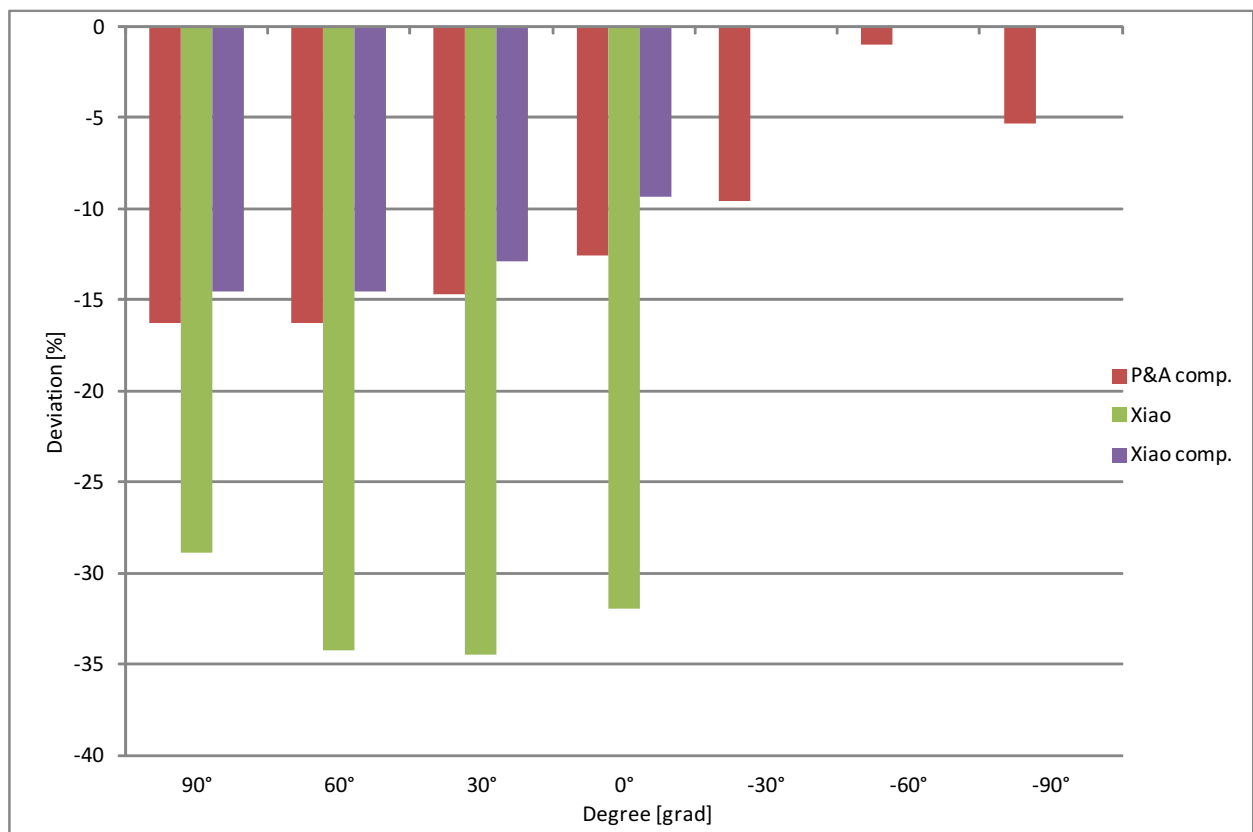
Figure 8.32: Average deviation of liquid hold up. (initial flow condition = IF)

differently in SEM-Flow and Hysys. The detailed evaluation can be found in Appendix C (Sec. C.2).
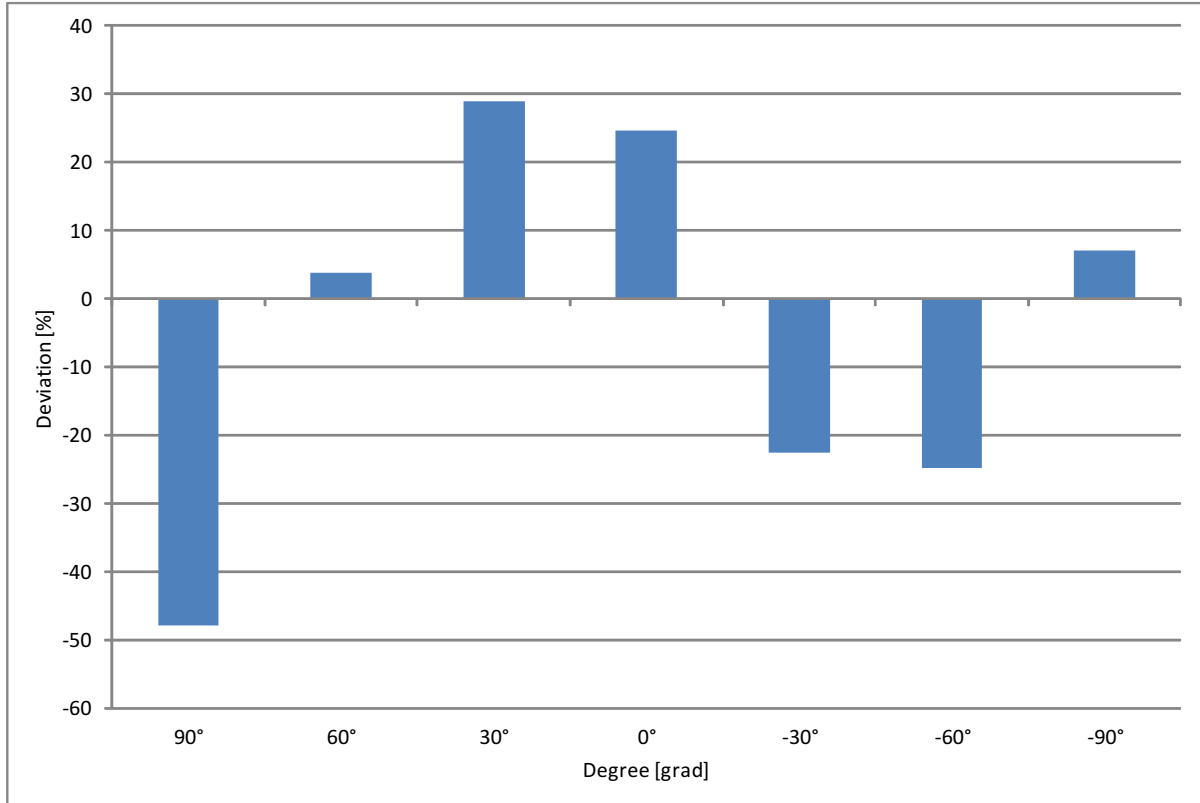
Figure 8.33: Deviation of temperature loss between SEM-Flow and Hysys over the pipeline inclination. (initial flow condition = SF)

8.4.2   Conclusion of the indivdual segments

The prediction of the flow patterns matches for most of the cases. The importance of the correct prediction of the flow patterns becomes obvious, if one takes a look on the large pressure drop deviations in those cases, where the flow pattern is different in SEM-Flow and Hysys.

It depends mostly on the flow condition whether the pressure drop is over or under predicted by SEM-Flow. In the SF and AF-case the pressure drop is mostly under predicted, but in the IF-case it is over predicted. Thus, the flow rates of the gas and liquid phase seem to play an important role for the predicted values. By comparing the pressure drop calculation models for the slug flow pattern, the Xiao comp. correlation combination constantly gives the smallest deviation. The same behavior occurs for the translational velocity and the liquid hold up. Thus, this model can be used as an alternative for upward inclined pipelines. The code is available in SEM-Flow, but has not been included so far in the overall algorithm so far. The reason therefore is the observed instability of the Xiao model during the evaluation process.

It has been mentioned several times, that the prediction of the slug length is a difficult task. It can be seen, that the predicted values are highly different, why it is recommended to use them carefully. Further investigation would have to be conducted to make a more rigorous statement concerning the validity of these values.
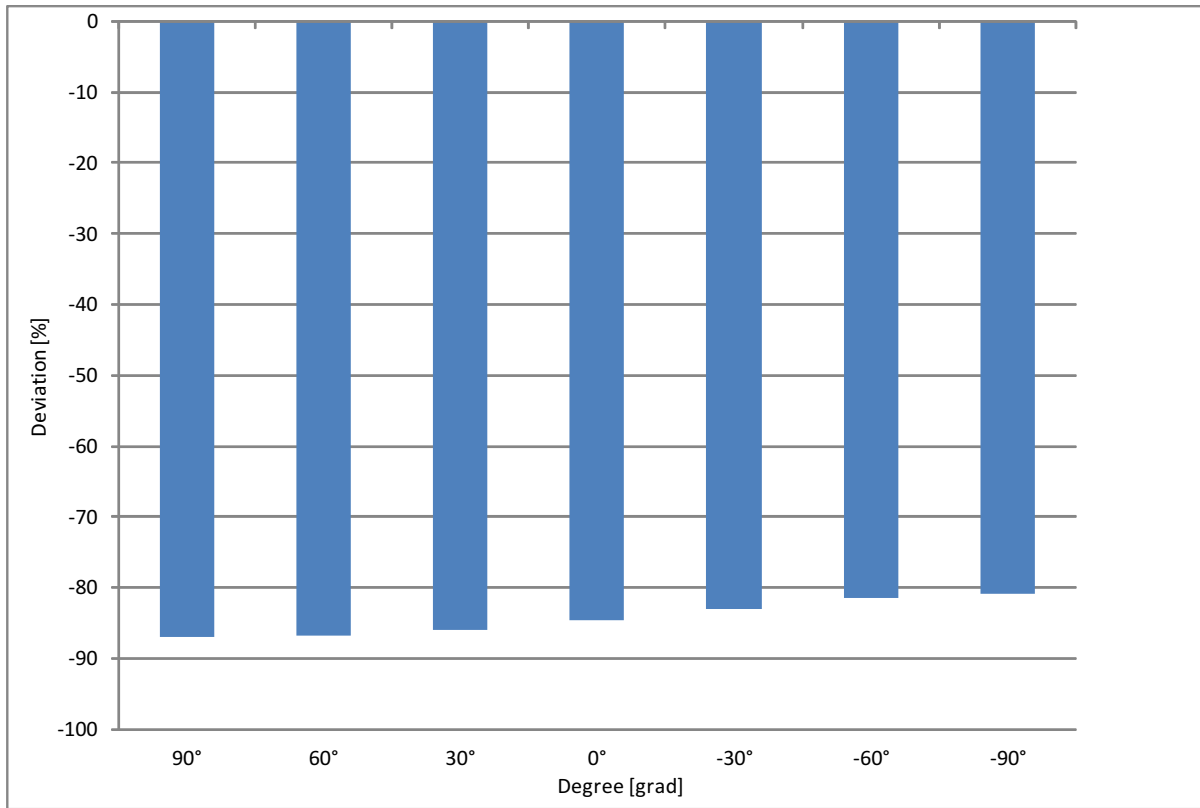
Figure 8.34: Deviation of temperature loss between SEM-Flow and Hysys over the pipeline inclination. (initial flow condition = AF)
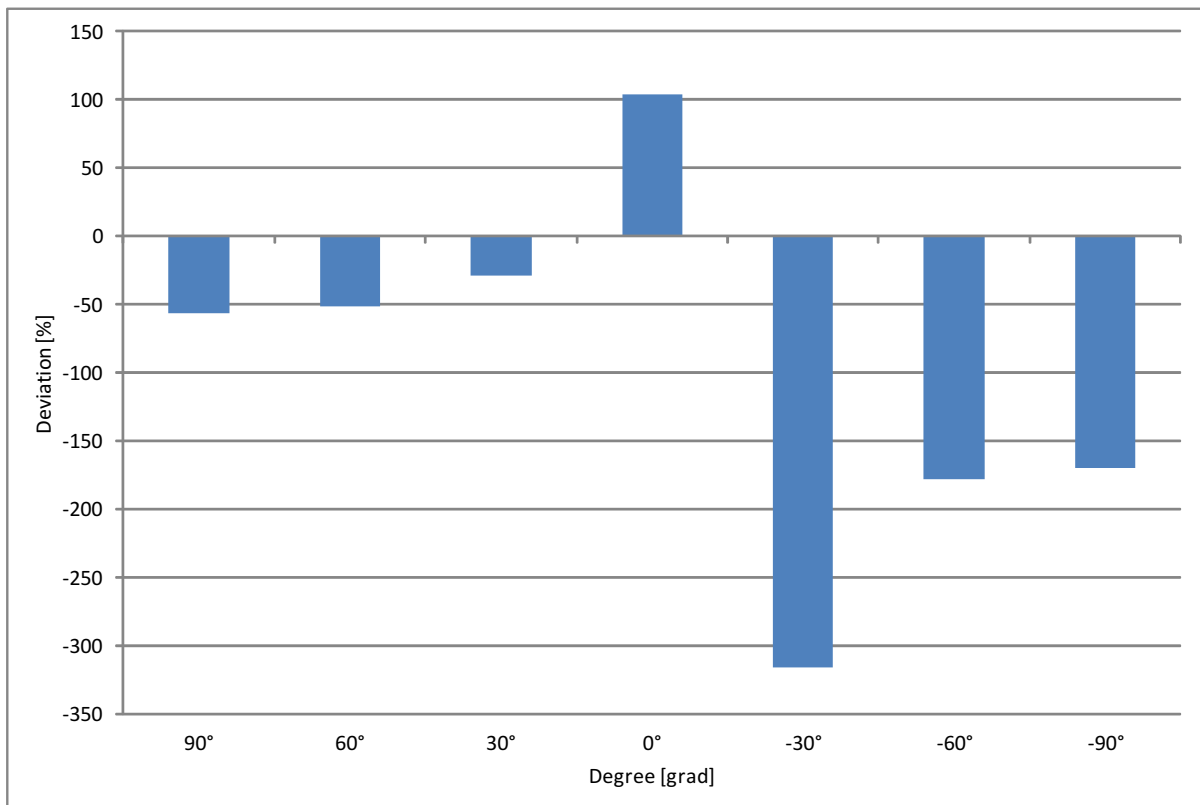
Figure 8.35: Deviation of temperature loss between SEM-Flow and Hysys over the pipeline inclination. (initial flow condition = IF)

8.4.3   Results multisegment pipeline

The flow behavior in a pipeline with several up- and downward inclined segments is simulated to test the performance of SEM-Flow in a real case scenario and to evaluate in which range the predicted pressure drop over a whole pipeline takes place .

In the previous section, one could see that the magnitude of the deviation between SEM-Flow and Hysys is dependent on the flow condition and the inclination angle. In some cases the pressure drop is overestimated by SEM-Flow and in some it is not. For practical applications the behavior and functionality of the program over a long pipeline is however more important.

At first the elevation profile from Fig. 8.15 is used and the starting pressure is set to 20 bara. The detailed analysis for each increment can be found in Appendix C (Sec. C.3). The flow pattern prediction matches 100%. In Fig. 8.36 , the pressure is plotted over the pipeline length. In addition to the SEM-Flow and Tulsa pressure profile, the results from the two other flow correlations, mentioned earlier are presented as well. The pressure, calculated by SEM-Flow is constantly higher than by the Tulsa model, which shows that SEM-Flow uses a more conservative approach. The pressure drop, calculated with SEM-Flow is in between the other models and it appears from Fig. 8.36 , that the tendency of the pressure gradient is a compromise between the Tulsa model and the model after Beggs and Brill. For horizontal and upward inclined segments the pressure gradient of SEM-flow is approximately parallel to the Beggs and Brill gradient. In these sections, the pressure drop calculated with the Tulsa model is constantly smaller. For downward inclined segments Beggs and Brill do not take into account the pressure increase however. For these sections the SEM-Flow pressure gradient is closer to the one by Tulsa. As presented in Tab. C.2 , the liquid hold up depends on the flow pattern and the inclination angle, which was stated in the previous section. The average deviation of the liquid hold up between SEM-Flow and Tulsa is 37%. Although the deviation of temperature loss is 90%, this does not seem to have a big influence on the pressure drop due to the fact, that the tendency is predicted very well. The simulation is further performed with a starting pressure of 5 bara and a more moderate elevation profile. As seen in Fig. 8.37 and Fig. 8.38 , the above mentioned observations occur in these cases as well, whereby the deviation for pressure drop and temperature loss decrease (Appendix C, Sec. C.3).

8.4.4   Conclusion multisegment pipeline

By comparing the results of the pressure drop calculation with the models available in Hysys, one can conclude, that the performance of SEM-Flow is practicable in terms of pressured gradient prediction. The pressure gradient has the same tendency over the pipeline and the predicted flow patterns match. Of course it cannot be denied that there is a deviation between SEM-Flow and Hysys of 115%. On the one hand this deviation must be seen in the context, that the deviation between Tulsa and the Model after Beggs and Brill, which are both available in the commercial simulation software Aspen Hysys, is 155%. On the other hand it must be mentioned again, that the models in Hysys, as well as the Petalas and Aziz model included in SEM-Flow are an image of the reality only and thus are not entitled to be accurate.

Furthermore it must be pointed out, that it would be necessary to perform more tests with SEM-Flow at other flow conditions, inclination angles and pipeline diameters. This would allow a more thorough evaluation of the program. Thus the program evaluation does not
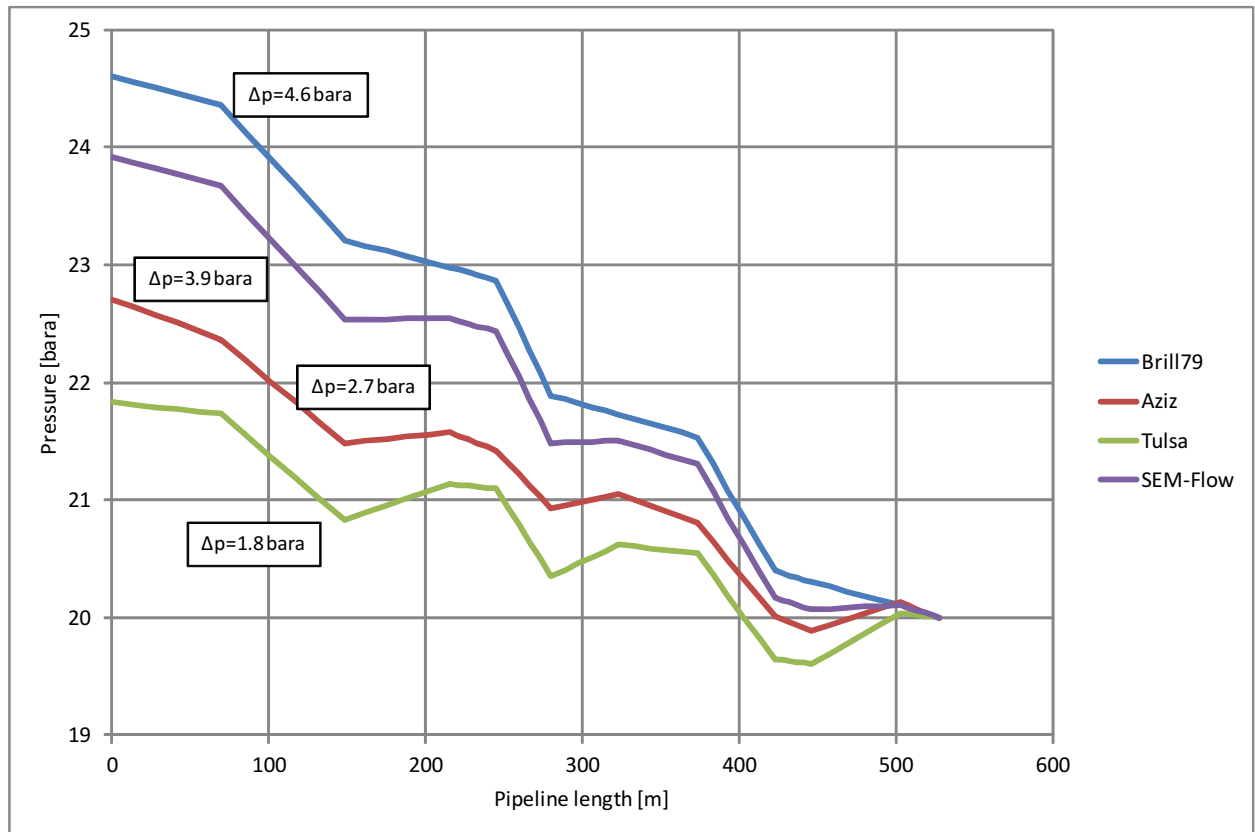
Figure 8.36: Pressure drop profile over the pipeline length. (20 bara, steep profile)
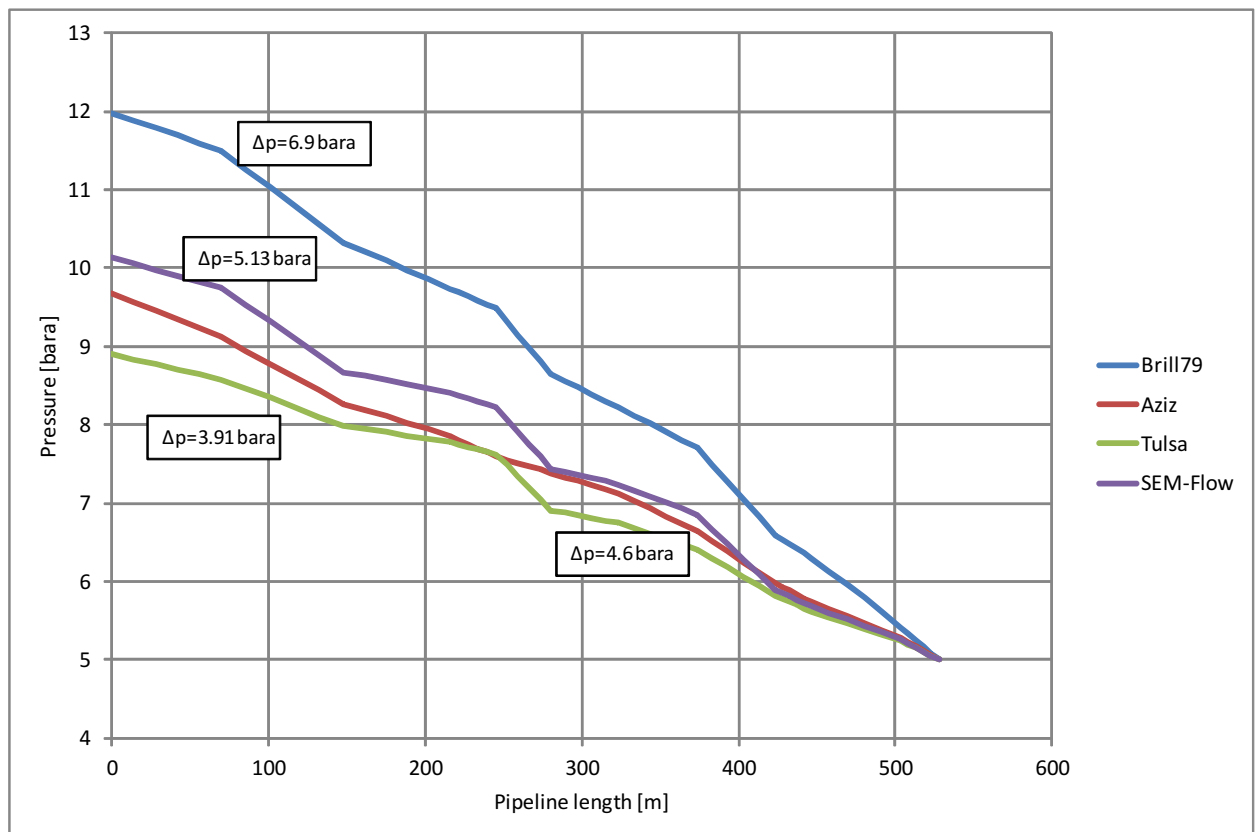

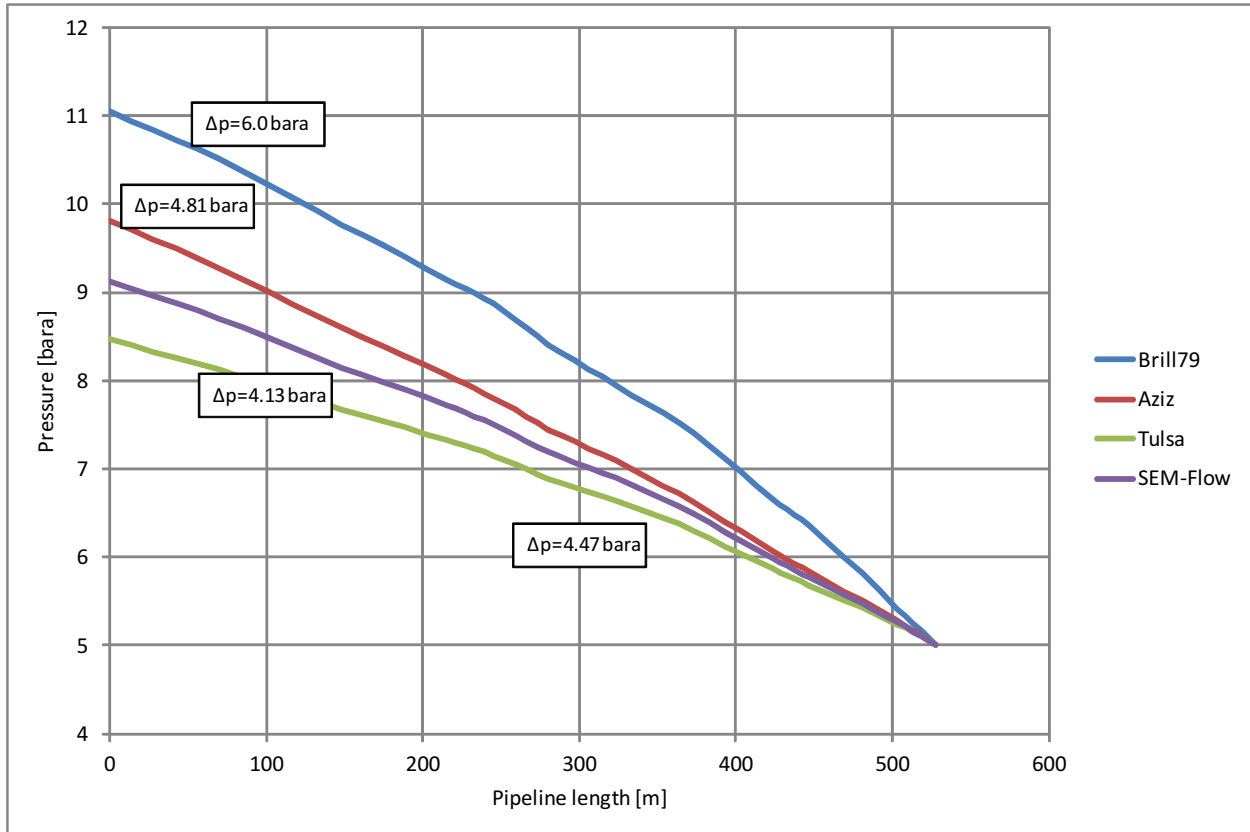Figure 8.37: Pressure drop profile over the pipeline length. (5 bara, steep profile)

Figure 8.38: Pressure drop profile over the pipeline length. (5 bara, moderate profile)

lay claim to be complete and is just intended to show the functionality of the program.

8.5   Summary

The requirements to SEM-Flow are to give a first estimation of the pressure drop and the occurring flow pattern with as few input parameters as possible. The prediction of the fluid properties, which is done by the program, works for most of the properties with a deviation of 20% between Hysys and SEM-Flow. Those properties with a higher deviation have proven to have a small influence on the overall simulation result of the program. The evaluation of the fluid properties is done for a dedicated pressure and temperature range, which is the common working area of a pipeline in practice. Thus the evaluation is only applicable to this range.

The pressure gradient over the whole pipeline has the same tendency as the other models in Hysys and thus is assumed to give a good prediction. The values for the pressure gradient calculated with the models in Hysys, as well as with SEM-Flow have deviations up to 150%, whereby SEM-Flow predicts the pressure drop rather conservative. Further testing of SEM-Flow would have to be performed to make universally valid evaluations, which is beyond the scope of this thesis.

Chapter 9

Outlook

The results from the fluid property calculation as well as the results from the multiphase flow calculation are reviewed for a limited range of pressure, temperature, fluid composition and flow condition. To receive a more profound result of the applicability of SEM-Flow a more intensive testing phase should be performed. Special attention must be paid thereby on selecting a broader range of gas and liquid velocities.

SEM-Flow as well as any model that comes with Aspen Hysys is only capable of giving an image of the reality. Although the performance of the model after Petalas and Aziz was evaluated with experimental data, it would be necessary to check the results obtained by SEM-Flow with data from the laboratory as well. Thus one can make better statements than just the deviation between two models.

During the evaluation phase the program was undertaken intensive testing. Thereby, the performance could be further improved and several bugs could be corrected. Nevertheless, there still might occur further bugs during the usage of the program in everyday use. Thus, the program will be constantly developed and improved.

For obtaining the roots of the several functions which have to be solved with an iterative procedure the Pegasus algorithm is used. To further shorten the calculation time of SEM-Flow additional investigation can be conducted in the area of numerical methods to find a faster converging method.

For another improvement to decrease the calculation time, the architecture of the algorithm could be undertaken some changes. At the moment the increments are increased for the whole segment and the calculation procedure starts from the outlet of the segment again if the limit of 5% is exceeded. It would be more efficient, however, to only increase the number of increments for the section of the segment where it is necessary.

The values for the slug length are strongly different. The reason therefore is of course their pure empirical basis but it is recommended as well that one checks the applied equations again if any misinterpretation has happened. Furthermore an additional literature review can be conducted to find other possibilities to calculate the slug length.

In the area of the fluid properties other equations available in the literature could be applied for those parameters with deviations greater than 50%. Due to the fact that no calculation method for the latent heat of vaporization could be found in the literature, data obtained with Aspen Hysys were used. An additional literature research could perhaps provide better equations to calculate the latent heat of vaporization.

Chapter 10

Bibliography

[1] Yemada Taitel and A. E. Dukler. A model for predicting flow regime transitions in horizontal and near horizontal gas-liquid flow. *AIChE Journal*, 22(1):47–55, 1976.

[2] Khalid Aziz and George W. Govier. Pressure drop in wells producing oil and gas. *Journal of Canadian Petroleum Technology*, 11(03), 2013.

[3] Herrmann Luisa. An integrated approach to modeling pipeline hydraulics in a gathering and production system: An industry white paper, 2013.

[4] Ove Bratland. *Pipe Flow 2: Multi-phase Flow Assurance.* 2010.

[5] Boyun Guo. *Offshore pipelines: Design, installation, and maintenance.* Gulf Professional Publishing, Waltham and MA, 2014.

[6] Ovadia Shoham. *Mechanistic modeling of gas-liquid two-phase flow in pipes.* Society of Petroleum Engineers, Richardson and TX, 2006.

[7] J. P. Brill and H. D. Beggs. *Two-phase Flow in Pipes.* 1984.

[8] Ovadia Shoham. *Flow pattern transition and characterisation in gas liquid two phase flow in inclined pipes.* PhD thesis, TelAviv University, Israel, 1982.

[9] Saeid Mokhatab, William A. Poe, and James G. Speight. *Handbook of natural gas transmission and processing.* Gulf Professional Pub., Burlington and MA, 2006.

[10] J. J. Xiao, O. Shonham, and J. P. Brill. *A Comprehensive Mechanistic Model for Two-Phase Flow in Pipelines.* PhD thesis, 1990.

[11] Edurne Carpintero Rogero. *Experimental Investigation of Developing Plug and Slug Flows.* PhD thesis, Technische Universität München, München, 2009.

[12] J. P. Brill and S. J. Arirachakaran. State of the art in multiphase flow. *Journal of Petroleum Technology*, 44(05):538–541, 2013.

[13] Mack Shippen and William J. Bailey. Steady-state multiphase flow—past, present, and future, with a perspective on flow assurance. *Energy & Fuels*, 26(7):4145–4157, 2012.

[14] Fred H. Poettman and Paul G. Carpenter. *The Multiphase Flow of Gas, Oil, and Water Through Vertical Flow Strings with Application to the Design of Gas-lift Installations.* American Petroleum Institute, 1952.

[15] P. B. Baxendell and R. Thomas. The calculation of pressure gradients in high-rate flowing wells. *Journal of Petroleum Technology*, 13(10):1023–1028, 2013.

[16] J. P. Brill and Hemanta Mukherjee. *Multiphase flow in wells*, volume 17 of *Monograph / SPE Henry L Doherty series*. Henry L. Doherty Memorial Fund of AIME, Society of Petroleum Engineers, Richardson and Tex, 1st print edition, 1999.

[17] D. H. Beggs and J. P. Brill. A study of two-phase flow in inclined pipes. *Journal of Petroleum Technology*, 25(05):607–617, 1973.

[18] G. A. Gregory, J. M. Mandhane, and K. Aziz. Some design considerations for two-phase flow in pipes. *Journal of Canadian Petroleum Technology*, 14(01), 2013.

[19] Technology Inc. Aspen. Hysys 2004.2 operations guide, 2005.

[20] N. Petalas and K. Aziz. A mechanistic model for multiphase flow in pipes. *Journal of Canadian Petroleum Technology*, 39(06), 2000.

[21] D. Barnea. A unified model for predicting flow-pattern transitions for the whole range of pipe inclinations. *International Journal of Multiphase Flow*, 13(1):1–12, 1987.

[22] R.V.A. Oliemans, B.F.M. Pots, and N. Trompé. Modelling of annular dispersed two-phase flow in vertical pipes. *International Journal of Multiphase Flow*, 12(5):711–732, 1986.

[23] Yehuda Taitel, Dvora Bornea, and A. E. Dukler. Modelling flow pattern transitions for steady upward gas-liquid flow in vertical tubes. *AIChE Journal*, 26(3):345–354, 1980.

[24] John J. McKetta. *Piping design handbook*. M. Dekker, New York, 1992.

[25] Kjell H. Bendiksen. An experimental investigation of the motion of long bubbles in inclined tubes. *International Journal of Multiphase Flow*, 10(4):467–483, 1984.

[26] Martin Cook and Masud Behnia. Pressure drop calculation and modelling of inclined intermittent gas–liquid flow. *Chemical Engineering Science*, 55(20):4699–4708, 2000.

[27] James P. Brill, Zelimir Schmidt, William A. Coberly, John D. Herring, and David W. Moore. Analysis of two-phase tests in large-diameter flow lines in prudhoe bay field. *SPE-8305-PA*, 1981.

[28] L. Norris. Correlation of prudhoe bay liquid slug lengths and holdups including 1981 large diameter flowline tests, 1982.

[29] Stuart L. Scott, Ovadia Shoham, and James P. Brill. Prediction of slug length in horizontal, large-diameter pipes. *SPE-15103-PA*, 1989.

[30] Ove Bratland. *Pipe flow 1: Single-phase Flow Assurance*. 2009.

[31] Kim Dongwoo, J. Ghajar Afshin, and L. Dougherty Ronald. Comparison of 20 two-phase heat transfer correlations with seven sets of experimental data, including flow pattern and tube inclination effects. *Heat Transfer Engineering*, 20(1):15–40, 1999.

[32] A. J. Ghajar. Non-boiling heat transfer in gas-liquid flow in pipes: a tutorial. *Journal of the Brazilian Society of Mechanical Sciences and Engineering*, 27(1):46–73, 2005.

[33] Jae-yong Kim and Afshin J. Ghajar. A general heat transfer correlation for non-boiling gas–liquid flow with different flow patterns in horizontal pipes. *International Journal of Multiphase Flow*, 32(4):447–465, 2006.

[34] Lixin Cheng and Dieter Mewes. *Advances in Multiphase Flow and Heat Transfer (Volume 1)*. Bentham Science Publisher, 2012.

[35] E. N. Sieder and G. E. Tate. Heat transfer and pressure drop of liquids in tubes. *Industrial & Engineering Chemistry*, 28(12):1429–1435, 1936.

[36] Yong Bai and Qiang Bai. *Subsea pipelines and risers*. Ocean engineering series. Elsevier, Amsterdam and Boston, 1st ed edition, 2005.

[37] M. Vazquez and H. D. Beggs. Correlations for fluid physical property prediction. *SPE-6719-PA*, 1980.

[38] Katz, D. L. V. *Handbook of natural gas engineering*. McGraw-Hill series in chemical engineering. McGraw-Hill, 1959.

[39] Kartoatmodjo, Trijana R. S. and Zelimir Schmidt. New correlations for crude oil physical properties. 1991.

[40] O. Baker and W. Swerdloff. Calculation of surface tension 6: Finding surface tension of hydrocarbon liquids. Oil Gas J., 1956.

[41] Howard B. Bradley and Fred W. Gipson. *Petroleum engineering handbook*. Society of Petroleum Engineers, Richardson and TX and U.S.A, 1987.

[42] T. H. Ahmed. *Hydrocarbon phase behavior*. Contributions in petroleum geology & engineering. Gulf Pub. Co, 1989.

[43] William D. McCain. *The properties of petroleum fluids*. PennWell Books, Tulsa and Okla, 2nd ed edition, 1990.

[44] N. van Wingen. *Viscosity of Oil´, Water, Natural Gas and Crude Oil at Varying Pressures and Temperature: Secondary Recovery of Oil in the United States*. American Petroleum Institute, 1950.

[45] M. B. Standing. *Volumetric and phase behavior of oil field hydrocarbon systems: PVT for engineers*. California Research Corp, 1951.

[46] P. M. Dranchuk and H. Abou-Kassem. Calculation of z factors for natural gases using equations of state. *PETSOC-75-03-03*, 1975.

[47] Anthony L. Lee, Mario H. Gonzalez, and Bertram E. Eakin. The viscosity of natural gases. *SPE-1340-PA*, 1966.

[48] Armin I. Kauerauf and Thomas Hantschel. *Fundamentals of Basin and Petroleum Systems Modeling*. Springer-Verlag Berlin Heidelberg, Berlin and Heidelberg, 2009.

[49] Dave Deming and David S. Chapman. Heat flow in the utah-wyoming thrust belt from analysis of bottom-hole temperature data measured in oil and gas wells. *Journal of Geophysical Research*, 93(B11):13657, 1988.

[50] Douglas W. Waples and Jacob S. Waples. A review and evaluation of specific heat capacities of rocks, minerals, and subsurface fluids. part 2: Fluids and porous rocks. *Natural Resources Research*, 13(2):123–130, 2004.

[51] Wilbur H. Somerton. *Thermal properties and temperature-related behavior of rock/fluid systems*, volume 37 of *Developments in petroleum science*. Elsevier, Amsterdam and New York, 1992.

[52] W. R. Gambill. You can predict heat capacities. Chemical Engineering:243–248, 1957.

[53] Schlumberger. Pipesim production system analysis software: User guide: Version 2011.1, 2011.

[54] Duane Birnbaum and Michael A. Vine. *Microsoft Excel VBA programming for the absolute beginner*. Thomson Course Technology, Boston and MA, 3rd ed edition, 2007.

[55] E. Joseph Billo. *Excel for scientists and engineering: Numerical methods*. Wiley-Interscience, Hoboken, 2007.

Appendices

Appendix A

SEM-Flow code

A.1   Frame-Module

```
1  Public Sub Frame()

3  '_____
   'Inputdata
5  '_____
   Dim p_1 As Single
7  Dim T_1 As Single
   Dim gamma_G As Single
9  Dim gamma_API As Single
   Dim R_p As Single
11 Dim T_sep As Single
   Dim p_sep As Single
13 Dim S As Single
   Dim q_L As Single
15 Dim f_w As Single
   Dim GOR As Single
17 Dim epsilon As Single
   Dim d As Single
19 Dim T_o As Single
   Dim s_w As Single
21 Dim v_o As Single
   Dim k_pipe As Single

23
   p_1 = Worksheets("Input_Data").Range("G11")
25 T_1 = Worksheets("Input_Data").Range("G12")
   gamma_API = Worksheets("Input_Data").Range("G20")
27 gamma_G = Worksheets("Input_Data").Range("G21")
   T_sep = Worksheets("Input_Data").Range("G27")
29 p_sep = Worksheets("Input_Data").Range("G26")
   R_p = Worksheets("Input_Data").Range("G25")
31 f_w = Worksheets("Input_Data").Range("G28")
   q_L = Worksheets("Input_Data").Range("G29")
```

```vba
S = Worksheets("Input_Data").Range("G22")
d = Worksheets("Input_Data").Range("G32")
epsilon = Worksheets("Input_Data").Range("G35")
T_o = Worksheets("Input_Data").Range("G39")
s_w = Worksheets("Input_Data").Range("G33")
v_o = Worksheets("Input_Data").Range("G38")
k_pipe = Worksheets("Input_Data").Range("G34")

'_____
'Increment Loop
'_____

Dim n_Section As Integer
Dim L_Section_V() As Single
Dim L_Section_H() As Single
Dim L_Section() As Single
Dim alpha_Section() As Single
Dim n_Increment() As Single
Dim n_Increment_tot() As Single
Dim L_Increment() As Single

n_Section = Worksheets("Elevation").Range("E11")

ReDim L_Section(1 To n_Section)
ReDim alpha_Section(1 To n_Section)
ReDim L_Section_H(1 To n_Section)
ReDim L_Section_V(1 To n_Section)
Dim Count As Integer

Count = 0
Do
Count = Count + 1
L_Section_H(Count) = Worksheets("Elevation").Range("E" & Count + 35)
L_Section_V(Count) = Worksheets("Elevation").Range("F" & Count + 35)

If L_Section_H(Count) <> 0 Then
    alpha_Section(Count) = Atn(L_Section_V(Count) / L_Section_H(Count))
ElseIf L_Section_V(Count) > 0 Then
    alpha_Section(Count) = WorksheetFunction.Pi() / 2
ElseIf L_Section_V(Count) < 0 Then
    alpha_Section(Count) = -WorksheetFunction.Pi() / 2
Inlet If

If L_Section_H(Count) <> 0 Then
```

```
77      L_Section(Count) = L_Section_H(Count) / Cos(Abs(alpha_Section(
            Count)))
   Else
79      L_Section(Count) = Abs(L_Section_V(Count))
   Inlet If
81
   Loop Until (Count = n_Section)
83


85
   ReDim n_Increment(1 To n_Section)
87 ReDim L_Increment(1 To n_Section)
   ReDim n_Increment_tot(n_Section)
89 Count = 0
   Do
91 Count = Count + 1
   n_Increment(Count) = 5
93 n_Increment_tot(Count) = n_Increment(Count) + n_Increment_tot(
       Count − 1)
   L_Increment(Count) = L_Section(Count) / n_Increment(Count)
95 Loop Until (Count = n_Section)

97 '_____
   'Calculation
99 '_____
   Dim T_Outlet As Single
101 Dim p_Outlet As Single
   Dim T_Inlet As Single
103 Dim p_Inlet As Single
   Dim Actalpha As Single
105 Dim ActIncrement As Single
   Dim ActSection As Single
107 Dim p_Inlet_Section() As Single
   Dim T_Inlet_Section() As Single
109 Dim delta_p_Increment As Single
   Dim E_L As Single
111 Dim Pattern As String
   Dim dp_dL As Single
113
   'Heat loss variables
115 Dim roh_o As Single
   Dim roh_w As Single
117 Dim cp_o As Single
   Dim cp_w As Single
119 Dim Z As Single
   Dim q_o_m As Single
121 Dim q_w_m As Single
   Dim deltaHv As Single
```

```vbnet
123
   Dim roh_L_Outlet As Single
125 Dim roh_G_Outlet As Single
   Dim my_L_Outlet As Single
127 Dim my_L_wall_Outlet As Single
   Dim my_G_Outlet As Single
129 Dim sigma_L_Outlet As Single
   Dim v_SL_Outlet As Single
131 Dim v_SG_Outlet As Single
   Dim k_L_Outlet As Single
133 Dim k_G_Outlet As Single
   Dim cp_L_Outlet As Single
135 Dim cp_G_Outlet As Single


137 Dim roh_L_Inlet As Single
   Dim roh_G_Inlet As Single
139 Dim my_L_Inlet As Single
   Dim my_L_wall_Inlet As Single
141 Dim my_G_Inlet As Single
   Dim sigma_L_Inlet As Single
143 Dim v_SL_Inlet As Single
   Dim v_SG_Inlet As Single
145 Dim k_L_Inlet As Single
   Dim k_G_Inlet As Single
147 Dim cp_L_Inlet As Single
   Dim cp_G_Inlet As Single
149
   T_Outlet = T_1
151 p_Outlet = p_1
   ActIncrement = 0
153 ActSection = 1
   ReDim p_Inlet_Section(n_Section)
155 ReDim T_Inlet_Section(n_Section)

157 p_Inlet_Section(0) = p_1
   T_Inlet_Section(0) = T_1
159
   Do
161
   Point1:
163
   ActIncrement = ActIncrement + 1
165

167 Call FluidPropertiesMain(p_Outlet, T_Outlet, T_o, d, gamma_G,
      gamma_API, R_p, p_sep, T_sep, S, q_L, f_w, roh_L_Outlet,
      roh_G_Outlet, my_L_Outlet, my_L_wall_Outlet, my_G_Outlet,
      sigma_L_Outlet, v_SL_Outlet, v_SG_Outlet, k_L_Outlet,
```

```vb
         k_G_Outlet , cp_L_Outlet , cp_G_Outlet , roh_o , roh_w , cp_o , cp_w ,
         Z, q_o_m, q_w_m, deltaHv)

169
     If ActIncrement <= n_Increment_tot(ActSection) Then
171        ActSection = ActSection
     Else
173        ActSection = ActSection + 1
     Inlet If
175


177  Actalpha = alpha_Section(ActSection)

179  Call FlowPatternPrediction(v_SL_Outlet , v_SG_Outlet , Actalpha ,
        sigma_L_Outlet , roh_L_Outlet , d, my_L_Outlet , roh_G_Outlet ,
        my_G_Outlet , epsilon , Pattern , E_L , dp_dL)

181  delta_p_Increment = -dp_dL * L_Increment(ActSection)

183  p_Inlet = p_Outlet + delta_p_Increment * 0.00001


185
     'Check if delta p is small enough
187  If p_Inlet <= (p_Outlet + p_Outlet * 0.05) Then
         If ActIncrement = n_Increment_tot(ActSection) Then
189          p_Inlet_Section(ActSection) = p_Inlet
             p_Outlet = p_Inlet
191      Else
              p_Outlet = p_Inlet
193      Inlet If
     Else
195      n_Increment(ActSection) = WorksheetFunction.Round(n_Increment(
             ActSection) * 1.25, 0)
         ActIncrement = n_Increment_tot(ActSection - 1)
197      p_Outlet = p_Inlet_Section(ActSection - 1)
         T_Outlet = T_Inlet_Section(ActSection - 1)
199
         Count = 0
201      Do
         Count = Count + 1
203      n_Increment_tot(Count) = n_Increment(Count) + n_Increment_tot(
             Count - 1)
         L_Increment(Count) = L_Section(Count) / n_Increment(Count)
205      Loop Until (Count = n_Section)
         GoTo Point1
207  Inlet If


209
```

```vb
    Call HeatLoss(d, E_L, s_w, T_Outlet, T_o, v_o, k_pipe, L_Increment
        (ActSection), p_Outlet, p_Inlet, T_o, gamma_G, gamma_API, R_p,
        p_sep, T_sep, S, q_L, f_w, GOR, T_Inlet)
211

    'Check if delta T is small enough
213
    If  T_Inlet <= (T_Outlet + T_Outlet * 0.05) Then
215     If  ActIncrement = n_Increment_tot(ActSection) Then
            T_Inlet_Section(ActSection) = T_Inlet
217         T_Outlet = T_Inlet
        Else
219         T_Outlet = T_Inlet
        Inlet If
221 Else
        n_Increment(ActSection) = WorksheetFunction.Round(n_Increment(
            ActSection) * 1.25, 0)
223     ActIncrement = n_Increment_tot(ActSection - 1)
        T_Outlet = T_Inlet_Section(ActSection - 1)
225     p_Outlet = p_Inlet_Section(ActSection - 1)

227     Count = 0
        Do
229     Count = Count + 1
        n_Increment_tot(Count) = n_Increment(Count) + n_Increment_tot(
            Count - 1)
231     L_Increment(Count) = L_Section(Count) / n_Increment(Count)
        Loop Until (Count = n_Section)
233     GoTo Point1
    Inlet If
235
    Call FluidPropertiesMain(p_Inlet, T_Inlet, T_o, d, gamma_G,
        gamma_API, R_p, p_sep, T_sep, S, q_L, f_w, roh_L_Inlet,
        roh_G_Inlet, my_L_Inlet, my_L_wall_Inlet, my_G_Inlet,
        sigma_L_Inlet, v_SL_Inlet, v_SG_Inlet, k_L_Inlet, k_G_Inlet,
        cp_L_Inlet, cp_G_Inlet, roh_o, roh_w, cp_o, cp_w, Z, q_o_m,
        q_w_m, deltaHv)
237
    If (roh_L_Inlet >= (roh_L_Outlet - roh_L_Outlet * 0.05)) And (
        roh_L_Inlet <= (roh_L_Outlet + roh_L_Outlet * 0.05)) And (
        roh_G_Inlet >= (roh_G_Outlet - roh_G_Outlet * 0.05)) And (
        roh_G_Inlet <= (roh_G_Outlet + roh_G_Outlet * 0.05)) And (
        my_L_Inlet >= (my_L_Outlet - my_L_Outlet * 0.05)) And (
        my_L_Inlet <= (my_L_Outlet + my_L_Outlet * 0.05)) And (
        my_G_Inlet >= (my_G_Outlet - my_G_Outlet * 0.05)) And (
        my_G_Inlet <= (my_G_Outlet + my_G_Outlet * 0.05)) And (
        sigma_L_Inlet >= (sigma_L_Outlet - sigma_L_Outlet * 0.05)) And
        (sigma_L_Inlet <= (sigma_L_Outlet + sigma_L_Outlet * 0.05)) And
         (k_L_Inlet >= (k_L_Outlet - k_L_Outlet * 0.05)) And (k_L_Inlet
```

```vbnet
        <= (k_L_Outlet + k_L_Outlet * 0.05)) And (k_G_Inlet >= (
     k_G_Outlet - k_G_Outlet * 0.05)) And (k_G_Inlet <= (k_G_Outlet
     + k_G_Outlet * 0.05)) And (cp_L_Inlet >= (cp_L_Outlet -
     cp_L_Outlet * 0.05)) And (cp_L_Inlet <= (cp_L_Outlet +
     cp_L_Outlet * 0.05)) And (cp_G_Inlet >= (cp_G_Outlet -
     cp_G_Outlet * 0.05)) And (cp_G_Inlet <= (cp_G_Outlet +
     cp_G_Outlet * 0.05)) Then
239     T_Outlet = T_Inlet
        p_Outlet = p_Inlet
241 Else
        n_Increment(ActSection) = WorksheetFunction.Round(n_Increment(
           ActSection) * 1.25, 0)
243     ActIncrement = n_Increment_tot(ActSection - 1)
        T_Outlet = T_Inlet_Section(ActSection - 1)
245     p_Outlet = p_Inlet_Section(ActSection - 1)

247     Count = 0
        Do
249     Count = Count + 1
        n_Increment_tot(Count) = n_Increment(Count) + n_Increment_tot(
           Count - 1)
251     L_Increment(Count) = L_Section(Count) / n_Increment(Count)
        Loop Until (Count = n_Section)
253     GoTo Point1
    Inlet If
255
    Loop Until (ActIncrement = n_Increment_tot(n_Section))
257
    End Sub
```

A.2   Colebrook equation

```vbnet
1 Public Function Fktf_iter(ByVal Re As Single, ByVal epsilon As
     Single, ByVal d As Single) As Single
     Start = 1
3
  Do
5     Count = Count + 1

7     f1 = Start
      f2 = 1 / (3.48 - 4 * WorksheetFunction.Log(2 * epsilon / d +
         9.35 / (Re * f1 ^ 0.5))) ^ 2
9     Start = f2
  Loop Until (Abs(f1 - f2) < 0.000001)
11
  Fktf_iter = f2
```

```
13 End Function
```

A.3 Iteration procedure

```
1  '——————————————
   'Iteration Loop
3  '——————————————
   Dim x0 As Double
5  Dim x1 As Double
   Dim a As Double
7  Dim b As Double
   Dim fxo As Double
9  Dim fx1 As Double
   Dim fa As Double
11 Dim fb As Double
   Dim fx_x As Double
13 Dim x_x As Double

15 'Find start value
   x0 = 0.000001
17 x1 = x0 + 0.01

19 FindStartValue:

21     fx0 = Fkth_L_snake(x0, v_SL, v_SG, alpha, g, roh_L, d, my_L,
             roh_G, my_G, epsilon)
       fx1 = Fkth_L_snake(x1, v_SL, v_SG, alpha, g, roh_L, d, my_L,
             roh_G, my_G, epsilon)
23
    If fx0 * fx1 < 0 Then
25          If fx0 < 0 Then
                b = x0
27              a = x1

29          Else
                b = x1
31              a = x0

33          End If

35      Else
            If x1 <= 1 Then
37              x1 = x1 + 0.01
                GoTo FindStartValue
39
```

```vb
            Else
                    MsgBox ("Stratified_Flow:_There_is_no_root.")
            End If

     End If

'Move lower start value closer to root

If a < b Then
     Do
          a = a + 0.001

          a1 = a + 0.001
          fa1 = Fkth_L_snake(a1, v_SL, v_SG, alpha, g, roh_L, d,
              my_L, roh_G, my_G, epsilon)
     Loop Until (fa1 < 0)
Else
     Do
          b = b + 0.001

          b1 = b + 0.001
          fb1 = Fkth_L_snake(b1, v_SL, v_SG, alpha, g, roh_L, d,
              my_L, roh_G, my_G, epsilon)
     Loop Until (fb1 > 0)
End If

'Peagasus algorithm

Dim Control As Double
Dim Count As Double
Dim chi As Double
Dim x() As Double
ReDim x(0 To 9) As Double
Dim Index As Integer
Count = 1
chi = 1
Index = 0

Do
     Count = Count + 1


     fa = chi * Fkth_L_snake(a, v_SL, v_SG, alpha, g, roh_L, d,
         my_L, roh_G, my_G, epsilon)
     fb = Fkth_L_snake(b, v_SL, v_SG, alpha, g, roh_L, d, my_L,
         roh_G, my_G, epsilon)

```

```
85
        x_x = b - fb * (a - b) / (fa - fb)
87      fx_x = Fkth_L_snake(x_x, v_SL, v_SG, alpha, g, roh_L, d, my_L,
            roh_G, my_G, epsilon)

89


91
        If fx_x < 0 Then

93
            chi = fb / (fb + fx_x)

95
            a = a
97          b = x_x


99      Else


101         chi = 1
            a = x_x
103         b = b


105     End If


107     x(Index) = x_x

109 Control = (x(0) - x(1)) + (x(0) - x(2)) + (x(0) - x(3)) + (x(0) -
        x(4)) + (x(0) - x(5)) + (x(0) - x(6)) + (x(0) - x(7)) + (x(0) -
        x(8)) + (x(0) - x(9))

111     Index = Index + 1
        If Index = 10 Then
113         Index = 0
        Else
115         Index = Index
        End If

117


119
    Loop Until (Abs(fx_x) < 0.0001 Or (Control < (10 ^ -10) And
        Control > (-10 ^ -10)))

121


123 h_L_snake = x_x
```

Appendix B

Input/Output-Interface

Fig. B.1 shows the input data page in SEM-Flow.

Fig. B.2 shows the page where the elevation profile is defined in SEM-Flow.

Fig. B.3 shows the output data page in SEM-Flow.

Input Data   SEM-Flow

Input Data

New Calculation

Boundary conditions

Initial Pressure	$p_{Outlet}=$	20,00	[bara]
Initial Temperature	$T_{Outlet}=$	40,00	[°C]

Fluid property data

API gravity	$\gamma_{API}=$	35,90	[°API]
Sepcific gas gravity	$\gamma_{G}=$	0,62	[-]
Salinity	$S=$	0,00	[%]

Flow data

Producing gas oil ratio	$R_{p}=$	125,22	[Sm^3/m^3]
Act. Sepeartion pressure	$p_{sep}=$	1,01	[bara]
Act. Sepeartion temperature	$T_{sep}=$	15,56	[°C]
Watercut	$f_{W}=$	0,03	[-]
Liquid flow rate	$q_{L}=$	5811,10	[m^3/d]

Pipeline data

Inner pipe diameter	$D=$	0,31	[m]
Wall thickness	$s=$	0,01	[m]
Wall thermal conductivity	$k_{pipe}=$	50,00	[W/mK]
Pipe roughness	$\varepsilon=$	0,00	[m]

Ambient fluid data

Fluid velocity	$v_{o}=$	1,00	[m/s]
Fluid temperature	$T_{o}=$	20,00	[°C]

Figure B.1: Input data page SEM-Flow.

Elevation profile SEM-Flow

Elevation profile

| Gennerate Table | Start calculation |

Total number of segments n= 11
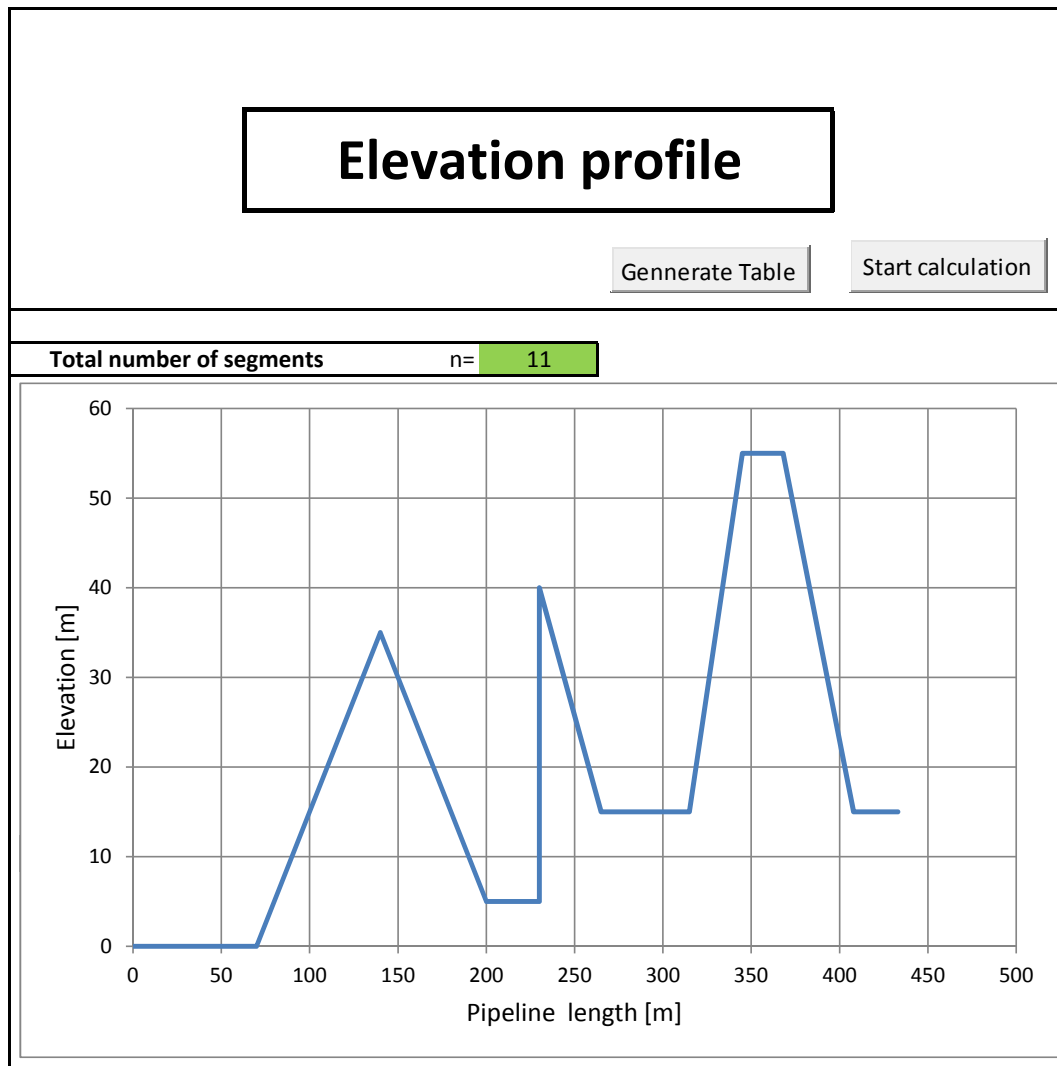
Segment number	Horizontal length [m]	Vertical length [m]
1	25	0
2	40	-40
3	23	0
4	30	40
5	50	0
6	35	-25
7	0	35
8	30	0
9	60	-30
10	70	35
11	70	0

tecon®
ENGINEERING

1 01.09.2014

Figure B.2: Elevation input page SEM-Flow.

Output data summary SEM-Flow

Output Data

Pressure Outlet	p_{Outlet}=	20,00	[bara]
Pressure Inlet	p_{Inlet}=	23,84	[bara]
Pressure loss	Δp=	3,84	[bara]
Temperature Outlet	T_{Outlet}=	40,00	[°C]
Temperature Inlet	T_{Inlet}=	41,13	[°C]
Temperature loss	ΔT=	1,13	[°C]
Flow pattern (Outlet)		Stratified Flow	
Superficial Gas Velocity Outlet	$v_{G,Outlet}$=	5,50	[m/s]
Superficial Gas Velocity Inlet	$v_{G,Inlet}$=	4,54	[m/s]
Superficial Gas Velocity Average	$v_{G,Average}$=	5,08	[m/s]
Superficial Liquid Velocity Outlet	$v_{L,Outlet}$=	0,94	[m/s]
Superficial Liquid Velocity Inlet	$v_{L,Inlet}$=	0,95	[m/s]
Superficial Liquid Velocity Average	$v_{L,Average}$=	0,95	[m/s]
Liquid Hold Up Outlet	$E_{L,Outlet}$=	0,24	[-]
Liquid Hold Up Inlet	$E_{L,Inlet}$=	0,27	[-]
Liquid Hold Up Average	$E_{L,Average}$=	0,24	[-]
Translational Slug Velocity (Outlet)	$v_{T,Outlet}$=	-	[m/s]
Translational Slug Velocity Average	$v_{T,Average}$=	7,11	[m/s]
Slug Unit Length (Outlet)	$L_{U,Outlet}$=	-	[m]
Slug Unit Length Average	$L_{U,Average}$=	186,51	[m]

01.09.2014

Figure B.3: Output data page SEM-Flow.

Appendix C

Results

C.1   Results fluid properties
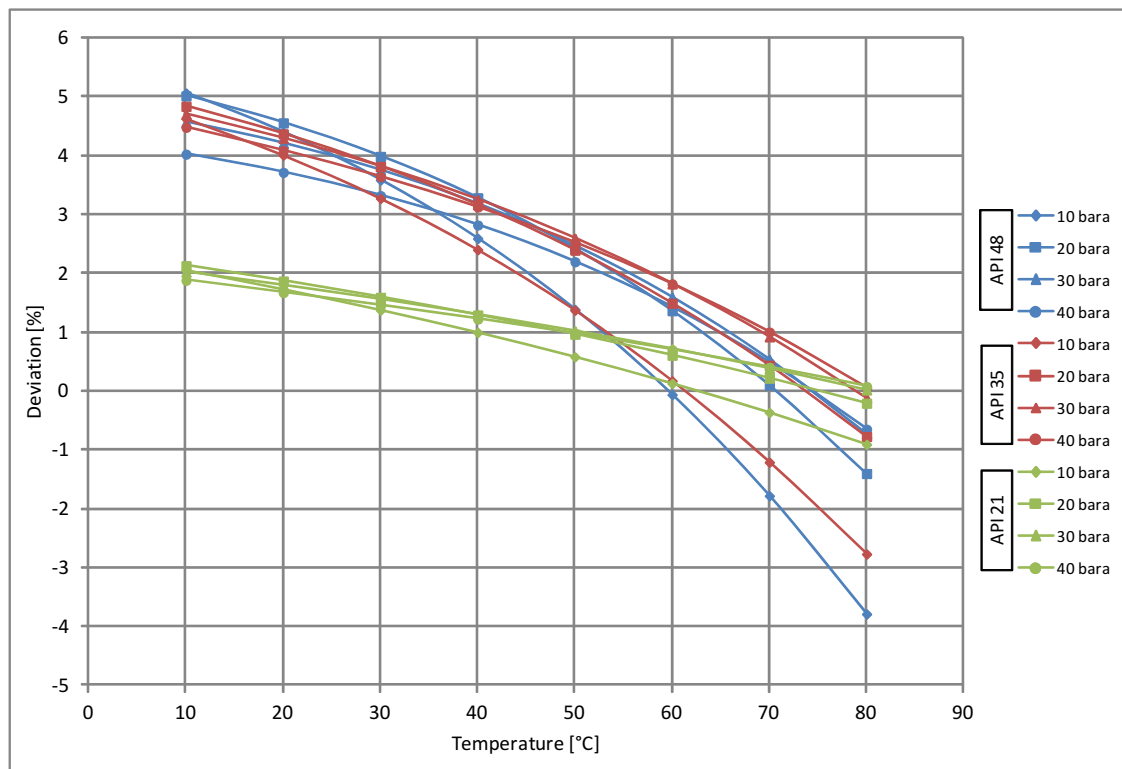
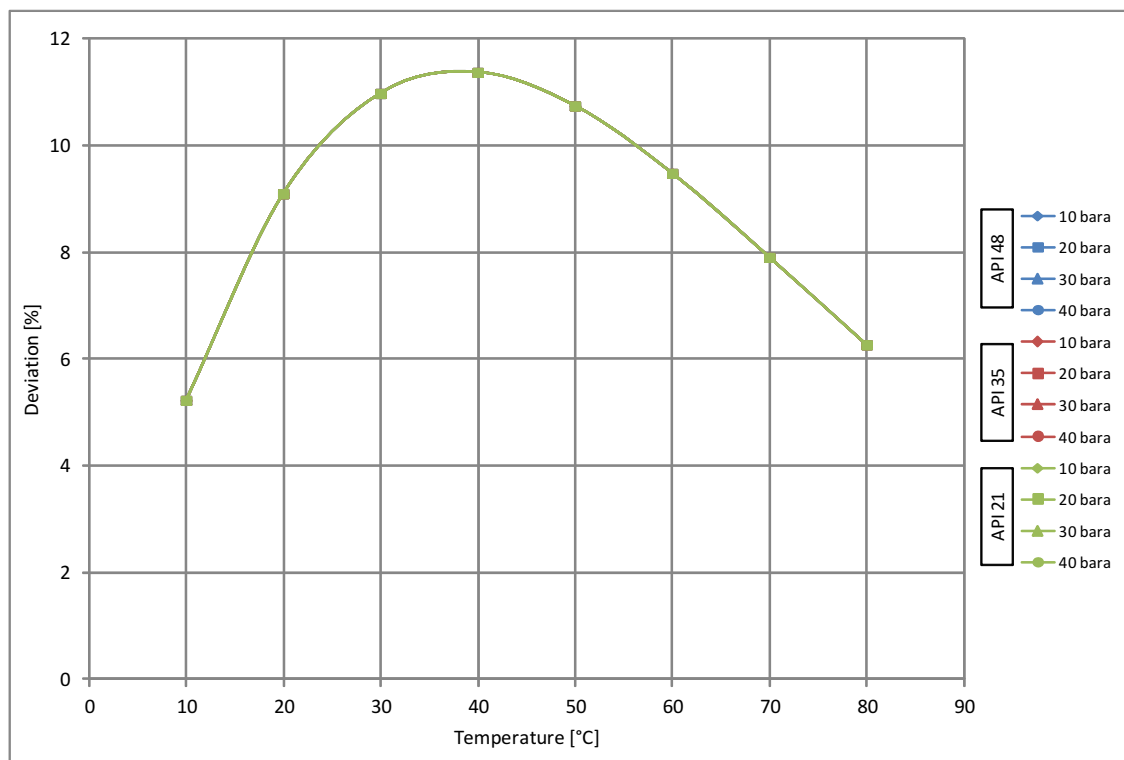Figure C.1: Deviation of the gas density for varying API gravities.
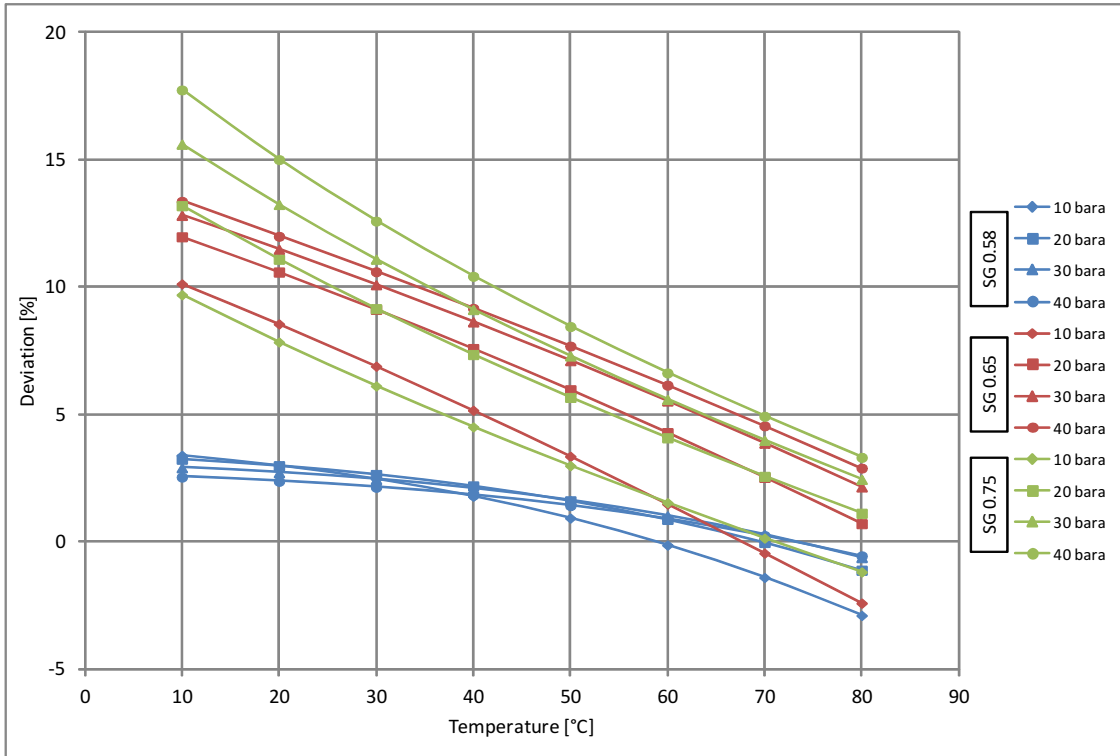
Figure C.2: Deviation of the gas density for varying specific gas gravities.
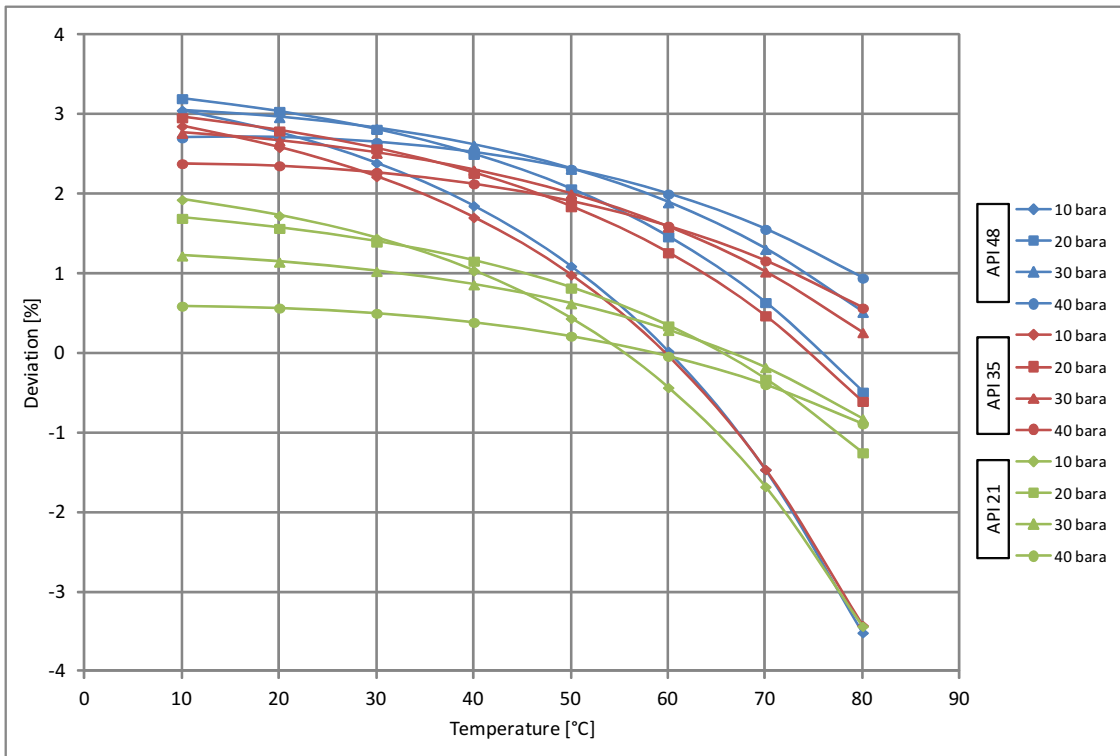
Figure C.3: Deviation of the volumetric gas flow rate for varying API gravities.
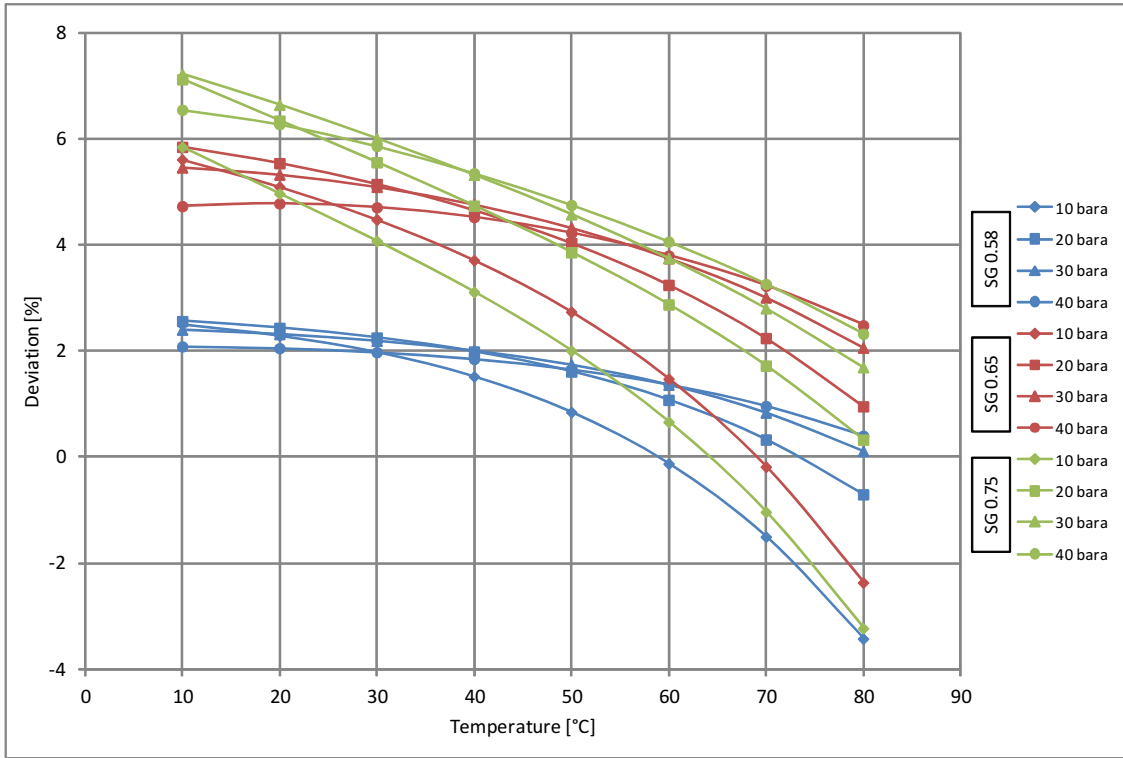
Figure C.4: Deviation of the volumetric gas flow rate for varying specific gas gravities.
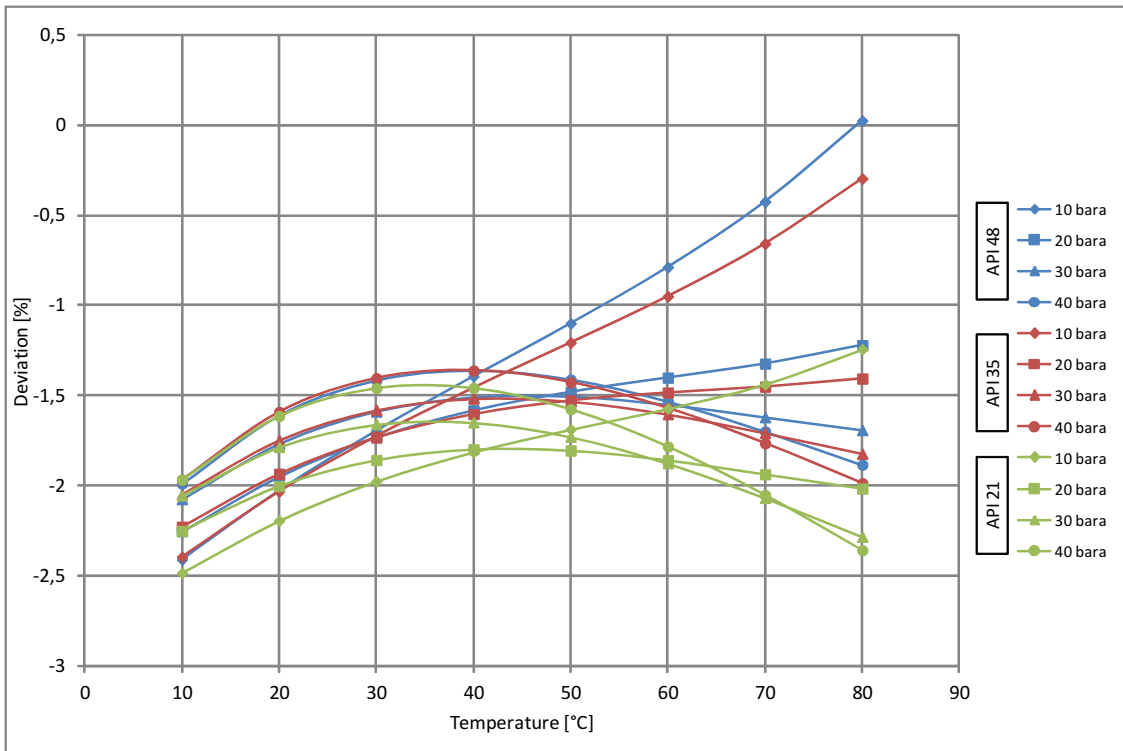
Figure C.5: Deviation of the gas specific heat capacity for varying API gravities.
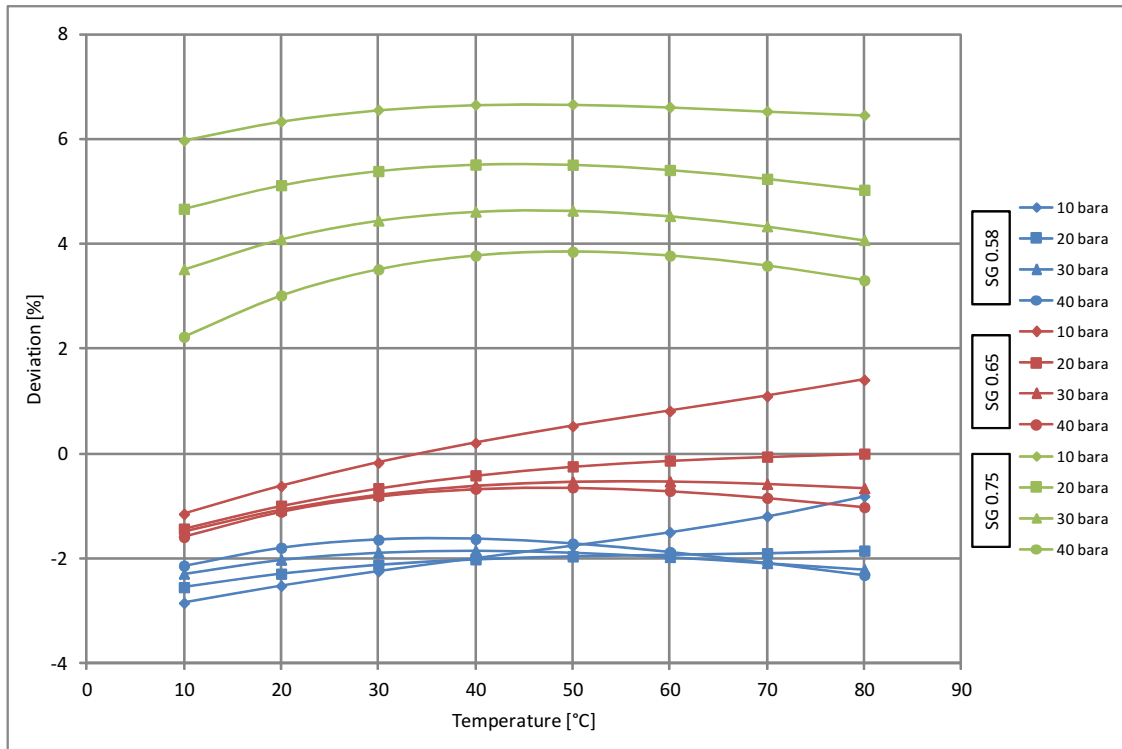
Figure C.6: Deviation of the gas specific heat capacity for varying specific gas gravities.
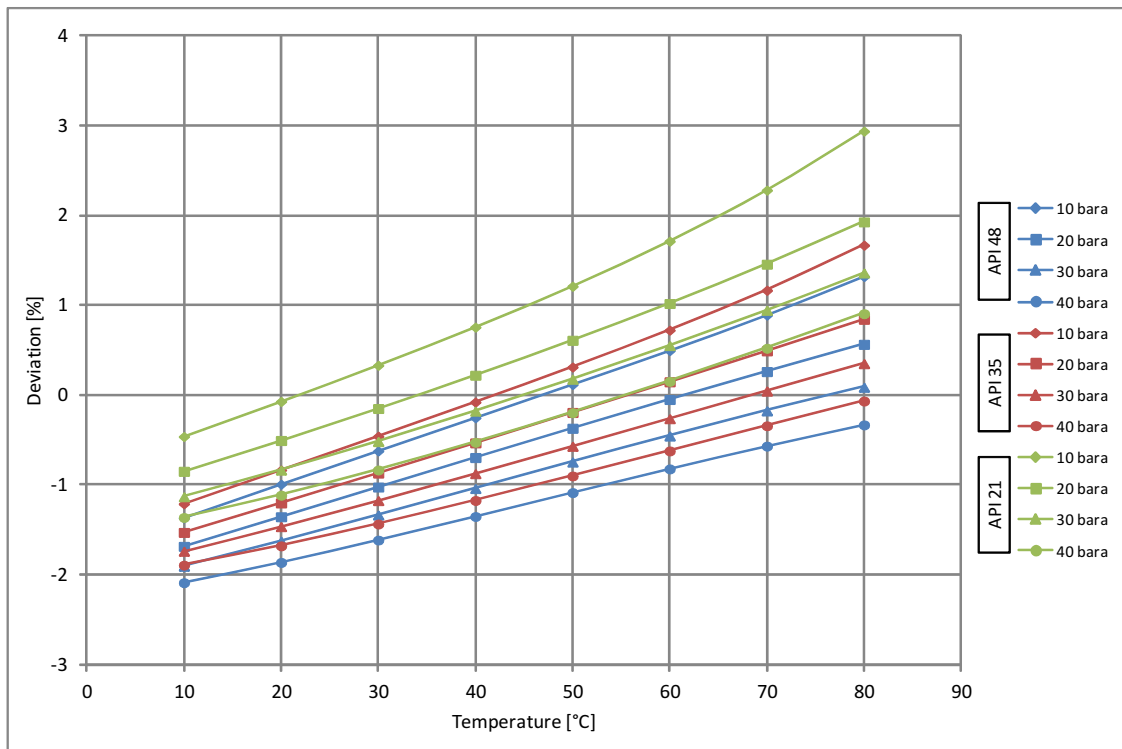
Figure C.7: Deviation of the gas viscosity for varying API gravities.
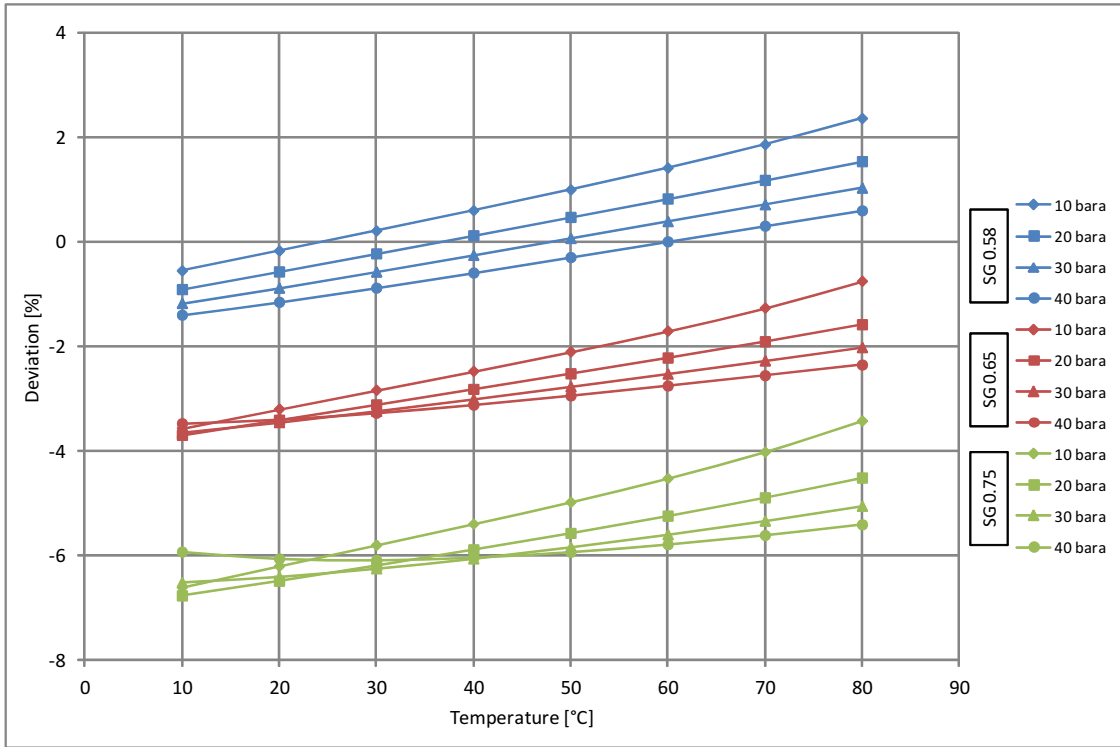
Figure C.8: Deviation of the gas viscosity for varying specific gas gravities.
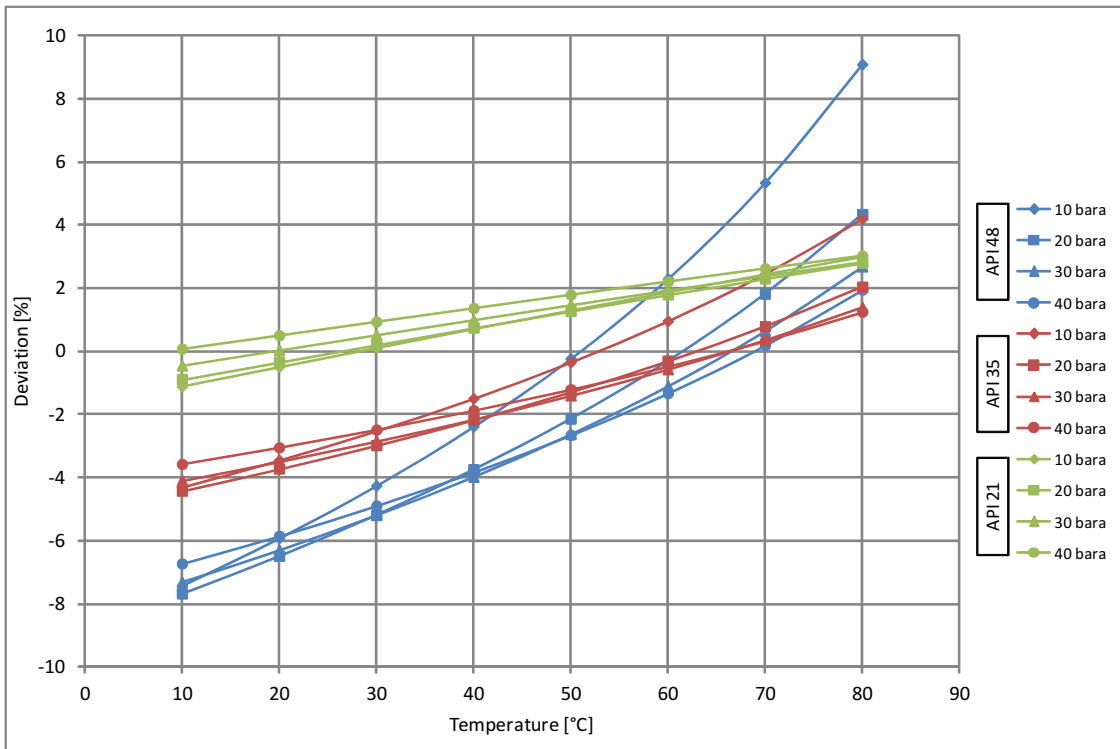
Figure C.9: Deviation of the volumetric oil flow rate for varying API gravities.
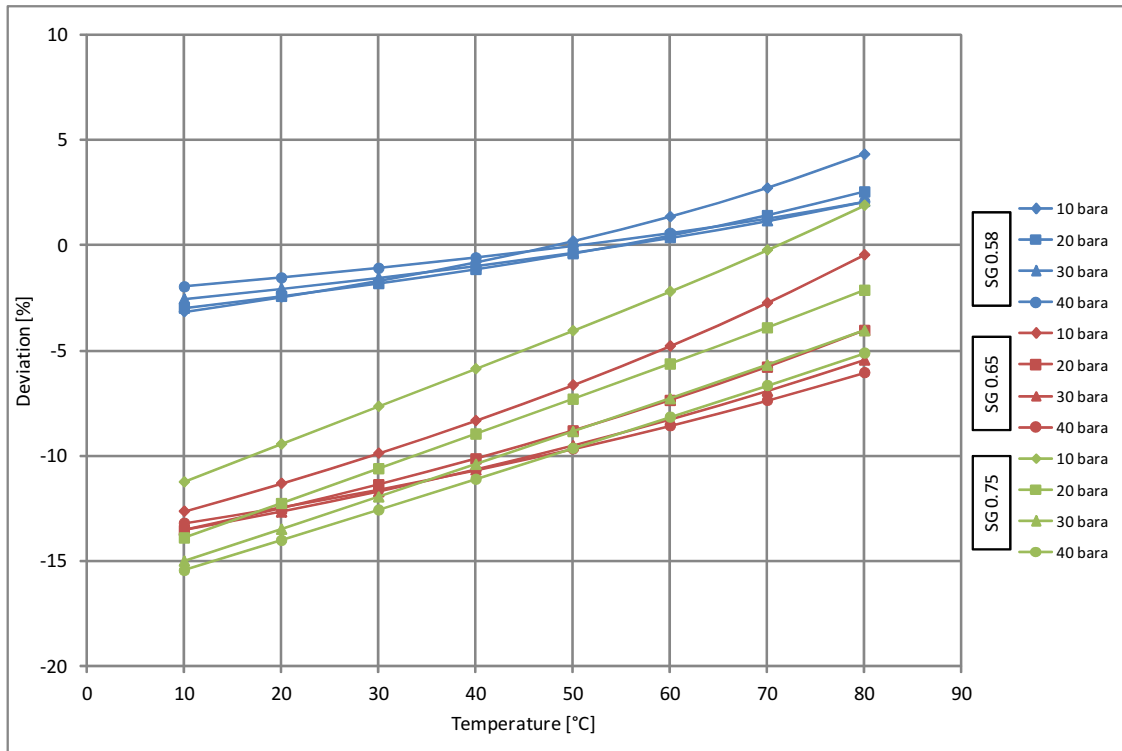
Figure C.10: Deviation of the volumetric oil flow rate for varying specific gas gravities.
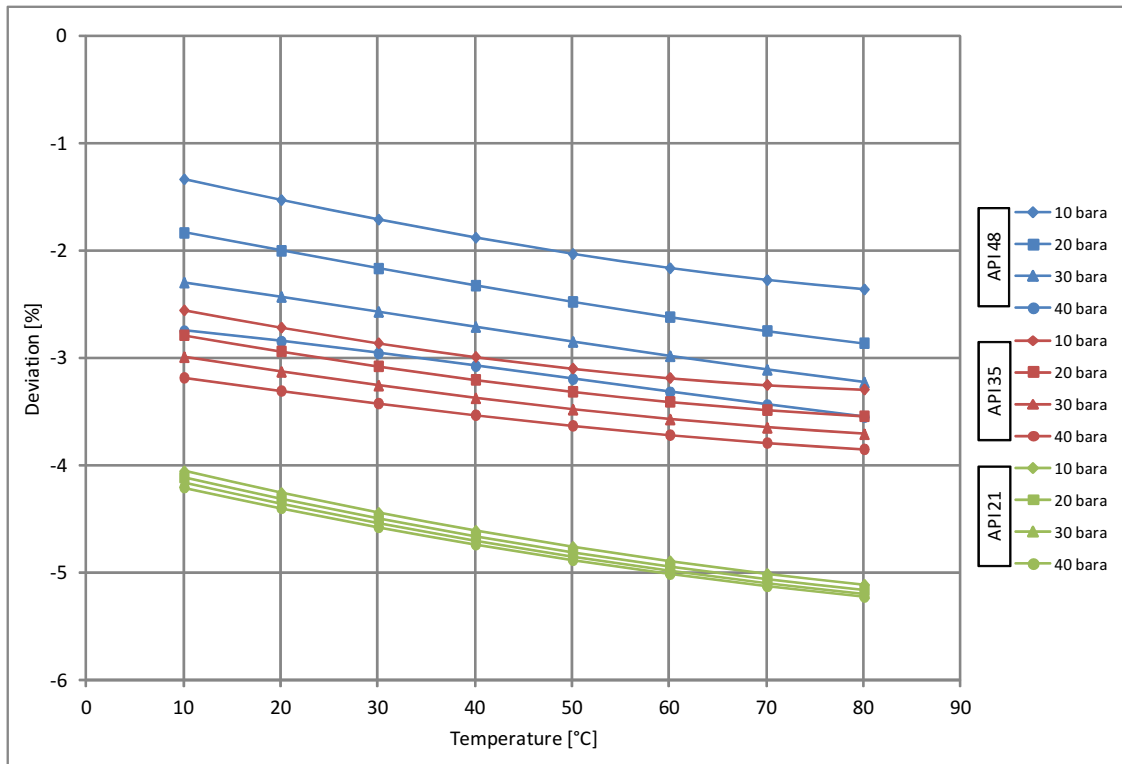
Figure C.11: Deviation of the oil specific heat capacity for varying API gravities.
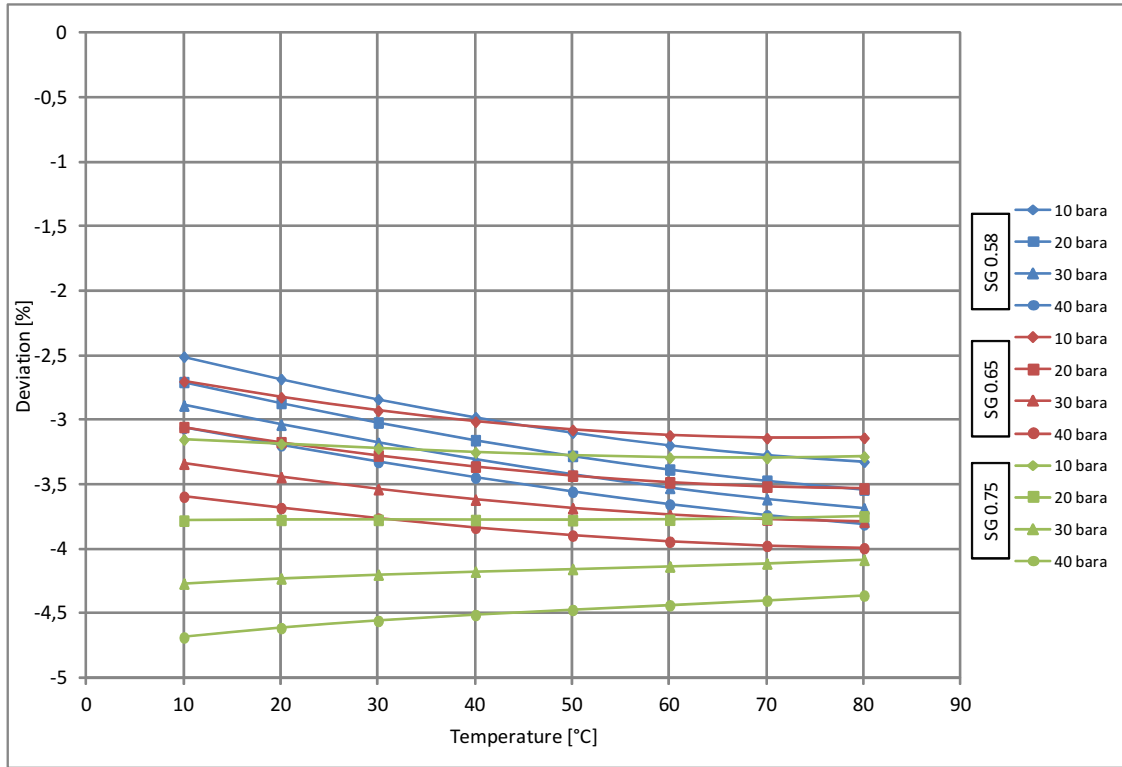
Figure C.12: Deviation of the oil specific heat capacity for varying specific gas gravities.
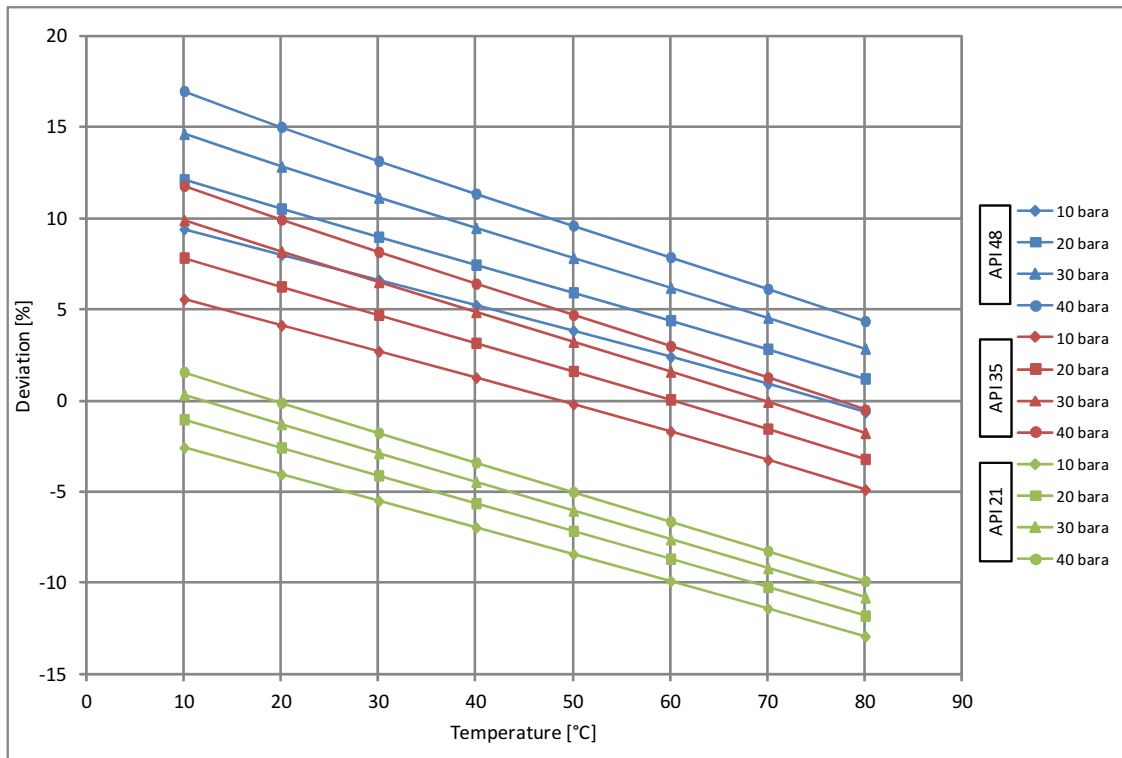
Figure C.13: Deviation of the oil thermal conductivity for varying API gravities.
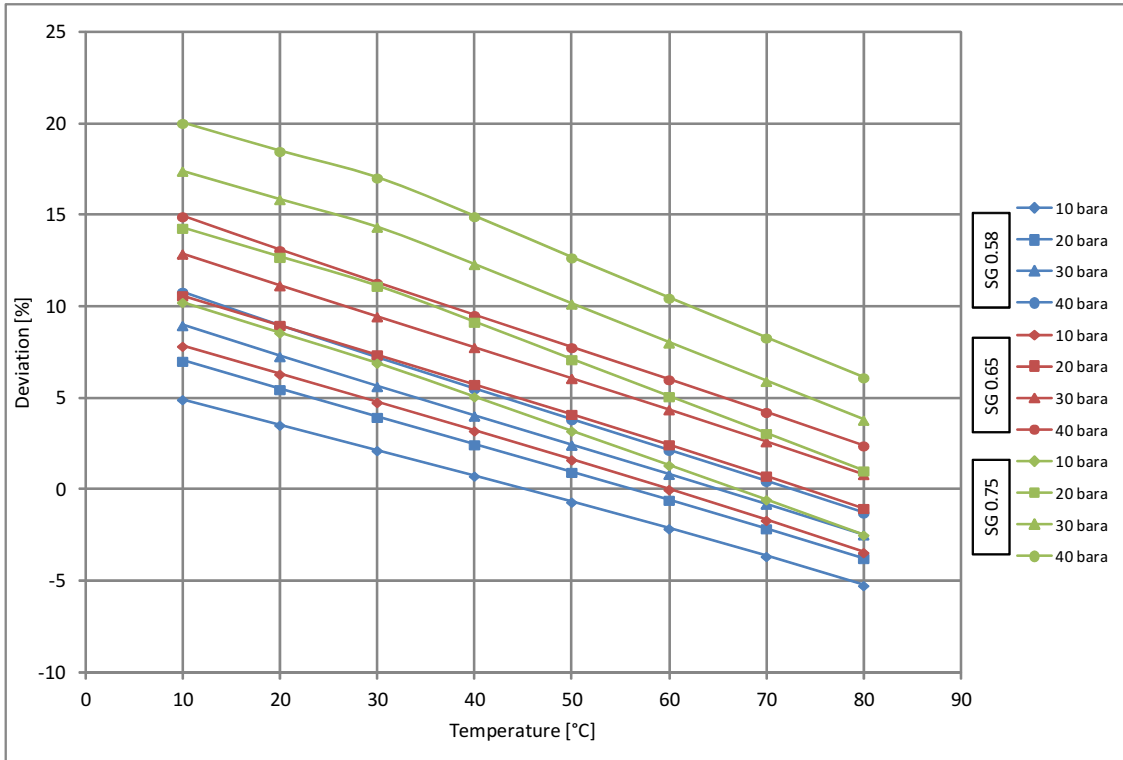
Figure C.14: Deviation of the oil thermal conductivity for varying specific gas gravities.
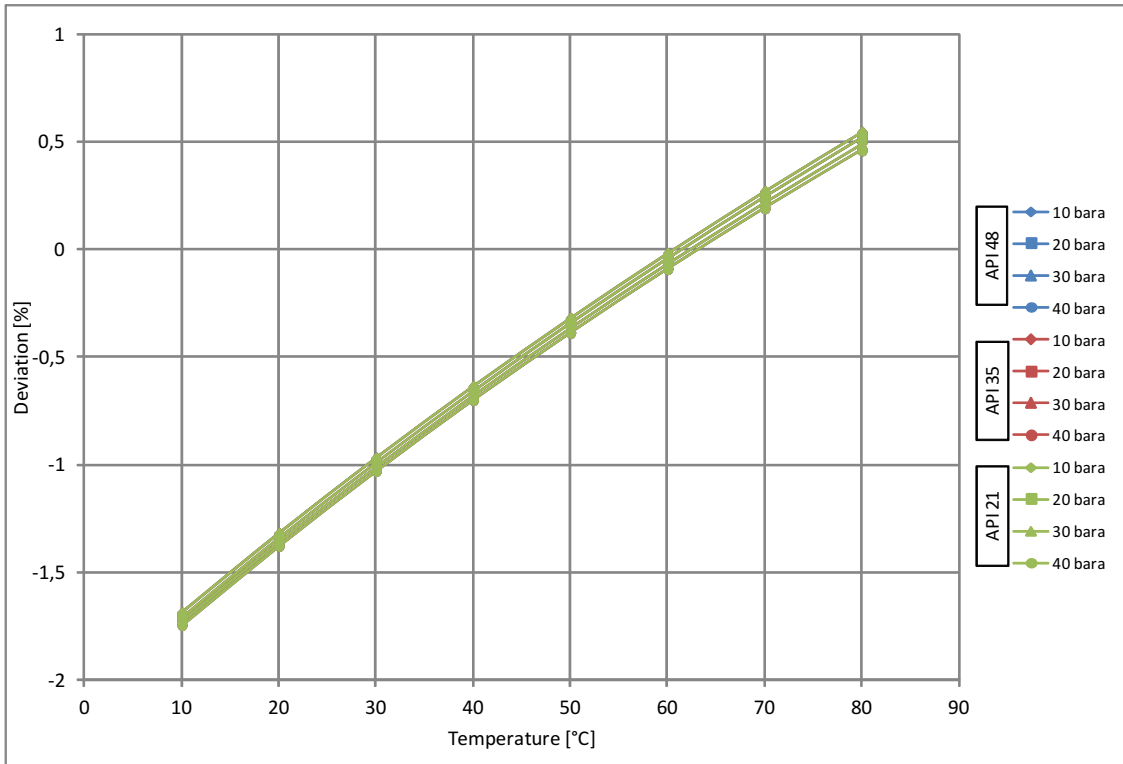
Figure C.15: Deviation of the water density for varying API gravities.
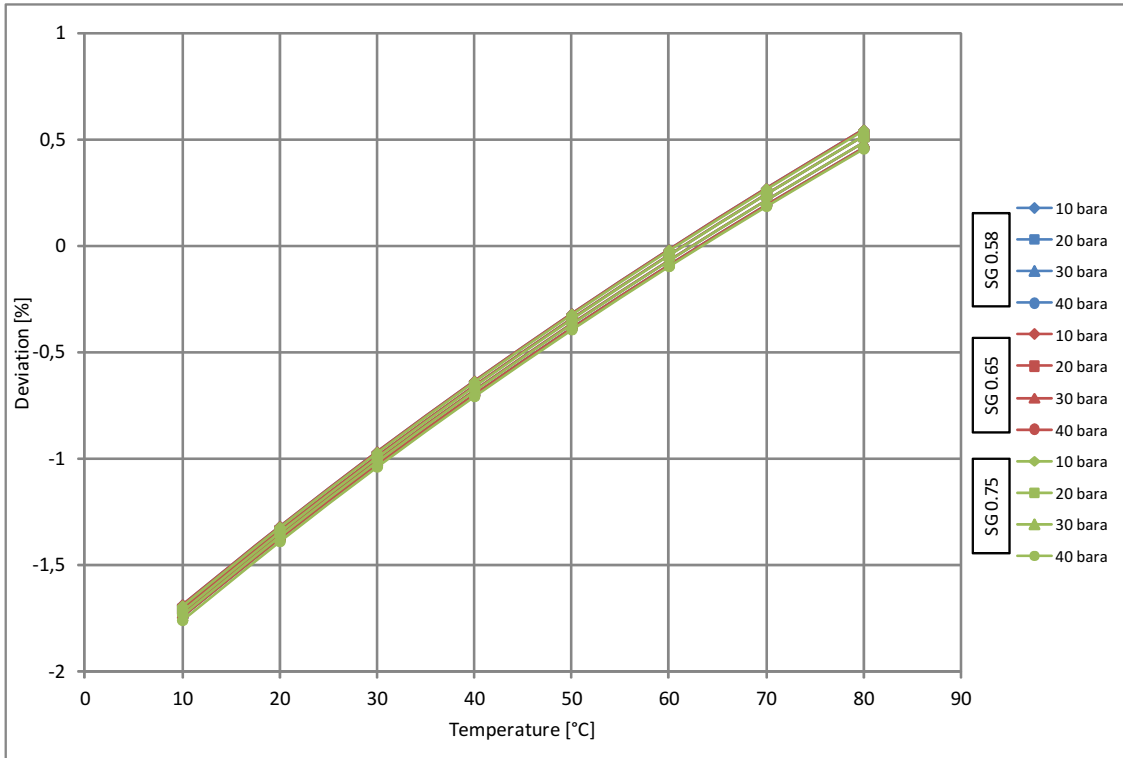
Figure C.16: Deviation of the water density for varying specific gas gravities.
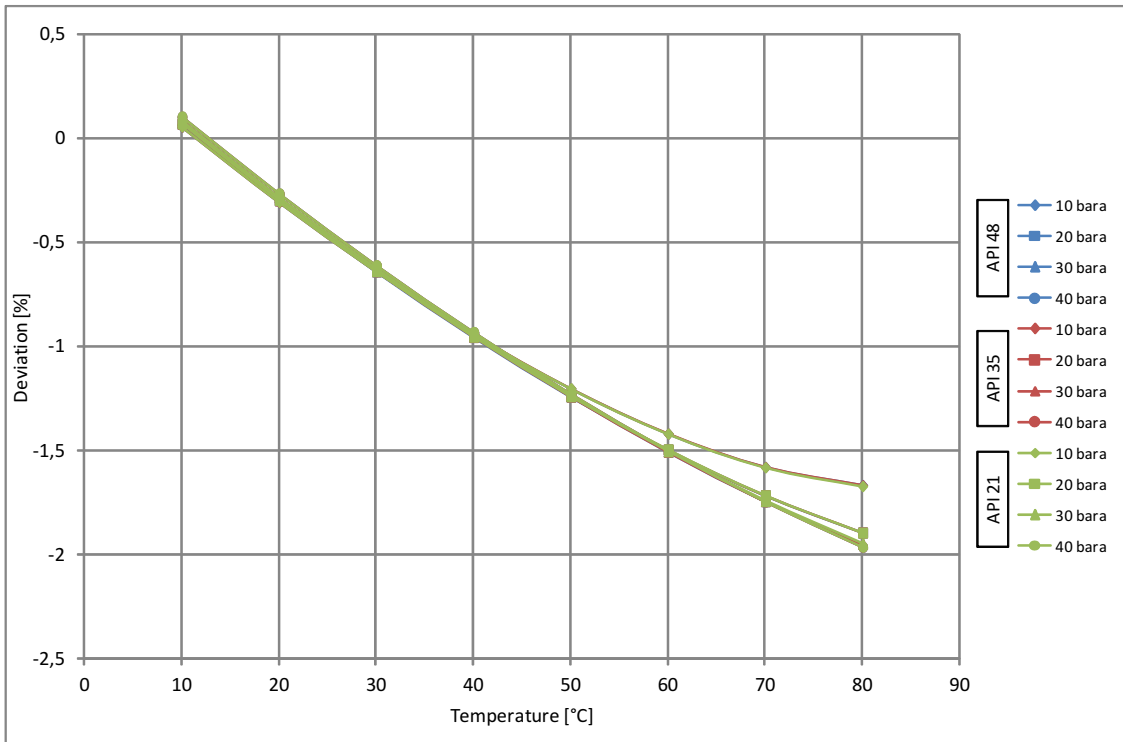
Figure C.17: Deviation of the volumetric water flow rate for varying API gravities.
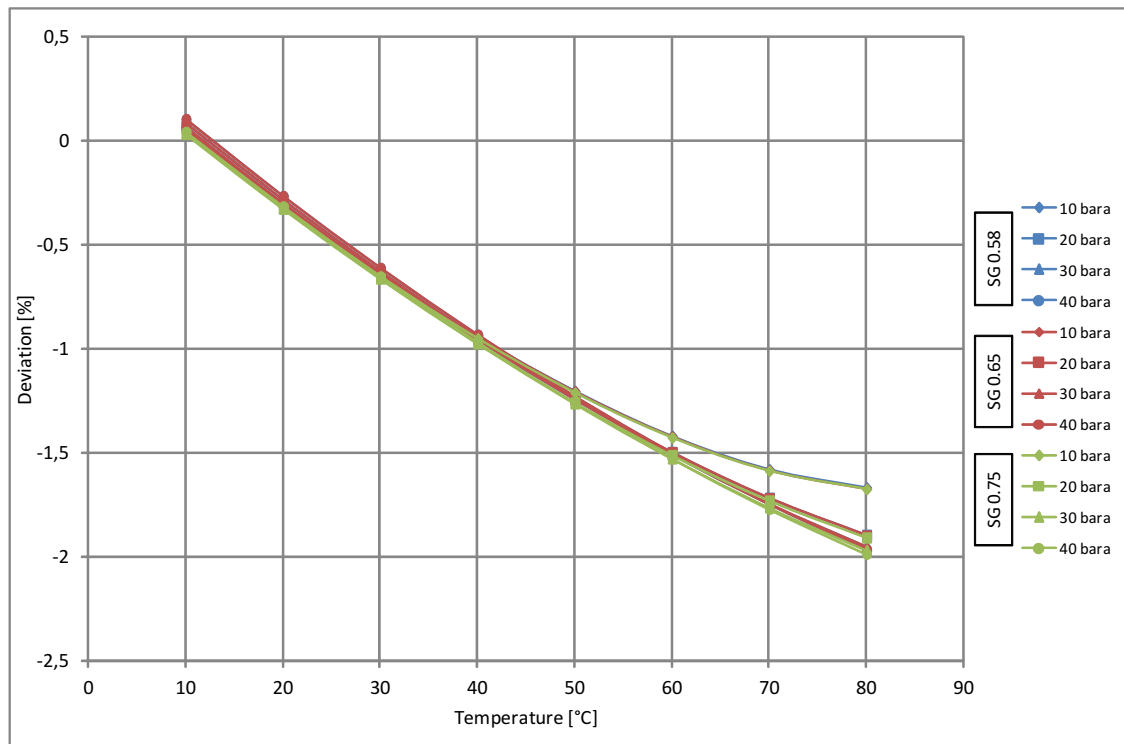
Figure C.18: Deviation of the volumetric water flow rate for varying specific gas gravities.
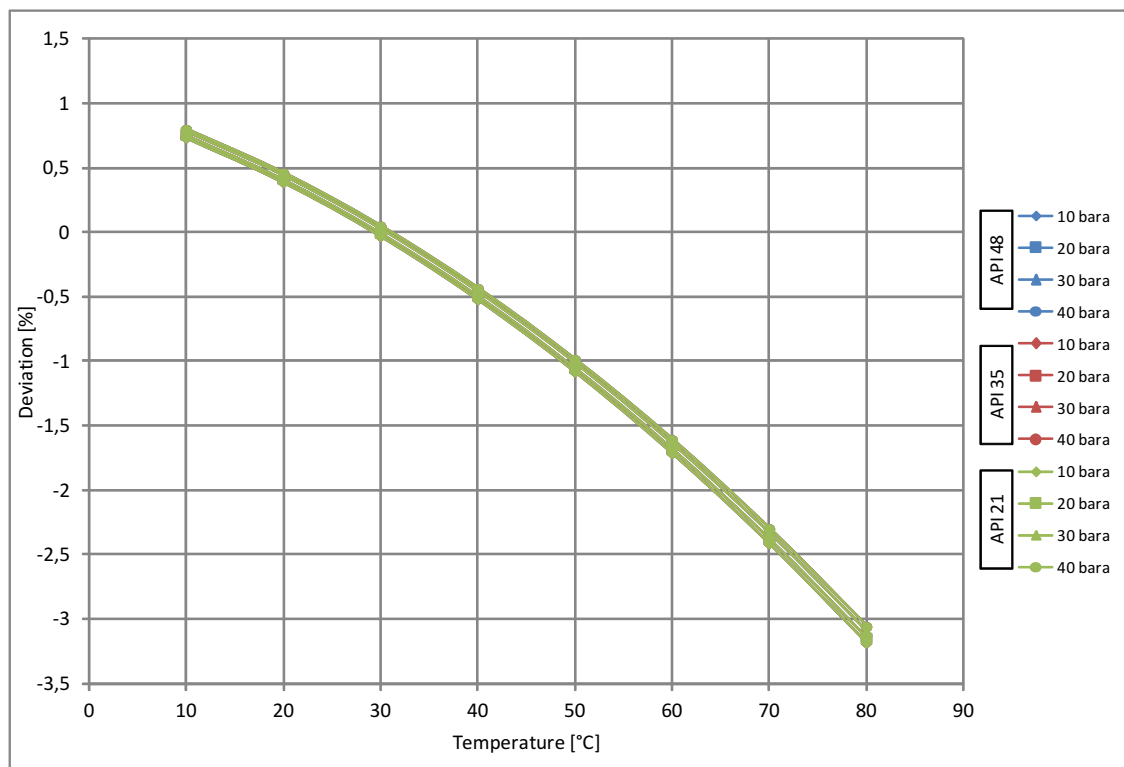
Figure C.19: Deviation of the water specific heat capacity for varying API gravities.
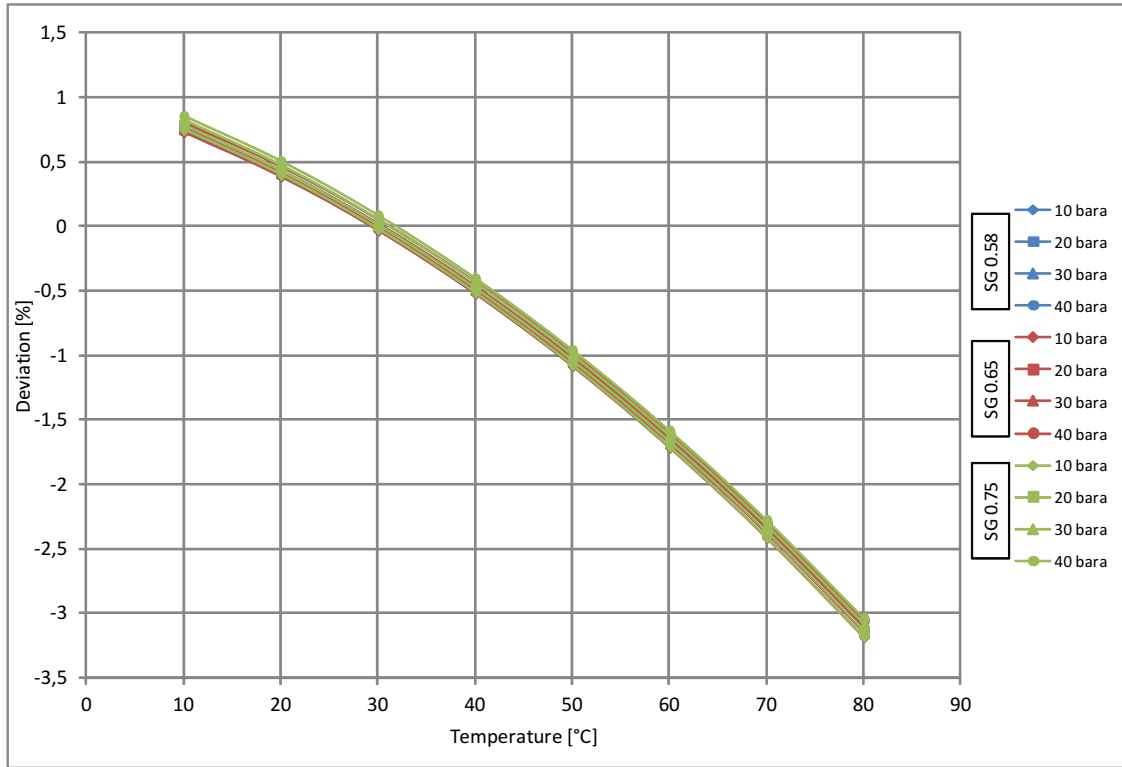
Figure C.20: Deviation of the water specific heat capacity for varying specific gas gravities.
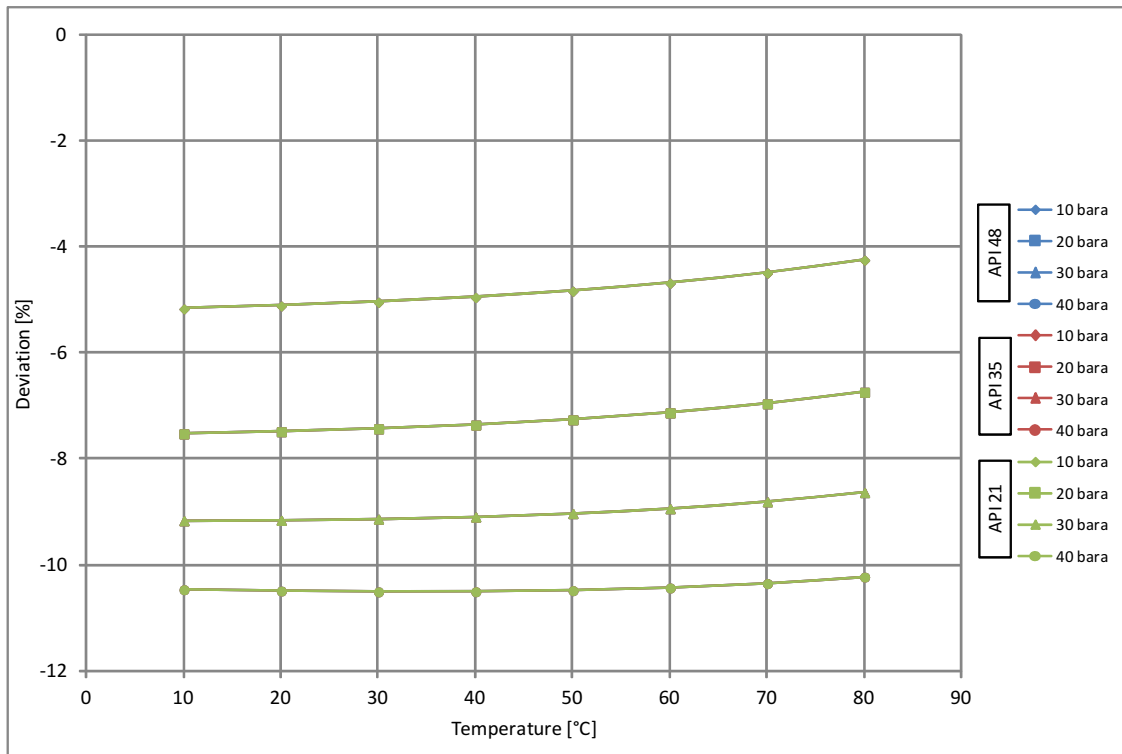
Figure C.21: Deviation of the water surface tension for varying API gravities.
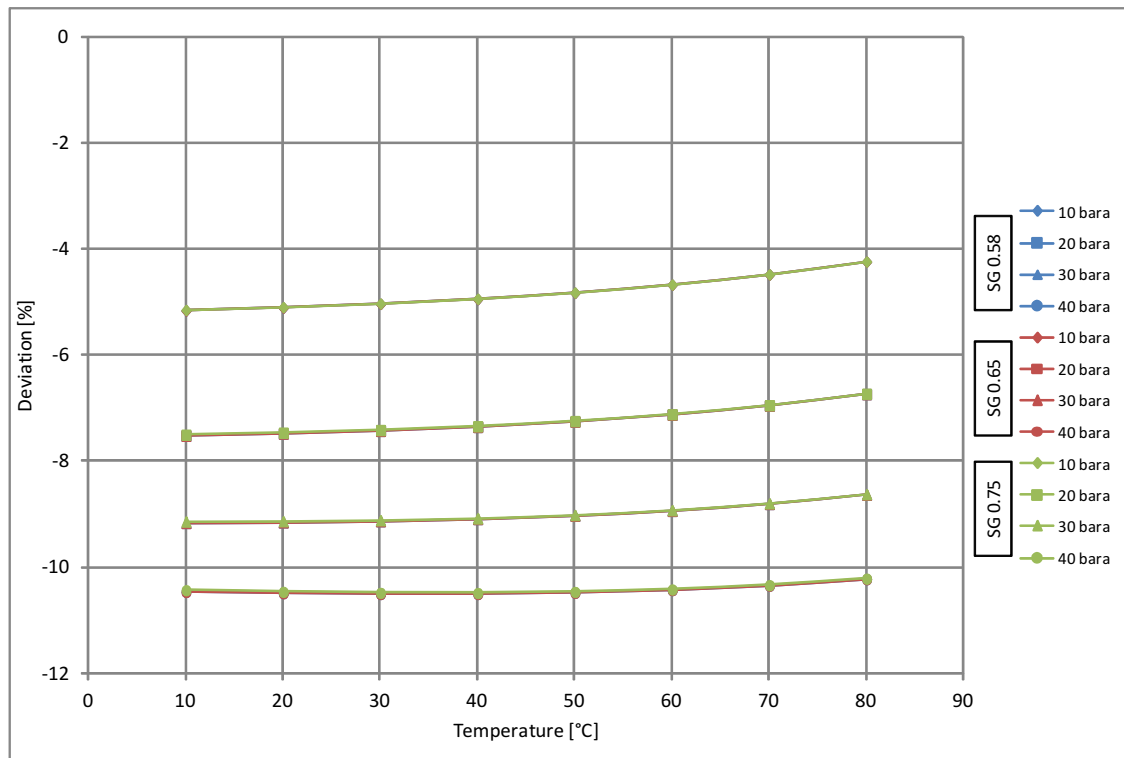
Figure C.22: Deviation of the water surface tension for varying specific gas gravities.

Figure C.23: Deviation of the water viscosity for varying API gravities.
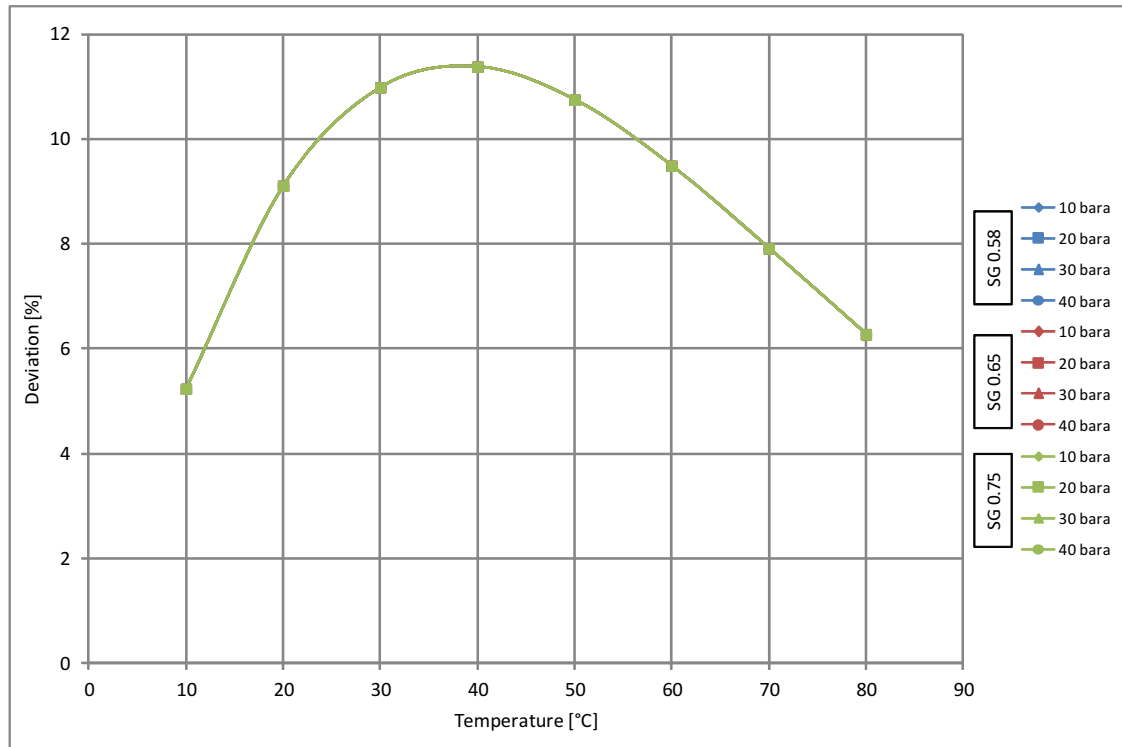
Figure C.24: Deviation of the water viscosity for varying specific gas gravities.

C.2   Summary individual segments

Tab. C.1 presents the pressure drop and temperature loss for the individual pipeline segments.

C.3   Multisegment pipeline

Tab. C.2 presents the detailed results for the evaluation of the multisegment pipeline profile with steep upward and downward inclined segments at 20 bara.

Tab. C.3 presents the detailed results for the evaluation of the multisegment pipeline profile with steep upward and downward inclined segments at 5 bara.

Tab. C.4 presents the detailed results for the evaluation of the multisegment pipeline profile with moderate inclined segments at 5 bara.

Table C.1: Detailed results for the individual pipeline segments.

		Hysys	P&A		P&A comp.		Xiao		Xiao comp.		Hysys	SEM-Flow	
Flow condition	Angle	Δp [bara]	Δp [bara]	Dev. [%]	Δp [bara]	Dev. [%]	Δp [bara]	Dev. [%]	Δp [bara]	Dev. [%]	ΔT [bara]	ΔT [°C]	Dev. [%]
SF	0	0.07	0.07	-1.04	OF	OF	OF	OF	OF	OF	11.70	14.58	24.59
SF	30	9.27	8.97	-3.25	10.41	12.27	9.60	3.50	8.95	-3.49	14.23	18.36	28.98
SF	60	15.41	11.32	-26.51	18.96	23.06	17.43	13.12	16.83	9.21	15.67	16.27	3.79
SF	90	7.21	3.70	-48.64	19.18	22.26	17.52	11.67	17.06	8.76	7.51	3.92	-47.87
SF	-30	-1.22	-0.67	-45.20	OF	OF	OF	OF	OF	OF	9.40	7.29	-22.42
SF	-60	-1.22	-1.29	5.47	OF	OF	OF	OF	OF	OF	9.40	7.08	-24.68
SF	-90	-2.33	-2.00	-14.07	OF	OF	OF	OF	OF	OF	7.67	8.21	7.13
AF	0	41.00	34.86	-14.97	OF	OF	OF	OF	OF	OF	11.09	1.71	-84.59
AF	30	41.90	35.77	-14.64	OF	OF	OF	OF	OF	OF	12.18	1.71	-85.95
AF	60	42.56	36.45	-14.36	OF	OF	OF	OF	OF	OF	12.98	1.71	-86.79
AF	90	42.81	36.71	-15.25	OF	OF	OF	OF	OF	OF	13.27	1.72	-87.07
AF	-30	40.13	33.99	-15.32	OF	OF	OF	OF	OF	OF	10.00	1.70	-82.94
AF	-60	39.51	33.36	-15.56	OF	OF	OF	OF	OF	OF	9.20	1.70	-81.49
AF	-90	39.29	33.14	-15.65	OF	OF	OF	OF	OF	OF	8.90	1.70	-80.89
IF	0	8.64	9.11	5.40	9.68	12.02	8.02	-7.20	8.09	-6.34	0.62	1.26	103.67
IF	30	15.76	17.77	12.80	17.21	9.22	17.56	11.46	16.12	2.30	1.77	1.26	-28.70
IF	60	21.97	25.69	16.97	24.16	9.96	25.39	15.57	22.97	4.55	2.59	1.27	-51.08
IF	90	24.69	28.65	16.04	26.98	16.04	28.65	16.04	25.74	4.21	2.89	1.27	-56.02
IF	-30	2.91	3.37	15.73	4.14	43.42	3.52	22.21	ER	ER	-0.58	1.24	-315.98
IF	-60	-5.09	1.09	-121.35	1.12	-122.09	ER	ER	ER	ER	-1.59	1.24	-177.78
IF	-90	-4.03	1.13	-128.00	4.84	-220.00	ER	ER	ER	ER	-1.77	1.23	-169.75

Table C.2: Results for multisegment pipeline. (20 bara, steep inclination)

Length	Pressure			Temperature			Flow Regime		Liquid hold up		
	Hysys	SEM-Flow	Dev.	Hysys	SEM-Flow	Dev.	Hysys	SEM-Flow	Hysys	SEM-Flow	Dev.
[m]	[bara]	[bara]	[%]	[°C]	[°C]	[%]	[−]	[−]	[−]	[−]	[%]
527.92	20.00	20.00		40.00	40.00		Stratified	Stratified Flow	0.16	0.24	54.57
522.92	20.01	20.02		40.00	40.01		Stratified	Stratified Flow	0.16	0.24	54.62
517.92	20.02	20.04		40.01	40.02		Stratified	Stratified Flow	0.16	0.24	54.68
512.92	20.02	20.06		40.01	40.03		Stratified	Stratified Flow	0.16	0.24	54.73
507.92	20.03	20.09		40.02	40.04		Stratified	Stratified Flow	0.16	0.24	54.78
502.92	20.04	20.11		40.02	40.05		Stratified	Stratified Flow	0.16	0.15	-1.89
491.61	19.95	20.10		39.99	40.08		Stratified	Stratified Flow	0.15	0.15	-1.51
480.3	19.86	20.09		39.96	40.10		Stratified	Stratified Flow	0.15	0.15	-1.13
468.98	19.78	20.08		39.93	40.12		Stratified	Stratified Flow	0.15	0.15	-0.76
457.67	19.69	20.08		39.90	40.14		Stratified	Stratified Flow	0.15	0.15	-0.38
446.36	19.61	20.07		39.87	40.16		Stratified	Stratified Flow	0.15	0.24	57.50
441.76	19.62	20.09		39.87	40.17		Stratified	Stratified Flow	0.15	0.24	57.55
437.16	19.62	20.11		39.88	40.18		Stratified	Stratified Flow	0.15	0.24	57.60
432.56	19.63	20.13		39.88	40.19		Stratified	Stratified Flow	0.15	0.24	57.64
427.96	19.64	20.15		39.89	40.20		Stratified	Stratified Flow	0.15	0.24	57.69
423.36	19.64	20.17		39.89	40.21		Intermittent	Slug Flow	0.21	0.28	32.66
413.36	19.82	20.39		39.94	40.24		Intermittent	Slug Flow	0.22	0.29	32.90
403.36	20.00	20.62		40.00	40.26		Intermittent	Slug Flow	0.22	0.29	33.13
393.36	20.18	20.85		40.05	40.28		Intermittent	Slug Flow	0.22	0.29	33.37
383.36	20.36	21.08		40.10	40.30		Intermittent	Slug Flow	0.22	0.29	33.60
373.36	20.55	21.31		40.15	40.32		Stratified	Stratified Flow	0.16	0.25	57.56
363.36	20.56	21.35		40.16	40.34		Stratified	Stratified Flow	0.16	0.25	57.64
353.36	20.58	21.39		40.17	40.37		Stratified	Stratified Flow	0.16	0.25	57.72
343.36	20.59	21.43		40.18	40.39		Stratified	Stratified Flow	0.16	0.25	57.81
333.36	20.61	21.47		40.19	40.41		Stratified	Stratified Flow	0.16	0.25	57.89
323.36	20.62	21.51		40.20	40.43		Stratified	Stratified Flow	0.16	0.16	2.86
314.75	20.57	21.50		40.18	40.45		Stratified	Stratified Flow	0.16	0.16	3.10
306.15	20.51	21.50		40.16	40.47		Stratified	Stratified Flow	0.16	0.16	3.34
297.55	20.46	21.49		40.15	40.48		Stratified	Stratified Flow	0.16	0.16	3.57
288.95	20.40	21.49		40.13	40.50		Stratified	Stratified Flow	0.16	0.16	3.81
280.34	20.35	21.48		40.11	40.52		Intermittent	Slug Flow	0.21	0.28	32.33
273.34	20.50	21.67		40.15	40.53		Intermittent	Slug Flow	0.21	0.28	32.36
266.34	20.65	21.86		40.20	40.55		Intermittent	Slug Flow	0.21	0.28	32.41
259.34	20.80	22.05		40.24	40.56		Intermittent	Slug Flow	0.21	0.28	32.41
252.34	20.95	22.24		40.29	40.58		Intermittent	Slug Flow	0.21	0.28	32.49
245.34	21.10	22.43		40.33	40.60		Stratified	Stratified Flow	0.16	0.26	59.35
239.34	21.11	22.46		40.34	40.61		Stratified	Stratified Flow	0.16	0.26	59.39
233.34	21.11	22.48		40.34	40.62		Stratified	Stratified Flow	0.16	0.26	59.43
227.34	21.12	22.50		40.35	40.63		Stratified	Stratified Flow	0.17	0.26	59.47
221.34	21.13	22.52		40.35	40.65		Stratified	Stratified Flow	0.17	0.26	59.51
215.34	21.14	22.55		40.36	40.66		Stratified	Stratified Flow	0.16	0.18	9.61
201.93	21.08	22.54		40.34	40.69		Stratified	Stratified Flow	0.16	0.18	9.89
188.51	21.01	22.54		40.32	40.72		Stratified	Stratified Flow	0.16	0.18	10.18
175.1	20.95	22.54		40.30	40.74		Stratified	Stratified Flow	0.16	0.18	10.46
161.68	20.89	22.54		40.28	40.77		Stratified	Stratified Flow	0.16	0.18	10.75
148.26	20.83	22.54		40.26	40.80		Intermittent	Slug Flow	0.22	0.30	34.84
132.61	21.01	22.76		40.32	40.84		Intermittent	Slug Flow	0.22	0.30	35.14
116.96	21.19	22.99		40.37	40.87		Intermittent	Slug Flow	0.22	0.30	35.44
101.3	21.37	23.22		40.42	40.91		Intermittent	Slug Flow	0.22	0.31	35.73
85.652	21.55	23.45		40.48	40.94		Intermittent	Slug Flow	0.23	0.31	36.03
70	21.73	23.67		40.53	40.98		Stratified	Stratified Flow	0.17	0.27	60.82
56	21.75	23.73		40.54	41.01		Stratified	Stratified Flow	0.17	0.27	60.89
42	21.77	23.78		40.55	41.04		Stratified	Stratified Flow	0.17	0.27	60.97
28	21.79	23.83		40.57	41.07		Stratified	Stratified Flow	0.17	0.27	61.05
14	21.81	23.88		40.58	41.10		Stratified	Stratified Flow	0.17	0.27	61.12
0	21.83	23.93		40.59	41.13		Stratified	Stratified Flow	0.17	0.27	61.00
	1.83	3.92	114.34	0.59	1.13	91.77					37.34

Table C.3: Results for multisegment pipeline. (5 bara, steep inclination)

Length	Pressure			Temperature			Flow Regime		Liquid hold up		
	Hysys	SEM-Flow	Dev.	Hysys	SEM-Flow	Dev.	Hysys	SEM-Flow	Hysys	SEM-Flow	Dev.
[m]	[bara]	[bara]	[%]	[°C]	[°C]	[%]	[−]	[−]	[−]	[−]	[%]
527.92	5	5		40	40		Stratified	Annular Flow	0.042	0.110	-161.33
522.92	5.05	5.05		40.03	40.01		Stratified	Annular Flow	0.043	0.111	-160.80
517.92	5.10	5.11		40.05	40.02		Stratified	Annular Flow	0.046	0.112	-141.57
512.92	5.15	5.16		40.08	40.03		Stratified	Annular Flow	0.043	0.113	-159.47
507.92	5.20	5.21		40.11	40.04		Stratified	Annular Flow	0.044	0.113	-158.99
502.92	5.24	5.27		40.13	40.05		Stratified	Annular Flow	0.044	0.102	-130.49
491.61	5.32	5.35		40.14	40.08		Stratified	Annular Flow	0.045	0.102	-129.16
480.3	5.40	5.44		40.15	40.10		Stratified	Annular Flow	0.049	0.103	-109.26
468.98	5.48	5.52		40.16	40.13		Stratified	Annular Flow	0.046	0.104	-126.74
457.67	5.55	5.60		40.16	40.15		Stratified	Annular Flow	0.047	0.105	-125.64
446.36	5.62	5.68		40.17	40.18		Stratified	Annular Flow	0.047	0.120	-154.37
441.76	5.66	5.72		40.18	40.19		Stratified	Annular Flow	0.047	0.121	-154.05
437.16	5.70	5.77		40.20	40.20		Stratified	Annular Flow	0.052	0.121	-133.98
432.56	5.74	5.81		40.22	40.21		Stratified	Annular Flow	0.048	0.122	-153.19
427.96	5.77	5.85		40.24	40.22		Stratified	Annular Flow	0.048	0.122	-152.89
423.36	5.81	5.90		40.26	40.23		Stratified	Froth Flow	0.049	0.149	-204.77
413.36	5.94	6.09		40.35	40.25		Stratified	Froth Flow	0.054	0.151	-182.77
403.36	6.06	6.28		40.43	40.27		Stratified	Froth Flow	0.051	0.154	-201.58
393.36	6.18	6.47		40.51	40.29		Stratified	Froth Flow	0.052	0.156	-200.44
383.36	6.29	6.66		40.59	40.31		Stratified	Froth Flow	0.053	0.158	-199.37
373.36	6.41	6.85		40.67	40.34		Stratified	Annular Flow	0.053	0.136	-154.54
363.36	6.47	6.93		40.70	40.36		Stratified	Annular Flow	0.054	0.137	-153.91
353.36	6.54	7.01		40.72	40.38		Stratified	Annular Flow	0.055	0.138	-153.30
343.36	6.61	7.09		40.75	40.40		Stratified	Annular Flow	0.055	0.139	-152.70
333.36	6.67	7.16		40.78	40.42		Stratified	Annular Flow	0.056	0.140	-152.13
323.36	6.75	7.24		40.81	40.44		Stratified	Annular Flow	0.056	0.123	-118.82
314.75	6.78	7.28		40.81	40.46		Stratified	Annular Flow	0.056	0.123	-118.43
306.15	6.81	7.32		40.80	40.48		Stratified	Annular Flow	0.057	0.123	-118.05
297.55	6.84	7.36		40.80	40.50		Stratified	Annular Flow	0.057	0.124	-117.68
288.95	6.88	7.40		40.79	40.52		Stratified	Annular Flow	0.057	0.124	-117.32
280.34	6.91	7.44		40.79	40.54		Intermittent	Froth Flow	0.130	0.176	-35.65
273.34	7.05	7.59		40.86	40.55		Intermittent	Froth Flow	0.131	0.178	-35.97
266.34	7.20	7.75		40.93	40.57		Intermittent	Froth Flow	0.132	0.179	-36.01
259.34	7.34	7.91		41.01	40.58		Intermittent	Froth Flow	0.133	0.181	-36.17
252.34	7.48	8.06		41.08	40.60		Intermittent	Froth Flow	0.134	0.182	-36.34
245.34	7.62	8.22		41.15	40.61		Stratified	Annular Flow	0.063	0.154	-143.27
239.34	7.66	8.26		41.16	40.63		Stratified	Annular Flow	0.063	0.154	-143.06
233.34	7.69	8.30		41.17	40.64		Stratified	Annular Flow	0.064	0.155	-142.85
227.34	7.72	8.34		41.19	40.65		Stratified	Annular Flow	0.064	0.155	-142.65
221.34	7.75	8.38		41.20	40.67		Stratified	Annular Flow	0.064	0.155	-142.45
215.34	7.78	8.42		41.21	40.68		Stratified	Annular Flow	0.064	0.136	-112.32
201.93	7.82	8.47		41.21	40.71		Stratified	Annular Flow	0.064	0.137	-112.00
188.51	7.86	8.52		41.20	40.74		Stratified	Annular Flow	0.065	0.137	-111.70
175.1	7.91	8.57		41.20	40.77		Stratified	Annular Flow	0.065	0.138	-111.09
161.68	7.95	8.62		41.19	40.80		Stratified	Annular Flow	0.065	0.138	-110.80
148.26	7.98	8.68		41.18	40.82		Stratified	Froth Flow	0.066	0.160	-142.08
132.61	8.10	8.89		41.25	40.86		Stratified	Froth Flow	0.067	0.163	-142.36
116.96	8.22	9.11		41.32	40.89		Stratified	Froth Flow	0.074	0.165	-122.92
101.3	8.35	9.32		41.39	40.93		Stratified	Froth Flow	0.069	0.167	-142.45
85.652	8.47	9.54		41.46	40.96		Stratified	Froth Flow	0.070	0.170	-142.69
70	8.58	9.75		41.52	41.00		Stratified	Annular Flow	0.071	0.172	-143.22
56	8.64	9.83		41.55	41.03		Stratified	Annular Flow	0.071	0.173	-142.77
42	8.71	9.90		41.57	41.06		Stratified	Annular Flow	0.072	0.174	-142.32
28	8.77	9.98		41.60	41.09		Stratified	Annular Flow	0.072	0.174	-141.89
14	8.83	10.06		41.62	41.12		Stratified	Annular Flow	0.081	0.175	-117.17
0	8.91	10.13		41.65	41.15		Stratified	Annular Flow	0.073	0.175	-139.55
	3.91	5.13	-31.31	1.65	1.15	29.92					133.38

Table C.4: Results for multisegment pipeline. (5 bara, moderate inclination)

Length	Pressure			Temperature			Flow Regime		Liquid hold up		
	Hysys	SEM-Flow	Dev.	Hysys	SEM-Flow	Dev.	Hysys	SEM-Flow	Hysys	SEM-Flow	Dev.
[m]	[bara]	[bara]	[%]	[°C]	[°C]	[%]	[−]	[−]	[−]	[−]	[%]
527.92	5.00	5.00		40.00	40.00		Stratified	Annular Flow	0.04	0.11	-161.33
522.92	5.05	5.05		40.03	40.01		Stratified	Annular Flow	0.04	0.11	-160.80
517.92	5.10	5.11		40.05	40.02		Stratified	Annular Flow	0.05	0.11	-141.57
512.92	5.15	5.16		40.08	40.03		Stratified	Annular Flow	0.04	0.11	-159.47
507.92	5.20	5.21		40.11	40.04		Stratified	Annular Flow	0.04	0.11	-158.99
502.92	5.24	5.27		40.13	40.05		Stratified	Annular Flow	0.04	0.11	-146.59
491.61	5.34	5.37		40.17	40.08		Stratified	Annular Flow	0.04	0.11	-145.45
480.30	5.42	5.47		40.20	40.10		Stratified	Annular Flow	0.05	0.11	-144.37
468.98	5.51	5.57		40.24	40.13		Stratified	Annular Flow	0.05	0.11	-143.34
457.67	5.60	5.67		40.27	40.15		Stratified	Annular Flow	0.05	0.11	-142.37
446.36	5.68	5.77		40.30	40.18		Stratified	Annular Flow	0.05	0.12	-134.94
441.76	5.72	5.81		40.32	40.19		Stratified	Annular Flow	0.05	0.12	-154.01
437.16	5.76	5.86		40.33	40.20		Stratified	Annular Flow	0.05	0.12	-153.70
432.56	5.79	5.90		40.35	40.21		Stratified	Annular Flow	0.05	0.12	-153.39
427.96	5.83	5.94		40.37	40.22		Stratified	Annular Flow	0.05	0.12	-153.09
423.36	5.87	5.98		40.38	40.23		Stratified	Annular Flow	0.05	0.13	-172.13
413.36	5.95	6.09		40.43	40.25		Stratified	Annular Flow	0.05	0.14	-171.95
403.36	6.04	6.19		40.48	40.27		Stratified	Annular Flow	0.05	0.14	-171.80
393.36	6.13	6.29		40.53	40.29		Stratified	Annular Flow	0.06	0.14	-151.05
383.36	6.21	6.39		40.58	40.31		Stratified	Annular Flow	0.05	0.14	-171.58
373.36	6.29	6.49		40.62	40.34		Stratified	Annular Flow	0.05	0.13	-149.62
363.36	6.37	6.57		40.66	40.36		Stratified	Annular Flow	0.06	0.13	-128.14
353.36	6.44	6.65		40.69	40.38		Stratified	Annular Flow	0.05	0.13	-148.22
343.36	6.51	6.73		40.72	40.40		Stratified	Annular Flow	0.05	0.13	-147.75
333.36	6.57	6.81		40.74	40.42		Stratified	Annular Flow	0.05	0.14	-147.30
323.36	6.64	6.89		40.77	40.45		Stratified	Annular Flow	0.06	0.13	-135.20
314.75	6.69	6.95		40.79	40.46		Stratified	Annular Flow	0.06	0.13	-134.78
306.15	6.74	7.01		40.80	40.48		Stratified	Annular Flow	0.06	0.13	-113.40
297.55	6.79	7.07		40.82	40.50		Stratified	Annular Flow	0.06	0.13	-133.67
288.95	6.84	7.13		40.83	40.52		Stratified	Annular Flow	0.06	0.13	-133.28
280.34	6.89	7.19		40.85	40.54		Stratified	Annular Flow	0.06	0.16	-173.21
273.34	6.94	7.25		40.87	40.55		Stratified	Annular Flow	0.06	0.16	-151.18
266.34	7.00	7.32		40.90	40.57		Stratified	Annular Flow	0.06	0.16	-173.16
259.34	7.05	7.38		40.93	40.59		Stratified	Annular Flow	0.06	0.16	-173.29
252.34	7.10	7.45		40.96	40.60		Stratified	Annular Flow	0.06	0.16	-173.43
245.34	7.15	7.51		40.99	40.62		Stratified	Annular Flow	0.06	0.14	-143.34
239.34	7.19	7.55		41.00	40.63		Stratified	Annular Flow	0.06	0.15	-143.13
233.34	7.22	7.60		41.02	40.64		Stratified	Annular Flow	0.06	0.15	-142.91
227.34	7.26	7.64		41.03	40.66		Stratified	Annular Flow	0.06	0.15	-142.71
221.34	7.29	7.68		41.04	40.67		Stratified	Annular Flow	0.06	0.15	-142.50
215.34	7.33	7.72		41.06	40.68		Stratified	Annular Flow	0.06	0.14	-135.33
201.93	7.40	7.81		41.08	40.71		Stratified	Annular Flow	0.06	0.14	-134.85
188.51	7.47	7.90		41.10	40.74		Stratified	Annular Flow	0.06	0.14	-134.38
175.10	7.53	7.98		41.13	40.77		Stratified	Annular Flow	0.06	0.15	-133.92
161.68	7.60	8.07		41.15	40.80		Stratified	Annular Flow	0.06	0.15	-133.47
148.26	7.67	8.15		41.17	40.83		Stratified	Annular Flow	0.06	0.16	-149.26
132.61	7.77	8.26		41.22	40.86		Stratified	Annular Flow	0.06	0.16	-148.46
116.96	7.86	8.37		41.25	40.90		Stratified	Annular Flow	0.07	0.16	-148.15
101.30	7.95	8.49		41.29	40.93		Stratified	Annular Flow	0.07	0.16	-147.84
85.65	8.04	8.59		41.33	40.97		Stratified	Annular Flow	0.07	0.16	-147.55
70.00	8.12	8.70		41.37	41.00		Stratified	Annular Flow	0.07	0.16	-137.67
56.00	8.19	8.79		41.40	41.03		Stratified	Annular Flow	0.07	0.16	-137.32
42.00	8.26	8.88		41.42	41.07		Stratified	Annular Flow	0.07	0.16	-136.97
28.00	8.33	8.96		41.45	41.10		Stratified	Annular Flow	0.07	0.16	-136.64
14.00	8.41	9.05		41.48	41.13		Stratified	Annular Flow	0.07	0.16	-135.96
0.00	8.47	9.13		41.50	41.16		Stratified	Annular Flow	0.07	0.16	-134.22
	3.47	4.13	-18.98	1.50	1.16	22.84					147.39

List of Figures

List of Tables